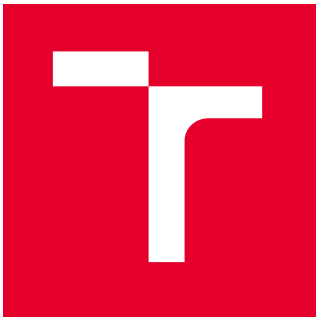

BRNO UNIVERSITY OF TECHNOLOGY

VYSOKÉ UČENÍ TECHNICKÉ V BRNĚ

FACULTY OF MECHANICAL ENGINEERING

FAKULTA STROJNÍHO INŽENÝRSTVÍ

INSTITUTE OF MACHINE AND INDUSTRIAL DESIGN

ÚSTAV KONSTRUOVÁNÍ

THE EFFECT OF CONTAMINATION ON FRICTION MODIFICATION IN THE WHEEL-RAIL CONTACT

VLIV KONTAMINACE NA MODIFIKACI TŘENÍ V KONTAKTU KOLA A KOLEJNICE

DOCTORAL THESIS

DIZERTAČNÍ PRÁCE

AUTHOR — **Ing. Šimon Skurka**

AUTOR PRÁCE

SUPERVISOR — **prof. Ing. Martin Hartl, Ph.D.**

ŠKOLITEL

BRNO 2026

Flight attendant: "Is there a doctor on board?"
Me: "Yes, but I'm not that kind of…"
Flight attendant: "It's 11:52 PM, and the passenger in 37F has a conference abstract due in seven minutes. It's currently 50 words over the limit."
Me: "Okay. I'm here."

— Leslie Berntsen, post on X (formerly Twitter), available online; no DOI assigned, accessed 22 December 2025.

Statement

I hereby declare that I have written the PhD thesis *The effect of contamination on friction modification in the wheel-rail contact,* on my own, according to the advice of my supervisor, prof. Ing. Martin Hartl, PhD and co-supervisor, doc. Ing. Radovan Galas, PhD, and using the sources listed in the references.

Šimon Skurka

Bibliographical Reference

SKURKA, Šimon. *The effect of contamination on friction modification in the wheel-rail contact*. Doctoral Thesis. Martin HARTL (supervisor). Brno: Brno University of Technology, Faculty of Mechanical Engineering, 2026.

Acknowledgement

The list of people who supported me during my doctoral studies and contributed, in different ways, to the completion of this thesis is indeed long.

I would like to begin by thanking my supervisor, prof. Ing. Martin Hartl, PhD, for his guidance, trust, and continuous support. I also thank prof. Ing. Ivan Křupka, PhD, as the head of the Tribology Research Group, for creating a research environment and providing opportunities that made this work possible. Special thanks go to doc. Ing. Milan Omasta, PhD, as the head of the wheel–rail tribology section, for his valuable advice and many helpful consultations, particularly during the preparation and publication of scientific articles.

A substantial part of this thesis was carried out during my research stay at Southwest Jiaotong University in Chengdu, China, where I spent nearly ten months. I am sincerely grateful to prof. Wenjian Wang and assoc. prof. Haohao Ding for their warm hospitality, guidance, and support. This internship had a strong influence on this work, on my development as a researcher, and was also an important personal life experience.

I am very thankful to my colleagues and friends for the great atmosphere at work and beyond, which made my doctoral studies both enjoyable and rewarding. Throughout this time, my family played a truly essential role, and I am deeply grateful for their lifelong support, patience, and encouragement.

Finally, I would like to thank my co-supervisor, and now also a friend, Radovan Galas, without whom this thesis would not have come to life. Our collaboration has lasted for more than six years and has been marked by countless discussions, valuable advice, many moments of humour, and unforgettable experiences from both here and the other side of the world. I believe that this shared journey does not end with the completion of this thesis.

Thank you.

Abstract

Top-of-rail products are used for friction modification on the railhead. Over the past three decades, intensive research has shown that they can reduce operational costs and extend the service life of wheels and rails by mitigating wear and rolling contact fatigue. Most of this research, however, has been performed under clean laboratory conditions. In reality, the wheel–rail interface is an open system in which various contaminants are always present, and conditions may change even between passing axles of the same vehicle. It is therefore reasonable to expect that these contaminants also affect the performance of top-of-rail products. For this reason, this PhD thesis investigates how contamination influences friction modification in the wheel–rail contact.

The experimental work combines friction measurements performed on a laboratory tribometer with rolling contact fatigue tests on a twin-disc machine. A climate chamber was used to simulate humid environments and to form oxide layers, while a humidifier unit and a peristaltic pump reproduced contamination modes such as dew or precipitation. Specimens were prepared as metallographic cross-sections, and scanning electron microscopy was used to evaluate crack morphology under the different test conditions.

The results showed that contamination has a strong effect on top-of-rail products. For water-based products, light moisture prolonged their effect, whereas larger amounts of water washed them away and ended their effect on friction, wear and rolling contact fatigue. Oil-based products behaved differently: water greatly amplified their lubricating effect, causing extremely low friction, suppressed wear and caused rapid liquid-assisted crack growth. Oxides had only a small influence on friction, but oxidation contributed to material weakening and had an unexpected effect on cracks, as it caused oxygen-assisted propagation.

These findings underline the importance of considering environmental conditions when optimising friction-modification strategies and provide insights into the mechanisms governing product behaviour under real operating conditions. In addition, a new benchmarking methodology for assessing the performance of top-of-rail products was proposed, offering a standardised and reliable approach for laboratory testing.

Keywords

Top-of-Rail Products, Wheel–Rail Adhesion, Rolling Contact Fatigue, Water Contamination, Iron Oxides

Abstrakt

Top-of-rail produkty se využívají pro modifikaci tření na temeni kolejnice. Roky výzkumu prokázaly jejich schopnost snižovat opotřebení, což má pozitivní vliv na životnost kolejnic i vlakových kol a s tím spojených nákladů na provoz a údržbu. Testování těchto produktů standardně probíhá v čistých laboratorních podmínkách. Na povrchu kolejnic se však kromě těchto produktů vyskytují i další látky (kontaminanty), které výrazným způsobem ovlivňují tření, a je tedy důvodné se domnívat, že budou ovlivňovat i jejich chování a výkonnost. Dizertační práce se proto věnuje zkoumání interakcí mezi top-of-rail produkty a kontaminanty, jako jsou voda nebo oxidy železa.

V rámci experimentální části byla provedena měření na laboratorním tribometru vybaveném klimatickou komorou pro vytvoření podmínek vysoké vzdušné vlhkosti a rosy. Déšť byl simulován pomocí aplikace vody v různých množstvích. Za účelem studia opotřebení a valivé kontaktní únavy bylo použito dvoudiskové zařízení v kombinaci s elektronovým mikroskopem pro pozorování trhlin. Příprava oxidických třecích vrstev probíhala v klimatické komoře za zvýšené teploty a vzdušné vlhkosti.

Výsledky ukázaly, že kontaminace vodou má významný vliv na funkci top-of-rail produktů. V případě produktů na vodní bázi docházelo vlivem menšího množství vody k prodlužení jejich účinků, větší množství vody je však vyplavilo z kontaktu a veškerý efekt byl ztracen. Produkty na olejové bázi se chovaly odlišně: voda měla výrazný zesilující efekt na jejich mazací účinek a způsobovala propady tření do velmi nízkých hodnot. To se ve finále negativně projevilo jak na problémech s adhezí, tak na valivé kontaktní únavě. Oxidické vrstvy měly na tření jen nepatrný vliv. Zajímavý však byl jejich účinek na únavové trhliny – oxidace uvnitř trhlin vedla k jejich šíření do větších hloubek v důsledku oslabení okolního materiálu na hranicích zrn a také objemové expanze oxidů.

Dizertační práce ukázala nutnost zohlednit klimatické podmínky při optimalizaci strategie modifikace tření na železničních i tramvajových tratích a poskytla nový vhled do mechanismů interakce mezi top-of-rail produkty a kontaminanty. Jedním z výstupů je také nová metodika pro hodnocení výkonnosti těchto produktů v kontrolovaných laboratorních podmínkách.

Klíčová slova

Top-of-rail produkty, adheze mezi kolem a kolejnicí, valivá kontaktní únava, kontaminace vodou, oxidy železa

Content

1. Introduction

Rail transport has long been a cornerstone of mobility and logistics, not only in Europe but worldwide. With a growing focus on environmental issues, demands for reducing carbon dioxide emissions, and the pursuit of sustainable development, rail transport is becoming more critical than ever before. However, numbers instead of words: Between 2021 and 2024, the European Union allocated more than €15 billion of funds directly to railway projects [1], preparing the infrastructure for a massive rise in passenger-kilometres travelled, from 470 billion in 2015 to 741 billion projected in 2050 [2]. To date, rail is recognised as the lowest-emission way of transport, far outperforming road and aviation [2].

The efficiency of rail transport relies on the effective use of forces that drive the vehicle and the minimisation of those that try to stop it. From a tribological perspective, it all comes down to the *wheel–rail interface* and *friction*. An honest answer to the question of whether friction should be low or high is: "It depends on where and when". The wheel–rail interface can be divided into two subsections: the contact between the *wheel flange* and the *rail gauge corner*, and the contact between the *wheel tread* and the *rail head* (hereafter referred to as "*top-of-rail contact*"). The first one primarily provides vehicle guidance in curves and acts as a safety feature against derailment. It is a highly loaded sliding contact, characterised by significant wear and energy losses. Therefore, minimising friction is of utmost importance.

Things become more complicated when it comes to friction in the *top-of-rail* (*TOR*) contact. High friction increases operational costs [3] through higher fuel consumption [4], more frequent wheel replacements, and rail grinding as a response to damage to contacting surfaces [5,6]. An additional problem is *friction-induced noise* [7,8]. It is estimated that up to 113 million people in Europe are exposed to excessive noise emissions from transport, with railways accounting for approximately 20% of this figure [9]. According to the World Health Organisation (WHO), long-term exposure to noise levels above 55 dB is harmful to human health. The European Environment Agency (EEA) estimates that chronic exposure to excessive noise leads to up to 12,000 premature deaths and 48,000 new cases of ischaemic heart disease annually. Additionally, approximately 6.5 million people residing near transport corridors experience sleep disorders due to excessive noise [9].

One could conclude that eliminating friction in the TOR contact would solve all issues once and for all, but that would be utterly wrong, as friction is crucial for the effective transmission of *tractive* (or *braking*) *forces*. Without that, vehicles experience various problems, with the most common being *station overruns* resulting from prolonged braking distances [10]. During the autumn period of 2023 in the United Kingdom alone, a total of 337,700 minutes of delay (equivalent to roughly two-thirds of a year in cumulative time!) was attributed to problems with friction. Last but not least, battling such issues can be highly costly, with some estimates suggesting annual expenditures of up to £350 million [11].

In recent years, extensive research has demonstrated that most of the problems mentioned above can be addressed through effective *friction management*. One established approach is the application of *TOR products*, typically delivered to the railhead either by wayside applicators or directly from passing vehicles. From traditional lubricants, TOR products differ in composition, as they contain solid particles designed to prevent friction from dropping too low. However, the wheel–rail interface is an *open system*, inevitably exposed to various *environmental contaminants* (such as water and leaves) that can substantially influence friction and, in turn, compromise the effectiveness of TOR products. Despite that, little attention has been paid to their mutual interaction, as most studies have tested TOR products under clean laboratory conditions or have not explicitly considered the role of contamination in field tests. Therefore, this thesis aims to describe the effect of environmental contamination on the performance of TOR products.

2. State of the Art

It is without any doubt that readers of this thesis are familiar with basic tribological terms like friction, creepage, or rolling-contact fatigue – concepts that have been explained countless times since Carter in 1926 [12]*. Yet, the Author cannot suppress the urge to explain them once again, as he believes it may be helpful for easier orientation in the text ahead.*

In wheel–rail tribology, frictional conditions are governed by *adhesion*. In simple terms, adhesion describes the friction that develops under a combination of rolling and sliding. More precisely, friction can be viewed as the limiting tangential force defined by material properties and contact conditions, while adhesion represents the actual tangential force that arises for a given ratio of rolling and sliding. Under pure sliding, adhesion reaches the friction limit, meaning that friction defines the upper boundary of the adhesion available in the contact.

When a wheel negotiates a curve or transmits traction or braking forces, a small difference in surface speed develops between the wheel and the rail, which produces frictional shear stresses. Under these conditions, part of the contact patch remains in stick while the rest slips, a behaviour typically described as rolling with partial sliding. This state is quantified by *creepage* or *slip*. In laboratory experiments, however, the *slide-to-roll ratio* (*SRR*) is often used instead, particularly in *ball-on-disc* tribometers such as the *Mini-Traction Machine* (*MTM*). Although creepage and SRR refer to a similar physical concept, they are not directly interchangeable, and the numerical value of slip does not correspond to the value of SRR.

Adhesion is quantitatively expressed by the *coefficient of adhesion* (*CoA*), which depends on creepage. An analogous parameter to the CoA is the *coefficient of traction* (*CoT*). Both parameters describe the transmission of tangential forces, but the distinction lies in the direction of force. In the case of CoA, these are braking forces, while in the case of CoT, they represent tractive forces. In simpler terms, the first corresponds to vehicle braking, while the second relates to vehicle acceleration. In the literature, CoA is typically used in studies addressing low-friction conditions due to contamination. In contrast, CoT is more common in research focused on problems related to high-friction or traction enhancement. In the context of this work, CoA will be used when discussing the effects of *contamination*, and CoT will be used in relation to *friction modification*.

The graphical representation of the relationship between CoT (or CoA) and creep is referred to as the *creep curve*. As creepage increases, the CoT increases up to a certain point, known as the *saturation point*. Increasing creepage beyond the saturation point may lead to either a further increase in CoT (*positive friction characteristic*) or a decrease (*negative friction characteristic*). The third option is that it does not increase or decrease (thus, a *neutral friction characteristic*). In railway operation, a negative friction characteristic is highly undesirable, as it induces *stick–slip oscillations*. This phenomenon occurs when two different

creepage values correspond to the same CoT, resulting in axle vibrations and wheel sliding, and often promoting rail corrugation [13].

The CoT measured between two dry and clean surfaces typically ranges between 0.4 and 0.8, depending on the measurement method and creepage [14–19]. From the perspective of efficient operation, this is too high, as it leads to several issues, such as excessive wear, noise generation, etc. Applying lubricants to the TOR contact could mitigate these problems, but it would simultaneously cause problems with traction or braking. This challenge has driven the development of a new class of materials designed to maintain friction at intermediate levels, where wear and noise are reduced compared to dry conditions, while simultaneously ensuring sufficient CoT.

Initially, these "TOR products" were developed in the form of solid sticks and were first applied in the late 1980s on the Vancouver SkyTrain system to address issues related to corrugation and noise [20]. Since then, TOR products have gradually spread worldwide. They were introduced across the United States [21], where they were used to control friction on both freight and passenger railways. In Asia, TOR products are employed mainly in Japan [22] and China [23]. Regarding Europe, TOR friction control is used in several national rail networks, including the UK [24] and Spain [25]. And lastly, in Czechia, TOR friction control is implemented in the urban rail networks of Prague and Brno. The Prague Metro, which operates more than 60 km of track and carries over half a billion passengers each year, ranks among the busiest systems in Europe. TOR products were adopted in the early 2000s after successful trials on Line C, aiming to limit rail corrugation and reduce wear. As a result, the expected wheel life increased to approximately 1.5 million kilometres [26].

2.1 Categorisation of TOR Products

TOR products can be either in the form of solid sticks composed of sintered solid lubricants that are pressed against the wheel [27–31], or in liquid form applied from a track-side applicator or directly sprayed from an on-board unit, see Fig. 1. According to Stock et al. [32], liquid TOR products can be categorised based on their base medium type into *friction modifiers* (water-based), *TOR lubricants* (oil/grease-based), and a marginal group of *TOR hybrids* (combining both water and oil). The base medium determines the friction modification mechanism. In the case of friction modifiers (*FMs*), water serves as a carrier that helps distribute solid lubricants over the rail surface. After the water evaporates, the resulting frictional conditions are governed by a dry layer with low shear strength, typically composed of graphite or molybdenum disulfide [33].

In contrast to the drying nature of FMs, TOR lubricants are non-drying [24]. They form a thin lubricating film on the railhead, and the reduction in friction results from a transition from dry to boundary or mixed lubrication regimes, where the load is transferred partly through asperity contact and partly through a thin fluid film. To ensure sufficient CoT, TOR lubricants

typically contain soft metal particles or their compounds [34,35]. The fundamental principles of TOR friction modification are depicted in Fig. 2.

a) b)

Fig. 1 Application methods: a) from a track-side unit [36] and b) from an onboard unit [37].

Two main requirements for TOR products are to maintain a positive friction characteristic [22] and to establish an *intermediate level of friction*. While the concept of a positive slope of the creep curve behind the saturation point is clear, the definition of the intermediate friction level varies across studies. This variation arises not only from different methodological approaches but also from the fact that dry contact conditions themselves can produce a wide range of friction levels [14]. For instance, Zakharov et al. [38] defined the intermediate range in relative terms as one-third to two-thirds of the CoT under dry conditions. However, most studies define it instead in absolute terms, typically between 0.2 and 0.4 [32,39].

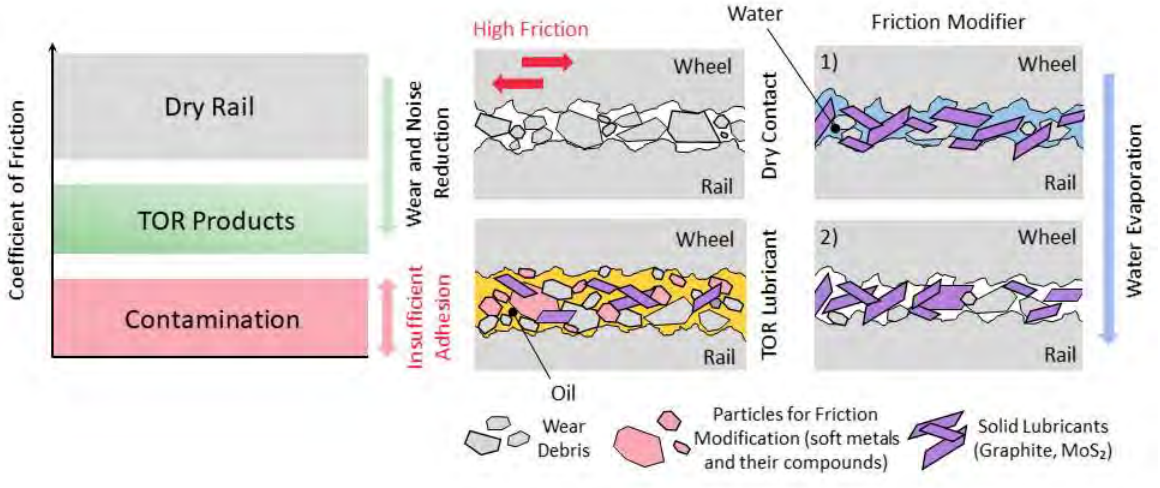

Fig. 2 Principles of top-of-rail friction modification – redrawn from [32] and modified.

2.2 TOR Products and Friction Control

One of the earliest field demonstrations of liquid TOR products was conducted by Tomeoka et al. [40] in 2002. Since then, numerous field and laboratory studies have examined the performance of TOR products with various compositions and under different operating

conditions [41–48]. Lundberg et al. [14] measured CoT between rails and wheels of a 360-ton locomotive. While CoT around 0.3 was measured on dry rails, values as low as 0.1 were observed on sections treated with an FM. This reduction had a positive impact on wear. Still, it is essential to note that the wheels of the locomotive often slipped, indicating that low adhesion problems occur at such a low CoT, which highlights the importance of precise dosing control and the composition of the product.

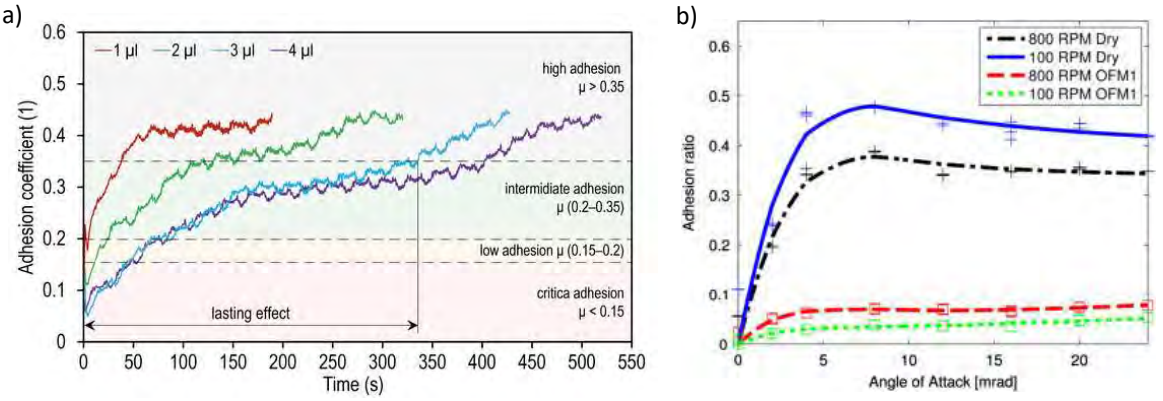

Fig. 3 Ability of TOR products to provide: a) intermediate friction [49] and b) positive creep curve slope [50].

The optimal dosing was further investigated by Galas et al. [49], who tested a TOR lubricant on a tram curve. The study demonstrated that overdosing significantly extended the braking distance of the passing vehicle (order of tens of metres). On the other hand, underdosing had a negligible effect on braking but did not achieve the desired noise reduction. Szablewski et al. [4] focused on differences between drying and non-drying products. In their tests, both FMs and TOR lubricants were able to maintain an intermediate level of friction. Measured CoT varied between 0.30 and 0.34, which is sufficient for traction and braking, while reducing lateral forces by up to 67% for the FM and 54% for the TOR lubricant. The longer effective carry distance was recorded for the TOR lubricant, as its non-drying nature allows it to spread further.

Evans et al. [51] focused on the ability of FMs to provide a positive friction characteristic. They conducted a comprehensive evaluation of the performance of one selected FM using two coupled locomotives at the VUZ Velim Test Centre, Czechia. One locomotive maintained a constant travel speed, while the other controlled slip on a single driven axle to simulate traction conditions. The FM was sprayed onto the railhead by an on-board unit mounted on one of the locomotives, enabling precise and repeatable dosing during each test. The measured CoT ranged between 0.1 and 0.25, and the creep curve exhibited a positive slope beyond the saturation point, confirming the desired traction behaviour.

Similarly, Matsumoto et al. [52] tested FM on a scaled bogie. The application of FM provided an intermediate level of friction and changed the slope of the creep curve from negative under dry conditions to positive. The endurance of the FM layer depended on the creepage level, as it was removed more slowly under low creepage, whereas higher creepage accelerated film loss. The ability of TOR products to maintain an intermediate level of friction and a positive slope of the creep curve was further confirmed in several other studies [25,53–56].

Galas et al. [57] focused on the role of the composition of TOR products. They tested two commercial TOR lubricants. The first one was based on plant oil containing copper and zinc particles, and the other on ester oil containing copper and aluminium particles. While the one with a higher metal-particle content maintained CoT near optimal levels, the other with higher oil content caused low adhesion problems due to over-lubrication. These results confirmed earlier conclusions [49] and demonstrated that particle content plays a key role in determining TOR lubricant performance.

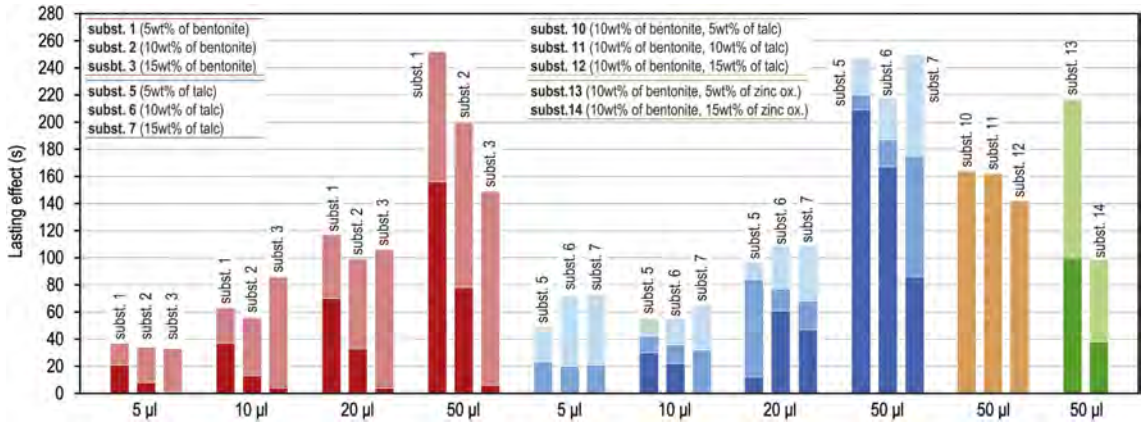

Fig. 4 Overview of the lasting effect of FMs with varying compositions and particle content [33].

The same authors further investigated the optimal ratio between liquid base and solid particles in FMs [33]. They prepared compositions based on water as a carrier with bentonite, talc, or zinc oxide particles, and solid lubricants such as molybdenum disulfide and graphite. The addition of bentonite was able to maintain CoT at intermediate levels even when overdosed.

The water–talc compositions provided sufficient CoT only when the talc content was below 10 wt%, while higher concentrations formed a soft, low-shear paste layer that reduced CoT to low values. The addition of zinc oxide promoted a positive friction characteristic. Large amounts of graphite or molybdenum disulfide reduced CoT below 0.1. An overview of the lasting effect of the tested compositions, based on their particle content, is shown in Fig. 4.

Kvarda et al. [58] extended the study for TOR lubricants. They used biodegradable ester oil thickened with bentonite as a base medium and different solid particles, including aluminium oxide, zinc oxide, copper sulfide, molybdenum disulfide, and graphite. Only alumina particles were able to balance the strong lubricating effect of the base oil, while zinc oxide and copper sulfide failed to provide intermediate friction. The combination of alumina particles with molybdenum disulfide or graphite resulted in stable CoT values corresponding to the desired range for TOR applications. These results indicate that hard particles such as aluminium oxide are essential for preventing over-lubrication. However, Oomen et al. [59] showed that the addition of aluminium oxide had an adverse effect on the surface, as it promoted abrasive wear. Therefore, soft particles such as copper or graphite should also be included in the product composition to balance the adverse effects of hard particles.

2.3 TOR Products and Wear and RCF

While the previous section focused mainly on the frictional behaviour of TOR products, it is equally important to consider their influence on wear and *rolling-contact fatigue* (*RCF*). Friction control not only determines traction but also directly affects the contact stress distribution, which governs the progression of material damage. So, the relationship between friction, wear, and RCF must be evaluated as a coupled system.

One motivating example for using TOR products for wear mitigation comes from the heavy-haul coal Shuohuang Railway line in China. Due to increased demand for coal supply, the transported load rose from 5.3 to 148 million net tons over a period of just 9 years. As the track had not been designed initially for such high loads, this led to severe wear and RCF. However, the introduction of a lubricating system combining gauge-face lubrication with TOR friction modification reduced rail wear by 18–52% (depending on track location) and lateral forces by up to 69%, effectively doubling the rail service life compared with the period before friction management was implemented [23].

Eadie et al. [54] conducted an extensive study, which utilised a full-scale testing rig to assess the effect of FMs on wear and RCF. The performed tests had a duration of 100,000 cycles, and the authors tested FMs at different dosages, along with an additional test under dry conditions for reference. In contrast, periodic FM application effectively prevented surface cracking and substantially reduced railhead wear, as can be seen in Fig. 5. Stock et al. [56] came up with a follow-up study that expanded previous experiments to 400,000 cycles and added additional steel grades (standard R260 and premium R350HT). FMs maintained CoT between 0.3 and 0.4, with positive friction characteristics, and no significant RCF cracks were detected at the end of the test. Compared to the dry reference test, wear was nearly eliminated.

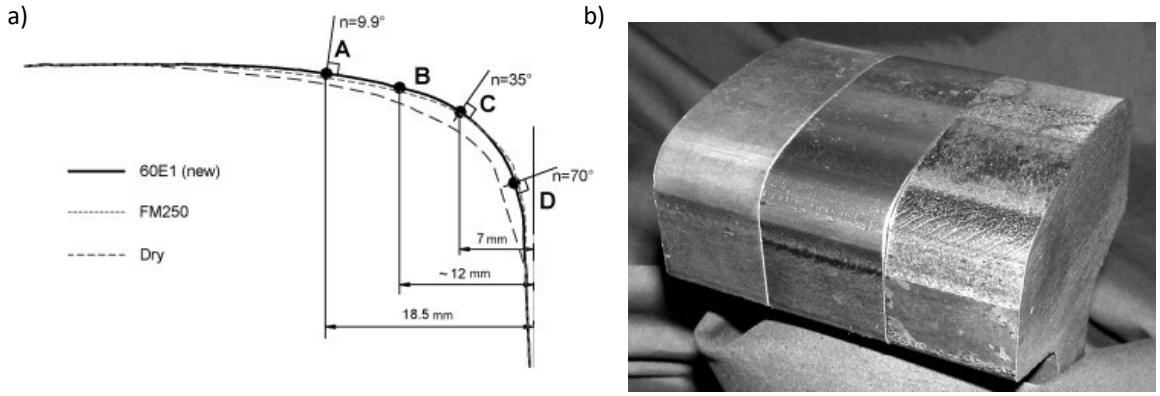

Fig. 5 Rail profile changes due to wear: reference (new) rail and for dry and FM test conditions in a), with photos of the corresponding specimens in the same order in b) [54].

When it comes to TOR lubricants, the RCF situation differs, as several studies have reported their adverse effects on crack propagation. Sánchez et al. [60] tested two TOR lubricants. While both of them significantly reduced CoT below 0.1 and subsurface deformation depth to one-third, microscopic observations revealed a transition from adhesive wear and *ratcheting* under

dry conditions to severe *delamination* under TOR lubricants, as low-viscosity oil used as a base medium penetrated subsurface cracks and accelerated crack growth by a *hydro-pressurisation mechanism*. A study by Gutsulyak et al. [61] reached similar conclusions, adding that hydro-pressurisation does not occur with FMs because their base dries rapidly after application. In this regard, it is essential to mention the study by Seo et al. [53], who tested the TOR hybrid. In this case, the product accelerated crack growth. Due to its partially drying base medium, it formed alternating dry and wet patches in the contact, combining the high CoT typical of dry contact with fluid entrapment, causing hydro-pressurisation.

Some of the mentioned studies demonstrated the ability of TOR products to prevent the formation of RCF cracks, but showed adverse effects of liquid base medium on cracks that already exist. A significant work was delivered by Hardwick et al. [62], who focused on the case when cracks were already present before the TOR product application. The authors used a twin-disc machine to initially run specimens for 4,000 dry cycles to create pre-existing cracks. Then, all categories of TOR products were tested together with water as a reference. In the case of FM, the base medium evaporated quickly, leaving behind a thin solid-particle film that maintained CoT between 0.1–0.2 and reduced wear by 44%. Crack depths remained shallow and parallel to the surface.

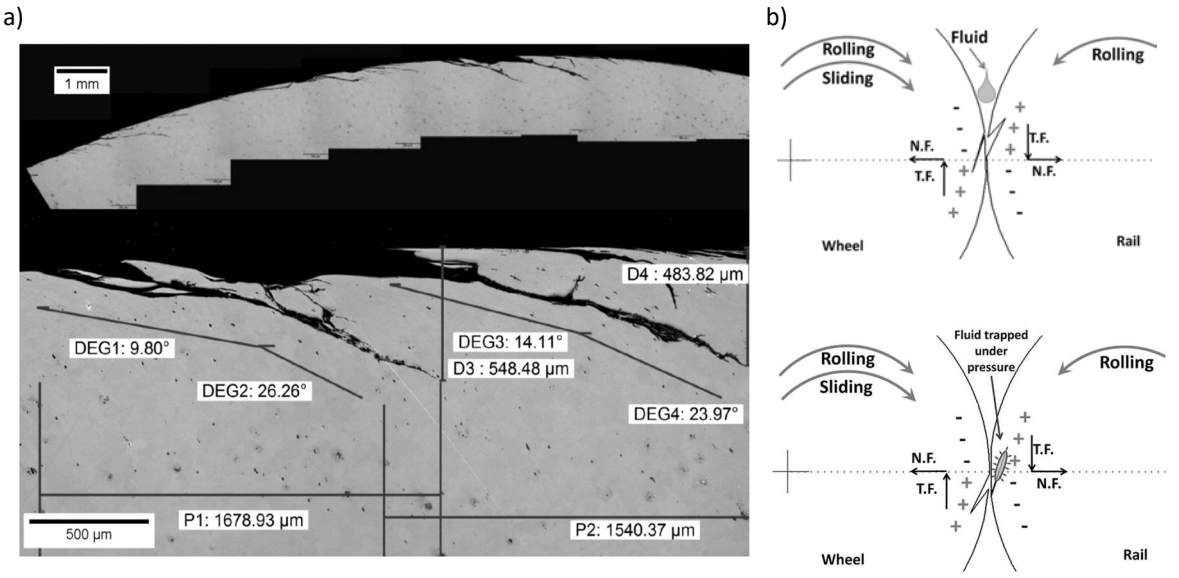

Fig. 6 a) Effect of TOR lubricant on RCF in the presence of pre-existing cracks [62] and b) fluid-assisted crack propagation mechanism (hydropressurisation) [63].

In contrast, TOR lubricants (oil- and grease-based), TOR hybrid and water promoted severe crack propagation, see Fig. 6 a). Water resulted in an average CoT of 0.2 and crack depths between 200 µm and 360 µm, as a result of hydropressurisation, as depicted in Fig. 6 b). The low-viscosity TOR lubricant resulted in a very low CoT (approximately 0.07) but caused a more than twelvefold increase in material loss, with crack depths reaching up to 0.8 mm. Similarly, the high-viscosity TOR lubricant and the TOR hybrid produced extremely low CoT (0.02–0.06), causing *spalling* and localised delamination with cracks as deep as 0.9 mm. The most severe RCF damage was observed under water-lubricated conditions, leading

to extensive delamination and an increase in total material loss of up to 17 times. Microscopic cross-sections confirmed that only the drying FM was able to prevent further crack propagation effectively. The study concluded that non-drying TOR products increase the risk of accelerated RCF in rails with pre-existing cracks, a conclusion consistent with the results of several other studies [63,64].

2.4 Other Benefits of TOR Products

In addition to wear and RCF, the wheel–rail system is also prone to rail corrugation, which is a periodic surface waviness that typically develops on the low rail in small-radius curves. This phenomenon arises from cyclic stick–slip oscillations, where cyclic stick–slip motion induces tangential oscillations and gradually deforms the rail surface. Over time, these oscillations result in characteristic long-pitch corrugation waves and increased vibration levels [41].

Eadie et al. [42] confirmed that proper friction management can prevent corrugation by maintaining an intermediate CoT and a positive friction characteristic. Moreover, corrugation is closely associated with acoustic emissions, as the same stick–slip instabilities that generate surface waviness also excite structural vibrations in the wheel and rail, producing squealing noise. The authors further reported that applying a friction modifier reduced squeal noise by 6–23 dB at the Metro Bilbao test site.

Although stick-slip oscillation is not the only mechanism of noise generation [65–67], other mechanisms can also be addressed through the application of TOR products. Galas et al. [49] measured a decrease in emitted noise from 97 dBA to 64–68 dBA thanks to the application of TOR lubricant, and Han et al. [7] demonstrated numerically that lowering the CoF from 0.3 to the range below 0.05 resulted in a 10–25 dB reduction in sound pressure levels. Liu et al. [50] further showed that both FMs and TOR lubricants changed the creep-curve slope from negative to positive and reduced squeal amplitude.

2.5 Wheel–Rail Interface as an Open System

The previous text explored materials that are added to the top of the rail intentionally. However, the wheel–rail interface is an open tribological system, where frictional conditions are strongly influenced by contaminants (e.g., water, leaves, oil or diesel) [68] and can change within a very short time frame, in some cases even over the passage of individual axles of a single train.

Water is arguably the most significant contaminant, as its occurrence on the rail is virtually unavoidable [69]. It may originate from rainfall, condensation of humid air, or leakage from passing vehicles, and even by itself, it acts as a strong lubricant, capable of significantly reducing adhesion [70–76]. Things get even worse when small amounts of water mix with

oxide layers and wear debris on the railhead, which typically happens in the early morning when dew is present [77]. Under such conditions, water and iron oxides form a viscous paste that can reduce CoA to values below 0.05 [17]. In the literature, this state is commonly referred to as the wet-rail phenomenon [78]. Countermeasures against low adhesion commonly involve the use of traction enhancers, typically sand, which restores adhesion by increasing surface roughness and breaking through the contaminant layer, enabling direct contact between the wheel and the rail [79–85].

Special attention must be paid to leaves. In autumn, leaves from nearby trees fall onto the track and are crushed under passing wheels, releasing organic compounds such as *tannins* [86] or *pectin* [87], that react with oxides on the rail surface [88]. This process forms a thin black layer on the railhead, commonly referred to in the literature as the *black leaf layer* [89]. Although the exact mechanism remains a subject of discussion [77], it has been observed that when this layer becomes wet, it has a significant effect on adhesion [77,89–93]. In the worst-case scenario, CoA can drop as low as 0.02 [94]. Spectroscopic analyses revealed that the black leaf layer is mainly composed of carbon and iron oxides [95]. However, experimental studies with leaf extracts [18] demonstrated that even without the black leaf layer, adhesion is still significantly reduced, as organic compounds released from leaves play a key role in the lubricating process [96]. However, their exact contribution remains to be clarified [77].

This work aims to study the interaction between TOR products and contaminants. In this context, some of them are less critical, as their occurrence can be effectively controlled. Oil or fuel leakage from passing vehicles can be largely prevented [69], and in the case of leaves, various measures are implemented in many countries. For example, trees along railway lines are often removed [97], while elsewhere the use of TOR products during autumn can be restricted. In contrast, the interaction of TOR products with water and iron oxides is inevitable. For this reason, the following literature review will provide a detailed examination of these two contaminants.

2.6 Water as a Contaminant

The most natural way for water to find its way on top of the rail is through condensation, precipitation, or from the melting of snow and ice. Over the last few decades, extensive research has investigated its influence on adhesion. Numerous studies reported that applying water to dry contact causes a decrease in CoA. Although exact values vary, most agree that water typically reduces CoA to the range of 0.2–0.3 [70–76].

The variability of reported values can be attributed not only to the type of experimental facility but also to the specific test conditions. For instance, Wang et al. [74] demonstrated that under standard conditions, water reduces CoA to approximately half of its dry value (see Fig. 7 a), but this decrease becomes even more significant at higher rolling speeds [75]. Another study highlighted the role of environmental temperature: while the CoA values themselves were similar across environments with different air temperatures, water retentivity was prolonged

at lower temperatures, most likely due to slower evaporation [98]. These observations clearly demonstrate that many parameters have an impact on the behaviour of water, underlining the need to examine its effect on adhesion under various operating scenarios. Many studies have focused on situations where a large amount of water is present (e.g., during rain), allowing for the formation of a thick lubricating film, and have attempted to explain its effect on adhesion based on elastohydrodynamic lubrication theory and its modifications [99–103].

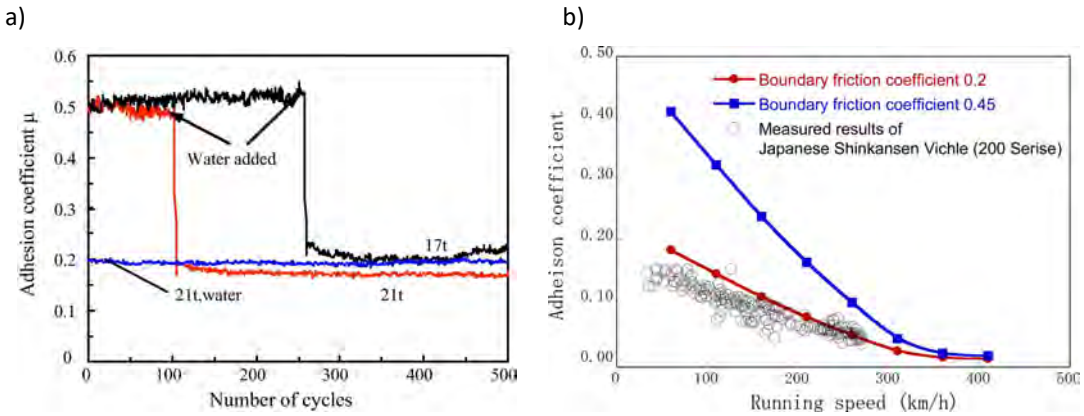

Fig. 7 a) Change in CoA after water application for different axle loads [74], and b) comparison of predicted and measured CoA for a Shinkansen train on wet rails [104].

Chen et al. [105] demonstrated that CoA is strongly dependent on water temperature and the height of the surface asperities. For cold water, CoA exhibits significantly lower values than for hot water, as depicted in Fig. 8 a). Regarding surface roughness, a higher CoA was calculated for surfaces with a higher height of surface asperities than for smooth surfaces, see Fig. 8 b) [103]. This finding suggests that a transition from boundary/mixed to fluid film lubrication may occur, which is also supported by the fact that the most significant effect was the vehicles' speed, as an increase in rolling speed resulted in a dramatic decrease in CoA.

In the follow-up study [106], they focused on this idea and analysed water film thickness as a function of rolling speed and temperature, showing that film thickness increased with higher rolling speed but decreased with higher temperature, as can be seen from Fig. 8 c). The observed evolution of film thickness is further supported by the study of Wang et al. [100], which shows that changes in fluid viscosity notably influence adhesion. As colder water has higher viscosity than warm water, it can form a thicker lubricating film, confirming earlier conclusions [106].

Later, the initial models were refined to simulate the mixed lubrication regime, which is more closely aligned with the actual conditions in wheel-rail contact. To achieve this, the authors employed ultrasonic methods to measure the real contact area directly and conducted twin-disc experiments to obtain the actual CoA data as input. The model confirmed the previous conclusions and validated them against full-scale data measured on the Shinkansen (Series 200), showing excellent agreement, see Fig. 7 b) [104].

Other authors focused closely on the role of surface roughness. Zhu et al. [107], who conducted experiments on both smooth and rough specimens, confirmed lower adhesion under wet

conditions for smooth specimens, experimentally confirming conclusions obtained by Chen et al. [103] through numerical simulation. Wu et al. [108] added that not only the height of asperities but also their orientation plays an important role. Additionally, the study [109] examined the effect of surface roughness with different axle loads (and thus contact pressures). For smooth surfaces below a certain roughness threshold, an increase in axle load enables the formation of a continuous water film, resulting in low adhesion. However, in the case of a rough surface, a high axle load enhances asperity contact and prevents water from forming a uniform lubricating film, resulting in increased adhesion.

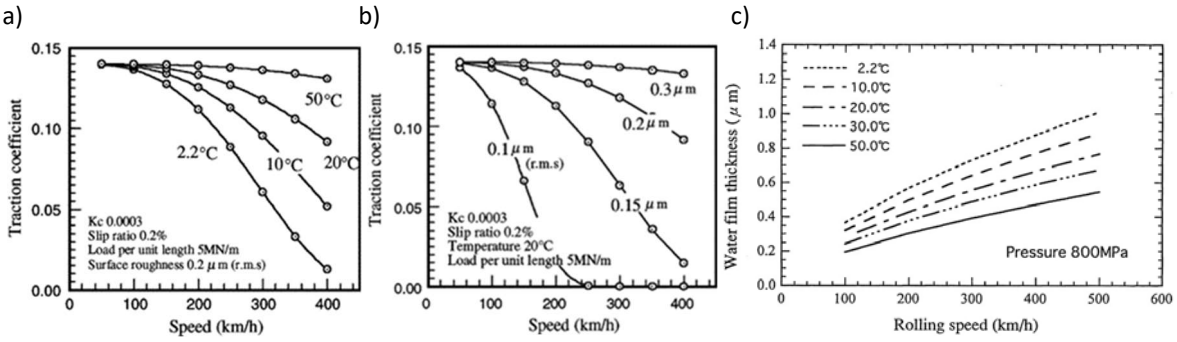

Fig. 8 a) CoT under water-lubricated conditions as a function of water temperature, b) surface roughness [103] and c) the resulting film thickness at different temperatures [106].

To prevent low-adhesion problems, modern locomotives are often equipped with on-board monitoring systems that run predictive models based on creep curves [99]. Thus, several studies [110–114] examined how water influences adhesion under different creepages, and it was found that in wet contacts, either neutral or slightly negative friction characteristics can be expected.

2.7 Moisture and Iron Oxides

Studies discussed in the previous text have shown that water reduces CoA, but none of them recreated the low adhesion problems. A paper by Buckley-Johnstone et al. [115] provided an explanation based on the amounts of water. The author conducted tests on a full-scale twin-disc machine. For higher amounts, CoA remained between 0.2 and 0.3, which is in accordance with [70–76]. However, after reducing the water amount, CoA dropped as low as 0.05. Boster et al. [116] explained that the effect of water on adhesion varies depending on its amount, as follows: during heavy rain, particles and contaminants are washed from the rail surface, which may lead to improved adhesion. However, in small amounts, the effect will be quite the opposite. On a clean surface, water acts as an additional boundary lubricant, reducing adhesion. If wear debris or oxide products were present, they would form a thick paste that would lubricate the rail surface even better. Experimental evidence can be seen in Fig. 9 a).

The two most common scenarios in which small amounts of water appear on the railhead are either due to the gradual evaporation of larger amounts (e.g. after rainfall, as the rail dries)

or through condensation from humid air. In the first case, as the water film thins during evaporation, the ratio between water and particles shifts in favour of the particles, and the viscosity of the mixture grows exponentially [117], resulting in the formation of a highly viscous paste that can cause very low adhesion [118]. The schematic of this process can be seen in Fig. 9 b). This phenomenon has been recognised for some time [116], but its understanding remains limited, as it is difficult to observe directly in the field.

The main challenge lies in the fact that it occurs over a very short time frame and only under specific conditions. Laboratory studies [17,18,33] and numerical models [119] have attempted to describe this transient behaviour of water just before complete evaporation. These studies showed that while sufficient quantities of water are present, the CoA remains at values comparable to those [70–76] observed under flooded conditions. As drying progresses, adhesion stays relatively stable until a critical point is reached, after which the CoA rapidly returns to dry-contact levels, often accompanied by increased noise [18]. However, just before complete drying, a short transitional phase occurs in which a critically small amount of water remains in the contact. During this phase, the CoA temporarily drops to values much lower than those under fully flooded conditions.

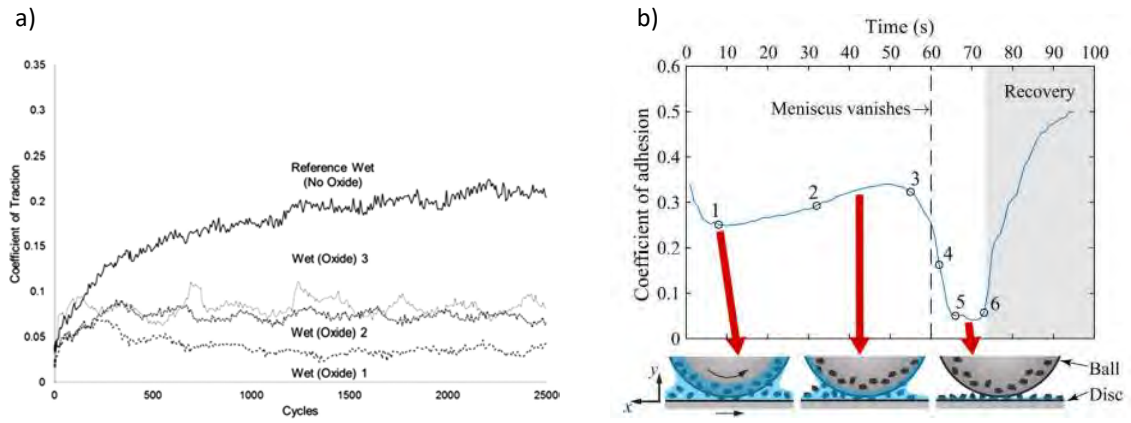

Fig. 9 a) Comparison of CoT for water and oxide mixtures [120], and b) the schematic of the transient behaviour of water during evaporation [119].

Incidents related to low adhesion are most often reported in the morning [77], and a large number of them can be directly linked to humidity [121]. One illustrative example is the 2002 derailment on the Tokyo Metro line in Japan, where changes in friction due to ambient temperature and humidity were identified as a contributing factor [122]. Several studies have highlighted that an increase in *relative humidity* (*RH*) of air, especially above 75%, leads to a decrease in CoA [123–129]. The situation becomes even more critical when the *dew point* is reached [18], which means that the air can no longer retain additional water vapour, and excess moisture begins to condense on the rail surface. This process depends strongly on ambient temperature, which determines how much water vapour the air can hold before condensation occurs. As the temperature drops, especially at night, the capacity of air to retain moisture decreases, leading to the formation of morning dew. Studies have concluded that,

although the effect is more significant at lower temperatures [127], low adhesion problems may occur even at ambient temperatures above 20 °C and higher [125,126].

Beagley described the mechanism by which oxide products lead to low adhesion as follows: while oxides are sufficiently strong to support wheel loads, their low shear strength limits the transmission of tangential forces and thereby reduces adhesion [117]. In another study, the same author tested a mixture of hematite powder and water, achieving extremely low adhesion levels [130]. White et al. [17] further examined the behaviour of hematite in comparison with magnetite and concluded that hematite suspension in water is considerably more prone to induce low adhesion conditions. In his tests, the lowest measured CoA dropped to 0.02. In a later study [78], the same authors successfully replicated the wet-rail phenomenon under laboratory conditions by using powders of different oxides, achieving very low adhesion during transient periods between wet and dry states.

In addition to testing oxides in powder form, attempts were made to create oxide layers in laboratory conditions in a more natural way. Sone et al. [131] proposed a procedure for generating oxides in a climatic chamber using vapours of oxidation-promoting agents. Suzumura subsequently demonstrated that oxides produced under such conditions behave similarly to those formed on actual rails [132]. Zhu et al. [133–136] adopted the procedure proposed by Sone et al. [131] and carried out extensive research on the effect of iron oxides and humidity on friction. The pin-on-disc tests demonstrated that *in situ* formation of iron oxides under severe mechanical conditions had a greater impact on friction than pre-applied oxide films. The CoF decreased with increasing RH until a saturation level was reached, where a boundary layer of adsorbed water molecules stabilised the contact. Beyond this point, additional humidity promoted the retention of hematite on the surface, slightly increasing friction and counteracting the lubricating effect of the water film. As a result, the CoF remained low and stable. The visual appearance of oxide layers prepared in laboratory conditions can be seen in Fig. 10 a–c).

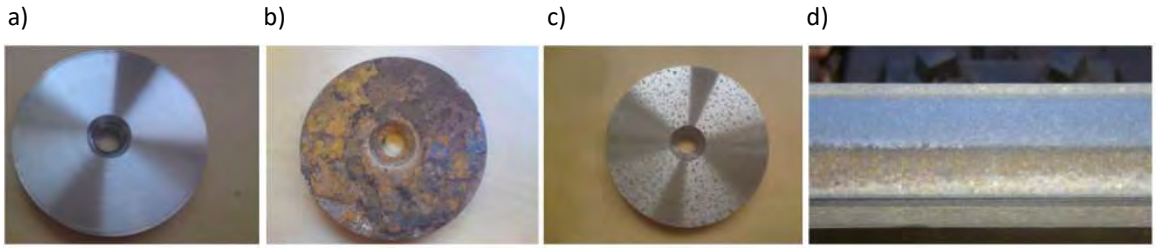

Fig. 10 The visual appearance of specimens after oxidation treatment: a) untreated, b) thick rust layers, c) typical light surface oxidation observed on railhead, and d) comparison with an actual oxidised rail segment – modified [133].

Oxidation of rail surfaces is a chemical reaction in which iron at the surface combines with oxygen from the air to form iron oxides. As the process progresses, the metallic surface gradually transforms into a layer of corrosion products. Several external factors influence the rate and nature of oxidation. Quinn et al. [137,138] noted that oxidation strongly depends on contact conditions such as temperature, load, and sliding speed, while Dillmann et al. [139] emphasised the critical role of ambient humidity and moisture. Hardwick et al. [120] further

demonstrated that the presence of salt in the environment (such as from winter road de-icing) accelerates oxide growth.

Several studies have attempted to associate specific types of iron oxides with particular environments (such as industrial, rural, or coastal areas) based on the typical conditions prevailing in those settings [140,141]. Godfrey et al. [142] compiled a comprehensive list of the most common iron oxides and their hydrated forms (*rusts*), along with their mechanical and tribological properties. In addition, Kempka et al. [143] explicitly focused on the wheel–rail contact, analysing the oxide layers formed on the rail surface using X-ray diffraction (XRD). The analyses revealed that the oxide layers consisted mainly of hematite, magnetite, goethite, and akaganeite.

2.8 Contamination of TOR Products

The previous section reviewed numerous studies that examined either TOR products or contamination individually. However, only a few investigations have addressed these factors simultaneously. Moreover, those that did often tested materials that would no longer meet the current definition of TOR products, as they have been designed for a different purpose than friction modification.

One of the earliest studies was conducted by Olofsson et al. [124], who utilised a laboratory pin-on-disc tribometer to investigate the effects of humidity, leaf contamination, and oil-based rail lubricant on friction. It is important to note that the used lubricant (Binol Rail 510A) does not meet the definition of TOR lubricant, as it is used to minimise friction regardless of traction/adhesion. Nevertheless, oil is the main component of TOR lubricants, so that any conclusion can be, to a limited extent, also applied to TOR lubricants.

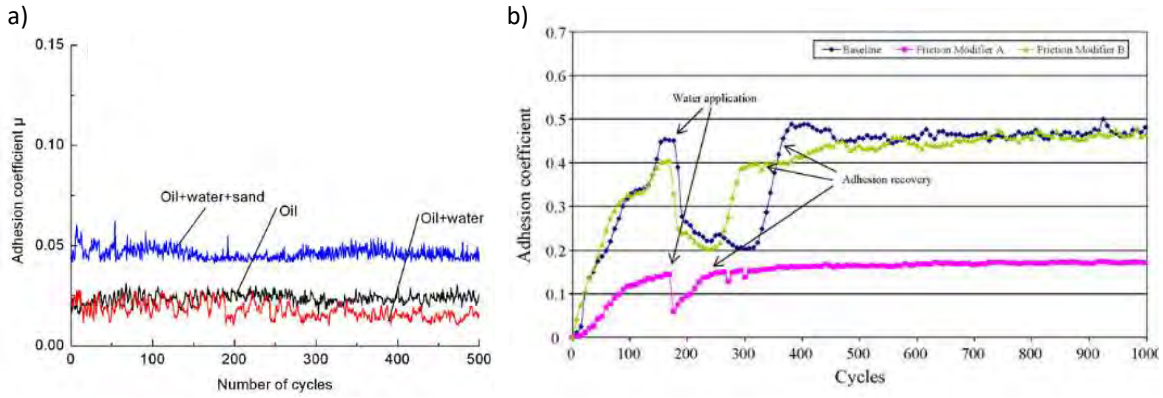

Fig. 11 a) Comparison of the lubricating effect of water, oil and their mixture [19], and b) performance of FMs in wet conditions [15].

Under clean conditions, the CoF of the lubricant ranged between 0.05 and 0.1. The addition of dry chopped leaves did not further reduce friction, indicating that the dry organic layer interfered with the lubricant film. When tested alone, dry leaves produced intermediate

friction levels (CoT = 0.3), which would not cause adhesion problems. Therefore, the combined presence of lubricant and dry leaf contamination did not lead to the extremely low friction typical of oil-lubricated contacts. Humidity slightly reduced friction under dry conditions, but its effect became negligible in the presence of both lubricant and leaf contamination.

Another study on an oil-based rail lubricant was conducted by Wang et al. [19], but in this case, the contaminant was water. The authors used a full-scale JD-1 simulation facility and tested sequentially three conditions: water, lubricant, and their mixture, under two different axle loads (21 t and 25 t). For the 21 t load, the CoT decreased from 0.17 under water to 0.025 under oil, and to only 0.018 when oil and water were combined. A similar trend was observed at 25 t, where the adhesion values were 0.18, 0.035, and 0.03, respectively. These results indicate that the mixture of oil and water produces an even lower CoT than either component alone, as can be seen in Fig. 11 a).

Arias-Cuevas and Li conducted two follow-up studies in which they tested the effect of water [15] and leaf [47] contamination on two commercial "friction modifiers". Both products were widely used on railways in Japan, the Netherlands, and Great Britain, primarily to restore adhesion under wet conditions rather than to optimise friction on dry track. This purpose was also reflected in their composition, as they contained stainless steel particles, which are not typically found in FMs. Furthermore, particles in the first product (labelled FMa) were up to 100 μm, and the second (labelled FMb) contained even larger particles in the range of hundreds of microns. Therefore, according to the current definition, these products would be considered traction enhancers rather than FMs [32].

Under wet conditions, FMb provided an intermediate level of friction, as the CoT did not drop below 0.2. In contrast, in the case of FMa, the CoT decreased to as low as 0.07 and, even after several hundred cycles, did not recover to 0.2, see Fig. 11 b). The size of the contained particles most likely caused the difference in performance between these two products, since FMb included much larger particles than FMa. However, this also led to surface damage and visible scratches, whereas in the tests with FMa, no significant damage was observed [15]. The same products were also tested under leaf contamination, with the authors focusing on their ability to restore adhesion. Once again, the product containing larger particles proved more effective, reducing the recovery period by up to 93%, though at the cost of surface indentations and scratches. The authors concluded that the size and hardness of the particles are key parameters, and that achieving an optimal balance between adhesion restoration and surface damage is crucial for product design [47].

Oldknow et al. [70] analysed how precipitation and FMs influence the lateral and vertical forces on a 300 m curve of a heavy-haul line. Four cases were compared: dry rail, rain without FM, FM under dry conditions, and FM under rain. Regarding the influence of water on FM, the results showed that when the rail was wet, and FM was applied, water interfered with the material transfer, delaying film formation and causing slightly higher L/V ratios (0.3–0.4) during the initial phase. Once the rail surface dried, the FM film re-formed, reducing the L/V ratio to approximately 0.2, which is comparable to FM performance under dry conditions. These findings indicate that the presence of water may temporarily suppress the effectiveness of FMs until the moisture evaporates.

Chen et al. [44] evaluated various lubricants under both dry and wet rail conditions to analyse their effect on adhesion, lateral forces and braking performance. The tested products included oil, grease, a water-soluble lubricant, and a solid lubricant, together with improved formulations. The oil and grease were primarily intended for flange lubrication to reduce wear at the wheel flange and gauge corner. In contrast, the solid and water-soluble lubricants (basically an FM) were developed for TOR applications.

Under dry conditions, products effectively reduced lateral forces, with the most substantial reduction observed for the solid lubricants. However, when water was present on the rail surface, the behaviour of the lubricants diverged. Oil and grease mixed with the moisture, forming an extended lubricating film that further reduced adhesion and led to longer braking distances. In contrast, the water-soluble lubricants and solid lubricants maintained more stable friction and shorter braking distances even on wet rails. Quantitatively, water-soluble lubricants produced similar lateral force reduction to the solid lubricants, but without the severe loss of adhesion seen for oil and grease. Thus, the study demonstrated that while oil and grease become risky under wet conditions, solid and water-soluble formulations maintain controlled friction and consistent braking performance, making them more suitable for safe TOR lubrication in humid environments.

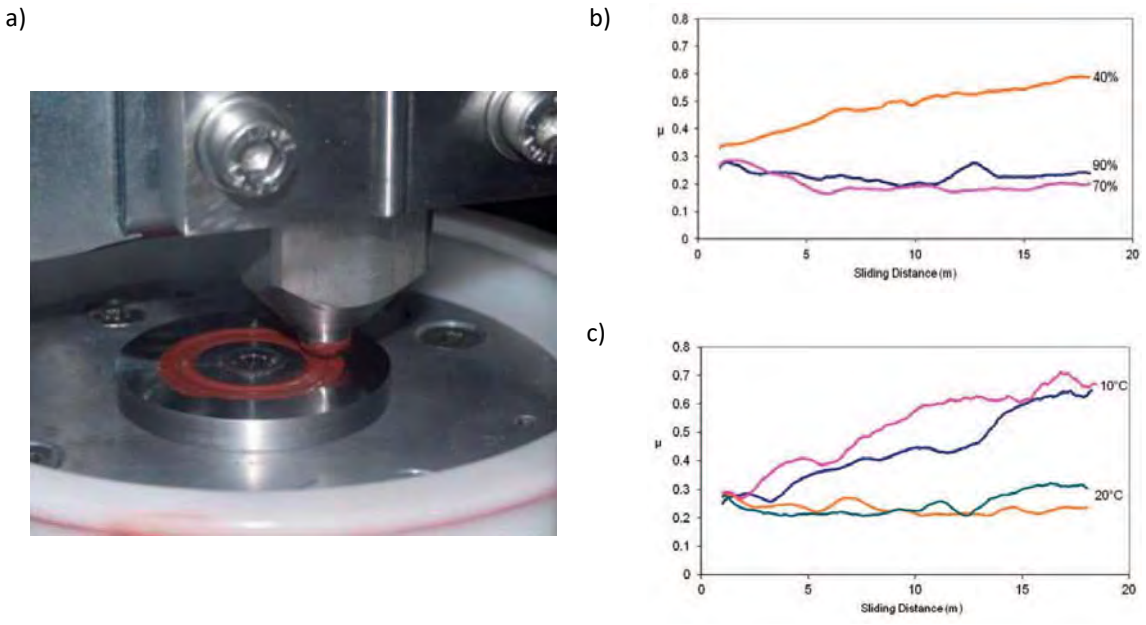

Fig. 12 a) Testing setup, b) effect of RH and c) effect of ambient temperature on CoF of FM–Fe_2O_3 mixture [123].

Using a custom-built pin-on-disc rheometer and Amsler twin-disc tester, Lu et al. [27] conducted a laboratory study to examine the effect of iron oxides (specifically Fe_2O_3 particles) and grease on performance FM. The iron oxide contamination had a strong structural and mechanical influence on the FM film. At high concentrations (75–90%), the shear stress–displacement curves exhibited a pronounced initial peak, attributed to the aggregation of oxide particles within the polymeric matrix, and CoT ranged between 0.3 and 0.35. Grease contamination, on the other hand, had a more substantial effect. When FM was applied

to a grease-contaminated surface, the lower surface tension of the oil compared to water and steel led to poor wetting, incomplete film adhesion, and crater formation. As a result, the shear strength of the FM–grease composite decreased from around 60 MPa (clean FM) to 40–47 MPa, and CoT decreased to 0.15-0.25. However, even under light grease contamination, the mixture still exhibits a positive friction characteristic, suggesting that FM could still maintain some level of traction control. Overall, the study highlighted that while iron oxide contamination only moderately affects FM performance, grease contamination substantially reduces film integrity and CoT.

Lewis et al. [123] used a pin-on-disc tribometer equipped with an environmental chamber to investigate how environmental conditions and iron oxides influence the performance of a commercial FM, see Fig. 12 a). Tests were carried out at 10 °C and 20 °C, relative humidity between 40 and 90 %, and oxide concentrations ranging from 25 to 45 %. Two types of oxide were studied: Fe_2O_3 and Fe_3O_4. The results showed that at high humidity (above 70 % RH), the CoF remained between 0.2 and 0.25 for the entire sliding distance, because the film retained moisture and did not dry out. In contrast, at 40 % RH, the FM dried after only a few meters of sliding, and CoF returned to dry contact values above around 0.6, see Fig. 12 b). Mixing iron oxides with the FM decreased its lubricating effect, with Fe_3O_4 having the stronger influence than Fe_2O_3 due to its larger particle size.

Subsequent tests examined the influence of oxide concentration and temperature. At 10 °C, friction rose rapidly for mixtures with 25% oxide but remained low for 45%, indicating that higher solid content improves film stability and moisture retention. At 20 °C, friction remained low regardless of oxide content, suggesting that higher temperatures delayed drying, as can be seen in Fig. 12 c). This is because, at the same relative humidity, warmer air contains more water vapour, which reduces the vapour pressure gradient and slows evaporation from the FM film. A humidity transition zone was identified between 40 and 45% RH, below which the film dried and friction increased, and above which the film remained wet, and friction stayed low. These findings highlight that both environmental moisture and oxide content critically affect film persistence and the frictional behaviour of railhead friction modifiers.

3. Analysis and Conclusions

Frictional phenomena in the wheel–rail interface have been studied for several decades. During this time, numerous studies have examined the effects of water [70–76], iron oxides [133–136], and leaves [86–88,95] on adhesion. Considerable attention has also been given to TOR products, where their effectiveness has been demonstrated in reducing wear [54,63,144] and noise [8,42,49,145]. In practice, friction modification and contamination cannot be entirely separated, as TOR products are always applied to a more or less contaminated contact. Despite this, only a few studies have addressed these issues simultaneously, which can be demonstrated by the results of a literature search performed in the *Web of Science* database (*valid as of 19 October 2025*):

- *Search query*: (wheel or rail) and (adhesion or friction or traction) and (water or humidity or dew or iron oxides or rusts or leaf) returns *727 publications*.
- *Search query*: (wheel or rail) and (adhesion or friction or traction) and (friction modifier or TOR product or TOR lubricant) returned *209 publications*,
- However, the *combined query*: (wheel or rail) and (adhesion or friction or traction) and (friction modifier or TOR lubricant or TOR product) and (water or humidity or dew or iron oxides or rusts or leaf) and contamination returned only *19 publications*.

Furthermore, several of these 19 publications do not entirely fit within the intended scope. For example, the study by Arias-Cuevas et al. [92] claims to use a friction modifier, which in fact refers to sand, and the work focuses on enhancing traction rather than friction management. After filtering these publications and adding several additional papers from the *Scopus* database, only eight studies were found to be relevant. These were discussed in the previous section, and the following summary outlines the most important findings of the literature review:

I. The ability of TOR products to maintain a positive friction characteristic [31] and to establish an intermediate level of friction typically between 0.2 and 0.4 [32,39] was well-proven.

II. In specific cases (such as overdosing), TOR products may cause low adhesion problems, like wheel slips [14] or extended braking distance [49].

III. TOR lubricants contain hard particles that balance the lubricating effect of the base oil or grease [58]. Any imbalance between the liquid and solid phases may cause undesired effects, such as over-lubrication when shifted toward the liquid content, or increased wear [59] when the composition of solid particles is non-optimal [57].

IV. FMs are generally effective in reducing wear [54,146] and usually do not have any adverse effects on RCF as their base medium evaporates [62]. In contrast, TOR

lubricants may enhance propagation of pre-existing cracks, as the base oil penetrates cracks and causes hydropressurisation [63,64].

V. In addition, Seo et al. [53] demonstrated that the TOR hybrid containing both water and oil negatively affected RCF. This was attributed to alternating dry and wet conditions, as the water component evaporated while the oil remained in the contact, combining the adverse effects of high CoT from dry contact with liquid-assisted crack propagation caused by the residual oil film.

VI. Contaminants related to low adhesion problems are water [70–76], oxide products [17] and leaves [77]. Regarding the contamination of TOR products, studying the effects of water, oxides, and their combination is crucial. The interaction between TOR products and leaves can be potentially prevented [97].

VII. Regarding laboratory testing, applying larger amounts of water reduces the CoA by half [19] but does not cause low-adhesion problems. Such issues occur only when small amounts of water are present [116]. Two approaches can be used in experiments: allowing the water to gradually evaporate until only a small amount remains [115] or water condensation from air at higher RH levels [18].

VIII. A study by Lewis et al. [123] thoroughly described the effect of high ambient RH on FMs. However, the impact on TOR lubricants remains unknown. While humidity was found to have rather a negligible effect, the situation is quite different when the dew point is reached, and condensation occurs [18].

IX. A mixture of oil and water results in a lower CoT compared to either component alone [19]. Furthermore, field tests showed that the use of oil/grease-based products on wet rail may result in prolonged braking distance [44]. But it is important to note that tested lubricants did not contain particles such as those used in TOR lubricants.

X. Contamination of FM with water may, in some cases, lead to a low CoT [15]. However, things are not entirely clear. Some studies have reported an enhanced lubricating effect caused by the slower evaporation of the base medium in wet or humid environments [123]. In contrast, others have shown that the presence of water can worsen film formation and produce the opposite effect [70]. In addition, field measurements showed that the use of FMs on wet rail should not cause low adhesion problems [44].

XI. Two approaches can be used to introduce oxides in laboratory testing: either by pre-forming an oxide layer in a climate chamber under oxidation-promoting conditions [131] or by directly adding oxides in powdered form [78]. Those most commonly found on rail surfaces and tested under laboratory conditions include hematite, magnetite, goethite, and lepidocrocite [143].

XII. Iron oxides were found to influence film formation of FMs [123]. Adding them in a powdered form to the FMs composition would have a rather increasing effect on adhesion [27].

XIII. Apart from the factors discussed above, the reported friction levels are also strongly affected by the experimental methodology itself. The measurements can be carried out

using a wide range of approaches, from hand-pushed tribometers [14,147] in the field to full-scale test rigs [91,115,148], scaled twin-disc machines [61,114,136,149], and small-scale laboratory tribometers in ball-on-disc [18,33,57] or pin-on-disc configurations [124,133,135]. Although there are clear requirements for TOR products, no universally accepted methodology exists for evaluating their performance. In practice, a variety of procedures and setups are used, which often yield different results even under seemingly identical conditions. For instance, Lundberg et al. [14] demonstrated that when the CoT was measured on the same rail section using two different methods, the first method produced values roughly twice as high as the second.

3.1 Research Gap

Many studies have explored the effect of TOR products on frictional phenomena in the wheel-rail interface, and even more have examined various types of contamination. However, Fig. 13 shows that less than 1% of them have investigated both aspects together, even though their interaction is inevitable under real operating conditions.

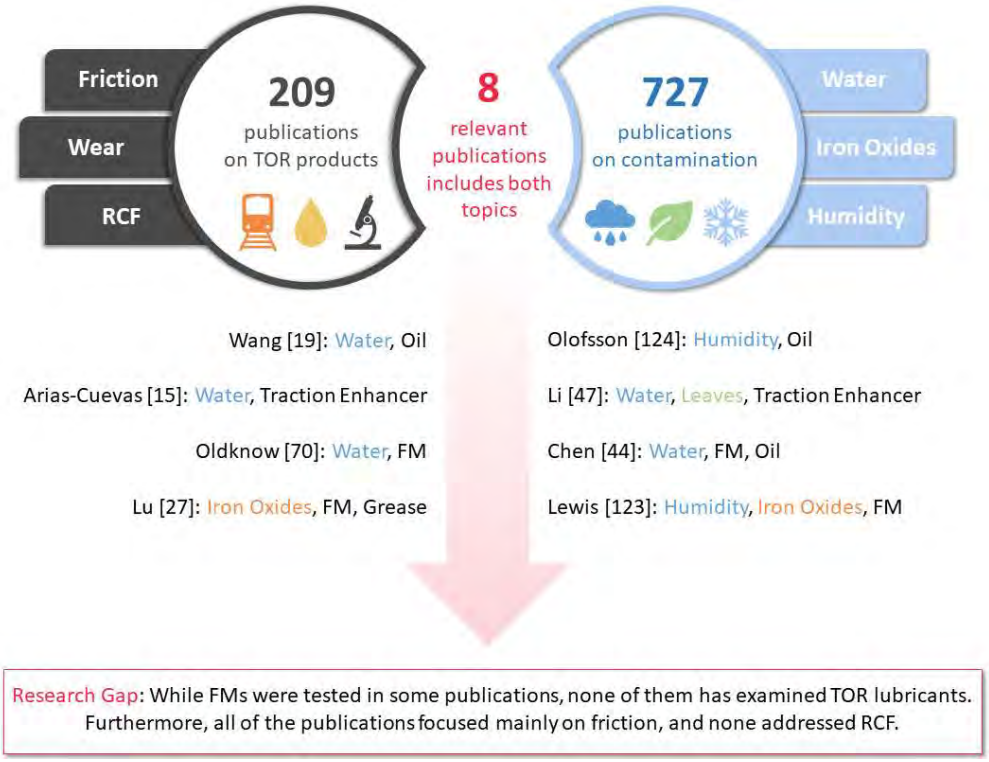

Fig. 13 Overview of publications on TOR products and contamination, highlighting the limited overlap between the two research areas.

During the literature review, eight publications were identified as particularly relevant and were examined in detail in Section 2.8. Although some of these studies included FMs, none of them examined TOR lubricants, as the products tested, for example, by Wang et al. [19] or Olofsson et al. [124], were simple oils not suitable for top-of-rail application. Furthermore, all of these studies focused mainly on friction (or traction and adhesion), and none investigated RCF, leaving the effect of TOR products on RCF in contaminated conditions entirely unknown.

The most commonly tested contaminants are moisture (in the form of humidity, dew or direct application of water) and iron oxides. Testing these conditions appears most reasonable, as they were identified as common causes of low-adhesion problems. Li et al. [47] also addressed leaf contamination. However, they used traction enhancers rather than TOR products, which are not designed to remove or disrupt leaf layers anyway. Overall, no study has systematically assessed TOR lubricants under moisture, water or iron oxide contamination, nor has any examined the effect of TOR products on RCF under contaminated conditions.

3.2 Scientific Questions and Hypotheses

Based on the identified research gap, three scientific questions were formulated. Corresponding hypotheses were proposed based on the conclusions I–XIII drawn from literature reviews:

Q1: *How does water contamination influence the ability of TOR products to modify friction?*

- H1.1: Under wet conditions, TOR lubricants are expected to cause over-lubrication because the presence of water disrupts the balance between the liquid and solid phases, shifting it in favour of a stronger lubricating effect. Since water–oil mixtures are known to produce very low friction, and oil is the main component of TOR lubricants, a similarly low-friction response is likely for TOR lubricants in wet conditions. (II, III, IX)
- H1.2: For friction modifiers, the effect of water contamination is expected to depend on the amount of water. Small amounts of water may enhance lubrication by slowing evaporation of the base medium. In contrast, larger quantities are likely to disrupt film formation and result in higher and less stable friction. (II, VIII, X)

Q2: *How does the performance of TOR lubricants change with increasing ambient humidity and under dew conditions?*

- H2: Ambient humidity alone is expected to have only a minor effect on friction and, therefore, is unlikely to influence the performance of TOR lubricants significantly. A substantial change is expected when the dew point is reached and water condenses on the rail surface. In this case, the condensed water can mix with TOR lubricants and cause over-lubrication. (II, III, VII, VIII, IX)

Q3: *How do TOR products affect wear and rolling contact fatigue in the presence of oxide layers under wet conditions?*

- H3.1: In wet conditions, TOR lubricants are expected to influence RCF in a way similar to TOR hybrids. The only difference is that water is intentionally added in the latter, whereas in the former, it enters the contact as an unwanted contaminant. This combination is expected to promote severe RCF due to the coexistence of high friction and liquid-assisted crack propagation. (V)
- H3.2: When mixed with friction modifiers, oxides are expected to disrupt film formation, reducing the effectiveness of the product and increasing wear. In contrast, the presence of water may partially counteract this effect by helping to rebalance the liquid–solid ratio and by slowing the evaporation of the base medium, thereby prolonging the lubricating effect. (X, XII)

4. Aims of the Thesis

This thesis aims to explore the effect of environmental contamination on the performance of TOR products. Based on the scientific questions Q1–Q3, three key research areas have been identified. This thesis aims to investigate:

a. The effect of larger quantities of water on both FMs and TOR lubricants, simulating wet rail conditions and precipitation,
b. The impact of small amounts of water in environments with high relative humidity and temperature gradients,
c. The combined effect of water and iron oxides on the ability of TOR products to reduce wear and RCF.

However, the literature review also revealed that different authors use diverse experimental approaches, testing devices, and measured parameters. Moreover, the commonly used CoT/CoA time-dependence tests, known as "time tests", are useful for studying transient phenomena but are not suitable for a comprehensive evaluation of TOR product performance. Therefore, an additional objective was formulated:

d. The development of a benchmarking methodology for assessing the performance of TOR products, specifically their ability to provide intermediate friction levels and a positive friction characteristic. The methodology will be designed for use on a commercial tribometer to ensure consistent repeatability and reproducibility across different laboratories.

5. Thesis Layout

The core of the thesis consists of four publications [150–153], each focusing on one of the objectives (a–d). The first two publications were carried out in parallel. Article I [150] deals with objective (a) and investigates the direct effect of water contamination on TOR products using time tests. During this work, it became clear that time tests are helpful in studying the immediate response of TOR products to contamination, but are not suitable for broader performance evaluation. This finding led to the development of a new benchmarking methodology based on creep curves rather than time tests. The methodology is described in Article II [151], which addresses objective (d). To be transparent, this objective was added later, as the need for a dedicated methodology emerged naturally during the work on the first publication.

The newly developed approach was then applied in Article III [152], which explores the effects of ambient humidity and temperature, corresponding to objective (b). To pursue the final objective (c), which required advanced facilities for RCF analysis, an internship at Southwest Jiaotong University in China was specifically arranged. This institution, with its long tradition and extensive experience in twin-disc RCF testing, offered the ideal environment to conduct the experiments and complete this part of this thesis. The result of this internship was published in Article IV [153].

During the final experiments, an unexpected phenomenon was observed: oxidation of the crack faces initiated crack propagation. This observation inspired a separate line of research. The results were presented at the *Contact Mechanics 2025* conference in Tokyo, and a shortened version was published in the conference proceedings. The full paper will be submitted to the *Wear* special issue by 30 April 2026. Although this study was not part of the original objectives (a–d), it emerged as a direct outcome of the PhD research and is closely related to the main thesis topic. The finding that oxidation seals cracks and prevents liquid ingress has direct implications for the behaviour of TOR products on oxidised surfaces, as it explains why liquid-assisted crack propagation was suppressed in the presence of an oxide layer (Article IV). For this reason, the study is included and discussed in this thesis as Article V.

Article I

[150] **Skurka S**, Galas R, Omasta M, Wu B, Ding H, et al.
The performance of top-of-rail products under water contamination.
Tribology International 2023; 188.

Author's contribution	40%
Journal impact factor (2023)	6.1
JIF/AIS Quartile	Q1/Q1
Citations (WoS/Scopus/Google Scholar)	7/9/9

Article II

[151] Galas R, **Skurka S**, Valena M, Kvarda D, Omasta M, et al. A benchmarking methodology for top-of-rail products. Tribology International 2023; 189.

Author's contribution	28%
Journal impact factor (2023)	6.1
JIF/AIS Quartile	Q1/Q1
Citations (WoS/Scopus/Google Scholar)	4/6/6

Article III

[152] **Skurka S**, Galas R, Omasta M, Ding H, Wang W, et al. Assessing the Performance of TOR Lubricants in Humid Environments and Under Dew Conditions. Tribology Letters 2024 72.

Author's contribution	50%
Journal impact factor (2024)	3.3
JIF/AIS Quartile	Q2/Q2
Citations (WoS/Scopus/Google Scholar)	1/1/1

Article IV

[153] **Skurka S**, Galas R, Li J, Wang H, Omasta M, Ding H, et al. Performance of top-of-rail products under contaminated conditions with pre-existing cracks: Impacts on traction and surface damage, Wear 588 (2026) 206520.

Author's contribution	50%
Journal impact factor (2025)	6.1
JIF/AIS Quartile	Q1/Q1
Citations (WoS/Scopus/Google Scholar)	0/0/0

Article V

CM 2025

Wear special issue (will be submitted before 30 April)

Skurka S, Li M, Wang H, Galas R, Omasta M, Ding H, et al. Inside RCF Crack: Oxidation as a Factor in Rail Damage.

Author's contribution	50%
Journal impact factor (2026)	
JIF/AIS Quartile	
Citations (WoS/Scopus/Google Scholar)	

6. Materials and Methods

This chapter provides a general overview of the experimental procedures and methods used throughout the PhD research. Experiments can be classified into two groups based on the type of tests: friction tests (addressing Q1 and Q2) and wear and RCF tests (Q3). According to the thesis layout, friction tests were used in Articles I–III (and, to a limited extent, also in Article IV). Wear and RCF tests were the main focus of Articles IV and V. A summary of the experimental design and workflow is provided in Fig. 14. In this chapter, the material that is common to several articles, like the specification of the TOR products or the description of the testing apparatus, is presented first. The methodology for each article is then described separately.

6.1 Tested TOR Products

All tested materials were commercial TOR products that are routinely used in railway operations. Because no formal agreement with the manufacturers was in place, the specific product names are not disclosed. Only the details necessary for the experimental work and for interpreting the results are reported. Three products were selected to cover both drying and non-drying formulations: one friction modifier (*FM-A*) and two TOR lubricants (*TORL-A* and *TORL-B*). The same products, FM-A and TORL-B, have also been used in several previous studies by other authors, which supports their relevance and representativeness.

Tab. 1 Characteristics of selected TOR lubricants.

Product	Structure	NLGI grade	Base oil	Thickener	Particles	Base oil viscosity at 40 °C (mm^2/s)
TORL-A	Paste	0	Biodegradable ester	Organic	Soft metal	41–53
TORL-B	Gel paste	00	Synthetic ester	Inorganic (silicate)		46

Product TORL-A was included as a reference to TORL-B because the two products differ in composition and several key parameters. The reason for selecting two TOR lubricants was that these materials are sensitive to over-lubrication, which is strongly affected by their formulation. As a result, the impact of contamination may vary between products with different compositions. The main difference between the two TOR lubricants is summarised in Tab. 1.

Experimental Workflow Diagram

Time tests (a) were used in Article I

1

- Water was applied to the TOR product at different time points (b)
- The lowest CoT and duration of the low adhesion period were evaluated
- Both single/continuous water applications were tested
- Two different TOR lubricants and one FM in wet and dry states

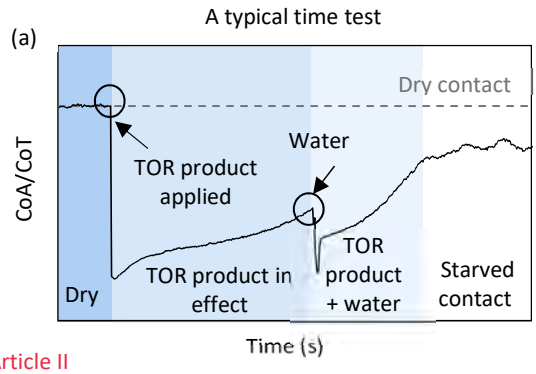

A new benchmarking methodology was developed in Article II

2

- Based on repeated creep curve measurement
- Sliding distances in low and intermediate traction zones are used to evaluate the performance parameters OLF, I and the performance class of the TOR product

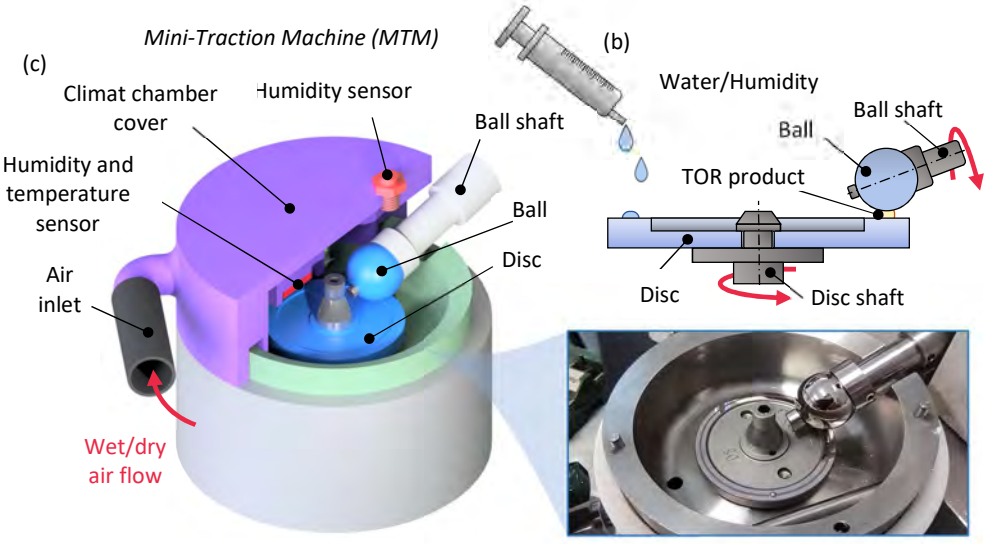

In Article III, the benchmarking methodology was used to test TOR lubricants in a humid environment

3

- MTM was equipped with a climate chamber (c) that enabled RH control in the 0–100% range
- Normal, humid and dew conditions were tested under a temperature gradient
- Effect of RH was evaluated based on changes in OLF, I and the performance class

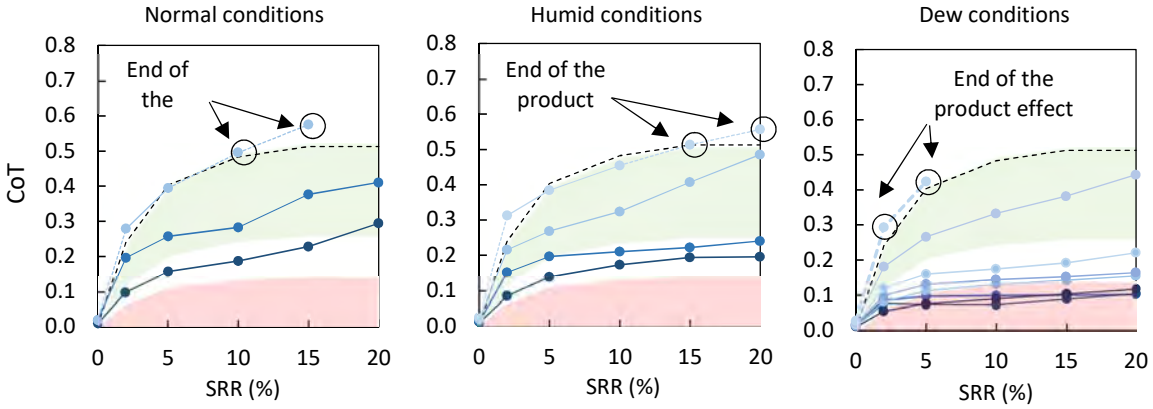

An increase in RH typically results in a higher number of creep curves and a lower CoT

4

In Article IV:

- A twin-disc machine MJP-30A (d) was used
- Specimens cut from an actual wheel/rail
- One TOR lubricant and one FM
- Contaminants: water, oxides
- Specimens with and without pre-existing surface damage
- Evaluated parameters: crack length and depth, wear rate, mass loss

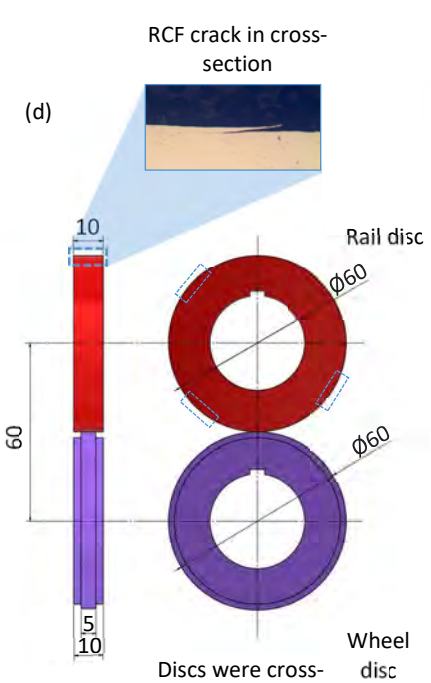

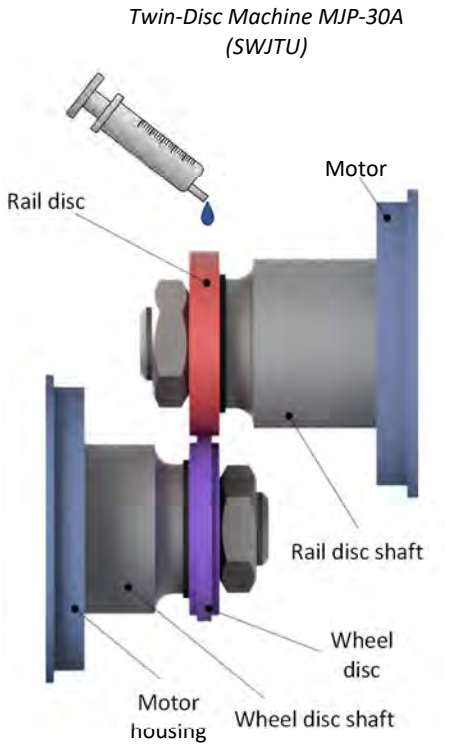

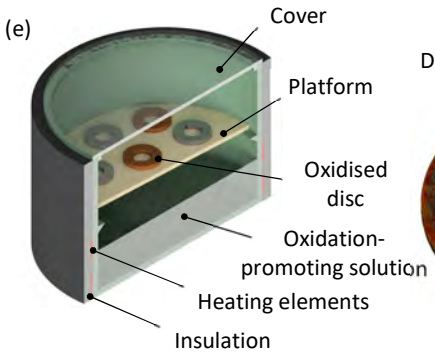

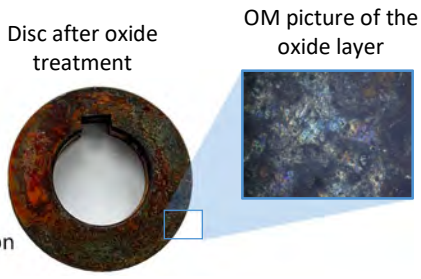

5

- MJP-30A was used to form pre-existing cracks
- Four different steel grades were tested
- Discs were placed in a climate chamber (e)
- At defined time points (f), samples were sectioned and crack length, depth and oxide progression were measured in Article V

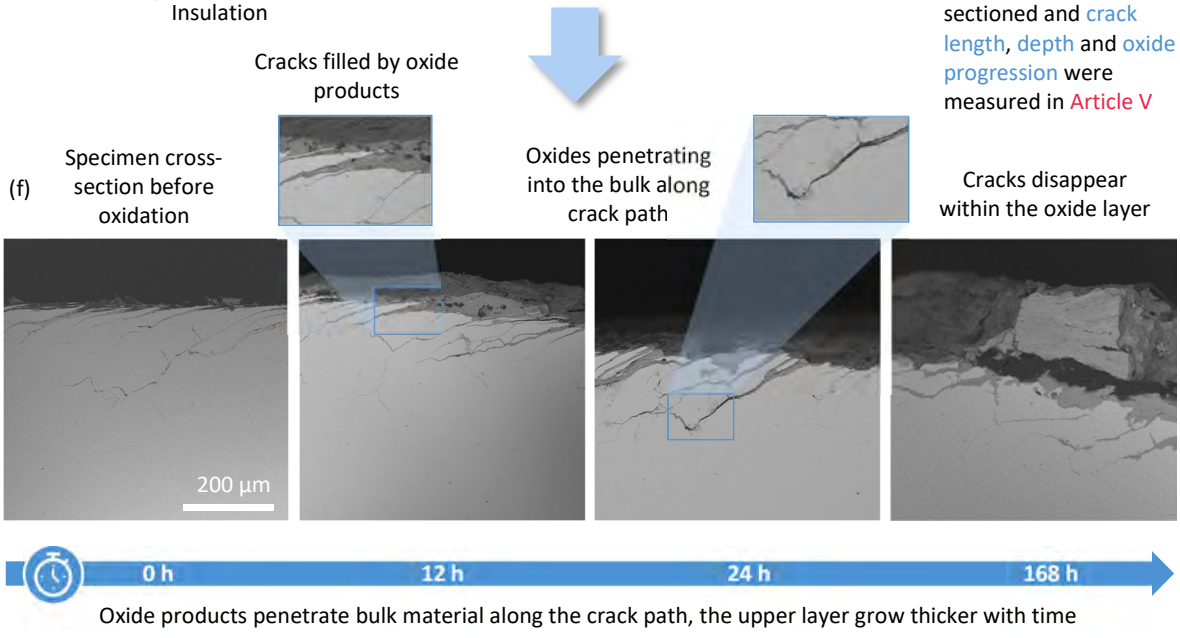

Fig. 14 Experimental workflow.

6.2 Tribometer Mini-Traction Machine

Mini-Traction Machine (MTM, PCS Instruments) is a universal tribometer that was chosen for the friction tests in Articles I–III. Its key advantage is that it is widely used worldwide, ensuring that the results are highly comparable and reproducible.

The ball-on-disc configuration was selected to simulate rolling–sliding contact. The test specimens were made of AISI 52100 bearing steel. Although this material is not a typical rail steel, it provides high mechanical stability and minimal wear, ensuring consistent contact conditions throughout repeated measurements. This setup was previously used, for example, in [18,33,57]. For specific parameters, see Tab. 2.

Both specimens were driven independently by separate servo motors, enabling precise control of SRR. The MTM is equipped with a high-precision load cell that continuously records normal and tangential forces, allowing real-time monitoring of the CoT/CoA. It can operate in three testing modes: time tests, creep curves, and Stribeck curves, where CoT/CoA is evaluated as a function of time, SRR, or rolling speed, respectively.

Tab. 2 Parameters of specimens used for MTM testing.

Specimen	Diameter (mm)	Material	Hardness ($HV_{0.5}$)	Initial roughness (µm)	Testing roughness (µm)
Ball	19.05	AISI 52100 bearing steel	800–920	Ra 0.01	Ra 0.15
Disc	46		720–780		Ra 0.3

In Article III [152], MTM was equipped with a climate chamber covering the tribometer bath. The chamber contained two RH sensors: one provided feedback to the humidification unit, which supplied a controlled flow of wet/dry air into the chamber, while the other continuously monitored environmental conditions during the experiments. The climate chamber lacked active temperature control, so all tests were conducted at room temperature. However, in some tests, specimens were pre-cooled in a freezer to create a temperature gradient and to study the effect of dew point.

6.3 Twin-Disc Machine MJP-30A

The MJP-30A (Southwest Jiaotong University, China) was used for wear and RCF tests in Article IV and to form pre-existing cracks in Article V. In this setup, the specimens are two independently driven discs, one representing the wheel and the other the rail. The device allows precise control of the normal load, rolling speed, and creepage within operating conditions similar to those in real wheel–rail contacts.

The specimens had a diameter of 60 mm, and the contact width was 5 mm. The discs used in Article IV [153] were made of C-class steel used for train wheels and U71MnH rail steel. The materials used in Article V consisted of CL60 wheel steel and three rail steels: U75V, U71MnH, and a newly developed material, which, for the same reason as in the case of the TOR products, is referred to as "hyper-eutectoid steel". All specimens were cut directly from used wheel and rail segments to ensure realistic material composition and properties.

Tab. 3 Composition and hardness of specimens used for wear and RCF tests.

Disc	Steel	C	Si	Mn	P	S	$HV_{0.5}$
Wheel	C-class	0.67–0.77	0.15–1.00	0.60–0.90	0.030	≤0.040	388±9
Wheel	CL60	0.56-0.60	≤0.40	≤0.80	≤0.020	≤0.015	298±11
Rail	U75V	0.71-0.80	0.5-0.80	0.70-1.05	≤0.030	≤0.030	310±11
Rail	U71MnH	0.65–0.75	0.10–0.50	0.80–1.30	≤0.025	≤0.025	290±9
Rail	Hyper-eutectoid	0.90–0.95	0.48–0.52	0.94–1.02	0.01–0.014	0.04–0.07	405±10

6.4 Oxidation Process in the Climate Chamber

Articles IV and V focused on the effect of the oxide layer. The specimens were placed in a climate chamber with the air temperature maintained at 60 °C and high ambient humidity. There, the specimens were exposed to vapours from a mixture of water, ethanol, and magnesium dichloride for 24 hours to speed up oxidation (in Article V, the exposure lasted up to 168 hours). The XRD analysis revealed that the formed oxide layers consisted primarily of four phases: magnetite, hematite, goethite, and akaganeite.

Before and after this treatment, the specimens were weighed to determine the mass increase caused by oxide formation. In Article V, the thickness of the oxide layer was additionally measured using SEM at specific time points during the oxidation process. A similar approach to form oxide layers was used in several other studies [134–136] with some modifications, e.g. the use of different oxidation-promoting agents and varying treatment durations.

6.5 Additional Experimental Equipment

In addition, several other instruments were used for surface analysis and supplementary testing. In Articles II and III, the surface topography was examined using an optical

profilometer, ContourGT-X (Bruker). A Phenom Desktop SEM (Thermo Fisher Scientific) was employed to observe RCF cracks in Articles IV and V, and an integrated EDX system was used to detect oxides and residual particles from TOR products within the cracks. Furthermore, an air-powered impact tester was used in Article V to examine how well the oxide layer adhered to the crack faces and how stable it remained under cyclic loading.

6.6 Experimental Design and Test Conditions

The following sections briefly describe the experimental procedures, test conditions, and overall experimental design for the experiments reported in each Article.

Article I

The objective of this study was to address the first scientific question, Q1. More specifically, it aimed to examine how water influences the performance of TOR products. The tests were performed on the MTM using the specimens described in Tab. 2. The tested TOR products included FM-A, TORL-A, and TORL-B. All tests were carried out at a normal load of 18 N (corresponding to a contact pressure of 0.8 GPa), rolling speed of 1 m/s, and an SRR of 2%. First, preliminary tests were conducted to determine the optimal dosage for each product. The test procedure consisted of four consecutive steps:

1) *Run-in:* The specimens were run under dry conditions for 15 minutes to reach a stable CoA characteristic for the dry contact (approximately 0.4) and to remove any remaining contaminant residue.
2) *Product application:* after CoA stabilised at dry levels, TOR products were applied directly to the contact using an electronic micropipette.
3) *Water application:* Water was applied at three points, T1–T3, where the trigger for application was a predefined CoA value, see Fig. 15. Specifically, T1 corresponded to the phase soon after application of the product, where the contact is flooded, and the risk of low adhesion is the highest. T2 belonged to the steady-state phase in the intermediate friction range, where the product performs as intended. Finally, T3 was defined in the region of relatively high friction, where the product no longer exhibits any significant effect, to evaluate whether water can replenish the starved lubricating film and prolong its effect. In single-application tests, water was added manually using a micropipette (up to 2 ml). In continuous-application tests, it was supplied by a peristaltic pump at the rate of 430 µl/min for 5 minutes.
4) *Post-test cleaning:* After each test, specimens were ultrasonically cleaned in an acetone bath to remove all residues and contaminants.

The following analysis focused on the magnitude of the CoA drop caused by water and the duration of the low adhesion period (CoA below 0.1). In addition to time tests,

Stribeck curve measurements for water, base oil of TORL-A, and their mixtures were conducted at speeds ranging from 50 to 2500 mm/s.

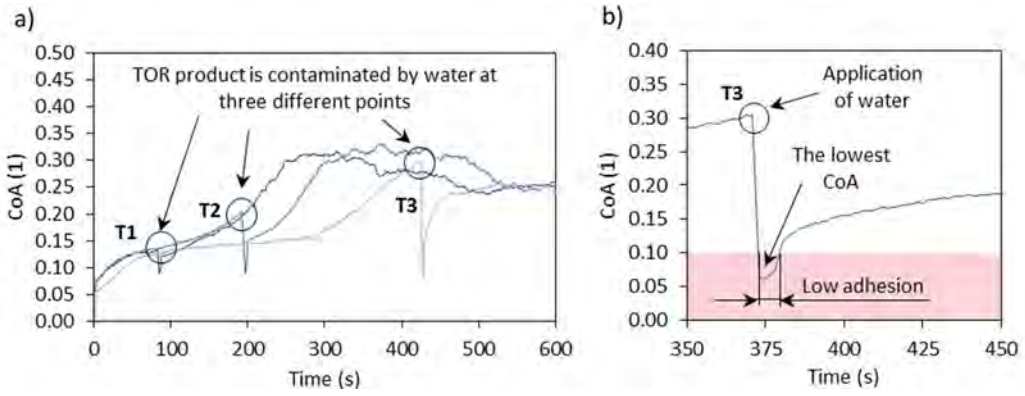

Fig. 15 Illustration of the water-application timing a) and the evaluated parameters b) [150].

Article II

While the first paper provided insights into the interactions between water and TOR products, it also revealed several drawbacks and limitations of the experimental procedure. Therefore, before moving forward, a new benchmarking methodology was developed to enable a consistent and comparable assessment of TOR product performance under water contamination. In the following text, the individual steps of the methodology are described. For a detailed explanation and reasoning behind each step, please see Article II [151].

The methodology can be divided into two phases, see Fig. 16. In the Experimental phase, MTM is used to obtain data from creep curve measurements that are later used in the Evaluation phase to calculate *performance parameters*, based on which the final assessment is assigned to the product. The Experimental phase consists of the following steps:

- *S1:* Before testing, specimens are cleaned ultrasonically in an acetone bath for 20 min to remove any residue from previous testing.
- *S2:* After cleaning, the specimens are run-in for 30 min to establish stable dry contact conditions. When a new pair of specimens is used, the run-in period is extended to 60 min to overcome the initial phase of accelerated wear, and is therefore referred to as *wear-in* for clarity.
- *S3:* TOR products were applied to the contact using an electronic micropipette (with a declared error ± 0.04 µl to ensure accurate and repeatable dosing,
- *S4:* The testing sequence consisted of repeated creep curve measurements within the 0–20 % SRR range. The TOR product was applied only once at the beginning of the test sequence. The test was then repeated using the same initial dosage, and no additional product was added until the stopping criterion was reached.
- *S5* and *S6:* The testing sequence was ended when CoT for two consecutive SRR points exceeded 2/3 of the CoT value for dry conditions. If this condition was not met, the excess lubricant was wiped from the ball with a paper towel (*S6*), and the sequence continued as described in *S4*.

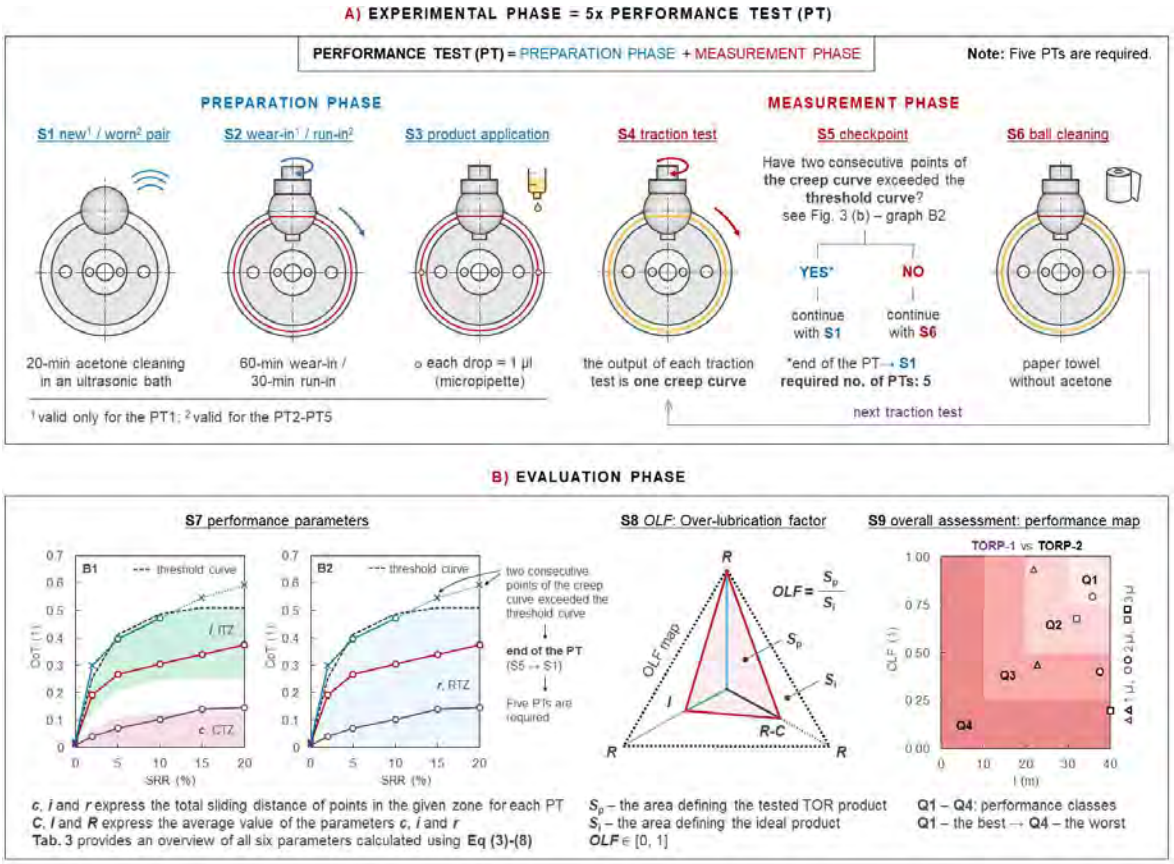

Fig. 16 Schematic illustration of the testing methodology [151].

The completion of *S1–S6* was labelled as a *performance test* (PT). To assess the performance of one product, five PTs in total are required to explore the behaviour of the product under a wide range of contact conditions and also to prevent any random error that may arise due to effects like oxidation, etc.

The first step (*S7* in Fig. 16) in the Evaluation phase is to define three different *traction zones* under the creep curve of a dry contact: a *critical traction zone* (*CTZ*, below 17% of dry contact CoT), an *intermediate traction zone* (*ITZ*, between 1/3 and 2/3), and a *retentivity zone* (*RTZ*, spanning across the whole test duration). Then, performance parameters *C* (*critical traction*), *I* (*intermediate traction*) and *R* (*retentivity*) are computed as the sliding distance spent in each of the corresponding traction zones (average from five PTs). Simply put, parameter *C* says for how long the contact operated in the low adhesion region, *I* says how long the product maintained intermediate friction, and *R* says how long there was any noticeable effect of the product.

In the next step (*S8*), the over-lubrication factor (*OLF*) is calculated from parameters *C*, *I* and *R*. The *OLF* express how likely the product is to cause low-adhesion problems. Then, in step *S9*, *OLF* and *I* are plotted in a 2-D *performance map*, divided into four *performance classes* that represent four quartiles Q1 to Q4. The final comparison between the two TOR products is based on their performance classes. In addition, the effect of contamination can be evaluated by examining how the performance class of each TOR product changes under different conditions.

Article III

The objective of the third paper was to apply the new methodology [151] to evaluate the influence of humidity and moisture on TORL-A and TORL-B. The only modification to the testing procedure, as depicted in Fig. 16, was the addition of an extra step between *S3* and *S4*. After the application of the TOR lubricant in *S3*, the tribometer bath was covered with a climate chamber, and a humidification phase followed. During this stage, two RH levels were tested: 70% and 100%, to simulate humid and dew conditions. In some cases, the specimens were pre-cooled in a freezer to create a temperature gradient, to lower the dew point and speed up condensation. The tests then proceeded as usual.

In the evaluation, the effect of RH and temperature was assessed based on changes in performance class, *OLF* and *C* parameters relative to their values in the reference test under normal conditions.

Article IV

All tests were conducted on the MJP-30A twin-disc machine. The tested TOR products were FM-A and TORL-A, and the specimens were cut from C-class wheel steel and U71Mn rail steel, see Tab. 3. Preliminary time tests were performed to determine the optimal dosage for both products. Afterwards, the main wear and RCF tests were carried out, see Fig. 17 a).

In some tests, the specimens were first run under dry conditions for 5,000 cycles to form pre-existing cracks. Then, they were placed in a climate chamber to undergo an oxidation process. Please note that all combinations of specimens' initial state were tested: clean and new, with pre-existing cracks, with pre-existing cracks and oxides, etc.

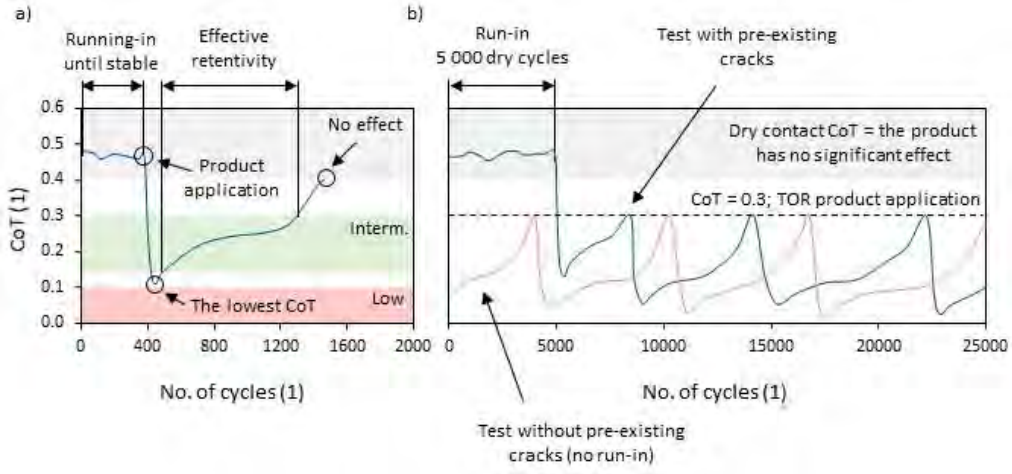

Fig. 17 Schematic illustration of: a) preliminary time test and b) wear and RCF test [153].

During testing, the TOR product was applied each time the CoT reached 0.3, which marked the upper boundary of the intermediate traction zone (see Fig. 17 b). Water was supplied continuously at a rate of one drop per second using a drip system positioned above the contact. Before and after each test, the discs were weighed to determine mass loss and to calculate

the wear rate. Afterwards, they were sectioned and prepared as metallographic samples for microscopic examination. Cracks were observed using SEM, and their lengths and depths were measured. In addition, EDX analysis was performed to determine whether any components of FM-A or TORL-A had entered the cracks.

Article V

Unlike in previous studies, this paper does not focus on friction or wear but instead on the effect of oxidation on the morphology and propagation of pre-existing cracks. In the preparation stage, the MJP-30A was used to form cracks. The tested materials included CL60 wheel steel and three rail steel grades: U75V, U71MnH, and the hyper-eutectoid steel (see Tab. 3 for details). These tests were run under alternating wet and dry conditions to form cracks with different sizes and geometries.

Afterwards, the specimens were placed in a climate chamber and exposed to the same oxidation treatment as in Article IV, with the only difference being the duration of the process. In this case, the duration was extended up to 168 hours. At specific time intervals, the specimens were removed, sectioned, and prepared as metallographic samples.

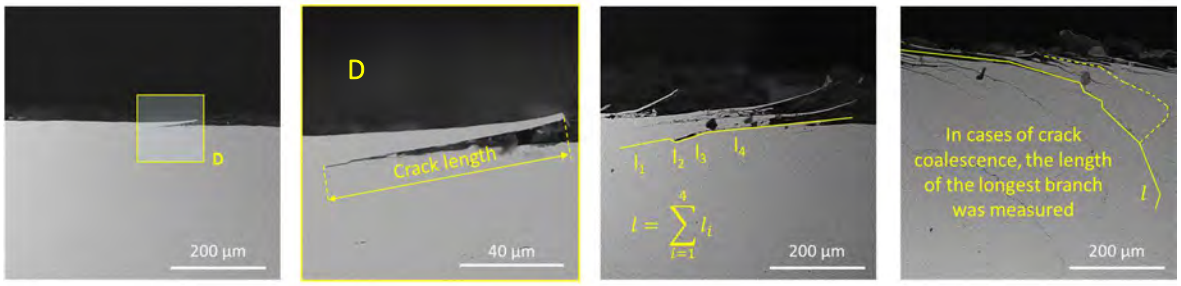

Fig. 18 Methodology of crack length measurement for cracks with different shapes.

The metallographic samples were then examined using SEM to measure the length and depth of cracks and to evaluate how oxidation affected their morphology. In some cases, the evaluation of crack length was challenging, particularly under wet conditions where cracks tended to branch and coalesce. The methodology used to measure crack length for cracks with different morphologies is shown in Fig. 18. The same method was also used for the measurement of crack parameters in Article IV.

Additionally, impact tests were performed on selected oxidised specimens. These samples were subjected to cyclic mechanical loading for varying durations to assess the adhesion and mechanical stability of the oxide layer within cracks and to determine whether the oxides could detach or fracture under repeated impacts.

7. Results and Discussion

This section summarises the main findings of the thesis and discusses their generalisation and implications for railway operations. Before evaluating the impact of contamination on the performance of TOR products, the effect of environmental conditions on wheel-rail friction in the absence of friction modification is addressed first. Since track conditions can vary depending on the environment, it is important to understand these basic conditions before interpreting the results in the following sections.

7.1 Identifying Critical Environmental Conditions

Ishizaka et al. [77] analysed low-adhesion incidents (such as station overruns and signals passed at danger) during the autumn seasons of 2010–2014 in the UK. The analysis shows that these incidents were more frequent during the day than at night, which can be partly explained by the higher traffic volume during the day. After normalising the number of incidents by the number of stopping attempts, a different pattern appears. The highest frequency of low-adhesion incidents occurs in the morning between 6:00 and 9:00, decreases during the day, and increases again in the evening, see Fig. 19.

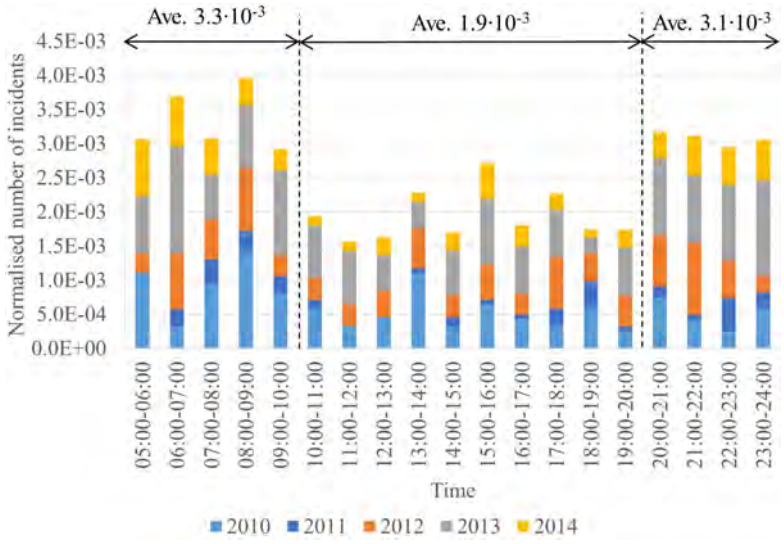

Fig. 19 Number of low-adhesion incidents normalised by stopping attempts [77].

The higher occurrence in the morning can be explained by a closer look at how environmental conditions change throughout the day. Kempka et al. [143] published data from a trackside environmental station in Warwickshire (also in the UK) that monitored railhead temperature, ambient temperature, dew point, and precipitation (see Fig. 20). The chart shows a clear

pattern: a period of light rain in the evening was followed by the railhead temperature dropping below the dew point overnight, resulting in water condensation in the morning. Since the railhead temperature rose above the dew point only about an hour before the first train passed, dew was still evaporating, and the rail surface had not yet fully dried. Therefore, the most likely cause of low adhesion was a combination of residual moisture with particles on the railhead, such as wear debris, iron oxides and rust. As a consequence, drivers reported low-adhesion incidents.

Based on this observation, the situation in the morning under humid conditions appears to be the most problematic in terms of low-adhesion problems. Galas et al. [18] examined the effect of RH on adhesion. They found that although the CoA decreases slightly with increasing RH, this effect remains relatively small. The situation changes markedly when condensation occurs. Once water appears on the surface and mixes with the particles, the CoA drops sharply, falling well below 0.1, see Fig. 21 a).

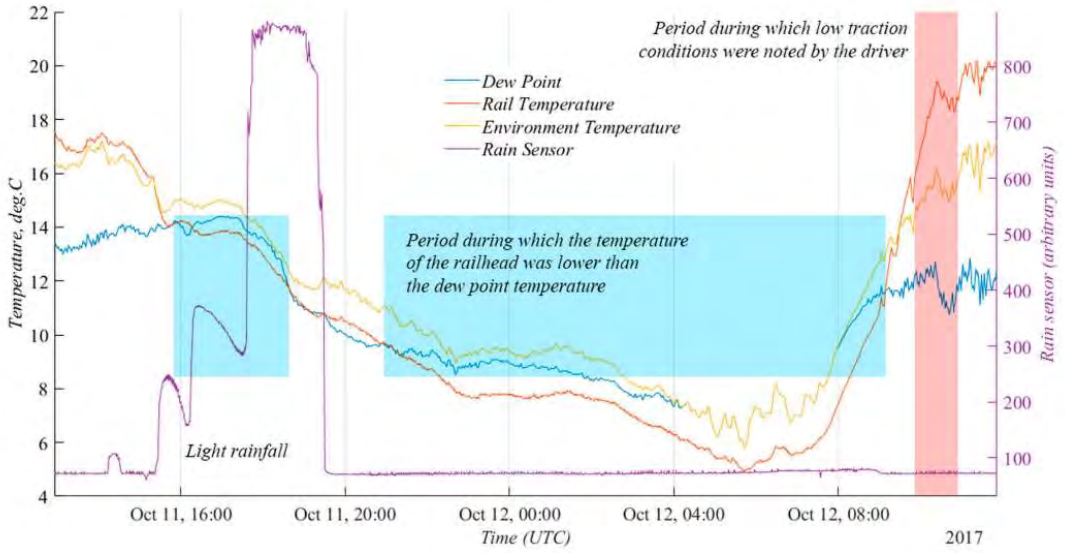

Fig. 20 Data from the trackside environmental station in Warwickshire, UK [143].

Furthermore, they showed that besides the RH value itself, the temperature is equally important. When the rail temperature falls below the dew point, the air can no longer hold its moisture. As a result, water vapour condenses on the railhead. In real operation, this situation often arises after a cold night. The surrounding air warms quickly after sunrise, while the railhead remains cold. If the temperature of the railhead surface stays below the dew point, condensation begins, and dew forms on the rail, exactly as observed in Fig. 20.

Therefore, Article III aimed to investigate the performance of TOR lubricants in this exact scenario. Tests were carried out under high-humidity levels and under dew conditions, and pre-cooled specimens were used to simulate a cold rail in the morning. The focus here was specifically on TOR lubricants, as Lewis et al. [123] had already tested the effect of RH on FMs. The impact on performance was assessed based on the newly developed methodology described in the Materials and Methods section [151].

7.2 TOR Lubricants under Humid and Dew Conditions

The previous subchapter identified the environmental conditions considered most relevant for this thesis. The following text, therefore, focuses on friction modification under these conditions. The performance of tested TOR lubricants under normal conditions (dry contact and normal ambient humidity) and under high humidity and dew can be seen in Fig. 21 b). Under normal conditions, the TOR lubricants provided an intermediate CoT without any risk of low adhesion, exhibiting the desired behaviour of TOR lubricants. However, due to its relatively short-lasting effect, its overall performance was classified only in the third-best category.

In a humid environment (RH 70%), the product classification improved to the second-best category, indicating that the TOR lubricant performs better under humid conditions. Although this improvement may appear counterintuitive, it becomes clear when the performance parameters are examined more closely. Under these conditions, only a negligible amount of water condensed. While this amount was insufficient to cause low adhesion, it was enough to prolong the lasting effect slightly. Consequently, the parameter reflecting the desired product behaviour increased, whereas the parameter related to low adhesion remained unchanged, leading to an overall improvement in the performance map score.

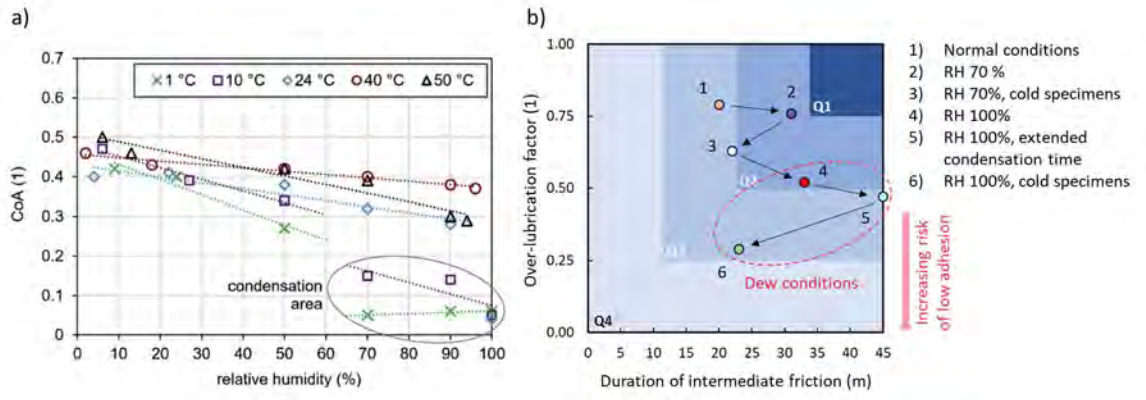

Fig. 21 a) Critical environmental conditions identified by Galas et al. [18] and b) performance of TOR lubricants under these conditions [152].

Next, RH was raised to 100% to simulate dew conditions. Now, visible water droplets start to appear on the surface, and their mixing with the TOR lubricant resulted in a short period of low adhesion, and the parameter describing product resistance to over-lubrication decreased by 40%. Furthermore, water changed the normally positive slope of the creep curve of the TOR lubricant to a negative one.

TOR lubricants performed the worst in a scenario where a cold rail was simulated. In these tests, the specimens were pre-cooled in a freezer, creating a temperature difference of approximately 10 °C between the surface and the ambient air, which strongly promoted condensation. In some cases, up to 25 times more water condensed compared with tests conducted at the same RH but without a temperature difference between the specimens

and the surrounding air. Mixing such a large amount of water with the TOR lubricant had a strongly adverse effect on its behaviour, as reflected by the lowest score in all evaluated parameters, and the product completely failed to fulfil its intended function.

7.3 The Effect of Water on TOR Products

The behaviour of TOR lubricants under different conditions can, to a large extent, be reduced to the effect of the amount of water. Thus, Article I examined the response of both TOR lubricants and the FM to direct contamination by progressively increasing amounts of water. In some tests, water was applied continuously through a peristaltic pump to simulate precipitation. The effect differs for each type of TOR product, as FMs are water-soluble and TOR lubricants are not.

In the case of FMs, the effect of water needs to be considered separately for small and large amounts (of water, the quantity of FM remains the same). For smaller amounts, a similar trend as for TOR lubricants under dew conditions was observed, as with increasing amount, the CoA progressively decreased to lower values (up to a 91% reduction). However, when the largest amount of water was applied (or in tests where water was applied continuously over a longer period), any lubricating effect was immediately lost, and friction instantly increased to the level of dry contact.

Similar behaviour was reported by Oldknow et al. [70], who described that water disrupts film formation and reduces the effectiveness of FMs. Simply put, because FMs are water-soluble, they have low resistance to water contamination and can be easily washed away from the rail surface, thereby eliminating their lubricating effect. Smaller amounts of water rehydrate the dried film and temporarily reduce the CoA [123]. However, this behaviour is essentially the same as during the initial product application and does not lead to any pronounced amplification of the effect (although its magnitude still depends on the amount of water). Therefore, under actual track conditions, low-adhesion problems caused by FM contamination are less likely.

Situation was quite different for TOR lubricants, as water amplified the lubricating effect and the larger the amounts, the lower the CoA (a reduction of up to 93%) and the longer the duration of low adhesion. Beyond a certain amount, the water effect became so strong that adhesion did not recover until the end of the test. Increasing the amount beyond this point produced no additional effect. The amount of water that caused over-lubrication was different for TORL-A and TORL-B, indicating that product characteristics such as composition, particle content, and viscosity influence the sensitivity of the product to water.

It was also shown that this effect occurred regardless of the moment at which the contamination took place, whether immediately after the product was applied, or during the steady-state phase with intermediate friction, or in the final phase when the contact is starved and approaches dry conditions. The interaction between water and the oil/grease was

identified as the key factor, and based on the moment at which the contamination occurred, it can be described by several theories.

At the beginning, when the contact is flooded by lubricant, the *oil-in-water emulsion* theories come into play. Although those do not deal with TOR lubricants, some conclusions may be applied even in this case. The plate-out theory may be used for lower sliding speeds [154,155]. Since oil has better wetting ability than water, it tends to spread over the surface and form an oil pool in front of the contact inlet, see Fig. 22 a). This pool effectively prevents water from entering the contact [156], so the lubricating film in the contact zone is formed primarily by oil, and its thickness is not adversely affected by the presence of water [157,158].

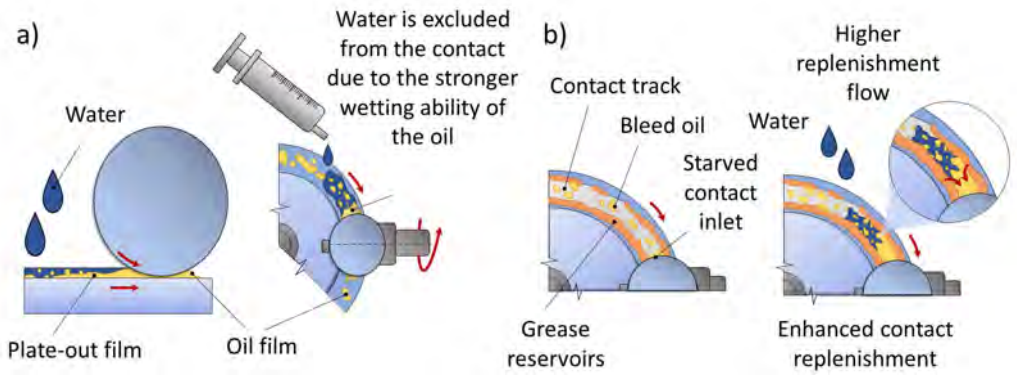

Fig. 22 Possible mechanisms of water and oil interaction: a) plate-out theory and b) enhanced replenishment in grease lubricated contacts [150].

According to the starvation theory [159], when a certain speed is reached, the oil pool becomes unstable, and the lubricant film thickness decreases, although full-film lubrication is still maintained [160–162]. In this stage, a thinner film leads to lower shear stress and, consequently, lower friction. However, as the film continues to thin, starvation eventually occurs. At this point, water can no longer be excluded from the contact and replenishes the starved lubricating film, improving lubrication [163]. So, in this case, the friction would be lower than in the absence of water. The described mechanisms may be relevant to the behaviour observed in the later part of the friction curve, where CoA rise to higher levels as starvation progresses.

When it comes to grease, the following hypothesis may be proposed. If the grease contains polar thickeners, it may absorb water. The absorption degree depends on the thickener type, as some greases are stiffer while others are softer. As a result, water alters the rheological behaviour of the grease, which affects the oil pool stability and, consequently, the contact replenishment [164].

In grease lubrication, the replenishment flow to the contact is inversely proportional to viscosity [165,166]. Depending on the thickener type, the absorbed water may lower viscosity and, in some cases, enhance the oil-bleeding ability and thus, by improving contact

replenishment, delay starvation [167,168], as depicted in Fig. 22 b). Therefore, in the presence of water, friction may remain lower for an extended period.

7.4 The Friction Control on a Wet Rail

The key findings about the frictional behaviour of TOR products under humid, dew and wet conditions are placed in the context of actual track operation in Fig. 23. On uncontaminated rail, CoT usually ranges between 0.4 and 0.6 [32]. The central part of the figure illustrates that in humid environments, CoT can be slightly lower, but generally remains comparable to that under dry conditions [124]. Once that dew formation begins [18], a substantial reduction can be seen, and in combination with other contaminants, such as wear debris, low adhesion may occur. On the contrary, precipitation is less likely to cause low-adhesion problems [73].

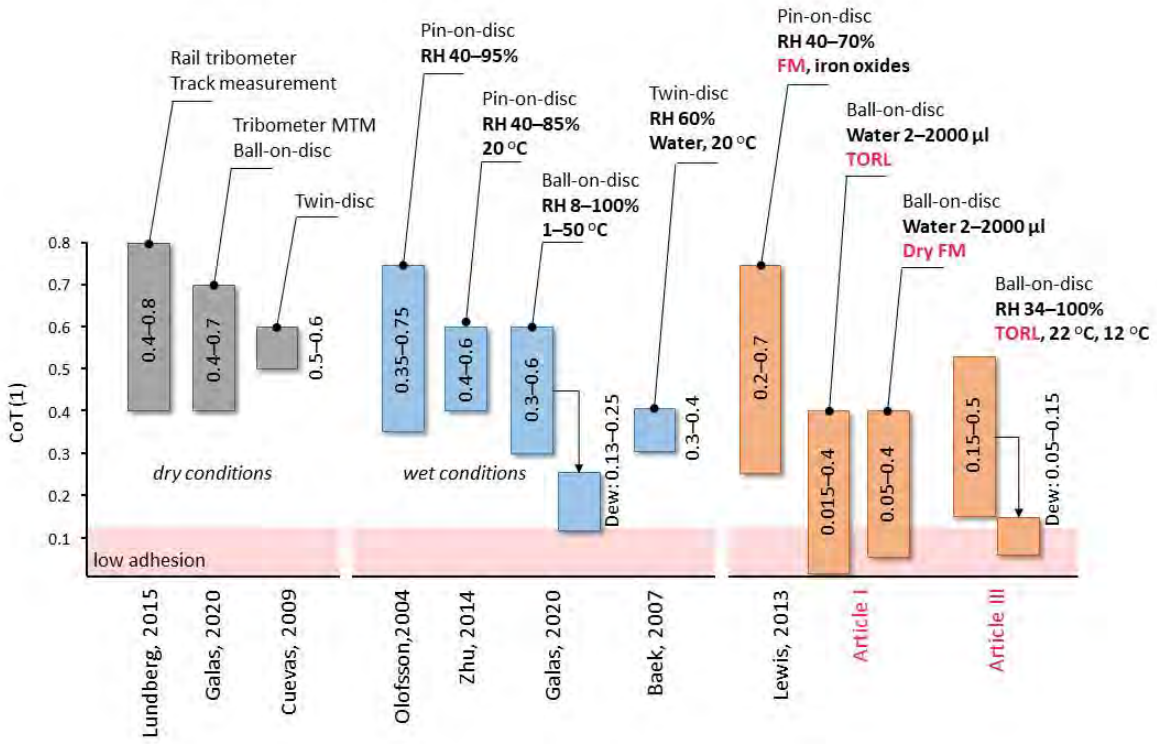

Fig. 23 Comparison of typical CoT ranges under different scenarios [152].

The final part of Fig. 23 presents the CoT ranges measured in Articles I and III, together with the results reported by Lewis et al. [123]. Basically, it combines the conditions from the central part of the figure with the application of TOR products and therefore addresses how these products would perform in the scenario previously identified as the most critical (humid air and moisture on a cold rail). Regarding the results of Article I for FMs, it should be noted that although the CoT briefly dropped into the low-adhesion region after the application of water, this reduction was very short and was followed by a quick recovery (which is not evident from

the graph). In contrast, the application of TOR lubricants resulted in a prolonged period of low adhesion without recovery. Based on a comparison across the individual CoT ranges, it can be concluded that, while the application of FMs is generally safe under a wide range of environmental conditions, TOR lubricants may lead to low adhesion, particularly when applied in the presence of larger amounts of water, such as during dew formation or precipitation.

Sufficient adhesion is the most important during acceleration and braking. While these situations are generally less frequent on long, straight heavy-haul lines, they are much more common in urban transport systems such as metro and tram networks, where vehicles start, stop and go to sharp curves all the time, which is particularly relevant in Brno, Czechia, where most of this PhD research was carried out. Trams play a central role in everyday travel and carried more than 200 million passengers in 2024, which is a remarkable number for a city with fewer than half a million residents. Rail lubrication is used at many locations in the network, especially near tram loops where vehicles queue after completing their routes.

Several incidents have been reported in which trams experienced reduced braking performance or even minor collisions due to low adhesion. Because application units are often placed directly before loops and curves, there is a realistic scenario where TOR products become contaminated with water. However, it is fair to note that drivers do not report contamination of the TOR products specifically as the cause. These incidents are usually recorded simply as low-adhesion incidents and are commonly attributed to leaves, moisture or general railhead contamination.

7.5 Effectiveness of TOR Products in Mitigating Wear and RCF under Wet Conditions

On the one hand, the reduced CoT in wet conditions may decrease adhesive wear of the rail surface due to the lubricating effect of water. On the other hand, however, water can adversely affect RCF. Liquid-assisted crack propagation has been a topic since the 1980s, when Kaneta et al. [169–171] provided important early insights into this mechanism. Since then, the effect of water on RCF has also been well described in the context of wheel–rail tribology. Hardwick et al. [62] and Maya-Johnson et al. [63] showed that these problems may arise not only due to water contamination but also as a result of the application of the TOR products. They found oil-based TOR lubricants to be the most problematic among TOR products, as FMs dry out, and in the case of grease-based TOR lubricants, the high viscosity limits the ability of the fluid to penetrate cracks. However, this may not apply under wet conditions, as it has already been discussed that FMs remain wet for longer and that water can influence the viscosity of greases. Therefore, the experiments conducted in Article IV aim to extend previous RCF testing of TOR products by incorporating the effect of contamination.

Under dry conditions, all selected TOR products greatly reduced wear. The TOR lubricant showed the best performance, achieving more than a thirtyfold reduction. The contact path

remained smooth with only minor spalling, and no significant cracking was observed. In contrast, the FM did not prevent crack growth as effectively. Cracks reached lengths and depths comparable to those observed in the dry reference tests. This can be explained by the fact that once the FM dried out, the CoT increased, and the resulting higher tangential forces promoted crack propagation.

The present results can be compared with those reported by Stock et al. [56], who observed that when FM application was initiated after 25,000 dry cycles, no further crack growth occurred. While this finding could be interpreted as an indication that the FMs can stop crack propagation, the results of this thesis show that crack growth continues and even progresses faster under well-lubricated conditions. A more probable explanation is that crack length and depth saturate at a certain limit determined by the competition between wear and rolling contact fatigue. This limit appears to be similar for dry conditions and for contacts with a dried friction modifier layer, which is consistent with the behaviour observed in the experiments presented in this thesis.

An increase in wear was observed in the tests where cracks had already formed before the product was applied, indicating that while TOR products are effective in preventing crack initiation, their effectiveness decreases when the surface contains pre-existing cracks, as liquid-assisted mechanisms of crack propagation come into play. Still, the application of both TOR products led to some improvement compared to unlubricated conditions. The average crack length and depth under the FM were more or less the same as in the previous tests. However, both parameters increased under the TOR lubricant, confirming that the crack propagation mechanisms differ between drying and non-drying products.

Testing both TOR products in wet conditions and with pre-existing cracks produced very different results. When the FM was applied to a wet surface, the material loss increased more than fivefold, and the crack length increased by an order of magnitude compared with the tests without water. Cracks that were only tens of micrometres deep in dry conditions grew to several hundred micrometres. A reference test with water only showed that this behaviour was caused mainly by water rather than by the FM itself. In fact, FM provided a slight improvement. However, its overall effect was negligible, and it failed to perform its intended function under wet conditions.

Application of TOR lubricant to a wet surface resulted in the lowest CoT among all tested conditions, which was also reflected in mass loss that was almost half that in tests where TOR lubrication was applied in dry conditions, see Fig. 24 a). However, this seemingly favourable performance appears much less positive after examination of metallographic cross-sections under SEM (Fig. 24 b). Here, cracks reached the greatest depths by far, even exceeding those observed in the tests with water or FM in wet conditions, and they were visible to the naked eye from the top of the surface, see Fig. 24 c). The cracks were turning towards the bulk, propagating under an angle almost reaching perpendicularity, branching and coalescing into a dense network reaching up to nearly a millimetre deep (compared to tens of micrometres in the case of TOR lubricant in dry conditions).

The question arises why the deepest cracks developed under the combined effect of water and the TOR lubricant, and why this was not reflected in the mass loss. Considering what is known about liquid-assisted crack propagation [99,172,173], the following explanation is likely. The tangential forces acting in the contact generate alternating tensile and compressive stresses. As a crack approaches the contact zone, the surface is in tension, the crack opens, and water, due to its low viscosity, easily penetrates into it. Once the contact passes, the stresses become compressive, the crack closes, and the trapped liquid becomes pressurised. As a result, the stress intensity at the crack tip increases and promotes crack growth [174].

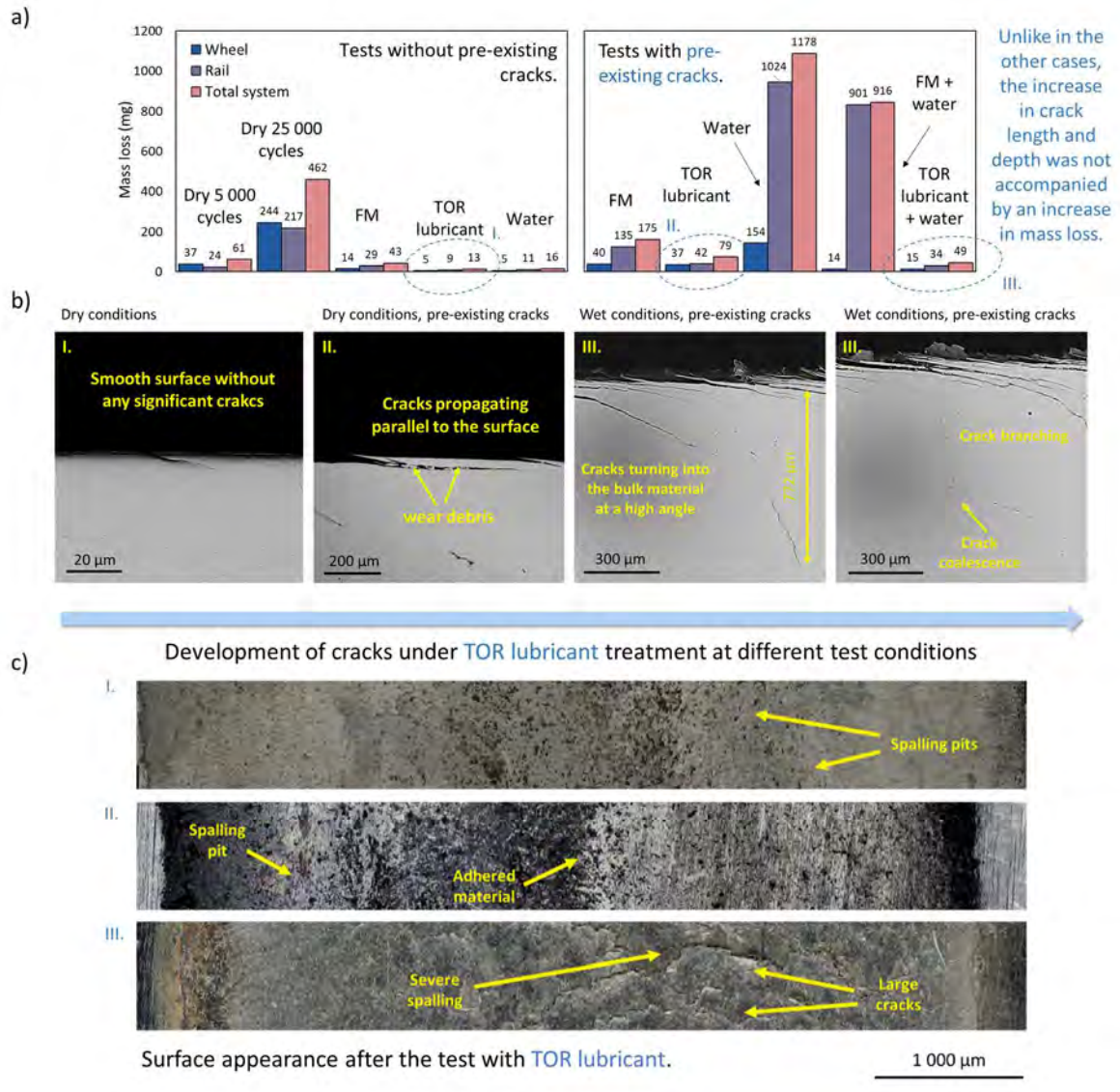

Fig. 24 Changes in a) mass loss, b) crack parameters and c) surface damage in tests with TOR lubricant under different conditions [153].

As the combination of the TOR lubricant and water produced a CoT of around 0.05, the wear of the surface layer was minimised (although signs of spalling were found at some locations, see Fig. 24 c). As a result, the cracks can propagate deeper due to hydropressurisation of oil,

while material removal remains minimal because a combination of TOR lubricant and water well lubricates the surface. Thus, the application of the TOR lubricant in wet conditions resulted in the deepest cracks, despite minimal mass loss.

From an operational perspective, this combination may lead to a potentially critical situation. Under FM in wet conditions, material is removed continuously, which makes the surface damage visible and allows it to be monitored and addressed in time. In contrast, under a TOR lubricant in wet conditions, the rail surface may appear relatively undamaged for a long period, while in reality, the cracks grow and gradually form a dense network deep in the material. At some point, this hidden damage may lead to a sudden failure.

7.6 The Role of Oxides

Regarding wear and material failure, corrosion and the formation of iron oxides can play a major role. Oxides influence the contact in several ways, as they modify friction and change the near-surface mechanical properties. A particularly significant contribution to this field was made by Zhu et al. [107,133–136]. In their work, they highlighted the need for a laboratory procedure capable of generating iron oxides with properties comparable to those produced under real operating conditions, as this is essential for representative testing in simplified laboratory environments. To address this, they adopted a multi-step procedure originally introduced by Sone et al. [131], which involves repeated exposure of specimens to NaCl vapours, alternating cycles of high and low humidity, and elevated temperatures.

In Articles IV and V, the procedure was simplified to a single step, and several parameters were adjusted. The specimens were placed in a climate chamber and exposed to vapours of water, ethanol and magnesium dichloride. The ambient temperature was increased from 40 °C to 60 °C, and the exposure time depended on the desired surface coverage and layer thickness. Usually, 24 h was sufficient to form a continuous layer across the entire surface. The XRD analysis showed that this procedure led to the formation of an oxide layer composed of hematite, magnetite, goethite and akaganeite.

In rail tribology, hematite and magnetite in the form of powder are arguably the most frequently tested. However, the range of oxides that may occur on the rail is broader [142]. In addition to the environmental data presented in Fig. 20, Kempka et al. [143] performed field XRD analysis of rail oxides and found that goethite and akaganeite were consistently present during low-adhesion incidents. Therefore, the oxide layer prepared in Articles IV and V can be considered well-suited for research focused on low-adhesion mechanisms.

Under dry conditions, the oxide layer had a reducing effect on CoT. Under lubricated conditions, however, its effect was not consistent. In some tests, FMs or TOR lubricants performed better, while in others, their lasting effect was shortened. No clear trend was identified. Godfrey reported that hematite tends to increase friction [142], whereas goethite and akaganeite lower it, particularly under wet conditions [143]. In reality, a single phase is rarely present (unlike in laboratory testing, when oxide powders are used). So, the behaviour

of the layer likely depends on which phase dominates at that time. Mechanical stability represents an additional issue. The oxide layer exhibits low shear strength and does not wear uniformly. Instead, it tends to crack and flake off in localised patches. The detachment of these oxide fragments alters the local contact conditions and, consequently, leads to less predictable frictional behaviour, which negatively affects test repeatability.

Oxidised discs experienced a higher mass loss under the TOR lubricant than unoxidised ones, showing that the oxidised material can be removed easily even under lubricated conditions. Similar mass loss was recorded for FM. However, it should be noted that compared to tests with unoxidised discs, it was significantly lower. This decrease was not due to a better performance of the FM. The higher mass loss on unoxidised discs resulted from liquid-assisted crack propagation and subsequent RCF damage. In contrast, oxidised discs were left with a smooth surface without visible cracks.

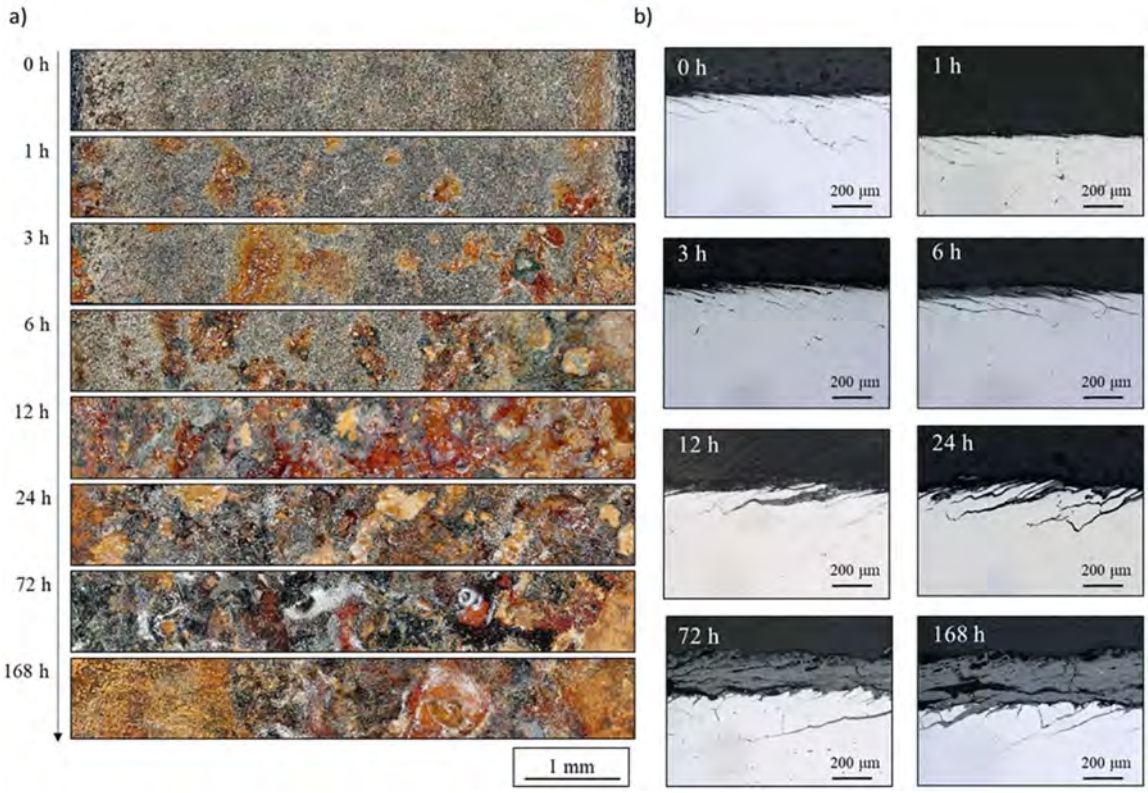

Fig. 25 a) Oxide coverage over time and b) oxidation of crack faces.

The effect of oxides on RCF was revealed by observing metallographic cross sections. The oxidation happens not only on the surface, but also internally along the crack faces. As the oxide products grew, they progressively filled the cracks and eventually sealed them (as can be seen from Fig. 25 b), preventing any liquid from entering and thus, effectively suppressing all liquid-assisted mechanisms of crack propagation. In addition, as the cracks became part of the oxide layer, they were removed together with it as wear progressed. As a result, all existing cracks were removed before they could propagate further, indicating that although oxidation promotes wear, it suppresses RCF. However, this conclusion applies to rolling–sliding conditions. During the preparation phase of the experiments

in Article IV, it was noted that some cracks were visibly larger after the oxidation process than before it, suggesting that oxidation may play a different role in contacts that have not been mechanically loaded yet.

Fig. 25 a) illustrates how the oxide layer gradually covers the surface as the oxidation time increases. During the first few hours, isolated oxide patches start to form, and full surface coverage is typically reached after roughly 24 hours under the used procedure. After that, the layer continues to grow in thickness, increasing from several tens to several hundreds of micrometres. Fig. 25 b) provides evidence for the previously discussed mechanism in which oxide products grow inside the crack and eventually seal it against any liquid ingress. In addition, oxidation progresses not only from the surface but also from the crack faces towards the bulk. As a result, the cracks appear wider, but more importantly, the underlying material becomes weakened from within and to a greater depth than in the case of surface oxidation only.

The measurements of crack parameters at the time points listed in Fig. 25 revealed an initial increase in crack length during the early stages of oxidation. However, after a certain period, the opposite trend was observed, as the cracks began to shorten. The turning point occurred earlier for cracks with smaller initial lengths than for longer ones. Regarding crack depth, it remained nearly constant at first, but then a sudden decrease occurred, and again this happened earlier for shallower cracks than for deeper ones. In most cases, the cracks disappeared completely after 24 hours of oxidation.

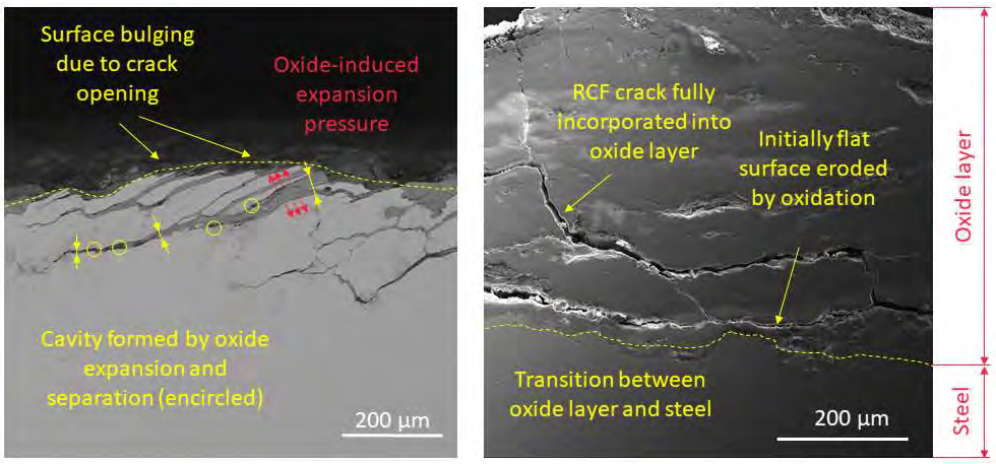

Fig. 26 a) Oxide-induced propagation and b) crack incorporated into the oxide layer.

The oxygen-assisted crack propagation has been observed before, although in areas unrelated to rail tribology. For example, studies on steam turbine components [175] have shown that oxides that grow inside cracks can act like a wedge and gradually force the crack open [176]. A comprehensive literature review on this topic was published by Jiang et al. [177] or later by Vasudevan et al. [178]. They pointed out that, depending on factors such as temperature [179], material compositions [180] or partial pressure [181], oxygen tends to diffuse along crack faces and grain boundaries, particularly near the crack tip where the local strain and stress are highest.

Under such conditions, two related mechanisms may happen. Oxygen can promote stress-assisted formation of oxide products on boundaries of individual grains, reducing cohesion [181–187], or it can cause oxygen enrichment that weakens the boundary without forming a continuous oxide layer, as described in studies focused on dynamic embrittlement [188–190]. Although these concepts were established mainly for high-temperature Ni-based superalloys, the underlying principles align with the observed behaviour. Analysed cracks commonly widen near the surface and taper with depth. This morphology suggests that oxygen may interact with crack faces and grain boundaries, and that the associated volumetric expansion or local weakening could influence the crack-tip geometry.

At the same time, the upper surface layers gradually transform into an oxide layer that grows progressively toward the centre, incorporating cracks, see Fig. 26 b). Smaller cracks disappear entirely, while longer ones are gradually consumed from the top down, which is clearly reflected in the measured crack depths over the oxidation period. Eventually, the length increase due to oxygen-assisted propagation becomes smaller than the decrease caused by the thickening layer of oxidised surface. Taken together, these effects explain why crack length and depth initially increase Fig. 26 a), but after a certain point, the trend reverses, and most cracks eventually vanish Fig. 26 b).

From an operational perspective, unlike liquid-assisted crack propagation, oxygen-assisted propagation is unlikely to cause severe RCF damage as it requires long exposure times. On frequently used tracks, such as in urban rail transportation systems, the oxidised layer is likely to be rapidly removed by passing vehicles. However, this may become an issue in marine environments and tunnels, where the combination of elevated temperatures, high humidity, and airborne salts accelerates oxidation processes [191,192]. What may realistically occur is that, as oxides penetrate the bulk through crack faces, it becomes weaker from within, which may potentially contribute to material failure. At the same time, the ability of oxides to seal cracks and suppress liquid-assisted crack propagation, as demonstrated in Article IV, suggests that the presence of a natural oxide layer on the rail surface may partially mitigate the adverse effects of TOR lubrication on rolling contact fatigue. Since some degree of oxidation is always present on real rail surfaces, this finding is relevant for understanding TOR product behaviour under field conditions and should be investigated further.

7.7 Significance of the Results

The results presented in this work were obtained under controlled laboratory conditions and are therefore not intended to provide a direct quantitative prediction of TOR product performance in real railway operation. The reported values should be understood as relative indicators showing general trends and differences between product types and operating scenarios. Furthermore, laboratory testing inevitably involves simplifications of the real wheel–rail system. For this reason, the conclusions and interpretations discussed here should be seen as informed assumptions based on laboratory observations, rather than as definitive statements on in-service performance. Within these limitations, this section aims to provide

practical guidance on when the use of TOR products can be considered safe, when increased caution is required, and which potential risks should be considered from an operational and practical point of view.

Tab. 4 Summary of TOR product performance under different contamination scenarios.

Conditions	Friction Modifier (FM)			TOR Lubricant (TORL)			Article
	Friction effect	Material loss	Crack propagation	Friction effect	Material loss	Crack propagation	
Dry, clean rail (RH ~ 34 %)	Intermediate (CoT 0.2–0.4)	Reduced (10×)	Tens of µm	Intermediate (CoT 0.15–0.25) OLF = 0.79	Reduced (35×)	No significant cracking	I–IV
Humidity (RH 70 %)	– [a)]	–	–	OLF = 0.76 (negligible effect)	–	–	III
Light moisture or dew (2–180 µl, RH 100 %)	CoA drop to 0.08–0.02 transient; recovery in seconds	–	–	OLF = 0.29 CoT < 0.1 long-lasting; negative slope of the creep curve	–	–	I, III
Water (continuous application)	CoT ~ 0.4 FM quickly washed away	Increased (2×)	Severe; hundreds of µm	CoT < 0.05 no recovery	Reduced (25×) [b)]	Most severe; up to 900 µm[b)]	I, IV
Iron oxides (24 h oxidation)	Variable (oxide layer unstable)	Increase[c)]	Suppressed (cracks sealed by oxides)	Slightly decreasing; variable	Increase[c)]	Suppressed (cracks sealed by oxides)	IV, V
Iron oxides + water	Variable	Lower than w/o oxides [d)]	Suppressed (oxide sealing)	Low CoT (water-dominated)	Higher than w/o oxides [d)]	Suppressed (oxide sealing)	IV

a) FM under humidity/dew was not tested. For FM in humid environments, see Lewis et al. [123].

b) Despite 25× lower material loss than under dry conditions, this condition produced the deepest cracks (up to 900 µm). Suppressed wear prevented crack removal, and water and oil promoted crack growth through hydropressurisation. The surface appeared undamaged while a deep crack network formed beneath.

c) Mass loss on oxidised specimens includes the removal of the oxide layer itself. As a result, the absolute values are not directly comparable to tests on unoxidised specimens, and no fold-change is reported. However, the trend (increased material removal) reflects both oxide wear and the underlying steel loss.

d) Comparison is between oxidised and unoxidised specimens under the same product and water conditions. FM: material loss lower than FM + water w/o oxides, because oxide sealing suppressed liquid-assisted crack propagation, which was the dominant damage mechanism on unoxidised discs. TORL: material loss higher than TORL + water w/o oxides, because the soft oxide layer was progressively removed, adding to the measured mass loss.

Tab. 4 summarises the measured results across all tested contamination scenarios, comparing the friction effect, material loss and crack propagation for both FMs and TORLs. For material loss, all reported fold-changes are referenced to dry unlubricated contact. Because these values are specific to the laboratory setup, they cannot be transferred directly to track conditions. To bridge this gap, the quantitative results from Tab. 4 were translated into a qualitative

performance assessment presented in Fig. 27, which aims to capture the general operational trends rather than exact numerical thresholds.

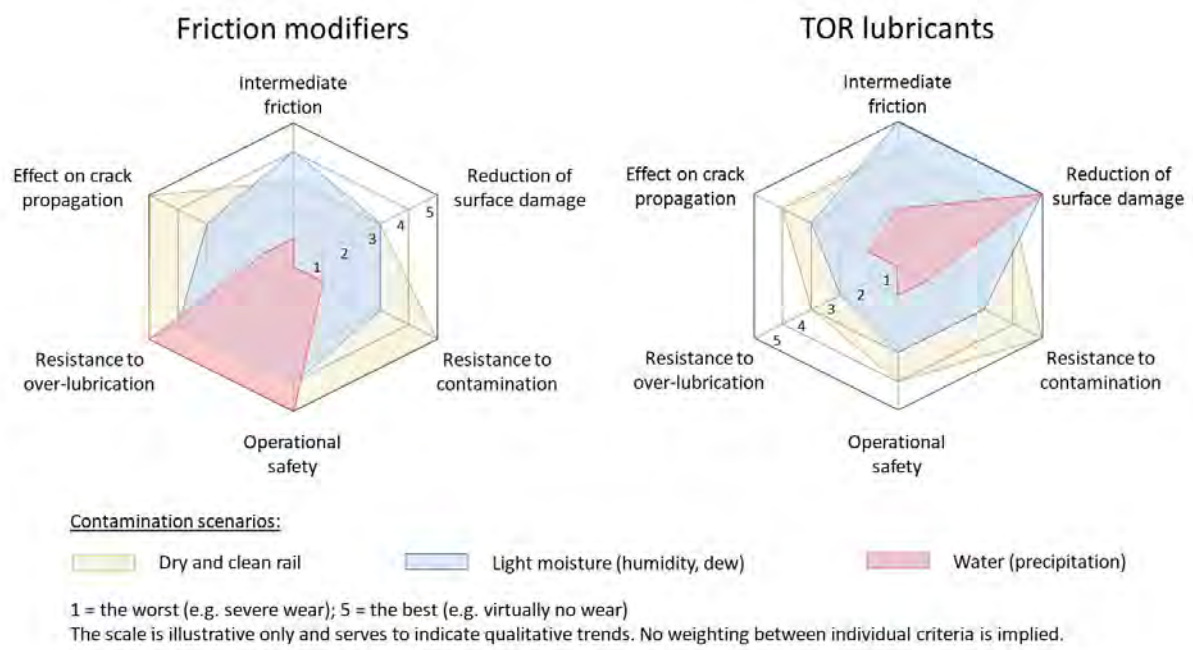

Fig. 27 Qualitative comparison illustrating the expected operational behaviour of FMs and TOR lubricants under different contamination scenarios.

The six performance categories in Fig. 27 address different aspects of TOR product behaviour. Four of them are directly linked to measured parameters, while the remaining two were assessed qualitatively by the author. *Intermediate friction* reflects the ability of a product to provide a desired friction level with CoT within the target range and is derived from the CoT values across Articles I–IV. *Resistance to over-lubrication* describes the susceptibility of the product to excessive lubrication, and is based on the OLF evaluated in Articles II and III. *Reduction of surface damage* accounts for material removal due to adhesive and abrasive wear as well as RCF, based on the mass loss reported in Article IV. *Effect on crack propagation* evaluates the influence of the tested conditions on crack initiation and growth, reflecting the crack length and depth from Article IV. The two remaining categories are based on the author's interpretation of the experimental trends. *Resistance to contamination* indicates how sensitive the product performance is to the presence of contaminants, which may affect its functionality either negatively or positively. *Operational safety* represents the overall risk of low-adhesion problems under realistic operating conditions, considering the sensitivity of CoT to different contamination scenarios. The difference between resistance to over-lubrication and operational safety is that the former mainly describes a product property, while the latter represents an operational effect, as it considers not only the product itself but also the influence of multiple additional factors and aims to predict what will occur on the real track. The performance in each category is rated on a scale from 1 (least favourable) to 5 (most favourable).

A direct comparison of the two groups of TOR products under dry conditions shows a clear trade-off in their behaviour. TOR lubricants provide stronger lubrication and optimise friction for a longer period. In real operation, this would correspond to a longer carry distance and higher retentivity. At the same time, this also makes TOR lubricants more sensitive to the applied amount. If too much product is applied, over-lubrication may occur even without contamination, and low-adhesion problems can arise [49]. In contrast, the performance of FMs depends less on the application amounts [32]. Their lubricating effect is lower, but this also limits the risk of over-lubrication and leads to higher operational safety.

The same trade-off is observed in damage-related behaviour. TOR lubricants were more effective in reducing wear due to their higher lubricating performance. However, because they do not dry out, they may promote liquid-assisted crack propagation. FMs, on the other hand, dry out after application, which reduces their lubricating effect and thus wear mitigation, but at the same time, it limits the crack growth. Overall, TOR lubricants offer higher performance, while FMs provide a more robust and safer behaviour.

Under conditions of light moisture, both TOR lubricants and FMs show improved scores in lubrication-related categories, while performance in safety-related categories tends to worsen. This effect is of less concern for FMs, as the measured results show that, although CoA may decrease due to moisture, this drop is usually short-term [150]. In contrast, the situation is more critical for TOR lubricants, as they are naturally more prone to over-lubrication even in the absence of contamination [49]. Therefore, additional caution is required when using TOR lubricants under conditions where moisture is expected, such as in the morning when the rail is cold, and water condenses on its surface [152]. From an operational perspective, this highlights the importance of adjusting application strategies to daily and seasonal changes [77].

Water has a strong effect on both types of TOR products, although for different reasons. In the case of FMs, water will wash the product off the rail surface, effectively terminating its action and eliminating the intended friction control effect [150]. In contrast, the application of TOR lubricants under wet conditions is likely to lead to over-lubrication, which may result in a loss of traction or adhesion and require sanding for acceleration or braking. For this reason, the application of TOR products should consider weather conditions, especially precipitation. Applying FMs during rain is mainly uneconomical, as the product is quickly removed and water itself already reduces friction [79]. In the case of TOR lubricants, the main concern is safety, and application when rain is expected should be avoided.

The role of iron oxides is more nuanced. Their direct effect on friction was limited and variable, largely due to the mechanical instability of the oxide layer. However, their influence on crack propagation was significant: oxide products sealed pre-existing cracks and prevented liquid ingress, effectively suppressing liquid-assisted crack propagation when water was present (Tab. 4). This finding suggests that a natural oxide layer on the rail surface may partially mitigate the adverse effects of TOR lubricants in RCF. At the same time, oxidation increases material removal, as the low shear strength of the oxide layer leads to accelerated surface wear.

The main takeaway of this thesis is that adapting the TOR product application to environmental conditions provides clear practical and economic benefits. Avoiding ineffective or unsafe application reduces unnecessary material use, limits the need for sanding, and lowers additional wear of wheels and rails. At the same time, improved operational safety and fewer incidents related to low adhesion or insufficient traction lead to higher service reliability and reduced delays, benefiting infrastructure managers, operators, and the overall sustainability of railway transport.

7.8 Study Limitations and Future Research

When testing TOR products, the majority of existing studies primarily focus on friction control (typically expressed in terms of CoT or CoA) and on the mitigation of wear and RCF. Accordingly, this PhD thesis concentrates on these three parameters and extends the current state of knowledge by introducing contamination as an additional variable. However, the evaluation of these parameters under laboratory conditions alone is not sufficient to fully capture the practical effectiveness of TOR products in real railway operation.

In the field, TOR product performance is additionally governed by mechanisms related to application, transfer, and redistribution on the rail. In particular, parameters such as carry distance, describing how far along the rail a product remains effective, and retentivity, referring to the durability of the frictional effect over the number of wheel passages, play a critical role in determining real-world performance [193]. However, they are rarely addressed in laboratory-based studies. This limitation is further emphasised by the study of Khan et al. [43], which demonstrates that, under real operating conditions, the effective carry distance of TOR products may be significantly shorter than commonly assumed.

Eadie et al. [194] highlighted that the effectiveness of redistribution is largely governed by lubricant-related properties, especially the ability of the product to be effectively picked up by the wheels and subsequently transferred back onto the rail surface. These aspects were not explicitly investigated within the scope of the present work, and it is reasonable to assume that contamination may significantly affect them. Nevertheless, this limitation is not specific to the present study but reflects a broader gap in the current understanding of TOR product behaviour and indicates a potential direction for future research.

The most significant limitation of this work, which is closely related to the aspects discussed above, lies in the testing approach itself. MTM testing is an efficient method for generating repeatable results, but its main drawback lies in simplification. The ball-on-disc configuration produces a small point contact that is highly susceptible to over-lubrication. The redistribution mechanism also differs. In the MTM, the contact repeatedly runs over the same track, so sufficient amounts of product remain available for a long time because there is nowhere for the lubricant to go. As a result, excessive lubricant can accumulate, and starvation is delayed.

On the actual track, the wheel passes any given point only once and redistributes the TOR product over several hundred metres of rail [195]. Larger amounts of lubricant are therefore present only near the application unit, and the quantity decreases with distance. Consequently, the effect of contamination on the CoT observed in laboratory tests may be stronger than the effect encountered under real operating conditions.

From this perspective, the use of a twin-disc machine with a wider line contact might appear to be a better option. However, twin-disc machines are often custom-built, such as SUROS [196], MJP-30A [197] or JD-1 [75], and therefore differ in characteristics such as loading system stiffness or disc alignment accuracy, which can affect the comparability of results. Moreover, the testing apparatus itself does not address the main problem identified in this work: deviations inherent to the time-test approach. Repeated testing often produced friction curves of different shapes, and the procedure was always affected by a certain degree of randomness. Although time tests are suitable for studying the immediate response of a TOR product to contamination (as in Article I), they proved unsuitable for any form of statistical analysis or quantitative evaluation. For this reason, a different approach that does not rely on time-based testing is required.

The recently published CEN/TS 15427–2–2:2021 standard introduced a methodology for the assessment of TOR products on the MTM tribometer based on the creep curve measurement approach [198]. Although this represents an important step forward, the method relies on a single performance criterion and therefore provides only limited insight into product behaviour. Thus, an alternative methodology was proposed in Article II. Its comparison with CEN/TS 15427–2–2:2021 standard can be seen in Tab. 5.

Both methodologies were designed for the MTM in the ball-on-disc configuration with specimens made of AISI 52100 steel. This material has a significantly higher hardness (800–920 HV) than typical pearlitic rail steels (approximately 275–350 HV) [199], which makes it unsuitable for studying wear and rolling contact fatigue, as these mechanisms are strongly influenced by hardness and microstructure. For this reason, Articles IV and V used specimens cut from authentic wheel and rail materials. For friction measurements, however, AISI 52100 offers a practical advantage: its high wear resistance ensures that the contact geometry remains stable throughout repeated testing, preventing changes in surface topography and contact pressure that would occur on softer steels due to progressive wear and flaking. As a result, the measured friction reflects the effect of TOR products and contaminants rather than evolving contact conditions. Although slightly lower friction may be expected on harder specimens [200] the results remain representative of the lubrication regime in the wheel-rail contact, as confirmed by Stribeck curve measurements in Article I. The same material has been used in several other studies on TOR products [18,33,107] and is specified in the CEN/TS 15427-2-2:2021 standard [198].

Regarding test parameters, both methodologies employ values representative of actual wheel–rail contact, with the CEN/TS standard using slightly higher contact pressure. However, applying 50% SRR during the dry run-in phase inevitably produces a wide and deep conformal contact path. Since the load is set on MTM as a normal force, it is questionable what the actual contact pressure would be during testing, as the increased contact area would lead

to a reduction in pressure. Therefore, the proposed methodology uses 2% SRR under dry conditions. This choice was further supported by preliminary tests at 50% SRR, which revealed that such a high sliding ratio generates excessive heat, promoting oxide formation that can affect friction measurements.

Another difference between the two methodologies is that the CEN/TS consists of only a single testing set. In contrast, the proposed methodology includes five sets of creep curve measurements, allowing assessment under a wider range of contact conditions and thus improving the representativeness of the obtained results. The final parameters are calculated as averages, which helps to minimise random errors. The drawback is that the procedure is considerably more time-consuming. Regarding the evaluation phase, the CEN/TS standard applies a single performance criterion based on the CoT measured at 10 % SRR, and the final assessment is limited to a simple good/bad. In contrast, the proposed methodology uses several parameters averaged from five sets of testing to construct a performance map.

Tab. 5 Comparison between the proposed methodology and the CEN/TS standard.

	Wear-in[1)] parameters	Run-in parameters	Test parameters	# of sets	Total time[2)]	Performance parameters	Overall assessment
Article II	0.8 GPa 1 m/s 2% SRR 60 min	0.8 GPa, 1 m/s, 2% SRR, 30 min	0.8 GPa 1 m/s 0–20% SRR 20–40 min	5	5–8h	I, OLF	Performance map (Q1–Q4)
CEN/TS standard	1 GPa 0.1 m/s 50% SRR 30 min	–	1 GPa 1, 3.8 m/s 0.25–10% SRR 22 min	1	1h	CoT at 10% SRR	Good/bad

1) CEN/TS standard uses run-in in the same way as wear-in in the proposed methodology.

2) Estimation, the exact time is dependent on the number of creep curves.

The author believes that an approach based on creep curves provides a more robust way of assessing TOR products in laboratory conditions than standard time tests. Laboratory tests on simplified apparatus can serve as useful screening tools in the early stages of research, as they are simple, fast and inexpensive. However, their results must be verified on facilities with more realistic geometries, such as those used by Eadie et al. [54] or Stock et al. [56]. Ultimately, the highest level of verification is field testing with a real vehicle. Conducting controlled braking tests under low-adhesion conditions is, however, methodologically complex, expensive and may pose safety risks for railway operations.

As a follow-up beyond the scope of this thesis, work continued to develop a methodology that combines the advantages of controlled laboratory testing while at the same time more closely models the wheel–rail conditions [193]. A test facility with a three-metre-long rail segment and a scaled wheel was built to study TOR products and contaminants. In this setup, frictional

characteristics and creep curves can be measured using a track-side tribometer [201]. Furthermore, this configuration also allows testing of less studied parameters, such as the pick-up ability of the wheel and redistribution mechanisms in general, which are directly linked to the limitations discussed above and can now be examined in a controlled manner using this setup.

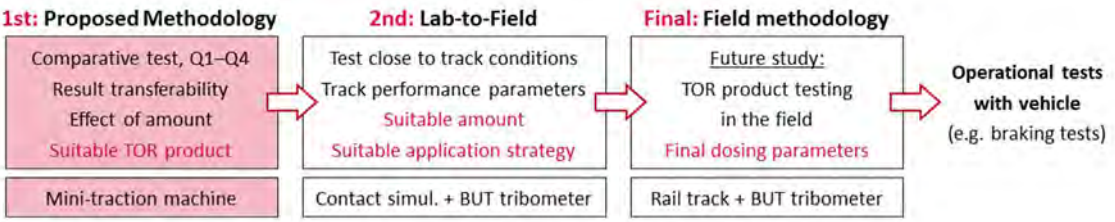

Fig. 28 Development stages of the TOR product testing methodology [151].

Fig. 28 illustrates how this new approach is linked to the methodology proposed in Article II. If the methodology introduced in Article II represents the initial step for assessing the performance of TOR products, the facility and track-side tribometer represent the second step, providing a more realistic but still controllable setup. The third step, to be carried out in future work, will involve validation through full-scale field tests. The final step will be operational tests with a vehicle on a real track, which would allow the inclusion of noise mitigation as an additional performance category in Fig. 27.

A possible addition for further development is the implementation of optical methods. Several hypotheses were formulated in this thesis regarding the interaction between water and TOR products. These hypotheses are based on the evaluation of friction curves, but the actual behaviour inside the contact remains unknown. A logical next step would therefore be to employ a tribometer equipped with optical interferometry to directly observe the formation of the lubricating film between TOR products and water, which could be, in the future, followed by the development of a portable fluorescence module that would enable similar observations on actual rails. Future progress may thus involve transferring established techniques from general tribology into wheel–rail applications and extending them from laboratory conditions to the field.

7.9 Evaluation of the Proposed Hypothesis

The three scientific questions raised in Section 3.2 were addressed through five hypotheses. Based on the results presented in Articles I–V, their evaluation can be summarised as follows:

H1.1: Under wet conditions, TOR lubricants are expected to cause over-lubrication because the presence of water disrupts the balance between the liquid and solid phases, shifting

it in favour of a stronger lubricating effect. Since water–oil mixtures are known to produce very low friction, and oil is the main component of TOR lubricants, a similarly low-friction response is likely for TOR lubricants in wet conditions. (II, III, IX)

- The results of Article I support this hypothesis, as water contamination of TOR lubricants consistently led to over-lubrication. However, the mechanism was more complex than initially assumed. While the disturbed ratio between the liquid and solid phases contributes to the effect in near-dry, starved conditions, the dominant influence arises from the interaction between water and the oil base, which together enhance the lubricating action of the liquid phase. Therefore, hypothesis H1.1 can be considered partially confirmed.

H1.2: For friction modifiers, the effect of water contamination is expected to depend on the amount of water. Small amounts of water may enhance lubrication by slowing evaporation of the base medium. In contrast, larger quantities are likely to disrupt film formation and result in higher and less stable friction. (II, VIII, X)

- Based on the results of Article I, this hypothesis was confirmed within the investigated range of operating conditions.

H2: Ambient humidity alone is expected to have only a minor effect on friction and, therefore, is unlikely to influence the performance of TOR lubricants significantly. A substantial change is expected when the dew point is reached, and water condenses on the rail surface. In this case, the condensed water can mix with TOR lubricants and cause over-lubrication. (II, III, VII, VIII, IX)

- Based on the observations and data presented in Article III, this hypothesis can be considered confirmed within the investigated range of operating conditions.

H3.1: In wet conditions, TOR lubricants are expected to influence RCF in a way similar to TOR hybrids. The only difference is that water is intentionally added in the latter, whereas in the former, it enters the contact as an unwanted contaminant. This combination is expected to promote severe RCF due to the coexistence of high friction and liquid-assisted crack propagation. (V)

- The hypothesis was not confirmed as formulated. The proposed mechanism, in which high friction combined with liquid-assisted crack propagation would drive RCF in a way similar to TOR hybrids, did not occur. Instead, the results presented in Article IV revealed a fundamentally different mechanism. Water amplified the lubricating effect of the TOR lubricant, reducing CoT to approximately 0.05. At such low friction, surface wear was effectively suppressed, and developing cracks were not removed by natural material loss. At the same time, water and oil entered opened cracks, where they promoted their growth through hydropressurisation and crack face

lubrication. This combined effect resulted in the deepest cracks observed across all tested conditions, reaching nearly 1 mm compared to tens of micrometres under TOR lubricant in dry conditions.

Nevertheless, the predicted outcome, that the combination of TOR lubricant and water promotes severe RCF, was confirmed, although through a different mechanism. Notably, this mechanism carries greater operational risk than the one originally assumed. High-friction-driven crack growth would be accompanied by visible surface wear, serving as a detectable warning sign. In contrast, the low-friction mechanism produces a rail surface that appears relatively undamaged while concealing a dense crack network beneath. This distinction has direct safety implications, as it limits the effectiveness of visual inspection methods.

In summary, based on Article IV, the hypothesis was not confirmed in terms of mechanism but confirmed in terms of outcome.

H3.2: When mixed with friction modifiers, oxides are expected to disrupt film formation, reducing the effectiveness of the product and increasing wear. In contrast, the presence of water may partially counteract this effect by helping to rebalance the liquid–solid ratio by slowing the evaporation of the base medium, thereby prolonging the lubricating effect. (X, XII)

- Based on the results of Article IV, the hypothesis can be considered partially confirmed. Regarding the first part, the presence of oxides led to less predictable FM performance and increased wear, which is consistent with the predicted outcome. However, the underlying mechanism differed from what was originally assumed. Rather than oxides chemically or compositionally disrupting the FM film, the effect was primarily mechanical: the oxide layer exhibited low shear strength and broke down non-uniformly, causing localised flaking that disrupted the FM film in an unpredictable manner. As a result, FM retentivity on oxidised specimens varied between tests, and no consistent trend could be identified.
- Regarding the second part, the role of water in prolonging the FM effect by slowing the evaporation of the base medium was confirmed on clean specimens, where retentivity consistently increased with water amounts. On oxidised specimens, a similar trend was observed in some tests, but the irregular breakdown of the oxide layer introduced additional variability that obscured the effect. Therefore, while the proposed mechanism of water counteracting the influence of oxides remains plausible and consistent with observations on clean surfaces, it could not be conclusively demonstrated on oxidised specimens due to the dominant and poorly controllable influence of oxide layer degradation.

8. Conclusions

Extensive research over the years has shown the many benefits of friction modifiers and top-of-rail lubricants, such as wear and noise mitigation due to the effective friction control. The knowledge gap highlighted at the beginning of this thesis lies in the fact that while top-of-rail products were proven effective in clean contacts, their performance under contaminated conditions remains unknown. In reality, contamination of the rail head is inevitable, and it is reasonable to suppose that, as contaminants significantly influence friction, they would also have an impact on the effectiveness of top-of-rail products. Thus, this thesis aimed to describe the influence of environmental contamination on the performance of top-of-rail products.

The following contamination scenarios were found to be the most relevant: high air humidity, dew, precipitation and iron oxides. One friction modifier and two top-of-rail lubricants were selected for testing. All of them were commercial products used on the actual track with a history of testing in scientific publications from other authors. The following conclusions are structured around the three scientific questions formulated in Section 3.2. The detailed evaluation of the corresponding hypotheses was provided in Section 7.9.

The first scientific question asked how water contamination influences the ability of top-of-rail products to modify friction. The two product types responded in fundamentally different ways. For friction modifiers, the effect depended on the amount of water. Light moisture prolonged retentivity by slowing the evaporation of the base medium, and medium amounts of water caused a temporary drop of the coefficient of adhesion by up to 91% (Article I). However, large amounts washed the product from the surface entirely, and friction returned to dry contact levels. Once removed, water drove severe crack propagation and material loss. Even in cases where the friction modifier was not washed away, it was unable to counteract the effect of water on crack propagation, as compared to dry conditions, significantly deeper cracks were observed (Article IV).

For top-of-rail lubricants, water amplified the lubricating effect, reducing the coefficient of adhesion to values below 0.05 (Articles I and IV), a level insufficient for safe braking. At such low values, surface wear was virtually eliminated, with the wear rate dropping 25 times compared to dry unlubricated contact and 3 times compared to TOR lubrication in dry conditions (Article IV). While this may appear beneficial, it also means that developing cracks are no longer removed by natural material loss and can propagate freely. Their growth was further accelerated by water ingress, leading to liquid-assisted crack propagation through hydropressurisation and crack face lubrication. To illustrate the magnitude of this effect, while crack depths under both dry and TOR-lubricated conditions remained in the order of tens of micrometres, the addition of water caused them to reach up to 900 μm (Article IV). These cracks branched and coalesced into a dense network beneath a seemingly undamaged surface.

Friction modifiers in wet conditions also led to severe crack propagation. However, the significantly higher material loss meant that damaged material was continuously removed, making the surface degradation visible. For top-of-rail lubricants, the opposite was true: material loss was nearly 20 times lower (Article IV), yet the cracks penetrated deeper into the bulk, making the situation potentially more dangerous, as the damage accumulates hidden beneath the surface and may remain undetected until sudden failure occurs.

The work also revealed a lack of a standardised approach for evaluating TOR product performance. To address this, a novel benchmarking methodology based on creep-curve measurements was developed (Article II). The methodology classifies products into performance categories based on their ability to provide the desired friction-modifying effect, and introduces the over-lubrication factor, a metric that quantifies the balance between the desired product effect and the risk of over-lubrication. This methodology has since been transferred to a test facility with a real rail, and future work should extend it to include product redistribution mechanisms and optical observation of friction layer formation, with the long-term aim of establishing a unified testing methodology under real operational conditions.

The second scientific question focused on the effect of ambient humidity and dew on TOR lubricants. To address this question, the benchmarking methodology developed in Article II was applied, enabling a systematic evaluation of product performance under controlled environmental conditions. Humidity alone had only a minor effect. The situation changed when the dew point was reached, and water began to condense on the specimen surface. From this point, it was the presence of liquid water, not humidity itself, that governed the product behaviour: the over-lubrication factor decreased by 40%, and the normally positive slope of the creep curve turned negative (Article III). The most critical scenario occurred when a cold rail was simulated: up to 25 times more water condensed on pre-cooled specimens, the over-lubrication factor decreased by more than 60%, and the product dropped from the second-best to the second-worst performance class (Article III).

The third scientific question addressed how TOR products affect wear and rolling contact fatigue in the presence of oxide layers under wet conditions. The effects of water contamination on both product types were already discussed above. Regarding oxides, their direct influence on friction was limited, but their role in crack behaviour was significant. Oxidised specimens did not exhibit severe rolling contact fatigue, as oxide products sealed the cracks and prevented liquid ingress, effectively suppressing liquid-assisted crack propagation (Article IV). At the same time, it was found that oxidation itself can drive crack growth. Oxygen diffuses along grain boundaries, and the volumetric expansion of the oxide products generates internal stresses that facilitate crack propagation even in the absence of external mechanical loading (Article V). Thus, oxidation plays a dual role: it suppresses liquid-driven damage but may contribute to progressive material degradation over extended service periods.

The key takeaways for real-world railway operation are that applying friction modifiers in wet conditions is primarily a matter of cost, as their effect is quickly lost. In contrast, applying top-of-rail lubricants under the same conditions represents a safety risk. Consequently, the application of top-of-rail products should be adapted to environmental conditions, particularly precipitation and early-morning dew.

9. Publications & Outcomes

9.1 Publications Related to the Thesis Topic

- S. Skurka, R. Galas, M. Omasta, B. Wu, H. Ding, W.J. Wang, I. Krupka, M. Hartl, The performance of top-of-rail products under water contamination, Tribol Int 188 (2023). https://doi.org/10.1016/j.triboint.2023.108872. [150]
- R. Galas, S. Skurka, M. Valena, D. Kvarda, M. Omasta, H. Ding, Q. Lin, W. Wang, I. Krupka, M. Hartl, A benchmarking methodology for top-of-rail products, Tribol Int 189 (2023) 108910. https://doi.org/10.1016/j.triboint.2023.108910. [151]
- S. Skurka, R. Galas, M. Omasta, H. Ding, W.-J. Wang, I. Krupka, M. Hartl, Assessing the Performance of TOR Lubricants in Humid Environments and Under Dew Conditions, Tribol Lett 72 (2024) 90. https://doi.org/10.1007/s11249-024-01889-7. [152]
- S. Skurka, R. Galas, J. Li, H. Wang, M. Omasta, H. Ding, W. Wang, I. Krupka, M. Hartl, Performance of top-of-rail products under contaminated conditions with pre-existing cracks: Impacts on traction and surface damage, Wear 588 (2026) 206520. https://doi.org/10.1016/j.wear.2026.206520. [153]
- Skurka S, Li M, Wang H, Galas R, Omasta M, Ding H, et al. Inside RCF Crack: Oxidation as a Factor in Rail Damage – the submission system opens on 15 February 2026.

9.2 Other Publications

- D. Kvarda, S. Skurka, R. Galas, M. Omasta, L. Shi, H. Ding, W. Wang, I. Krupka, M. Hartl, The effect of top of rail lubricant composition on adhesion and rheological behaviour, Engineering Science and Technology, an International Journal 35 (2022) 101100. https://doi.org/10.1016/j.jestch.2022.101100. [58]
- R. Galas, M. Valena, T. Jordan, D. Kvarda, M. Omasta, S. Skurka, B. Wu, H. Ding, W. Wang, I. Krupka, M. Hartl, A benchmarking methodology for top-of-rail products: Carry distance and retentivity, Tribol Int 197 (2024) 109810. https://doi.org/10.1016/j.triboint.2024.109810. [193]

9.3 Scientific Conferences

- 48th Leeds-Lyon Symposium on Tribology, Tribology for a Sustainable and Resilient Future, 5–7 September 2023, University of Leeds, UK
- 3rd International Conference on Rail Transportation (ICRT), 7–9 August 2024, Shanghai, China
- 13th International Conference on Contact Mechanics and Wear of Rail/Wheel Systems (CM 2025), 22–26 September 2025, Tokyo, Japan

9.4 Scientific Mobilities

- Southwest Jiaotong University, Tribology Research Institute, State Key Laboratory of Rail Transit Vehicle System, Supervisor Prof. Wenjian Wang, March–August 2024, Chengdu, China
- Southwest Jiaotong University, Tribology Research Institute, State Key Laboratory of Rail Transit Vehicle System, Supervisor Prof. Wenjian Wang, May–August 2025, Chengdu, China

Literature

[1] European Commission, Report from the Commission to the European Parliament, the Council, the European Economic and Social Committee and the Committee of the Regions – Progress report on the implementation of the 2021–2027 Connecting Europe Facility for the years 2021–2024, Brussels, 2025. https://eur-lex.europa.eu/legal-content/EN/TXT/?uri=CELEX:52025DC0516 (accessed September 30, 2025).

[2] European Environment Agency, TERM 2022: Transport and Environment Reporting Mechanism, Copenhagen, 2023. https://www.eea.europa.eu/en/analysis/publications/transport-and-environment-report-2022 (accessed September 30, 2025).

[3] V. V. Krishna, S. Hossein-Nia, C. Casanueva, S. Stichel, Long term rail surface damage considering maintenance interventions, Wear 460–461 (2020). https://doi.org/10.1016/j.wear.2020.203462.

[4] D. Szablewski, J. LoPresti, T. Sultana, Testing of latest top-of-rail friction modification materials at FAST, Railway Track and Structures 111 (2015) 13.

[5] R.X. Wang, K. Zhou, J.Y. Yang, H.H. Ding, W.J. Wang, J. Guo, Q.Y. Liu, Effects of abrasive material and hardness of grinding wheel on rail grinding behaviors, Wear 454–455 (2020). https://doi.org/10.1016/j.wear.2020.203332.

[6] L. Niu, F. Yang, X. Deng, P. Zhang, G. Jing, W. Qiang, Y. Guo, An assessment method of rail corrugation based on wheel–rail vertical force and its application for rail grinding, J. Civ. Struct. Health Monit. 13 (2023) 1131–1150. https://doi.org/10.1007/s13349-023-00700-w.

[7] J. Han, Y. He, X. Xiao, X. Sheng, G. Zhao, X. Jin, Effect of Control Measures on Wheel/Rail Noise When the Vehicle Curves, Applied Sciences 7 (2017) 1144. https://doi.org/10.3390/app7111144.

[8] P.A. Meehan, X. Liu, Wheel squeal noise control under water-based friction modifiers based on instantaneous rolling contact mechanics, Wear 440–441 (2019) 203052. https://doi.org/10.1016/j.wear.2019.203052.

[9] Number of Europeans exposed to harmful noise pollution expected to increase — European Environment Agency, (n.d.). https://www.eea.europa.eu/highlights/number-of-europeans-exposed-to (accessed August 12, 2022).

[10] B. White, M. Watson, R. Lewis, A year-round analysis of railway station overruns due to low adhesion conditions, Proc. Inst. Mech. Eng. F J. Rail Rapid Transit 237 (2023) 458–469. https://doi.org/10.1177/09544097221117314.

[11] K. Allan, A sticky situation: managing rail adhesion - Railway Technology, (2024). https://www.railway-technology.com/features/a-sticky-situation-managing-rail-adhesion/ (accessed September 30, 2025).

[12] F.W. Carter, On the action of a locomotive driving wheel, Proceedings of the Royal Society of London. Series A, Containing Papers of a Mathematical and Physical Character 112 (1926) 151–157. https://doi.org/10.1098/rspa.1926.0100.

[13] J. Valehrach, P. Guziur, T. Riha, O. Plasek, Assessment of rail long-pitch corrugation, in: IOP Conf. Ser. Mater. Sci. Eng., Institute of Physics Publishing, 2017. https://doi.org/10.1088/1757-899X/236/1/012048.

[14] J. Lundberg, M. Rantatalo, C. Wanhainen, J. Casselgren, Measurements of friction coefficients between rails lubricated with a friction modifier and the wheels of an IORE locomotive during real working conditions, Wear 324–325 (2015) 109–117. https://doi.org/10.1016/j.wear.2014.12.002.

[15] O. Arias-Cuevas, Z. Li, R. Lewis, E.A. Gallardo-Hernández, Rolling–sliding laboratory tests of friction modifiers in dry and wet wheel–rail contacts, Wear 268 (2010) 543–551. https://doi.org/10.1016/j.wear.2009.09.015.

[16] Y. Zhu, Y. Lyu, U. Olofsson, Mapping the friction between railway wheels and rails focusing on environmental conditions, Wear 324–325 (2015) 122–128. https://doi.org/10.1016/j.wear.2014.12.028.

[17] B. White, R. Lewis, Simulation and understanding the wet-rail phenomenon using twin disc testing, Tribol. Int. 136 (2019) 475–486. https://doi.org/10.1016/j.triboint.2019.03.067.

[18] R. Galas, M. Omasta, L. Shi, H. Ding, W. Wang, I. Krupka, M. Hartl, The low adhesion problem: The effect of environmental conditions on adhesion in rolling-sliding contact, Tribol. Int. 151 (2020) 106521. https://doi.org/10.1016/j.triboint.2020.106521.

[19] W.J. Wang, H.F. Zhang, H.Y. Wang, Q.Y. Liu, M.H. Zhu, Study on the adhesion behavior of wheel/rail under oil, water and sanding conditions, Wear 271 (2011) 2693–2698. https://doi.org/10.1016/j.wear.2010.12.019.

[20] J. Kalousek, K.L. Johnson, An Investigation of Short Pitch Wheel and Rail Corrugations on the Vancouver Mass Transit System, Proc. Inst. Mech. Eng. F J. Rail Rapid Transit 206 (1992) 127–135. https://doi.org/10.1243/PIME_PROC_1992_206_226_02.

[21] Y. Pan, A. Radmehr, A. Tajaddini, M. Ahmadian, An Experimental Study of the Influence of the Amount of Top-Of-Rail Friction Modifiers on Traction, in: 2021 Joint Rail Conference, American Society of Mechanical Engineers, 2021. https://doi.org/10.1115/JRC2021-58433.

[22] Y. Suda, T. Iwasa, H. Komine, T. Fuji, K. Matsumoto, N. Ubukata, T. Nakai, M. Tanimoto, Y. Kishimoto, The basic study on friction control between wheel and rail (experiments by test machine and scale model vehicle), in: Proceedings of the Sixth International

Conference on Contact Mechanics and Wear of Rail/Wheel Systems (CM2003), Chalmers University of Technology, Gothenburg, 2003: pp. 343–348.

[23] X. Lu, T.W. Makowsky, D.T. Eadie, K. Oldknow, J. Xue, J. Jia, G. Li, X. Meng, Y. Xu, Y. Zhou, Friction management on a Chinese heavy haul coal line, Proc. Inst. Mech. Eng. F J. Rail Rapid Transit 226 (2012) 630–640. https://doi.org/10.1177/0954409712447170.

[24] M. Harmon, R. Lewis, Review of top of rail friction modifier tribology, Tribology - Materials, Surfaces and Interfaces 10 (2016) 150–162. https://doi.org/10.1080/17515831.2016.1216265.

[25] J.I. Egana, J. Vinolas, N. Gil-Negrete, Effect of liquid high positive friction (HPF) modifier on wheel-rail contact and rail corrugation, Tribol. Int. 38 (2005) 769–774. https://doi.org/10.1016/j.triboint.2004.11.006.

[26] Solid stick Friction Management for Prague Metro | L.B. Foster, (n.d.). https://lbfoster.com/news/solid-stick-friction-management-for-prague-metro (accessed November 24, 2025).

[27] X. Lu, J. Cotter, D.T. Eadie, Laboratory study of the tribological properties of friction modifier thin films for friction control at the wheel/rail interface, Wear 259 (2005) 1262–1269. https://doi.org/10.1016/j.wear.2005.01.018.

[28] C. Hardwick, S. Lewis, R. Lewis, The effect of friction modifiers on wheel/rail isolation at low axle loads, Proc. Inst. Mech. Eng. F J. Rail Rapid Transit 228 (2014) 768–783. https://doi.org/10.1177/0954409713488102.

[29] D.T. Eadie, J. Kalousek, K.C. Chiddick, The role of high positive friction (HPF) modifier in the control of short pitch corrugations and related phenomena, 2002.

[30] R. Lewis, E.A. Gallardo, J. Cotter, D.T. Eadie, The effect of friction modifiers on wheel/rail isolation, Wear 271 (2011) 71–77. https://doi.org/10.1016/j.wear.2010.10.036.

[31] J. Song, L. Shi, H. Ding, R. Galas, M. Omasta, W. Wang, J. Guo, Q. Liu, M. Hartl, Effects of solid friction modifier on friction and rolling contact fatigue damage of wheel-rail surfaces, Friction 10 (2022) 597–607. https://doi.org/10.1007/s40544-021-0521-5.

[32] R. Stock, L. Stanlake, C. Hardwick, M. Yu, D. Eadie, R. Lewis, Material concepts for top of rail friction management – Classification, characterisation and application, Wear 366–367 (2016) 225–232. https://doi.org/10.1016/j.wear.2016.05.028.

[33] R. Galas, D. Kvarda, M. Omasta, I. Krupka, M. Hartl, The role of constituents contained in water–based friction modifiers for top–of–rail application, Tribol. Int. 117 (2018) 87–97. https://doi.org/10.1016/j.triboint.2017.08.019.

[34] Chiddik Kelvin, Solid lubricants and friction modifiers for heavy loads and rail applications, 6,136,757 A, 2000.

[35] Cotter John, Friction control composition with enhanced retentivity, 6,759,372 B2, 2004.

[36] Trackside Top of Rail Friction Management | L.B. Foster, (n.d.). https://lbfoster.com/rail/friction-management/friction-management-products/top-of-rail-and-wheel-tread-friction-management/trackside-top-of-rail-friction-management#keltrack-water-based-friction-modifiers (accessed November 24, 2025).

[37] HeadLub®90 solid friction modifiers for rail head crown (TOR) - Sklenář Tribotechnika, (n.d.). https://www.sklenar-tribotechnika.cz/en/products/liquid-lubricants-and-friction-modifiers/for-mobile-applications/headlub90-solid-friction-modifiers-for-rail-head-crown-tor/ (accessed November 24, 2025).

[38] S.M. Zakharov, I.G. Goryacheva, A.P. Krasnov, A.S. Yudin, A. V. Morozov, D.P. Markov, A. V. Naumkin, A. V. Ovechkin, Tribological studies for developing friction modifiers in the wheel–rail system, Journal of Friction and Wear 36 (2015) 468–475. https://doi.org/10.3103/S1068366615060173.

[39] J. Kalousek, E. Magel, Modifying and managing friction, 93 (1997) 31-X4.

[40] M. Tomeoka, N. Kabe, M. Tanimoto, E. Miyauchi, M. Nakata, Friction control between wheel and rail by means of on-board lubrication, Wear 253 (2002) 124–129. https://doi.org/10.1016/S0043-1648(02)00091-1.

[41] S.L. Grassie, Rail corrugation: advances in measurement, understanding and treatment, Wear 258 (2005) 1224–1234. https://doi.org/10.1016/j.wear.2004.03.066.

[42] D.T. Eadie, M. Santoro, Top-of-rail friction control for curve noise mitigation and corrugation rate reduction, J. Sound Vib. 293 (2006) 747–757. https://doi.org/10.1016/j.jsv.2005.12.007.

[43] S.A. Khan, J. Lundberg, C. Stenström, Carry distance of top-of-rail friction modifiers, Proc. Inst. Mech. Eng. F J. Rail Rapid Transit 232 (2018) 2418–2430. https://doi.org/10.1177/0954409718772981.

[44] H. Chen, S. Fukagai, Y. Sone, T. Ban, A. Namura, Assessment of lubricant applied to wheel/rail interface in curves, Wear 314 (2014) 228–235. https://doi.org/10.1016/j.wear.2013.12.006.

[45] Z. Yang, P. Zhang, J. Moraal, Z. Li, An experimental study on the effects of friction modifiers on wheel–rail dynamic interactions with various angles of attack, Railway Engineering Science 30 (2022) 360–382. https://doi.org/10.1007/s40534-022-00285-y.

[46] A. Matsumoto, Y. Sato, H. Ohno, M. Tomeoka, K. Matsumoto, T. Ogino, M. Tanimoto, Y. Oka, M. Okano, Improvement of bogie curving performance by using friction modifier to rail/wheel interface Verification by full-scale rolling stand test, in: Wear, 2005: pp. 1201–1208. https://doi.org/10.1016/j.wear.2004.03.063.

[47] Z. Li, O. Arias-Cuevas, R. Lewis, E.A. Gallardo-Hernández, Rolling-sliding laboratory tests of friction modifiers in leaf contaminated wheel-rail contacts, Tribol. Lett. 33 (2009) 97–109. https://doi.org/10.1007/s11249-008-9393-3.

[48] B. Wu, L. Shi, J. Li, H. Ding, R. Galas, M. Omasta, J. Guo, W. Wang, M. Hartl, Rheological and tribological performance of top-of-rail friction modifiers with different viscosities, Wear 538–539 (2024). https://doi.org/10.1016/j.wear.2023.205229.

[49] R. Galas, M. Omasta, M. Klapka, S. Kaewunruen, I. Krupka, M. Hartl, Case study: The influence of oil-based friction modifier quantity on tram braking distance and noise, Tribology in Industry 39 (2017) 198–206. https://doi.org/10.24874/ti.2017.39.02.06.

[50] X. Liu, P.A. Meehan, Investigation of squeal noise under positive friction characteristics condition provided by friction modifiers, J. Sound Vib. 371 (2016) 393–405. https://doi.org/10.1016/j.jsv.2016.02.028.

[51] M.D. Evans, Z.S. Lee, M. Harmon, K. Six, A. Meierhofer, R. Stock, D.V. Gutsulyak, R. Lewis, Top-of-rail friction modifier performance assessment: High pressure torsion testing; creep force modelling and field validation, Wear 532–533 (2023) 205073. https://doi.org/10.1016/j.wear.2023.205073.

[52] A. Matsumoto, Y. Sato, H. Ono, Y. Wang, M. Yamamoto, M. Tanimoto, Y. Oka, Creep force characteristics between rail and wheel on scaled model, Wear 253 (2002) 199–203. https://doi.org/10.1016/S0043-1648(02)00100-X.

[53] J.-W. Seo, H.-K. Jun, S.-J. Kwon, D.-H. Lee, Effect of Friction Modifier on Rolling Contact Fatigue and Wear of Wheel and Rail Materials, Tribology Transactions 61 (2018) 19–30. https://doi.org/10.1080/10402004.2016.1271487.

[54] D.T. Eadie, D. Elvidge, K. Oldknow, R. Stock, P. Pointner, J. Kalousek, P. Klauser, The effects of top of rail friction modifier on wear and rolling contact fatigue: Full-scale rail–wheel test rig evaluation, analysis and modelling, Wear 265 (2008) 1222–1230. https://doi.org/10.1016/j.wear.2008.02.029.

[55] D.T. Eadie, M. Santoro, K. Oldknow, Y. Oka, Field studies of the effect of friction modifiers on short pitch corrugation generation in curves, Wear 265 (2008) 1212–1221. https://doi.org/10.1016/j.wear.2008.02.028.

[56] R. Stock, D.T. Eadie, D. Elvidge, K. Oldknow, Influencing rolling contact fatigue through top of rail friction modifier application – A full scale wheel–rail test rig study, Wear 271 (2011) 134–142. https://doi.org/10.1016/j.wear.2010.10.006.

[57] R. Galas, M. Omasta, I. Krupka, M. Hartl, Laboratory investigation of ability of oil-based friction modifiers to control adhesion at wheel-rail interface, Wear 368–369 (2016) 230–238. https://doi.org/10.1016/j.wear.2016.09.015.

[58] D. Kvarda, S. Skurka, R. Galas, M. Omasta, L. Shi, H. Ding, W. Wang, I. Krupka, M. Hartl, The effect of top of rail lubricant composition on adhesion and rheological behaviour, Engineering Science and Technology, an International Journal 35 (2022) 101100. https://doi.org/10.1016/j.jestch.2022.101100.

[59] M.A. Oomen, R. Bosman, P.M. Lugt, Characterization of Friction and Wear Behavior of Friction Modifiers used in Wheel-Rail Contacts, Int. J. Progn. Health Manag. 8 (2020) 22. https://doi.org/10.36001/ijphm.2017.v8i3.2663.

[60] J. Sanchez, J. Alberto Jaramillo, J.F. Santa, J.C. Sánchez, J.A. Jaramillo, J.F. Santa, A. Toro, TWIN-DISC ASSESSMENT OF THE EFFECT OF TOP-OF-RAIL FRICTION MODIFIERS ON THE TRIBOLOGICAL RESPONSE OF ER8-R370HT PAIRS FOR USE IN WHEEL-RAIL SYSTEMS, Rev. LatinAm. Metal. Mat 39 (2019) pp-pp. www.rlmm.orgwww.rlmm.org.

[61] D. V. Gutsulyak, L.J.E. Stanlake, H. Qi, Twin disc evaluation of third body materials in the wheel/rail interface, Tribology - Materials, Surfaces and Interfaces 15 (2021) 115–126. https://doi.org/10.1080/17515831.2020.1829878.

[62] C. Hardwick, R. Lewis, R. Stock, The effects of friction management materials on rail with pre existing rcf surface damage, Wear 384–385 (2017) 50–60. https://doi.org/10.1016/j.wear.2017.04.016.

[63] S. Maya-Johnson, J. Felipe Santa, A. Toro, Dry and lubricated wear of rail steel under rolling contact fatigue - Wear mechanisms and crack growth, Wear 380–381 (2017) 240–250. https://doi.org/10.1016/j.wear.2017.03.025.

[64] Y.L. Xavier, A.B. Rezende, S.T. Fonseca, E. Jun Kina, P.R. Mei, Friction Modifier Performance in Twin-Disk Tests Using Disks of the Same Microstructure and Hardness, Tribology Transactions 68 (2025) 1–11. https://doi.org/10.1080/10402004.2024.2429716.

[65] U. Fingberg, A model of wheel-rail squealing noise, J. Sound Vib. 143 (1990) 365–377. https://doi.org/10.1016/0022-460X(90)90729-J.

[66] N. Hoffmann, L. Gaul, Effects of damping on mode-coupling instability in friction induced oscillations, ZAMM - Journal of Applied Mathematics and Mechanics / Zeitschrift Für Angewandte Mathematik Und Mechanik 83 (2003) 524–534. https://doi.org/10.1002/zamm.200310022.

[67] N. Hoffmann, M. Fischer, R. Allgaier, L. Gaul, A minimal model for studying properties of the mode-coupling type instability in friction induced oscillations, Mech. Res. Commun. 29 (2002) 197–205. https://doi.org/10.1016/S0093-6413(02)00254-9.

[68] R. Lewis, U. Olofsson, Wheel-rail interface handbook, CRC Press, Cambridge: Boca Raton: Woodhead, 2009.

[69] U. Olofsson, Y. Lyu, Open System Tribology in the Wheel–Rail Contact—A Literature Review, Appl. Mech. Rev. 69 (2017) 1–10. https://doi.org/10.1115/1.4038229.

[70] K. Oldknow, D.T. Eadie, R. Stock, The influence of precipitation and friction control agents on forces at the wheel/rail interface in heavy haul railways, Proc. Inst. Mech. Eng. F J. Rail Rapid Transit 227 (2013) 86–93. https://doi.org/10.1177/0954409712452240.

[71] R. Lewis, E.A. Gallardo-Hernandez, T. Hilton, T. Armitage, Effect of oil and water mixtures on adhesion in the wheel/rail contact, Proc. Inst. Mech. Eng. F J. Rail Rapid Transit 223 (2009) 275–283. https://doi.org/10.1243/09544097JRRT248.

[72] T. Nakahara, K.-S. Baek, H. Chen, M. Ishida, Relationship between surface oxide layer and transient traction characteristics for two steel rollers under unlubricated and

water lubricated conditions, Wear 271 (2011) 25–31. https://doi.org/10.1016/j.wear.2010.10.030.

[73] K.-S. Baek, K. Kyogoku, T. Nakahara, An experimental investigation of transient traction characteristics in rolling–sliding wheel/rail contacts under dry–wet conditions, Wear 263 (2007) 169–179. https://doi.org/10.1016/j.wear.2007.01.067.

[74] W.J. Wang, P. Shen, J.H. Song, J. Guo, Q.Y. Liu, X.S. Jin, Experimental study on adhesion behavior of wheel/rail under dry and water conditions, Wear 271 (2011) 2699–2705. https://doi.org/10.1016/j.wear.2011.01.070.

[75] W.J. Wang, H. Wang, H.Y. Wang, J. Guo, Q.Y. Liu, M.H. Zhu, X.S. Jin, Sub-scale simulation and measurement of railroad wheel/rail adhesion under dry and wet conditions, Wear 302 (2013) 1461–1467. https://doi.org/10.1016/j.wear.2012.12.014.

[76] W.J. Wang, T.F. Liu, H.Y. Wang, Q.Y. Liu, M.H. Zhu, X.S. Jin, Influence of friction modifiers on improving adhesion and surface damage of wheel/rail under low adhesion conditions, Tribol. Int. 75 (2014) 16–23. https://doi.org/10.1016/j.triboint.2014.03.008.

[77] K. Ishizaka, S.R. Lewis, R. Lewis, The low adhesion problem due to leaf contamination in the wheel/rail contact: Bonding and low adhesion mechanisms, Wear 378–379 (2017) 183–197. https://doi.org/10.1016/j.wear.2017.02.044.

[78] B. White, R. Kempka, P. Laity, C. Holland, K. Six, G. Trummer, L. Buckley-Johnstone, R. Lewis, Iron Oxide and Water Paste Rheology and Its Effect on Low Adhesion in the Wheel/Rail Interface, Tribol. Lett. 70 (2022) 8. https://doi.org/10.1007/s11249-021-01549-0.

[79] C. Wang, L.B. Shi, H.H. Ding, W.J. Wang, R. Galas, J. Guo, Q.Y. Liu, Z.R. Zhou, M. Omasta, Adhesion and damage characteristics of wheel/rail using different mineral particles as adhesion enhancers, Wear 477 (2021). https://doi.org/10.1016/j.wear.2021.203796.

[80] R. Lewis, R.S. Dwyer-Joyce, J. Lewis, Disc machine study of contact isolation during railway track sanding, Proc. Inst. Mech. Eng. F J. Rail Rapid Transit 217 (2003) 11–24. https://doi.org/10.1243/095440903762727311.

[81] O. Arias-Cuevas, Z. Li, R. Lewis, Investigating the lubricity and electrical insulation caused by sanding in dry wheel-rail contacts, Tribol. Lett. 37 (2010) 623–635. https://doi.org/10.1007/s11249-009-9560-1.

[82] R. Lewis, R.S. Dwyer-Joyce, Wear at the wheel/rail interface when sanding is used to increase adhesion, Proc. Inst. Mech. Eng. F J. Rail Rapid Transit 220 (2006) 29–41. https://doi.org/10.1243/095440905x33260.

[83] X. Cao, W.L. Huang, C.G. He, J.F. Peng, J. Guo, W.J. Wang, Q.Y. Liu, M.H. Zhu, The effect of alumina particle on improving adhesion and wear damage of wheel/rail under wet conditions, Wear 348–349 (2016) 98–115. https://doi.org/10.1016/j.wear.2015.12.004.

[84] L.B. Shi, Q. Li, D. Kvarda, R. Galas, M. Omasta, W.J. Wang, J. Guo, Q.Y. Liu, Study on the wheel/rail adhesion restoration and damage evolution in the single application of alumina particles, Wear 426–427 (2019) 1807–1819. https://doi.org/10.1016/j.wear.2019.01.021.

[85] L.B. Shi, C. Wang, H.H. Ding, D. Kvarda, R. Galas, M. Omasta, W.J. Wang, Q.Y. Liu, M. Hartl, Laboratory investigation on the particle-size effects in railway sanding: Comparisons between standard sand and its micro fragments, Tribol. Int. 146 (2020). https://doi.org/10.1016/j.triboint.2020.106259.

[86] M. Watson, B. White, J. Lanigan, T. Slatter, R. Lewis, The composition and friction-reducing properties of leaf layers, Proceedings of the Royal Society A: Mathematical, Physical and Engineering Sciences 476 (2020) 20200057. https://doi.org/10.1098/rspa.2020.0057.

[87] P.M. Cann, The “leaves on the line” problem - A study of leaf residue film formation and lubricity under laboratory test conditions, Tribol. Lett. 24 (2006) 151–158. https://doi.org/10.1007/s11249-006-9152-2.

[88] K. Ishizaka, S.R. Lewis, D. Hammond, R. Lewis, Chemistry of black leaf films synthesised using rail steels and their influence on the low friction mechanism, RSC Adv. 8 (2018) 32506–32521. https://doi.org/10.1039/C8RA06080K.

[89] R. Lewis, G. Trummer, K. Six, J. Stow, H. Alturbeh, B. Bryce, P. Shackleton, L.B. Johnstone, Leaves on the line: Characterising leaf based low adhesion on railway rails, Tribol. Int. 185 (2023) 108529. https://doi.org/10.1016/j.triboint.2023.108529.

[90] N. Kumar, A. Radmehr, M. Ahmadian, Experimental Evaluation of Effect of Leaves on Railroad Tracks in Loss of Braking, Machines 12 (2024). https://doi.org/10.3390/machines12050301.

[91] J. Jaffe, B. White, J. Lanigan, R. Lewis, “A novel methodology for developing ultra-low adhesion leaf layers on a full-scale wheel/rail rig,” Proc. Inst. Mech. Eng. F J. Rail Rapid Transit 238 (2024) 736–741. https://doi.org/10.1177/09544097231216521.

[92] O. Arias-Cuevas, Z. Li, R. Lewis, A laboratory investigation on the influence of the particle size and slip during sanding on the adhesion and wear in the wheel–rail contact, Wear 271 (2011) 14–24. https://doi.org/10.1016/j.wear.2010.10.050.

[93] H. Chen, T. Furuya, S. Fukagai, S. Saga, J. Ikoma, K. Kimura, J. Suzumura, Wheel slip/Slide and low adhesion caused by fallen leaves, Wear 446–447 (2020) 203187. https://doi.org/10.1016/j.wear.2020.203187.

[94] O. Arias-Cuevas, Z. Li, Field investigations into the adhesion recovery in leaf-contaminated wheel–rail contacts with locomotive sanders, Proc. Inst. Mech. Eng. F J. Rail Rapid Transit 225 (2011) 443–456. https://doi.org/10.1177/2041301710394921.

[95] Y. Zhu, U. Olofsson, R. Nilsson, A field test study of leaf contamination on railhead surfaces, Proc. Inst. Mech. Eng. F J. Rail Rapid Transit 228 (2014) 71–84. https://doi.org/10.1177/0954409712464860.

[96] M. Omasta, M. Machatka, D. Smejkal, M. Hartl, I. Křupka, Influence of sanding parameters on adhesion recovery in contaminated wheel–rail contact, Wear 322–323 (2015) 218–225. https://doi.org/10.1016/j.wear.2014.11.017.

[97] K.M. Briggs, J.A. Smethurst, W. Powrie, A.S. O'Brien, D.J.E. Butcher, Managing the extent of tree removal from railway earthwork slopes, Ecol. Eng. 61 (2013) 690–696. https://doi.org/10.1016/j.ecoleng.2012.12.076.

[98] L.B. Shi, L. Ma, J. Guo, Q.Y. Liu, Z.R. Zhou, W.J. Wang, Influence of low temperature environment on the adhesion characteristics of wheel-rail contact, Tribol. Int. 127 (2018) 59–68. https://doi.org/10.1016/j.triboint.2018.05.037.

[99] D. Fletcher, A new two-dimensional model of rolling–sliding contact creep curves for a range of lubrication types, Proceedings of the Institution of Mechanical Engineers, Part J: Journal of Engineering Tribology 227 (2013) 529–537. https://doi.org/10.1177/1350650112465694.

[100] H. Wang, W. Wang, Q. Liu, Numerical and experimental investigation on adhesion characteristic of wheel/rail under the third body condition, Proceedings of the Institution of Mechanical Engineers, Part J: Journal of Engineering Tribology 230 (2016) 111–118. https://doi.org/10.1177/1350650115591232.

[101] H. Chen, T. Ban, M. Ishida, T. Nakahara, Experimental investigation of influential factors on adhesion between wheel and rail under wet conditions, Wear 265 (2008) 1504–1511. https://doi.org/10.1016/j.wear.2008.02.034.

[102] B. Wu, Z. Wen, H. Wang, X. Jin, Numerical analysis on wheel/rail adhesion under mixed contamination of oil and water with surface roughness, Wear 314 (2014) 140–147. https://doi.org/10.1016/j.wear.2013.11.041.

[103] H. Chen, T. Ban, M. Ishida, T. Nakahara, Adhesion between rail/wheel under water lubricated contact, Wear 253 (2002) 75–81. https://doi.org/https://doi.org/10.1016/S0043-1648(02)00085-6.

[104] H. Chen, M. Ishida, A. Namura, K.-S. Baek, T. Nakahara, B. Leban, M. Pau, Estimation of wheel/rail adhesion coefficient under wet condition with measured boundary friction coefficient and real contact area, Wear 271 (2011) 32–39. https://doi.org/10.1016/j.wear.2010.10.022.

[105] H. Chen, T. Ban, M. Ishida, T. Nakahara, Effect of water temperature on the adhesion between rail and wheel, Proceedings of the Institution of Mechanical Engineers, Part J: Journal of Engineering Tribology 220 (2006) 571–579. https://doi.org/10.1243/13506501JET75.

[106] H. Chen, A. Yoshimura, T. Ohyama, Numerical analysis for the influence of water film on adhesion between rail and wheel, Proceedings of the Institution of Mechanical

Engineers, Part J: Journal of Engineering Tribology 212 (1998) 359–368. https://doi.org/10.1243/1350650981542173.

[107] Y. Zhu, U. Olofsson, K. Persson, Investigation of factors influencing wheel–rail adhesion using a mini-traction machine, Wear 292–293 (2012) 218–231. https://doi.org/10.1016/j.wear.2012.05.006.

[108] B. Wu, Z. Wen, T. Wu, X. Jin, Analysis on thermal effect on high-speed wheel/rail adhesion under interfacial contamination using a three-dimensional model with surface roughness, Wear 366–367 (2016) 95–104. https://doi.org/10.1016/j.wear.2016.06.002.

[109] H. Chen, A. Namura, M. Ishida, T. Nakahara, Influence of axle load on wheel/rail adhesion under wet conditions in consideration of running speed and surface roughness, Wear 366–367 (2016) 303–309. https://doi.org/10.1016/j.wear.2016.05.012.

[110] B. Wu, G. Xiao, B. An, T. Wu, Q. Shen, Numerical study of wheel/rail dynamic interactions for high-speed rail vehicles under low adhesion conditions during traction, Eng. Fail. Anal. 137 (2022). https://doi.org/10.1016/j.engfailanal.2022.106266.

[111] X. Wang, H. Hua, K. Peng, B. Wu, Z. Tang, Study on the wheel/rail adhesion characteristic under water and oil conditions by using mixed lubrication model, Wear 544–545 (2024). https://doi.org/10.1016/j.wear.2024.205279.

[112] G. Trummer, L.E. Buckley-Johnstone, P. Voltr, A. Meierhofer, R. Lewis, K. Six, Wheel-rail creep force model for predicting water induced low adhesion phenomena, Tribol. Int. 109 (2017) 409–415. https://doi.org/10.1016/j.triboint.2016.12.056.

[113] D. Kvarda, R. Galas, M. Omasta, L. Shi, H. Ding, W. Wang, I. Krupka, M. Hartl, Asperity-based model for prediction of traction in water-contaminated wheel-rail contact, Tribol. Int. 157 (2021) 106900. https://doi.org/10.1016/j.triboint.2021.106900.

[114] E.A. Gallardo-Hernandez, R. Lewis, Twin disc assessment of wheel/rail adhesion, Wear 265 (2008) 1309–1316. https://doi.org/10.1016/j.wear.2008.03.020.

[115] L.E. Buckley-Johnstone, G. Trummer, P. Voltr, K. Six, R. Lewis, Full-scale testing of low adhesion effects with small amounts of water in the wheel/rail interface, Tribol. Int. 141 (2020). https://doi.org/10.1016/j.triboint.2019.105907.

[116] M. Broster, C. Pritchard, D.A. Smith, Wheel/rail adhesion: its relation to rail contamination on british railways, Wear 29 (1974) 309–321. https://doi.org/10.1016/0043-1648(74)90017-9.

[117] T.M. Beagley, The Rheological Properties of Solid Rail Contaminants and their Effect on Wheel/Rail Adhesion, Proceedings of the Institution of Mechanical Engineers 190 (1976) 419–428. https://doi.org/10.1243/PIME_PROC_1976_190_044_02.

[118] T.M. Beagley, C. Pritchard, Wheel/rail adhesion — the overriding influence of water, Wear 35 (1975) 299–313. https://doi.org/10.1016/0043-1648(75)90078-2.

[119] D. Kvarda, A. Meierhofer, K. Six, Testing and modelling of transient adhesion phenomena in rolling-sliding contacts, Friction 12 (2024) 1016–1027. https://doi.org/10.1007/s40544-023-0825-8.

[120] C. Hardwick, R. Lewis, U. Olofsson, Low adhesion due to oxide formation in the presence of salt, Proc. Inst. Mech. Eng. F J. Rail Rapid Transit 228 (2014) 887–897. https://doi.org/10.1177/0954409713495666.

[121] B. White, R. Nilsson, U. Olofsson, A. Arnall, M. Evans, T. Armitage, J. Fisk, D. Fletcher, R. Lewis, Effect of the presence of moisture at the wheel–rail interface during dew and damp conditions, Proc. Inst. Mech. Eng. F J. Rail Rapid Transit 232 (2018) 979–989. https://doi.org/10.1177/0954409717706251.

[122] M. Ishida, T. Nakahara, Derailment Accident in Hibiya Line and Tribology, Journal-Japanese Society of Tribologists 46 (2001) 548–555.

[123] S.R. Lewis, R. Lewis, U. Olofsson, D.T. Eadie, J. Cotter, X. Lu, Effect of humidity, temperature and railhead contamination on the performance of friction modifiers: Pin-on-disk study, Proc. Inst. Mech. Eng. F J. Rail Rapid Transit 227 (2013) 115–127. https://doi.org/10.1177/0954409712452239.

[124] U. Olofsson, K. Sundvall, Influence of leaf, humidity and applied lubrication on friction in the wheel-rail contact: Pin-on-disc experiments, Proc. Inst. Mech. Eng. F J. Rail Rapid Transit 218 (2004) 235–242. https://doi.org/10.1243/0954409042389364.

[125] M.O. Folorunso, R. Lewis, J.L. Lanigan, Effects of temperature and humidity on railhead friction levels, Proc. Inst. Mech. Eng. F J. Rail Rapid Transit 237 (2023) 1009–1024. https://doi.org/10.1177/09544097221148236.

[126] C. He, P. Zhang, G. Zou, Y. Gan, R. Ye, P. Li, J. Liu, Experimental Investigation of the Wear and Damage of CL60 Wheel Material in a Humid Hot Environment, J. Mater. Eng. Perform. 32 (2023) 3500–3514. https://doi.org/10.1007/s11665-022-07338-7.

[127] M. xue Shen, J. qiang Li, L. Li, S. xin Li, C. ying Ma, Adhesion and Damage Behaviour of Wheel–Rail Rolling–Sliding Contact Suffering Intermittent Airflow with Different Humidities and Ambient Temperatures, Tribol. Lett. 72 (2024). https://doi.org/10.1007/s11249-023-01817-1.

[128] K. jie Rong, Y. long Xiao, M. xue Shen, H. ping Zhao, W.J. Wang, G. yao Xiong, Influence of ambient humidity on the adhesion and damage behavior of wheel–rail interface under hot weather condition, Wear 486–487 (2021). https://doi.org/10.1016/j.wear.2021.204091.

[129] W.Y.H. Liew, Effect of relative humidity on the unlubricated wear of metals, Wear 260 (2006) 720–727. https://doi.org/10.1016/j.wear.2005.04.011.

[130] T.M. Beagley, I.J. McEwen, C. Pritchard, Wheel/rail adhesion — the influence of railhead debris, Wear 33 (1975) 141–152. https://doi.org/10.1016/0043-1648(75)90230-6.

[131] Y. Sone, J. Suzumura, T. Ban, F. Aoki, M. Ishida, Possibility of in situ spectroscopic analysis for iron rust on the running band of rail, Wear 265 (2008) 1396–1401. https://doi.org/10.1016/j.wear.2008.02.027.

[132] J. Suzumura, Y. Sone, A. Ishizaki, D. Yamashita, Y. Nakajima, M. Ishida, In situ X-ray analytical study on the alteration process of iron oxide layers at the railhead surface while under railway traffic, Wear 271 (2011) 47–53. https://doi.org/10.1016/j.wear.2010.10.054.

[133] Y. Zhu, U. Olofsson, H. Chen, Friction between wheel and rail: A pin-on-disc study of environmental conditions and iron oxides, Tribol. Lett. 52 (2013) 327–339. https://doi.org/10.1007/s11249-013-0220-0.

[134] Y. Zhu, X. Chen, W. Wang, H. Yang, A study on iron oxides and surface roughness in dry and wet wheel-rail contacts, Wear 328–329 (2015) 241–248. https://doi.org/10.1016/j.wear.2015.02.025.

[135] Y. Lyu, Y. Zhu, U. Olofsson, Wear between wheel and rail: A pin-on-disc study of environmental conditions and iron oxides, Wear 328–329 (2015) 277–285. https://doi.org/10.1016/j.wear.2015.02.057.

[136] Y. Zhu, H. Yang, W. Wang, Twin-disc tests of iron oxides in dry and wet wheel–rail contacts, Proc. Inst. Mech. Eng. F J. Rail Rapid Transit 230 (2016) 1066–1076. https://doi.org/10.1177/0954409715575093.

[137] T.F.J. Quinn, Oxidational wear modelling Part III. The effects of speed and elevated temperatures, Wear 216 (1998) 262–275. https://doi.org/10.1016/S0043-1648(98)00137-9.

[138] T.F.J. Quinn, The oxidational wear of low alloy steels, Tribol. Int. 35 (2002) 691–715. https://doi.org/10.1016/S0301-679X(02)00039-7.

[139] P. Dillmann, F. Mazaudier, S. Hœrlé, Advances in understanding atmospheric corrosion of iron. I. Rust characterisation of ancient ferrous artefacts exposed to indoor atmospheric corrosion, Corros. Sci. 46 (2004) 1401–1429. https://doi.org/10.1016/j.corsci.2003.09.027.

[140] T. Kamimura, S. Hara, H. Miyuki, M. Yamashita, H. Uchida, Composition and protective ability of rust layer formed on weathering steel exposed to various environments, Corros. Sci. 48 (2006) 2799–2812. https://doi.org/10.1016/j.corsci.2005.10.004.

[141] D. de la Fuente, I. Díaz, J. Simancas, B. Chico, M. Morcillo, Long-term atmospheric corrosion of mild steel, Corros. Sci. 53 (2011) 604–617. https://doi.org/10.1016/j.corsci.2010.10.007.

[142] D. Godfrey, Iron oxides and rust (hydrated iron oxides) in tribology, Tribology & Lubrication Technology 55 (1999) 33.

[143] R. Kempka, R. Falconer, D. Gutsulyak, R. Lewis, Effects of oxide and water on friction of rail steel–new test method and friction mapping, Tribology - Materials, Surfaces and Interfaces 15 (2021) 80–91. https://doi.org/10.1080/17515831.2020.1765611.

[144] R. Lewis, U. Olofsson, Mapping rail wear regimes and transitions, Wear 257 (2004) 721–729. https://doi.org/10.1016/j.wear.2004.03.019.

[145] D.T. Eadie, M. Santoro, J. Kalousek, Railway noise and the effect of top of rail liquid friction modifiers: changes in sound and vibration spectral distributions in curves, Wear 258 (2005) 1148–1155. https://doi.org/10.1016/j.wear.2004.03.061.

[146] J.X. Li, B.N. Wu, H.H. Ding, R. Galas, M. Omasta, Z.F. Wen, J. Guo, W.J. Wang, Wear and damage behaviours of wheel and rail materials: Effects of friction modifier and environmental temperature, Wear 523 (2023). https://doi.org/10.1016/j.wear.2023.204796.

[147] Y.A. Areiza, S.I. Garcés, J.F. Santa, G. Vargas, A. Toro, Field measurement of coefficient of friction in rails using a hand-pushed tribometer, Tribol. Int. 82 (2015) 274–279. https://doi.org/10.1016/j.triboint.2014.08.009.

[148] U. Olofsson, T. Telliskivi, Wear, plastic deformation and friction of two rail steels-a full-scale test and a laboratory study, 2003.

[149] T.P. Leso, C.W. Siyasiya, R.J. Mostert, J. Moema, Study of rolling contact fatigue, rolling and sliding wear of class B wheel steels against R350HT and R260 rail steels under dry contact conditions using the twin disc setup, Tribol. Int. 174 (2022). https://doi.org/10.1016/j.triboint.2022.107711.

[150] S. Skurka, R. Galas, M. Omasta, B. Wu, H. Ding, W.J. Wang, I. Krupka, M. Hartl, The performance of top-of-rail products under water contamination, Tribol. Int. 188 (2023). https://doi.org/10.1016/j.triboint.2023.108872.

[151] R. Galas, S. Skurka, M. Valena, D. Kvarda, M. Omasta, H. Ding, Q. Lin, W. Wang, I. Krupka, M. Hartl, A benchmarking methodology for top-of-rail products, Tribol. Int. 189 (2023) 108910. https://doi.org/10.1016/j.triboint.2023.108910.

[152] S. Skurka, R. Galas, M. Omasta, H. Ding, W.-J. Wang, I. Krupka, M. Hartl, Assessing the Performance of TOR Lubricants in Humid Environments and Under Dew Conditions, Tribol. Lett. 72 (2024) 90. https://doi.org/10.1007/s11249-024-01889-7.

[153] S. Skurka, R. Galas, J. Li, H. Wang, M. Omasta, H. Ding, W. Wang, I. Krupka, M. Hartl, Performance of top-of-rail products under contaminated conditions with pre-existing cracks: Impacts on traction and surface damage, Wear 588 (2026) 206520. https://doi.org/10.1016/j.wear.2026.206520.

[154] Y. Kimura, K. Okada, Lubricating Properties of Oil-In-Water Emulsions, Tribology Transactions 32 (1989) 524–532. https://doi.org/10.1080/10402008908981921.

[155] N. Fujita, Y. Kimura, K. Kobayashi, Y. Amanuma, Y. Sodani, Estimation model of plate-out oil film in high-speed tandem cold rolling, J. Mater. Process. Technol. 219 (2015) 295–302. https://doi.org/10.1016/j.jmatprotec.2015.01.002.

[156] W.R.D. Wilson, Y. Sakaguchi, S.R. Schmid, A dynamic concentration model for lubrication with oil-in-water emulsions, Wear 161 (1993) 207–212. https://doi.org/10.1016/0043-1648(93)90471-W.

[157] T. Nakahara, T. Makino, K. Kyogoku, Observations of Liquid Droplet Behavior and Oil Film Formation in O/W Type Emulsion Lubrication, J. Tribol. 110 (1988) 348–353. https://doi.org/10.1115/1.3261630.

[158] J.J. Benner, F. Sadeghi, M.R. Hoeprich, M.C. Frank, Lubricating Properties of Water in Oil Emulsions, J. Tribol. 128 (2006) 296–311. https://doi.org/10.1115/1.2164464.

[159] Y.P. Chiu, An Analysis and Prediction of Lubricant Film Starvation in Rolling Contact Systems, A S L E Transactions 17 (1974) 22–35. https://doi.org/10.1080/05698197408981435.

[160] D. Zhu, G. Biresaw, S.J. Clark, T.J. Kasun, Elastohydrodynamic Lubrication With O/W Emulsions, J. Tribol. 116 (1994) 310–319. https://doi.org/10.1115/1.2927216.

[161] H. YANG, S.R. SCHMID, T.J. KASUN, R.A. REICH, Elastohydrodynamic Film Thickness and Tractions for Oil-in-Water Emulsions, Tribology Transactions 47 (2004) 123–129. https://doi.org/10.1080/05698190490278976.

[162] H. Liang, D. Guo, L. Ma, J. Luo, Investigation of film formation mechanism of oil-in-water (O/W) emulsions at high speeds, Tribol. Int. 109 (2017) 428–434. https://doi.org/10.1016/j.triboint.2017.01.006.

[163] X. Liu, J. Wang, L. Huang, J. Zhang, C. Xu, L. Tong, D. Guo, Direct observation of the impact of water droplets on oil replenishment in EHD lubricated contacts, Friction 10 (2022) 388–397. https://doi.org/10.1007/s40544-020-0466-0.

[164] F. Cyriac, P.M. Lugt, R. Bosman, Impact of Water on the Rheology of Lubricating Greases, Tribology Transactions 59 (2016) 679–689. https://doi.org/10.1080/10402004.2015.1107929.

[165] P.M.E. Cann, B. Damiens, A.A. Lubrecht, The transition between fully flooded and starved regimes in EHL, Tribol. Int. 37 (2004) 859–864. https://doi.org/10.1016/j.triboint.2004.05.005.

[166] B. Jacod, F. Pubilier, P.M. E. Cann, A.A. Lubrecht, An Analysis of Track Replenishment Mechanisms in the Starved Regime, in: 1999: pp. 483–492. https://doi.org/10.1016/S0167-8922(99)80069-8.

[167] F. Cyriac, P.M. Lugt, R. Bosman, C.H. Venner, Impact of Water on EHL Film Thickness of Lubricating Greases in Rolling Point Contacts, Tribol. Lett. 61 (2016) 23. https://doi.org/10.1007/s11249-016-0642-6.

[168] C.B. Hudedagaddi, A.G. Raghav, A.M. Tortora, D.H. Veeregowda, Water molecules influence the lubricity of greases and fuel, Wear 376–377 (2017) 831–835. https://doi.org/10.1016/j.wear.2017.02.002.

[169] M. Kaneta, K. Matsuda, K. Murakami, H. Nishikawa, A Possible Mechanism for Rail Dark Spot Defects, J. Tribol. 120 (1998) 304–309. https://doi.org/10.1115/1.2834426.

[170] Y. Murakami, M. Kaneta, H. Yatsuzuka, Analysis of Surface Crack Propagation in Lubricated Rolling Contact, A S L E Transactions 28 (1985) 60–68. https://doi.org/10.1080/05698198508981595.

[171] M. Kaneta, H. Yatsuzuka, Y. Murakami, Mechanism of Crack Growth in Lubricated Rolling/Sliding Contact, A S L E Transactions 28 (1985) 407–414. https://doi.org/10.1080/05698198508981637.

[172] A.F. Bower, The Influence of Crack Face Friction and Trapped Fluid on Surface Initiated Rolling Contact Fatigue Cracks, J. Tribol. 110 (1988) 704–711. https://doi.org/10.1115/1.3261717.

[173] S. BOGDAÑSKI, A rolling contact fatigue crack driven by squeeze fluid film, Fatigue Fract. Eng. Mater. Struct. 25 (2002) 1061–1071. https://doi.org/10.1046/j.1460-2695.2000.00563.x.

[174] I.I. Kudish, K.W. Burris, Modeling of surface and subsurface crack behavior under contact load in the presence of lubricant, 2004.

[175] F.F. Lyle, H.C. Burghard, Cracking of Low-Pressure Turbine Rotor Discs in U.S. Nuclear Power Plants, in: CORROSION 1982, NACE International, 1982: pp. 1–23. https://doi.org/10.5006/C1982-82216.

[176] S.J. Hudak, R.A. Page, Analysis of Oxide Wedging During Environment Assisted Crack Growth, Corrosion 39 (1983) 285–290. https://doi.org/10.5006/1.3581914.

[177] R. Jiang, P.A.S. Reed, Critical Assessment 21: Oxygen-assisted fatigue crack propagation in turbine disc superalloys, Materials Science and Technology 32 (2016) 401–406. https://doi.org/10.1080/02670836.2016.1148227.

[178] A.K. Vasudevan, R.E. Ricker, A.C. Miller, D. Kujawski, Fatigue crack tip corrosion processes and oxide induced closure, Materials Science and Engineering: A 861 (2022) 144383. https://doi.org/10.1016/j.msea.2022.144383.

[179] R. Jiang, S. Everitt, M. Lewandowski, N. Gao, P.A.S. Reed, Grain size effects in a Ni-based turbine disc alloy in the time and cycle dependent crack growth regimes, Int. J. Fatigue 62 (2014) 217–227. https://doi.org/10.1016/j.ijfatigue.2013.07.014.

[180] J. Gayda, R.V. Miner, Fatigue crack initiation and propagation in several nickel-base superalloys at 650°C, Int. J. Fatigue 5 (1983) 135–143. https://doi.org/10.1016/0142-1123(83)90026-9.

[181] R. Molins, G. Hochstetter, J.C. Chassaigne, E. Andrieu, Oxidation effects on the fatigue crack growth behaviour of alloy 718 at high temperature, Acta Mater. 45 (1997) 663–674. https://doi.org/10.1016/S1359-6454(96)00192-9.

[182] A. Karabela, L.G. Zhao, J. Tong, N.J. Simms, J.R. Nicholls, M.C. Hardy, Effects of cyclic stress and temperature on oxidation damage of a nickel-based superalloy, Materials Science and Engineering: A 528 (2011) 6194–6202. https://doi.org/10.1016/j.msea.2011.04.029.

[183] L. Ma, K.-M. Chang, Identification of SAGBO-induced damage zone ahead of crack tip to characterize sustained loading crack growth in alloy 783, Scr. Mater. 48 (2003) 1271–1276. https://doi.org/10.1016/S1359-6462(03)00049-6.

[184] L. Viskari, M. Hörnqvist, K.L. Moore, Y. Cao, K. Stiller, Intergranular crack tip oxidation in a Ni-base superalloy, Acta Mater. 61 (2013) 3630–3639. https://doi.org/10.1016/j.actamat.2013.02.050.

[185] H.S. Kitaguchi, H.Y. Li, H.E. Evans, R.G. Ding, I.P. Jones, G. Baxter, P. Bowen, Oxidation ahead of a crack tip in an advanced Ni-based superalloy, Acta Mater. 61 (2013) 1968–1981. https://doi.org/10.1016/j.actamat.2012.12.017.

[186] E. Andrieu, R. Molins, H. Ghonem, A. Pineau, Intergranular crack tip oxidation mechanism in a nickel-based superalloy, Materials Science and Engineering: A 154 (1992) 21–28. https://doi.org/10.1016/0921-5093(92)90358-8.

[187] A. Pineau, S.D. Antolovich, High temperature fatigue of nickel-base superalloys – A review with special emphasis on deformation modes and oxidation, Eng. Fail. Anal. 16 (2009) 2668–2697. https://doi.org/10.1016/j.engfailanal.2009.01.010.

[188] U. Krupp, W.M. Kane, C. Laird, C.J. McMahon, Brittle intergranular fracture of a Ni-base superalloy at high temperatures by dynamic embrittlement, Materials Science and Engineering: A 387–389 (2004) 409–413. https://doi.org/10.1016/j.msea.2004.05.053.

[189] J.A. Pfaendtner, C.J. McMahon Jr, Oxygen-induced intergranular cracking of a Ni-base alloy at elevated temperatures—an example of dynamic embrittlement, Acta Mater. 49 (2001) 3369–3377. https://doi.org/10.1016/S1359-6454(01)00005-2.

[190] D. Bika, C.J. McMahon, A model for dynamic embrittlement, Acta Metallurgica et Materialia 43 (1995) 1909–1916. https://doi.org/10.1016/0956-7151(94)00387-W.

[191] C.R. Shastry, J.J. Friel, H. Townsend, Sixteen-year atmospheric corrosion performance of weathering steels in marine, rural, and industrial environments, ASTM Special Technical Publication (1988) 5–15.

[192] S.J. Oh, D.C. Cook, H.E. Townsend, Atmospheric corrosion of different steels in marine, rural and industrial environments, Corros. Sci. 41 (1999) 1687–1702. https://doi.org/10.1016/S0010-938X(99)00005-0.

[193] R. Galas, M. Valena, T. Jordan, D. Kvarda, M. Omasta, S. Skurka, B. Wu, H. Ding, W. Wang, I. Krupka, M. Hartl, A benchmarking methodology for top-of-rail products: Carry distance and retentivity, Tribol. Int. 197 (2024) 109810. https://doi.org/10.1016/j.triboint.2024.109810.

[194] D.T. Eadie, K. Oldknow, M. Santoro, G. Kwan, M. Yu, X. Lu, Wayside gauge face lubrication: How much do we really understand?, Proc. Inst. Mech. Eng. F J. Rail Rapid Transit 227 (2013) 245–253. https://doi.org/10.1177/0954409712459306.

[195] G. Trummer, Z.S. Lee, R. Lewis, K. Six, Modelling of frictional conditions in the wheel–rail interface due to application of top-of-rail products, Lubricants 9 (2021). https://doi.org/10.3390/lubricants9100100.

[196] C. Hardwick, R. Lewis, D.T. Eadie, Wheel and rail wear—Understanding the effects of water and grease, Wear 314 (2014) 198–204. https://doi.org/10.1016/j.wear.2013.11.020.

[197] X. Song, S. Zhang, M. Xu, H. Ding, J. Guo, X. Zhao, H. Qi, Q. Liu, W. Wang, R. Lewis, Experimental investigation on dynamic adhesion characteristics of wheel-rail under various media conditions at a large slip ratio range, Wear 580–581 (2025) 206217. https://doi.org/10.1016/j.wear.2025.206217.

[198] CEN/TS 15427-2-2:2021. Railway applications - Wheel/Rail friction management - Part 2-2: Properties and Characteristics - Top of Rail materials, (2021).

[199] R. Lewis, P. Christoforou, W.J. Wang, A. Beagles, M. Burstow, S.R. Lewis, Investigation of the influence of rail hardness on the wear of rail and wheel materials under dry conditions (ICRI wear mapping project), Wear 430–431 (2019) 383–392. https://doi.org/10.1016/j.wear.2019.05.030.

[200] M. Harmon, J.F. Santa, J.A. Jaramillo, A. Toro, A. Beagles, R. Lewis, Evaluation of the coefficient of friction of rail in the field and laboratory using several devices, Tribology - Materials, Surfaces & Interfaces 14 (2020) 119–129. https://doi.org/10.1080/17515831.2020.1712111.

[201] M. Valena, M. Omasta, D. Kvarda, R. Galas, I. Krupka, M. Hartl, An approach for the creep-curve assessment using a new rail tribometer, Tribol. Int. 191 (2024) 109153. https://doi.org/10.1016/j.triboint.2023.109153.

List of Figures

List of Tables

List of Abbreviations

TOR	Top-of-Rail
WHO	World Health Organisation
EEA	European Environment Agency
SRR	Slide-to-Roll Ratio
MTM	Mini-Traction Machine
CoA	Coefficient of Adhesion
CoT	Coefficient of Traction
FM	Friction Modifier
TORL	Top-of-Rail Lubricant
RH	Relative Humidity
OLF	Over-Lubrication Factor
NLGI	National Lubricating Grease Institute
CoF	Coefficient of Friction
PT	Performance Test
OM	Optical Microscopy
CTZ	Critical Traction Zone
ITZ	Intermediate Traction Zone
RTZ	Retentivity Traction Zone
RCF	Rolling Contact Fatigue
SEM	Scanning Electron Microscopy
EDX	Energy Dispersive X-Ray
XRD	X-Ray Diffraction
UK	The United Kingdom

Declaration of Generative AI

During the preparation of this thesis, the Author used ChatGPT and Grammarly to improve the clarity and correctness of the English language. After using these tools/services, the Author reviewed and edited the content as needed and takes full responsibility for the content of the thesis.

Declaration on Published Articles

The appended publications are either published under open access or are included with the permission of the rights holder (*Elsevier*). As an author of the published works, I retain the right to include the articles in my thesis for non-commercial academic purposes, and all included articles are properly cited in this thesis.

Appendix

The appended section contains the publications as described in the thesis, arranged in the same order as referenced in the text, from Article I to Article V. As of today (*26 March 2026*), Article V is included in the version used for the corresponding conference contribution until its journal publication.

Tribology International 188 (2023) 108872

Contents lists available at ScienceDirect

Tribology International

journal homepage: www.elsevier.com/locate/triboint

The performance of top-of-rail products under water contamination

Simon Skurka [a,*], Radovan Galas [a], Milan Omasta [a], Bingnan Wu [b], Haohao Ding [b], Wen-Jian Wang [b], Ivan Krupka [a], Martin Hartl [a]

[a] Faculty of Mechanical Engineering, Brno University of Technology, Technicka 2896/2, 616 69 Brno, Czech Republic
[b] Tribology Research Institute, State Key Laboratory of Traction Power, Southwest Jiaotong University, Chengdu 610031, China

ARTICLE INFO

Keywords:
Wheel-rail tribology
Friction modification
Low adhesion
Water contamination

ABSTRACT

Top-of-rail products are commonly used for friction modification in wheel-rail contact. However, the effect of environmental conditions and contaminants on their performance remains unclear. In this study, three commercial top-of-rail products were contaminated by different amounts of water. The laboratory tribometer in ball-on-disc configuration was used to measure the coefficient of adhesion in contaminated contact. The results show that water influenced tested top-of-rail products significantly. A very low coefficient of adhesion occurred in tests with oil-based top-of-rail products suggesting that water could cause traction problems on the actual railway where friction modification is being used. Water-based top-of-rail products showed more resistance to water contamination.

1. Introduction

Friction modification presents a practical approach to dealing with high friction in railway transportation. Nowadays, top-of-rail (TOR) products are applied on railheads via trackside applicators or systems mounted on a train [1]. Initially, these products were used as solid sticks containing solid lubricants like graphite or molybdenum disulfide [2]. However, liquid-based products containing water [3] or oil with thickeners [4] as a base medium are often used. Dealing with friction is an important task to improve the energy efficiency of rail transportation and decrease maintenance costs. High friction causes rail corrugation [5] and is also the leading cause of excessive wear on both wheels and rail [6–9]. Also, friction in the wheel-rail contact and the shape of the traction curve contribute to noise pollution. According to WHO, the noise limit of 55 dB is harmful in case of long-term exposure. It is estimated that up to 113 million people in Europe (of which rail transport contributes approximately 20%) are exposed to traffic noise above this limit [10]. Various field and laboratory tests confirmed the ability of TOR products to reduce friction [11] and influence corresponding effects like wear [12–14], noise [15,16] and energy consumption [17].

On the other hand, maintaining a sufficient level of friction is required to transmit traction forces from wheel to rail to accelerate or stop the vehicle. The coefficient of adhesion (CoA) describes the effectivity of this transmission. Generally, CoA lower than 0.2 and 0.09 is considered insufficient for traction and braking, respectively [18]. Thus, TOR products often contain mineral or metal particles to secure sufficient CoA. A liquid base (water, oil or less often a combination of both) is included to carry these particles along the rail [4]. The performance of some TOR products, especially oil-based ones, strongly depends on the applied amount [19]. As shown in [20], excessive amounts of product could cause low CoA problems resulting in an extension of the braking distance. TOR products are developed and tested to reduce friction while maintaining a required level of CoA for traction/braking. This can be achieved only with a suitable composition of the product and its optimal dosing.

Both water and oil-based TOR products are commonly referred to as friction modifiers (FMs) in literature. However, the mechanism of friction modification differs significantly for both types. In the case of water-based TOR products, the base medium quickly evaporates after application, and solid particles mix with the third body layer on the rail surface, providing a shear displacement compensation mechanism [21]. On the other hand, oil-based TOR products do not dry up and rely on a mixed/boundary lubrication regime. Because the base medium stays liquid, these TOR products can be redistributed for longer distances than water-based ones. However, it also carries the risk of low CoA occurrence close to the application unit due to overdosing [20]. Following [19], this paper will refer to water-based TOR products as "friction modifiers" and oil-based TOR products as "TOR lubricants" for clarity.

As stated above, the performance of friction modifiers and TOR lubricants in dry and clean contact has been well examined. However,

* Corresponding author.
E-mail address: Simon.Skurka@vut.cz (S. Skurka).

https://doi.org/10.1016/j.triboint.2023.108872
Received 27 April 2023; Received in revised form 8 August 2023; Accepted 12 August 2023
Available online 21 August 2023

while the coefficient of friction in dry wheel-rail contact is usually between 0.5 and 0.6 [22], in contaminated contact, the friction decreases significantly, causing also drop in CoA. It is caused by third body layers naturally occurring on the rail surface and environmental contaminants [23]. Water is one of the most common environmental contaminants. It can be found on the track from rain, morning dew, or even leakage from passing vehicles. Several laboratory studies show that water can reduce the CoA under 0.2 [23–25] and even lower depending on quantity and temperature. Also, water forms a highly viscous mixture if combined with iron oxides, leading to a CoA of 0.05 or lower [24].

Although contamination of wheel-rail contact is practically inevitable in reality, very little is known about the interaction between contaminants and TOR products. In most studies, TOR products were tested only in laboratory-clean conditions without contamination, or the effect of contamination was not considered. Chen et al. compared the lubrication performance of several lubricants on dry and wet rails [25]. They showed that the reduction of lateral forces was greater on the wet rail for all tested lubricants. Lewis et al. tested the influence of air humidity on friction modifiers. They discovered that when exposed to air with a higher % of relative humidity, CoF reaches lower values than in less humid air [26]. This phenomenon could be explained by water condensation and contamination of friction modifiers. The case study [27] shows that the combined effect of water and oil can cause traction problems on the top of the railhead. As oil is the main component in TOR lubricants, a question arises as to if a similar phenomenon can happen when a TOR product is contaminated by water. TOR products usually maintain CoA sufficient for traction/braking thanks to the balance between base medium and solid particles. However, there is a possibility that if TOR products are contaminated with water, the balance will be disturbed, product performance will decrease, and the minimum required CoA will not be kept.

This study uses three commercial TOR products. Two of them are TOR lubricants, and one is a friction modifier. All CoA tests were conducted on a laboratory tribometer in a ball-on-disc configuration. On an actual railway, contamination by water can occur, resulting in an insufficient CoA level. The degree of the contamination can differ depending on the water source (dew, rain, leakage from passing trains). Therefore, all TOR products were tested in dry and wet conditions. Small and large amounts of water were applied. Also, single and continuous water application was tested to simulate different ways of contamination. This study aims to describe the influence of water and its amount on the TOR product performance in terms of CoA.

2. Material and methods

2.1. Test setup and specimens

A laboratory tribometer MTM (Mini-Traction Machine, PCS Instruments) in a ball-on-disc configuration was used for all tests, see Fig. 1. Technical norms specify the measuring procedure on this device. However, these norms are mainly focused on traction curve evaluation. Therefore, they are unsuitable for observation of CoA drop caused by contamination. Thus, a different approach previously used in papers [3,4] will be used in this study. The contact bodies were discs and balls of 46 mm and 19.05 mm in diameter, so the contact has a circular shape. Both specimens were made of AISI 52100 bearing steel with a Vickers macro-hardness of 800–920 HV and 720–780 HV for ball and disc. The bearing steel is not a typical rail material. However, higher hardness ensures stable conditions during experiments and better repeatability due to reduced wear compared to standard wheel/rail steel. The initial roughness of the surface of both specimens was Ra 0.01 μm; however, it grew to Ra 0.15 μm (ball) and Ra 0.3 μm (disc) after the initial wear-in and the following run-in.

Both specimens were loaded against each other and driven by independent servo motors so the required slide–roll ratio (SRR) could be achieved according to the given equation:

$$SRR = \frac{w_{ball} \bullet r_{ball} - w_{disc} \bullet r_{disc}}{w_{ball} \bullet r_{ball} + w_{disc} \bullet r_{disc}} \bullet 200\% \quad (1)$$

where w_{ball} and w_{disc} are angular speeds of specimens and r_{ball} and r_{disc} stands for its radii. The embedded sensor measures the normal force (N) with ± 0.3 N accuracy. Traction force (T) is calculated from the torque measured by the transducer attached to the disc shaft, so the adhesion coefficient (CoA) could be determined as follows:

$$CoA = \frac{N}{T} \quad (2)$$

Data from force sensors are acquired with a 1 Hz sampling frequency. However, this signal results from averaging a non-specified higher frequency input signal.

2.2. Tested TOR products and contaminants

Two commercial TOR lubricants (referred to as "TORL-A" and "TORL-B"; oil-based TOR products) and one friction modifier ("FM-A"; water-based TOR product) were used in this study. Essential information about the composition of both TOR lubricants can be read from datasheets, see Table 1.

Although water-based TOR products are meant to form a dry film after base medium evaporation, wet film lubrication occurs immediately after application. Thus FM-A was tested both before and after the evaporation of the base medium. Distilled water was used as a contaminant in all tests.

2.3. Wear-in, run-in and cleaning of specimens

Before any experiments, an initial 60-minute dry wear-in of specimens was conducted. This is because severe wear of contact surfaces occurs with a new pair of specimens. After 60 min of wear-in, the wear rate decreases significantly, and stable test conditions could be secured. According to Hertz's Theory, the diameter of the contact is calculated to be 0.2 mm for a new pair of specimens. However, due to wear and topography changes caused by the wear-in, the actual contact will differ from the theory, and the diameter will be higher. Please note that described 60-minute wear-in is performed only once at the beginning for

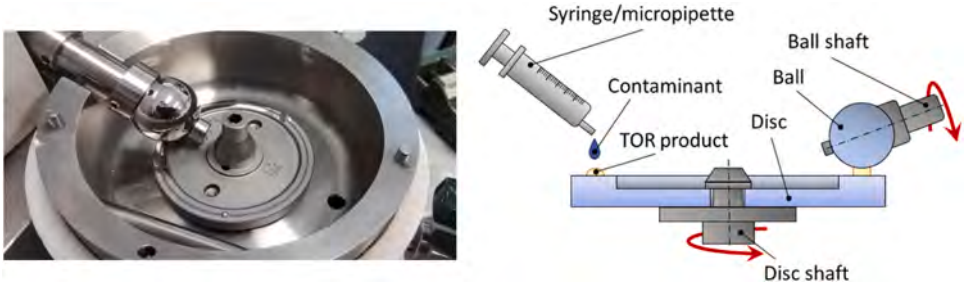

Fig. 1. Photo (left) and scheme (right) of the apparatus.

Table 1
Composition and characteristics of tested TOR lubricants.

TOR product	Structure	NLGI grade	Base oil	Thickener	Particles	Base oil viscosity at 40 °C (mm^2/s)
TORL-A	Paste	0	Biodegradable ester	Organic	Soft metal	41–53
TORL-B	Gel paste	00	Synthetic ester	Inorganic (silicate)	Soft metal	46

each new pair of specimens. The wear-in parameters (speed, load and SRR) are the same as for adhesion tests and run-ins and will be described later.

A 15-minute run-in was performed before every adhesion test to remove the oxide layer and TOR product residual from the track and to stabilize surface roughness. During this process, the CoA stabilized around 0.39 (a reference value for dry contact), ensuring that every test started from the same initial conditions. Unlike a wear-in, a run-in was performed before every adhesion test, not only at the beginning for a new pair of specimens. Specimens were cleaned manually with a paper towel and ultrasonically in an acetone bath for 10 min after each test.

The wear-in/run-in and cleaning parameters are based on a preliminary study conducted before this work in the experiment design process. The base value of 0.39 for the dry contact CoA and the duration of 60 min and 15 min for wear-in and run-in were selected based on the results of 20 tests focusing on adhesion and wear development. After the end of every test, the surface topography was checked on an optical profilometer. Also, the contact path surface was checked under a microscope to visually confirm that the cleaning process removed any remaining lubricant residue or particles.

2.4. Adhesion test: performance of water/TOR product under dry conditions

Firstly, different amounts of water and TOR products were tested in dry conditions to investigate their separate influence on CoA, see Table 2. The following parameters were set for all tests: a fixed value of 2% SRR, a mean speed of 1 m/s, and a load of 18 ± 0.01 N normal force (corresponding to 0.8 GPa Hertzian contact pressure). The same parameters were used in wear-ins and run-ins. The set SRR represents a value from the effective linear part of the traction curve near the saturation point commonly found in actual railway operations. Moreover, higher values of SRR could cause excessive wear. According to [28], the chosen value of the mean speed represents the velocity of approx. 60 km/h in actual wheel-rail contact corresponding to the light-rail system.

The performance of oil-based TOR products strongly depends on applied quantity [19]. Thus, choosing the optimal amount for tests in the main part of this work was necessary. Different amounts of each TOR product were tested to determine the optimal amount (regarding retentivity, low/intermediate CoA). The 15-minute run-in was performed before each test.

2.5. Stribeck test: water, oil and water-oil mixture under fully flooded conditions

A Stribeck test of water, oil, and a 1:1 water-oil (W/O) mixture under fully flooded conditions was conducted. TORL-A bleed oil with a viscosity of 64 mPa.s was used in this test. The set parameters for this test were 18 N of load and 2% SRR. The mean speed of specimens was 100–2500 mm/s for water and 50–2500 mm/s for oil and W/O mixture. For each tested speed, one mean value of CoA was calculated from the 6-second test. This test revealed the lubrication regime and thickness of the lubrication film and will be further discussed in the Sections Results and Discussion.

2.6. Adhesion test: performance of TOR product under wet conditions

In the main part of this work, TOR products were tested under wet conditions. Please note that water was applied to the contact only after the TOR product. The moment of application varied and is specified in Table 2. The parameters of these tests were the same as in adhesion tests under dry contact conditions (see Section 2.4). The tested amount of each product was determined regarding optimal performance in dry conditions. TOR products were applied to the disc surface using an electronic micropipette (error ± 0.04 μl). There were two types of tests: (1) single water application using a syringe/electronic micropipette and (2) continuous water application via a peristaltic pump. The procedure of all adhesion tests is summarised in Table 2.

In addition, water-based FM-A was tested both before ("wet film") and after ("dry film") base medium evaporation. To prepare a dry film, a short 30-second test immediately followed the application of FM-A to spread it on contact bodies. The parameters of this test were: 0% SRR, 300 mm/s mean speed, and 18 N load. A 10-minute pause follows to provide enough time for water evaporation. These two steps ensure the formation of an evenly distributed dry film. This procedure only applies to FM-A (dry film) tests.

In the case of single application tests, the TORL-A and FM-A (wet/dry

Table 2
Procedure of adhesion tests: dry and wet conditions (see 2.4 and 2.6).

Type of test	Water/TOR product	Run-in duration (min)	Amount of TOR product (μl)	T1–T3[a] (CoA)	Amount of water (μl)	Test duration (s)	Fig. # in Results
Dry conditions, a single water/TOR product application	TORL-A	15	1; 2; 3; 4	-	-	600	3 a)
	TORL-B	15	1; 2; 3; 4	-	-	900	3 b)
	FMA-(wet film)	15	2; 4; 6; 8	-	-	600	3c)
	FM-A (dry film)	15	4	-	-	600	3c)
	Water	15	-	-	2; 8; 32; 2000	150	3 d)
Wet conditions, a single water application	TORL-A	15	2	0.13; 0.2; 0.3	2; 8; 32; 2000	600	5
	TORL-B	15	1	0.13; 0.2; 0.3	2; 8; 32; 2000	900	6
	FM-A (wet film)	15	4	0.13; 0.2; 0.3	2; 8; 32; 2000	600	7
	FM-A (dry film)	15	4	0.3	2; 8; 32; 2000	600	8
Wet conditions, continuous water application	TORL-A	15	2	0.18	2150	2000	9
	TORL-B	15	1	0.18	2150	2000	9
	FM-A (wet film)	15	4	0.23	2150	1000	10
	FM-A (dry film)	15	4	0.32	2150	1000	10

[a] T1–T3 are defined values of CoA. When reached during the test, water was applied to the TOR product.

film) test duration was 600 s. For TORL-B, the test duration was extended to 900 s due to its longer retentivity. For the continuous application of water, the duration was 2 000 s for TOR lubricants and 1 000 s for friction modifiers.

In various tests, water was applied at different times after the start of the test. The reason for this was to observe the effect of water on TOR products at different phases of its performance. The exact moment of application was determined by the value of CoA defined in Table 2. Water was applied only once per adhesion test when CoA reached the specified value. In the Section Results, points where water was applied, are marked as T1–T3 in the graphs. These values vary for TOR lubricants and friction modifiers because both types of TOR products led to different CoA.

A typical adhesion test of TOR product with a single and continuous water application can be seen in Fig. 2a) and b). First, a 15-minute run-in was conducted before every test. Only the final parts of the run-in are shown in Fig. 2. Second, a TOR product was applied. In the FM-A (dry film) tests, the spreading and drying procedure followed (not shown in Fig. 2). After that, the adhesion test with described parameters started. The CoA development during the typical test was as follows: after a TOR product application, an initial drop caused by a large amount of TOR product occurred. However, part of the TOR product dosage was quickly pushed away from the track, and the CoA slowly rose to 0.15–0.25. When the trigger value of CoA was reached (T1–T3), water was applied either by a) a micropipette/syringe or b) a peristaltic pump. The magnitude and duration of the drop of CoA caused by the water application on the disc with the tested TOR product depended on the amount of applied water. During test b), 430 µl/min of water was continuously applied for 5 min (2 150 µl in total). Both small and large amounts of water were used to determine the influence on product performance (2–2 000 µl for a single application and 430 µl/min for a continuous application).

3. Results

3.1. Results: performance of water/TOR product under dry conditions

First, TOR products and distilled water were tested separately in a series of adhesion tests. Each TOR product was tested in different amounts to determine the best-performing amount, which was later used for the adhesion tests of TOR products in wet conditions in the main part of this work. The term "best-performing amount" means the amount of TOR product, which ensures a good ratio between the duration of the initial drop of CoA under 0.1 (which is undesired but inevitable in most cases for TOR lubricants) and the duration of a period of intermediate CoA (desired effect of TOR products). Also, the three phases after application can be distinguished: the initial rise in CoA, stabilization at the desired adhesion level, and starvation and dry contact restoration.

In the case of TORL-A (Fig. 3a), the amount of 4 µl was unsuitable for further testing as it caused over-lubrication, and the CoA restoration did not occur during the standard test duration. On the contrary, both 1 µl and 2 µl led to desired adhesion development. Finally, the amount of 2 µl was chosen because, for this amount, the product stays in effect slightly longer than for 1 µl. Also, the repeatability of the measurement was tested. Two dashed lines in Fig. 3a) represent additional measurements of 2 µl of TORL-A. After comparing all three curves, it can be said that in all three tests, very similar values of CoA were measured. The curves slightly differ only at the end when the starvation occurs, which should not be a problem as contamination will not be tested at this part of the curve.

In the case of TORL-B (Fig. 3b), 4 µl of the product led to over-lubrication of the contact. Although 2 µl did not cause the over-lubrication, the tests would be inefficiently long for this amount. As the 1 µl showed desired adhesion development in the standard test duration, this amount was chosen for the rest of the experiments.

Contrary to TOR lubricants, the over-lubrication did not occur for any tested amount of FM-A. Although it shows some adhesion-amount dependency, generally, it is much less significant than in the case of TOR lubricants. The 4 µl was chosen from all tested amounts as it led to a similar test duration compared to TORL-A and TORL-B. Afterward, this amount was also tested as dry film (red dashed line in Fig. 3c).

Four different amounts of water (2, 8, 32 µl, and 2 ml) were tested). These exact amounts were later used for adhesion tests under wet conditions. Fig. 3d) shows that with the increase of water amount, the duration of CoA drop also increases. However, there is no significant difference between 32 µl and 2 ml. The effect of the amount on the CoA level is relatively negligible. For tested amounts, the CoA ranged from 0.32 to 0.35.

3.2. Results: Stribeck test of water, oil and W/O mixture

The results of the Stribeck test are displayed in Fig. 4. Please note that each line represents the mean value calculated from three measurements. The lubrication parameter λ was calculated for water and oil to determine the lubrication regime. Value $\lambda = 1$, often used in literature as a transition between boundary and mixed lubrication regime [29], is marked for oil conditions in the figure.

For water, the boundary regime occurs for all tested speeds. For oil, the boundary regime occurs up to 280 mm/s. Above this speed, the contact operates mainly in the mixed lubrication regime. For the W/O mixture, parameter λ was not calculated. In addition, Fig. 4 shows that with the increase in speed, the CoA decreased. The highest CoA of 0.56 was measured for water. With increasing speed, the decrease of CoA was somewhat limited, and the lowest value of 0.43 was measured for a mean speed of 2 500 mm/s. On the other hand, a W/O mixture led to significantly lower CoA. The measured value for a speed of 1000 mm/s was 0.04 and 0.02 for the oil and W/O mixture, respectively. Meanwhile, the CoA of water was 0.45 at this speed.

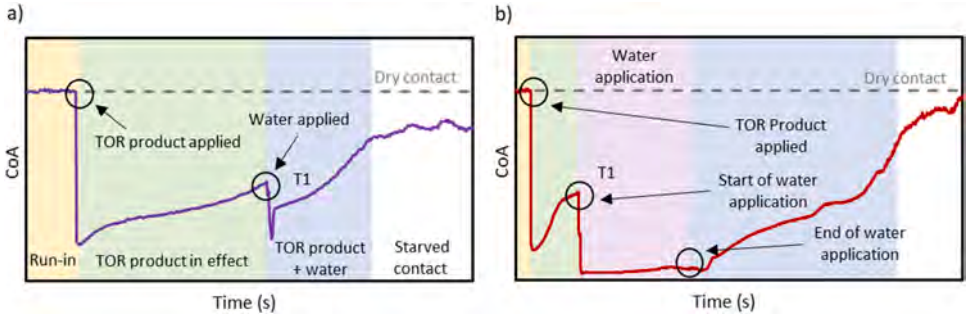

Fig. 2. (a) Adhesion test – a single application of water, (b) adhesion test – continuous application of water.

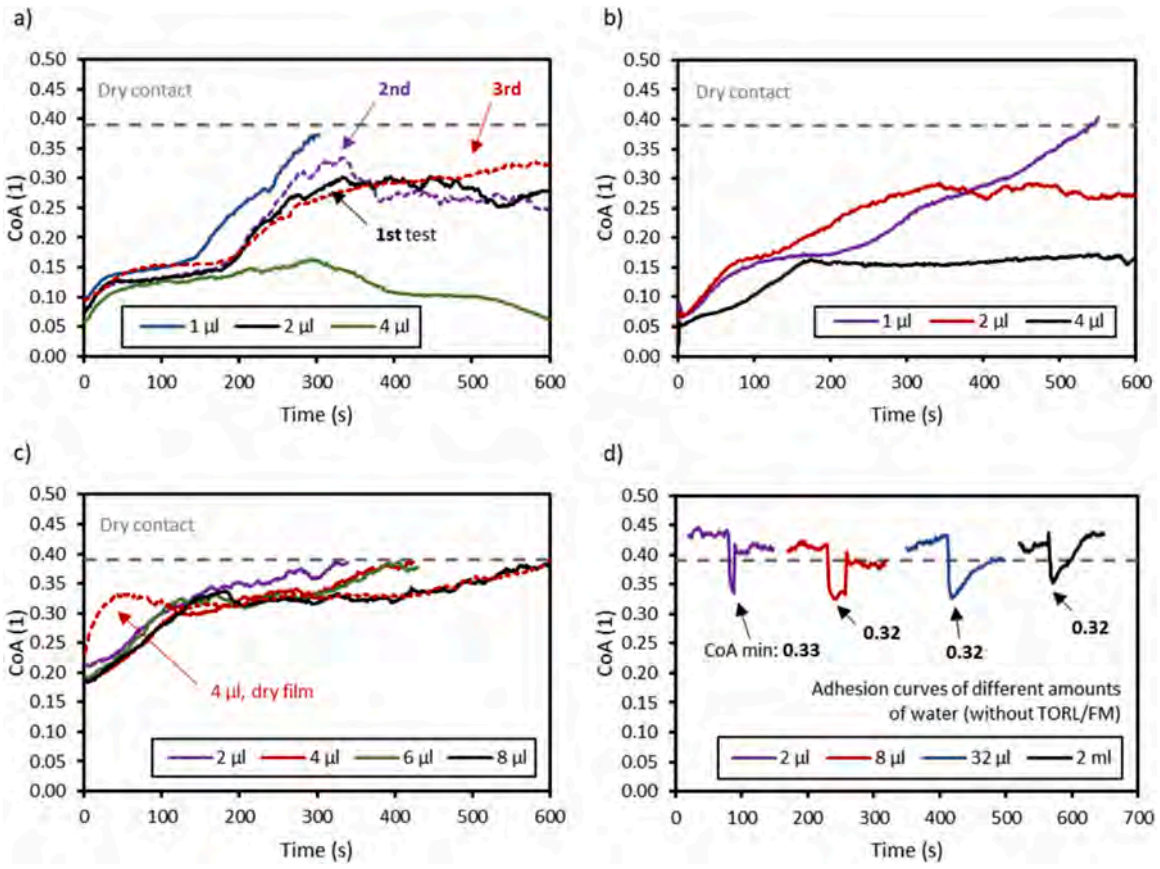

Fig. 3. Adhesion tests: different amounts of (a) TORL-A, (b) TORL-B, (c) FM-A, and (d) distilled water.

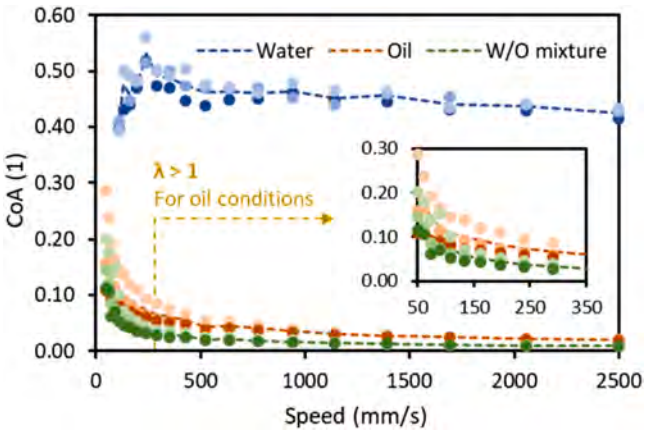

Fig. 4. Stribeck test of water, oil, and W/O mixture.

3.3. Results: performance of TOR products under a single water application

Figs. 5 and 6 represent TORL-A and TORL-B adhesion tests after a single water application. Both figures consist of four independent graphs marked as a–d). In each graph, a different amount of water was applied, see the upper left corner. There are two types of curves in these graphs. Dashed lines represent the dry contact CoA level (grey) and adhesion tests of TOR products measured under dry conditions (black). These curves are already depicted in Fig. 3a) and b). The purpose of showing them again in these graphs is to enable a quick comparison between adhesion tests with and without water application. Solid lines represent adhesion tests where water was applied into contact with TORL-A and TORL-B. Each graph includes three curves because three measurements were conducted for the same amount of water. Although each has a different color, this is only for clarity, and the test parameters for the triplet of tests were the same. The only difference was the time when water was applied to the contact. Water was applied when a specific value of CoA was reached. These values are for each TOR product listed in.

Table 2 and are marked as T1–T3 in all graphs. In addition, the minimum values of CoA reached during the initial adhesion drop are displayed. There are slight differences between curves of the same TOR product measured at different tests. These could be caused by different contact temperatures, surface topography changes as wear progresses during the experiment, or slightly different amounts of TOR product in the contact path. However, these differences are not statistically significant.

Fig. 5 shows results for TORL-A. For 2 µl of water, a drop to the lowest CoA value of 0.084 was observed when water was applied in T3. Similar drops were also observed in T1 and T2 applications. Compared to b–d), the CoA drop caused by 2 µl of water had the shortest duration. The CoA was restored to the level before water application in all three measurements. For the rest of the tests, the lowest CoA measured were: 0.037 in T3 for b); 0.035 in T3 for c) and 0.026 in T1 for d). As can be seen, with an increase in water amount, the CoA decreases to lower levels. Moreover, larger amounts of water also slow the CoA restoration after the initial drop. In c) and d), the CoA was not restored during the standard test duration (except for T3; 2 ml). The CoA stayed in the 0.05–0.1 interval until the end of the test.

The curves for TORL-B measured in dry conditions are more flattened than those of TORL-A. However, under wet conditions, they show similar behavior, see Fig. 6. With the increasing amount of water, CoA decrease, and it takes more time for CoA to reach dry contact levels. The lowest CoA measured: 0.069 in T3 for a); 0.028 in T2 for b); 0.017 in T1

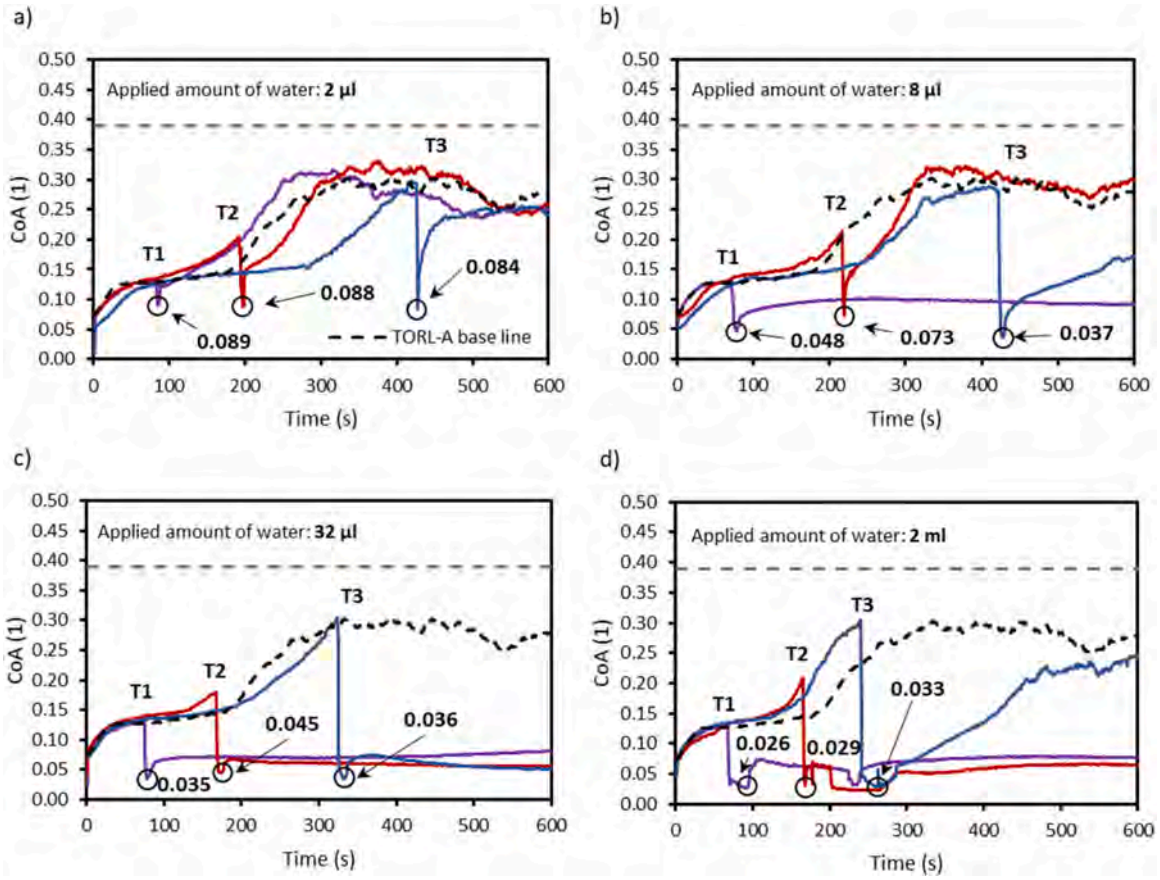

Fig. 5. Adhesion tests of TORL-A under wet conditions. Amounts of water: a) 2 µl; b) 8 µl; c) 32 µl; and d) 2 ml.

for c) and 0.026 in T1 for d). Compared to TORL-A, lower values of minimum CoA were reached after water application in the case of TORL-B. In addition, except for experiments with 2 µl of water a), the dry adhesion level restoration did not occur during the standard test duration.

Fig. 7 shows the results of tests with FM-A (wet film). Please note that points T1–T3, where water was applied, now have different values of CoA than in the case of TOR lubricants (see Table 2). This is because FM-A generally led to the different development of CoA than tested TOR lubricants. From a–c), a clear relationship between the increase in the amount of water and the magnitude of the initial drop of CoA after water was applied can be seen. The lowest reached CoA was 0.086 in T1 for a); 0.042 in T2 for b), and 0.021 in T1 for c). Moreover, the CoA restoration slows down with the increase in the amount of water. For the lowest amount, the CoA drop lasts only a couple of seconds after water application. On the contrary, CoA recovery in case c) took more than 100 s. Still, the duration of the drop is relatively short compared to tests with TOR lubricants. Case d) does not fit this trend. From all tested amounts of water, in tests where 2 ml was applied, the initial adhesion drop was the shortest, and the CoA was quickly restored to a dry level and even higher. This behavior will be further discussed in the Section Discussion.

Fig. 8 shows the results of experiments with dry friction film. Contrary to wet film experiments, water was only applied at one value of CoA marked as T1 for all tested amounts. Thus different line colors in the graph represent different amounts of water; please see the legend. Similarly to the wet film tests, the higher the amount of water applied, the lower the CoA and the longer the adhesion recovery. The only exception is the test with 2 ml of water, where CoA first rises after contamination but then decreases to 0.061. This value is higher than 0.047 in the case of 32 µl of water but lower compared to tests with 2 µl and 8 µl, with measured values of 0.151 and 0.077, respectively. The CoA drop is slow and divided into two parts – after the first initial drop, second to lower values follow. Water significantly reduces CoA compared to non-contaminated dry friction modifier film in all cases.

3.4. *Results: performance of TOR products under continuous water application*

Figs. 9 and 10 show the results for continuous water application, and in terms of visualization, they follow the same rules as the figures in the previous section. In Fig. 9, it can be seen that TORL-A shows a similar behavior under continuous water application as in tests with a single application of large amounts of water. The lowest reached CoA for TORL-A was 0.025. TORL-B reached an even lower value of 0.015, the same value as in the test with a single application of 2 ml of water, see Fig. 6d). In terms of CoA restoration, even though TORL-B led to lower CoA than TORL-A, approx. 100 s from the end of the water application, the CoA starts to rise, reaching dry-level CoA significantly quicker. The CoA restoration is also faster than in the tests with a single application of larger amounts of water (8 µl, 32 µl, and 2 ml). The gradient of the CoA increase in tests with TORL-A is comparable to tests with a single application of water.

Regarding water-based product FM-A, wet and dry film behaves differently compared to tests with a single application, see Fig. 10. In the case of the wet film, the lowest measured CoA was 0.073, which is lower than in tests with a single application (2 ml). Also, the CoA restoration to dry level takes longer (183 s). On the other hand, the CoA drops only to 0.168 in the case of dry film, and it takes approximately 180 s to restore CoA to dry levels. In both cases (dry/wet film), CoA was restored before the end of the water application.

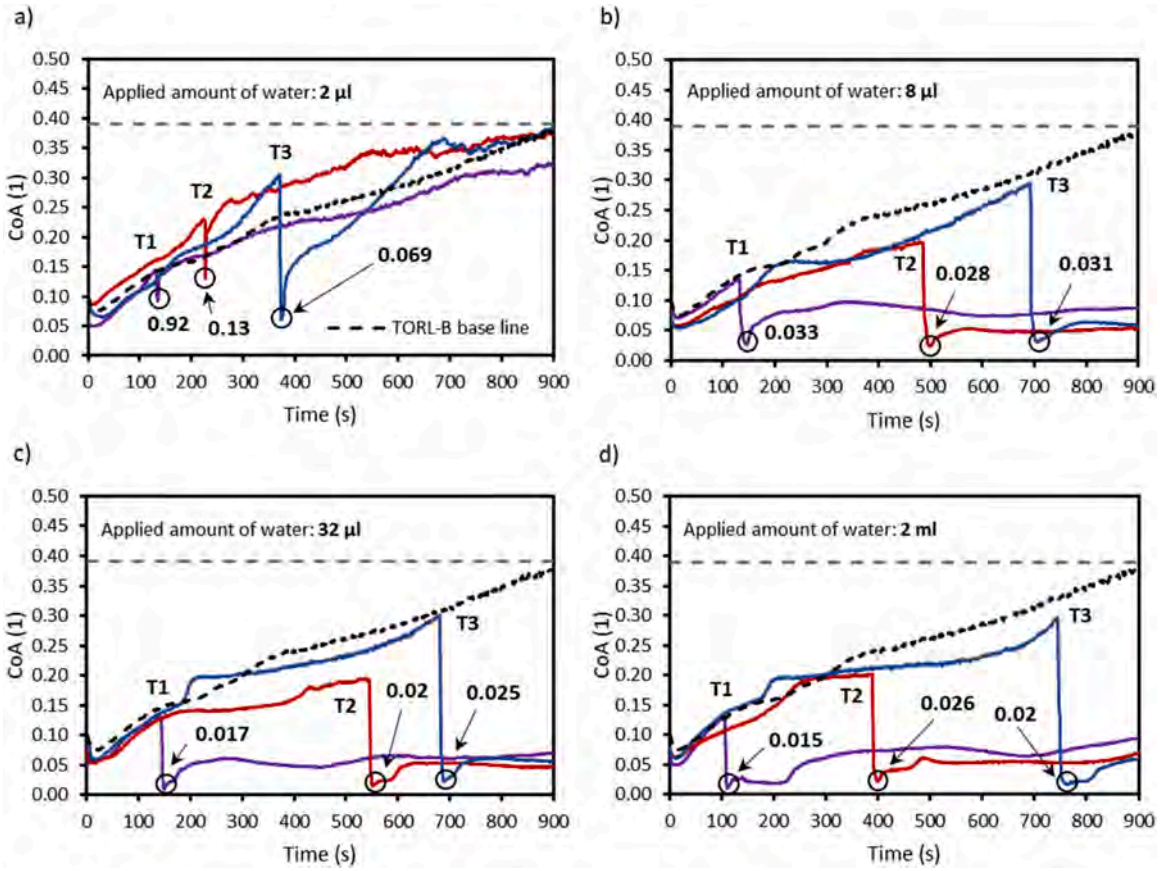

Fig. 6. Adhesion tests of TORL-B under wet conditions. Amounts of water: a) 2 µl; b) 8 µl; c) 32 µl; and d) 2 ml.

4. Discussion

4.1. The influence of the water amount on CoA

The Section Results show that water affects oil-based and water-based TOR products differently. In data evaluation, two main parameters were examined: (1) the lowest CoA reached after water was applied to the TOR product and (2) the duration of the interval of CoA < 0.1 (low adhesion). The overall results of experiments are summarised in the bar graphs in Fig. 11a) and b). Bars of different colors represent mean values evaluated from three measurements (applications in T1–T3), except FM-A (dry film), where water was applied only once at T1. Each color refers to a specific TOR product. Different shades of the same color indicate the amount of water applied, see the label of each bar. For Fig. 11a), the height of each bar represents the lowest CoA reached after water was applied to the TOR product. In Fig. 11b), the height of each bar represents the time duration in seconds for which the CoA was lower than 0.1. Note that a CoA did not drop under 0.1 in some tests. On the other hand, in some tests, the CoA restoration did not occur after water was applied, and the CoA did not reach 0.1 again during the test duration. These tests are marked with the "* " symbol in Fig. 11b). Please note that only tests with single water application were included in this evaluation. During tests with continuous water application, the CoA stays under 0.1 during the whole water application process. So, the CoA remained under the limit value for five extra minutes compared to tests with a single water application. Thus, time durations of CoA lower than 0.1 in those two types of tests cannot be compared.

For TORL-A, Fig. 11a) shows that as the amount of water increases, the CoA decreases to lower minimal values. For comparison, the mean CoA of 0.029 reached after 2 ml of water was applied is nearly three times lower than CoA of 0.086 in the case of 2 µl. TORL-B follows the same trend with an exception between 32 µl and 2 ml, where CoA decreases to a slightly lower value of 0.017 for 32 µl compared to CoA of 0.02 for 2 ml of water. For both oil-based TOR products, it can be said that the higher the amount of water, the longer the CoA stays under 0.1. In the case of a larger amount of water, the CoA restoration did not occur at all. Under continuous water application, both oil-based TOR products behaved similarly to a single application of 2 ml.

In the case of the FM-A (wet film), with an increasing amount of water, CoA reaches lower minimal values. The only exception was between 32 µl and 2 ml, which was caused due to a large amount of water flushing TOR product away from the track, causing quick CoA recovery. When water was applied to dried FM-A film, the drop of CoA was less significant compared to wet FM-A film, and the time of CoA lower than 0.1 was also shorter. Higher values of minimal CoA and shorter duration of the low adhesion period are probably caused by the absence of the evaporated base medium. An exception was the tests with 2 ml of water, where the combined effect of water and dried particles led to better lubrication than in the case of FM-A (wet film). Under continuous water application, the CoA restoration was quicker for dried FM-A film than for wet film.

In most tests, the CoA drop was not as high for water-based TOR products as for oil-based TOR products. Although the oil does not easily mix with water, contamination of oil-based TOR products poses a more significant risk in terms of low CoA. This is mainly supported by the fact that CoA stayed below 0.1 for no or very little time for water-based TOR products.

From a practical point of view, the amount of water on an actual rail can be either small (morning dew, leakage from passing train) or large (mostly rain). By comparing the approximate contact area of tested samples under set conditions to the expected size of the actual wheel-rail contact, the amounts of water tested in this paper correspond to the following amounts in the field conditions: 2 µl $\approx$ 3 ml; 8 µl $\approx$ 12 ml; 32 µl $\approx$ 46 ml; 2 ml and 2.15 ml $\approx$ 3 l. Single contamination of the

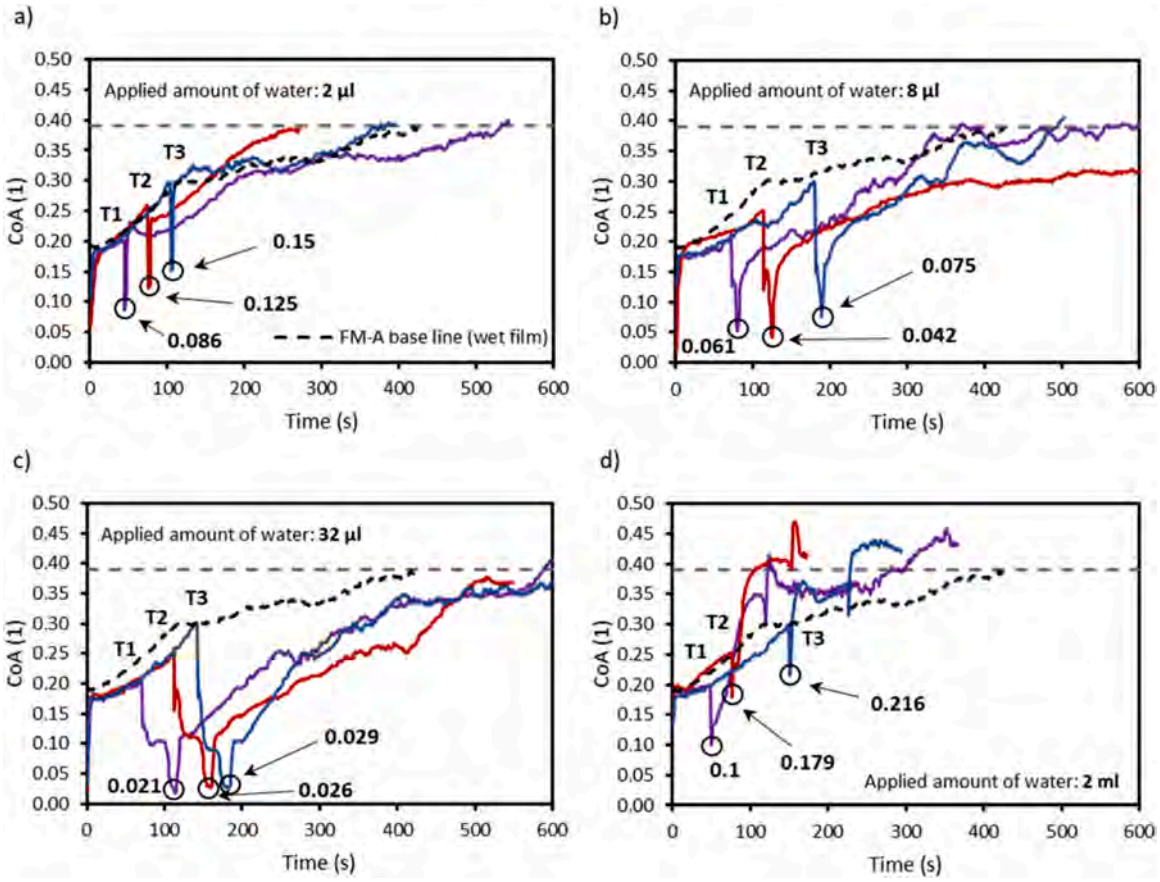

Fig. 7. Adhesion tests of FM-A (wet film) under wet conditions. Amounts of water: a) 2 µl; b) 8 µl; c) 32 µl; and d) 2 ml.

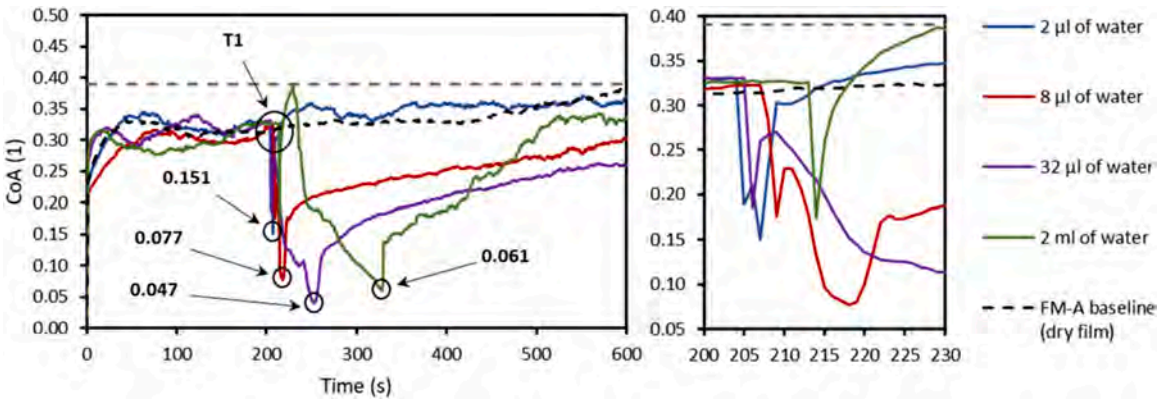

Fig. 8. Adhesion tests of FM-A (dry film) under wet conditions. Each line represents a different amount of water, see the legend.

contact by liters of water in actual railway operation seems to be unlikely. However, knowing the worst-case scenario is still necessary when dealing with passenger safety. On the other hand, it is possible for the smaller amounts in the order of milliliters to be accumulated over a short period from the rain or the overnight condensation from the humid air. Thus, tested amounts of water (especially 2 µl and 8 µl) are relevant to actual field conditions.

Results indicate that the risk of low CoA rises with the amount of water. However, this is contrary to field measurements, which suggest that it is rather a small amount of water leading to low CoA. The analysis in [5] shows that low CoA-related incidents are most probable when morning dew is on a rail. Similarly, findings in [24] show that when a small amount of water is mixed with particles of iron oxides, CoA lower than 0.05 can occur. On the other hand, several papers showed that although the exact value of CoA depends on water temperature [30], larger amounts generally lead to much higher CoA [31,32]. The effect of water also depends on the presence of the third-body layer, consisting of iron oxides, wear particles, environmental contaminants, or even TOR product residua. Thus, possible mechanisms of water contamination of TOR products will be discussed next.

4.2. *Fluid-film regime / Mechanisms relevant to oil-water system*

First, the question arises as to why the CoA of the W/O mixture is lower than that of bleed oil, as revealed by the Stribeck test under fully flooded conditions in Chapter 3.2. Similar observations were made in

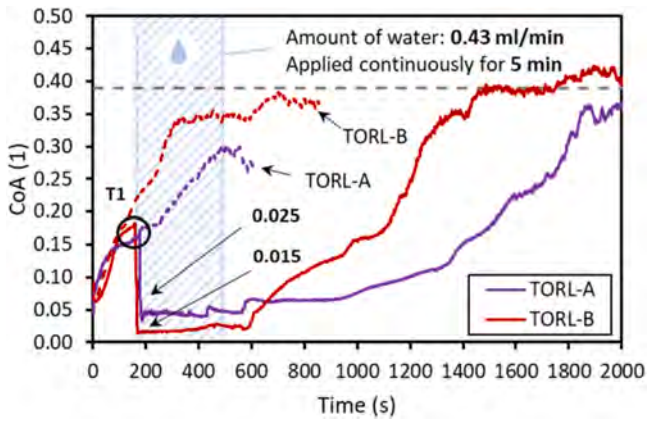

Fig. 9. Adhesion tests of TORL-A and TORL-B under wet conditions. Water was applied continuously for 5 min.

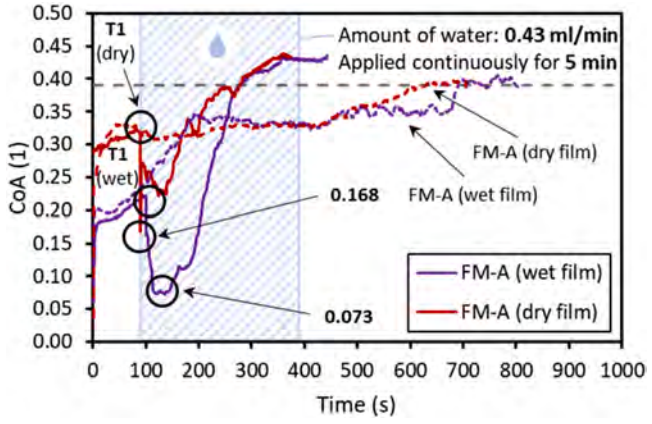

Fig. 10. Adhesion tests of FM-A (dry film) and FM-A (wet film) under wet conditions. Water was applied continuously for 5 min.

simulated wheel-rail contact [31]. Over the last decades, several theories have been proposed on the lubrication mechanism of water-in-oil (W/O) or oil-in-water (O/W) emulsions. Those theories can help to explain the behavior of water-contaminated EHL contacts.

At low speeds, the behavior can be explained by the well-accepted plate-out theory [33,34]. This theory assumes that water is excluded from the contact due to the stronger wetting ability of oil, creating an oil pool around EHL contact, see Fig. 12a). This mechanism is in accordance with the theory of energy displacement [33]. Ideally, a lubricant film in the contact is fully composed of the oil phase, and there is no negative effect on lubricant film thickness [35,36]. For larger droplets, dynamic concentration theory describing the increasing concentration of oil in the inlet zone as water is gradually excluded from the gap is more appropriate [37].

According to a starvation theory [38], the first critical speed exists, after which the oil pool becomes unstable, and lubricant film thickness in the contact decreases [39–41]. While remaining in full-film lubrication, lower film thickness means lower shear stress in lubricating film and, therefore, lower traction [40]. After the second critical speed, lubricant film thickness starts to increase. However, due to starvation, water can no longer be excluded from the contact inlet, and a certain amount of water phase, given by the dynamic concentration theory [37], passes through the contact resulting in a much lower coefficient of traction. This behavior strongly depends on the size of water droplets [42]. A single application of a water droplet may differ from the behavior of emulsified water. A large water droplet is more easily expelled from the oil. If it occurs under contact starvation, water can easily enter the contact [43]. Those theories can explain low CoA in the water-contaminated oil-lubricated contact.

4.3. Starved fluid-film regime / Mechanisms relevant to grease-water system

Oil-based TOR products are usually based on grease, i.e., they contain thickener and base oil. In this case, water influences the oil pool in the contact and structure and the rheology of bulk grease [44]. Evaluation of its water resistance is covered by industry standards [45]. Unlike lubricating oil, grease can absorb a larger amount of water due to the polar nature of its thickener and additives. This ability strongly depends on a thickener type, while some greases become stiffer and others soften [44].

Grease-lubricated contact is much more susceptible to starvation since a relatively thick grease is being pushed out of the contact track. Lubricant replenishment from the reservoirs on track sides is very slow, and the replenishment flow is inversely proportional to viscosity [46,47]. Absorbed water influences stiffness and oil-bleeding, i.e., the ability to replenish the contacts. The effects can be positive or negative depending on the type of thickener [48,49]. If the water absorption leads to an enhanced contact replenishment, higher oil film thickness under starved conditions and lower friction in the mixed regime may occur, which is consistent with our observations. For visualization of this mechanism, please see Fig. 12b). On the other hand, oil-based TOR products intended for the open tribology system are designed as water-repellent with low water adsorption, so the "free water" should rather occur in the contact.

4.4. Mixed regime / Mechanisms relevant to TOR-water system

When severe starvation occurs, lubricant film thickness further decreases, resulting in a mixed regime, where a part of the load is transmitted by the contacts of surface asperities and CoA increases [50]. Under these conditions, boundary friction is given by the composition of the created tribological layer. TOR products contain solid lubricants like graphite or molybdenum disulfide. The frictional properties of those particles are affected by water in different ways. The coefficient of friction of graphite usually decreases in the presence of water because of the dissociative chemisorption of water. On the contrary, the lubricity of MoS_2 decreases due to oxidation and physisorption of water molecules. However, the effect may be reduced by interaction with metal particles, which are also a common component of TOR products [51].

More significant is probably the interaction of water with other components of TOR products as particles for friction modification or wear particles. When mixed with a small amount of water, solid particles create a paste that causes a transient decrease in friction. This mechanism is known as a "wet-rail" phenomenon [52] and is depicted in Fig. 12c). Since the decrease in CoA appears to be independent of the water application time during friction development, it can be assumed to be due to particles contained in the TOR products rather than wear particles.

4.5. Mechanisms relevant to water-based TOR product contamination

Regarding the water-based TOR product, a similar dependence of magnitude and duration of CoA drop on the applied amount of water exists up to 32 μl. However, large amounts (2 ml) flush the product out of the surface, quickly restoring CoA to dry contact levels. This happened for both single and continuous applications, although in dry film test single application, the results are not entirely clear. Even if a CoA lower than 0.1 occurs immediately after the contamination, it remains below this limit only for a short period and then rises.

The drop of CoA can be divided into two parts. After the first drop, the second more significant follows, see Fig. 7a-c). This behavior was already seen in the study [53], in which the authors performed various

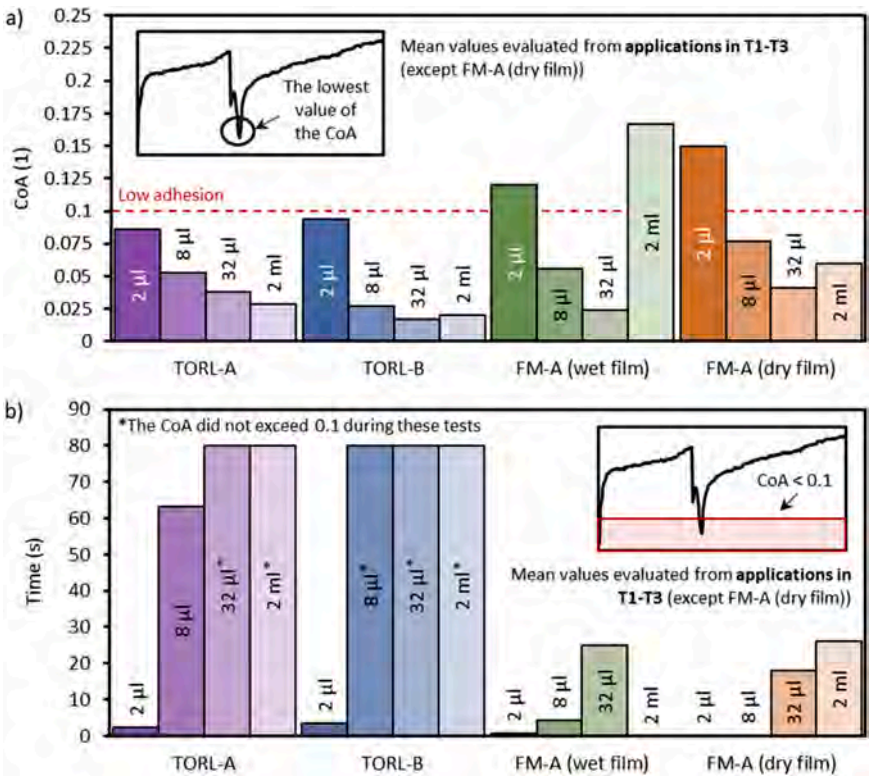

Fig. 11. Mean (a) adhesion drop after water application and (b) duration of a period when CoA was lower than 0.1.

tests with water alone. Similar behavior was also observed in a paper [3] focused on water-based TOR products. It can be assumed that this behavior relates to the water contained in the product and thus did not occur in tests with oil-based TOR products.

Results presented in this study are comparable with findings in [54], where two water-based TOR products were tested under various slips and water contamination. Although both products differ from those tested in this study in the type of particles contained, the trends in CoA development seem similar. In an extreme case, the CoA after water contamination drops to approx. 0.05, which is comparable to tests with FM-A (8 µl). In other cases, the magnitude of the drop was not as high, probably caused by different product particles. As was shown in [2], product performance strongly depends on the type of contained particles. Tested products in [54] had particles of metals with a diameter as large as 100 µm. Particles in [3] were mainly minerals like bentonite or talc, and their diameter did not exceed 10 µm. Substances with mineral particles of smaller diameters reach lower CoA comparable to one of the products used in this study. Thus, the type and scale of the particles play an essential role in achieving sufficient CoA. In both studies, it seems that water slows CoA development rather than interrupts it, contrary to the case of oil-based TOR products. As shown in Fig. 7a-c), the CoA develops similarly to the situation before contamination, only starting again from lower values.

Authors propose that the contamination mechanism of water-based TOR products lay in the refill of the evaporated base medium. After contamination, water mixes with dried particles and the mixture act as a freshly applied product. This is supported by Fig. 8, which summarises the results of dry FM-A film tests. The dry film leads to higher CoA (higher than 0.3) than the wet film. However, after contamination, water mixes with dried particles, and the CoA drops to values comparable to values of the original TOR product before base medium evaporation, see Fig. 7. After that, the mixture behaves similarly to tests with FM-A (wet film).

4.6. Limitations of the Study

The CoA values and performance of tested oil-based TOR products measured in this study follow results published in [13], which were also measured on a ball-on-disc tribometer. As was shown in [11], measured adhesion strongly depends on the measuring device. The point contact between the ball and the disc simplifies actual rail conditions. However, many previous studies on wheel-rail tribology already used universal tribometers in the ball-on-disc configuration, obtaining useful results [3,4,28]. Although conclusions from laboratory tests can be limited due to simplifications, they are suitable for preliminary studies as these tests are more controllable than field tests. Regarding used specimens, there are three main differences compared to actual wheel-rail contact: the contact shape, the surface roughness, and the material hardness.

As for the point contact, Chen et al. [30] measured the adhesion of water-contaminated contact on a twin disc machine. The use of discs as contact bodies led to line contact, and still, values obtained for given conditions correspond to values represented in Fig. 3d) or published in [53].

Pieringer et al. [55] measured the surface roughness of wheel and rail to be tens of micrometers which is significantly higher compared to Ra 0.15–0.3 µm of specimens in this study. Conversely, Chen et al. assumed that surface roughness depends on the current state of the wheel and rail (new/worn/after grinding) and can be expected in the range of 0.3–1.5 µm [56]. Previously, Galas et al. [13] used specimens with surface roughness varying from 0.05 to 0.45 µm to conduct similar experiments and achieved representative results. Furthermore, Zhu et al. [57] used discs with Ra as low as 0.2 µm to measure CoA in contaminated contact on a twin disc machine. Since surface roughness influences the lubrication regime, Stribeck tests were conducted in this study. Fig. 4 shows that the tested configuration operated in similar conditions to the actual wheel-rail contact. So, in theory, measured CoA should be representative.

Regarding hardness, sets of standard material grades were established around the world. In Europe, rail steels are typically perlitic and

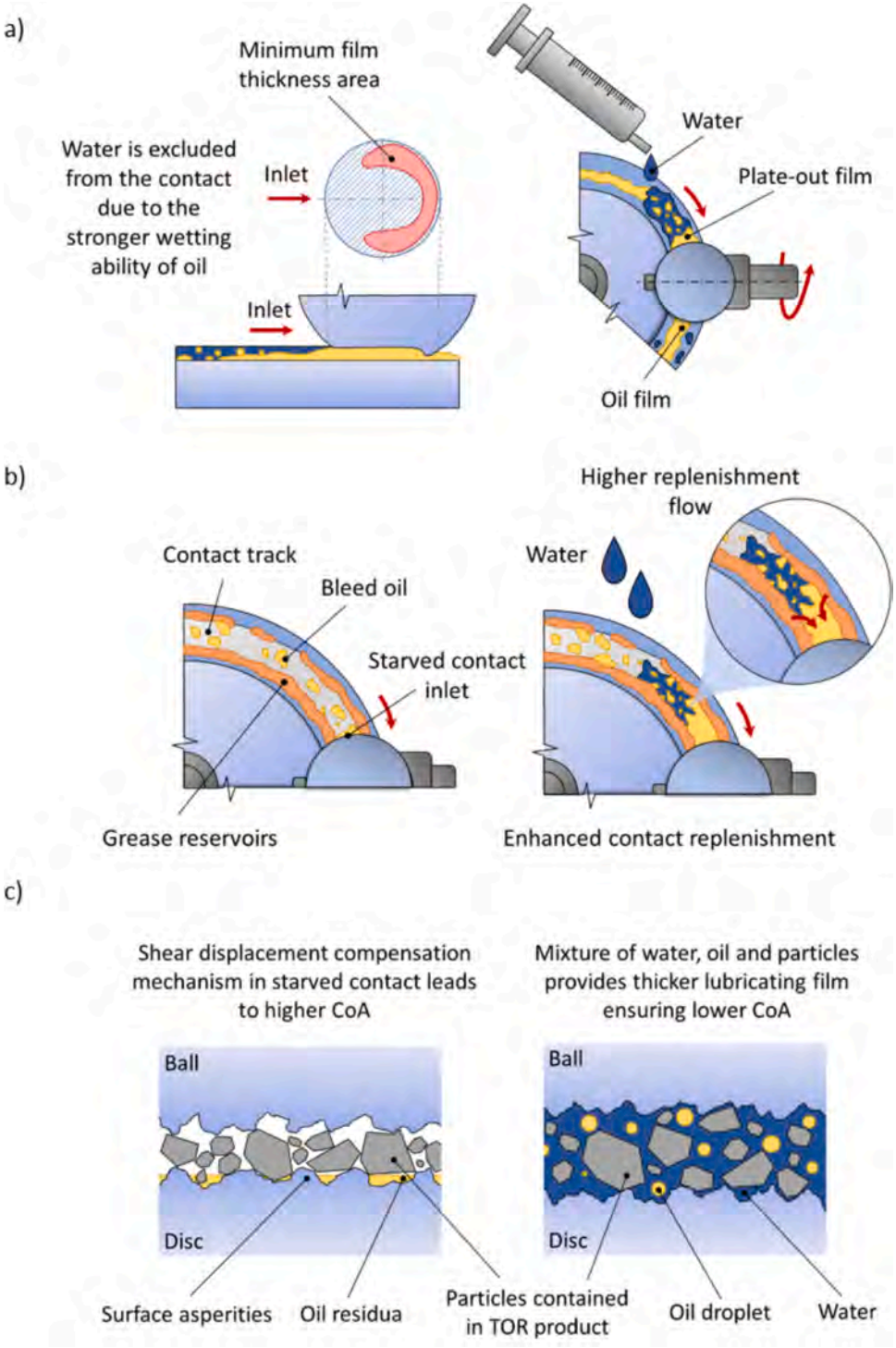

Fig. 12. Discussed mechanisms: a) Fluid-film regime, b) Starved fluid-film regime, c) Mixed regime.

could be heat-treated. Lewis et al., in their paper, compared the hardness of several materials [7]. They showed that the bulk hardness of conventional R260 steel was approx. 275 HV, and for heat-treated R350HT steel was 350 HV. It should also be noted that due to the work-hardening effect, the hardness close to the surface can be 2.5 times higher than the hardness of the bulk [58]. On the other hand, the hardness of specimens in this study was 800–920 HV and 720–780 HV for ball and disc, which is significantly higher, meaning their behavior can differ from actual rail materials. Harmon et al. showed that with a higher hardness of specimens, the slightly lower values of CoA will be measured compared to specimens made of softer materials [59].

The main purpose of choosing harder material was to reduce wear. The surface topography changes as the wear progresses during the test, causing a decrease in contact pressure. It was observed that the most severe wear occurred during the first 60 min of the test with new pair of specimens. But after this period, the wear becomes stable, and the width and depth of the contact path increased only a little. Thus, contact pressure remains relatively constant. The wear-in period was conducted on all new specimens to overcome the initial rapid wear and ensure stable test conditions. Although the actual contact pressure during tests

was probably lower than the initial 800 MPa, it remains relatively the same for all tests, so the results should be comparable.

A similar approach was used before in [3,4,13] and enabled focusing primarily on the effect of tested substances without bias from other factors that were not in the scope of the study. Measured results show a clear influence of water on TOR products. However, their transferability into railway operation could be limited and should be validated on specimens made from authentic rail material with more realistic geometry.

There is one more significant difference compared to the actual rail track. While in the laboratory tribometer, the contact between bodies occurs on the same spots as both bodies rotate, in reality, the wheel passes an exact location on the rail only once per ride. In laboratory conditions, this means that enough amount of lubricant is always present because it has nowhere to go. However, as shown in [15], the product is carried by wheels on an actual track for several hundred meters. Thus, larger amounts of lubricant are present only for a limited distance from an application unit. It is unclear if this increases or decreases the probability of low CoA. On one side, the probability of overdosing decreases with distance from the application unit. On the other, it was shown that water is most likely to cause low CoA when only a small amount is mixed with the third body layer [18,24]. From this point of view, the effect of water will be more significant if only a thin layer of TOR product is present, which could be expected farther away from the application unit. Either way, water will always influence the performance of TOR product, and the extent of this influence should be known for the safety of passengers and the efficiency of rail transport.

5. Conclusion

The ball-on-disc tribometer MTM was used in this study to investigate the influence of water contamination on TOR product performance. One commercial water-based and two oil-based TOR products were tested. The water-based TOR product was tested both before and after the base medium evaporation. Four different amounts of water were applied by syringe/electronic micropipette to TOR products. Also, continuous water application by a peristaltic pump was tested. The results could be summarized in the following points:

1) A low amount of water (2 μl) had a limited effect on tested TOR products and did not cause low CoA. However, it is important to mention that the contact surfaces of specimens were cleaned before every test. In actual railway, water could mix with third body layer particles and form a highly-viscous paste known for lowering CoA to insufficient levels.
2) Contamination of oil-based TOR products by a large amount of water resulted in a long-lasting period of low CoA (the lowest measured value was 0.015). A suggested explanation for this derives from W/O emulsion lubrication theories. Due to its low viscosity, water helped the oil to move into contact. Thus, lower values of CoA could be achieved for a prolonged time.
3) Low CoA rarely occurred in tests with water-based TOR products. Although CoA dropped after water was applied, after several dozen seconds, it was restored to the level before contamination. The water and dried solid particles formed a mixture similar to the original TOR product before the base medium evaporation. From this point of view, adding water to the dried water-based TOR product extended its lasting effect rather than causing low CoA problems. However, excessive amounts of water (2 ml) flushed the TOR product out of the contacting surfaces and significantly shortened its performance.
4) No significant difference existed between a single or continuous application of the same amount of water that contaminated oil-based TOR products. In the case of a water-based TOR product, CoA was restored slightly slower under continuous application.

The wheel-rail interface is an open system, meaning water and other contaminants can enter the contact. The presented results showed the strong influence of water contamination on the performance of TOR products. A long-lasting period of CoA lower than 0.1 occurred in several tests, suggesting that traction problems could also happen in actual railway conditions. This potential risk should be taken into account in the TOR conditioning deployment. Also, the interaction of TOR products with water should be considered in product development and testing. Although several hypotheses were proposed, the exact mechanism of the described phenomenon was not revealed and thus will be the object of the following research work.

Statement of Originality

As a corresponding author, I, Simon Skurka, hereby confirm on behalf of all authors that:

1) The authors have obtained the necessary authority for publication.
2) The paper has not been published previously, that it is not under consideration for publication elsewhere, and that if accepted it will not be published elsewhere in the same form, in English or in any other language, without the written consent of the publisher.
3) The paper does not contain material which has been published previously, by the current authors or by others, of which the source is not explicitly cited in the paper.

Upon acceptance of an article by the journal, the author(s) will be asked to transfer the copyright of the article to the publisher. This transfer will ensure the widest possible dissemination of information.

CRediT authorship contribution statement

Simon Skurka: Conceptualization, Methodology, Investigation, Data curation, Writing – original draft. **Radovan Galas:** Conceptualization, Investigation, Methodology, Writing – review & editing. **Milan Omasta:** Conceptualization, Investigation, Methodology, Writing – review & editing, Project administration. **Bingnan Wu:** Data curation, Writing – review & editing, Visualization. **Haohao Ding:** Writing – review & editing, Visualization. **Wen-Jian Wang:** Conceptualization, Data curation, Writing – review & editing, Project administration. **Ivan Krupka:** Data curation, Writing – review & editing. **Martin Hartl:** Supervision, Funding acquisition.

Declaration of Competing Interest

The authors declare that they have no known competing financial interests or personal relationships that could have appeared to influence the work reported in this paper.

Data Availability

Data will be made available on request.

Acknowledgments

This research was carried out under project EG20_321/0025198 with financial support from the Ministry of Industry and Trade of the Czech Republic and under project GA20-23482S with financial support from the Czech Science Foundation. Also, the authors thank the support of the National Natural Science Foundation of China (No. 52272443).

References

[1] Suda Y, Iwasa T, Komine H, Tomeoka M, Nakazawa H, Matsumoto K, et al. Development of onboard friction control. Wear 2005;258:1109–14. https://doi.org/10.1016/j.wear.2004.03.059.

[2] Kalousek J, Johnson KL. An investigation of short pitch wheel and rail corrugations on the vancouver mass transit system. Proc Inst Mech Eng F J Rail Rapid Transit 1992;206:127–35. https://doi.org/10.1243/PIME_PROC_1992_206_226_02.

[3] Galas R, Kvarda D, Omasta M, Krupka I, Hartl M. The role of constituents contained in water–based friction modifiers for top–of–rail application. Tribol Int 2018;117:87–97. https://doi.org/10.1016/j.triboint.2017.08.019.

[4] Kvarda D, Skurka S, Galas R, Omasta M, Shi L, Ding H, et al. The effect of top of rail lubricant composition on adhesion and rheological behaviour. Eng Sci Technol, Int J 2022;35:101100. https://doi.org/10.1016/j.jestch.2022.101100.

[5] Valehrach J, Guziur P, Riha T, Plasek O. Assessment of rail long-pitch corrugation. IOP Conf Ser Mater Sci Eng 2017;236:012048. https://doi.org/10.1088/1757-899X/236/1/012048.

[6] Stock R, Pippan R. RCF and wear in theory and practice—The influence of rail grade on wear and RCF. Wear 2011;271:125–33. https://doi.org/10.1016/j.wear.2010.10.015.

[7] Lewis R, Christoforou P, Wang WJ, Beagles A, Burstow M, Lewis SR. Investigation of the influence of rail hardness on the wear of rail and wheel materials under dry conditions (ICRI wear mapping project). Wear 2019;430–431:383–92. https://doi.org/10.1016/j.wear.2019.05.030.

[8] Braghin F, Lewis R, Dwyer-Joyce RS, Bruni S. A mathematical model to predict railway wheel profile evolution due to wear. Wear 2006;261:1253–64. https://doi.org/10.1016/j.wear.2006.03.025.

[9] Olofsson U, Telliskivi T. Wear, plastic deformation and friction of two rail steels—a full-scale test and a laboratory study. Wear 2003;254:80–93. https://doi.org/10.1016/S0043-1648(02)00291-0.

[10] Number of Europeans exposed to harmful noise pollution expected to increase — European Environment Agency n.d. ⟨https://www.eea.europa.eu/highlights/number-of-europeans-exposed-to⟩ (accessed August 12, 2022).

[11] Lundberg J, Rantatalo M, Wanhainen C, Casselgren J. Measurements of friction coefficients between rails lubricated with a friction modifier and the wheels of an IORE locomotive during real working conditions. Wear 2015;324–325:109–17. https://doi.org/10.1016/j.wear.2014.12.002.

[12] Eadie DT, Elvidge D, Oldknow K, Stock R, Pointner P, Kalousek J, et al. The effects of top of rail friction modifier on wear and rolling contact fatigue: Full-scale rail–wheel test rig evaluation, analysis and modelling. Wear 2008;265:1222–30. https://doi.org/10.1016/j.wear.2008.02.029.

[13] Galas R, Omasta M, Krupka I, Hartl M. Laboratory investigation of ability of oil-based friction modifiers to control adhesion at wheel-rail interface. Wear 2016;368–369:230–8. https://doi.org/10.1016/j.wear.2016.09.015.

[14] Abbasi S, Olofsson U, Zhu Y, Sellgren U. Pin-on-disc study of the effects of railway friction modifiers on airborne wear particles from wheel–rail contacts. Tribol Int 2013;60:136–9. https://doi.org/10.1016/j.triboint.2012.11.013.

[15] Han J, He Y, Xiao X, Sheng X, Zhao G, Jin X. Effect of Control Measures on Wheel/Rail Noise When the Vehicle Curves. Appl Sci 2017;7:1144. https://doi.org/10.3390/app7111144.

[16] Meehan PA, Liu X. Wheel squeal noise control under water-based friction modifiers based on instantaneous rolling contact mechanics. Wear 2019;440–441:203052. https://doi.org/10.1016/j.wear.2019.203052.

[17] Szablewski D, LoPresti J, Sultana T. Testing of latest top-of-rail friction modification materials at FAST. Railw Track Struct 2015;111:13–6.

[18] Ishizaka K, Lewis SR, Lewis R. The low adhesion problem due to leaf contamination in the wheel/rail contact: Bonding and low adhesion mechanisms. Wear 2017;378–379:183–97. https://doi.org/10.1016/j.wear.2017.02.044.

[19] Stock R, Stanlake L, Hardwick C, Yu M, Eadie D, Lewis R. Material concepts for top of rail friction management – Classification, characterisation and application. Wear 2016;366–367:225–32. https://doi.org/10.1016/j.wear.2016.05.028.

[20] Galas R, Omasta M, Klapka M, Kaewunruen S, Krupka I, Hartl M. Case study: case study: the influence of oil-based friction modifier quantity on tram braking distance and noise. Tribol Ind 2017;39:198–206. https://doi.org/10.24874/ti.2017.39.02.06.

[21] Harmon M, Lewis R. Review of top of rail friction modifier tribology. Tribology - Mater, Surf Interfaces 2016;10:150–62. https://doi.org/10.1080/17515831.2016.1216265.

[22] Areiza YA, Garcés SI, Santa JF, Vargas G, Toro A. Field measurement of coefficient of friction in rails using a hand-pushed tribometer. Tribol Int 2015;82:274–9. https://doi.org/10.1016/j.triboint.2014.08.009.

[23] Olofsson U, Lyu Y. Open system tribology in the wheel–rail contact—a literature review. Appl Mech Rev 2017;69. https://doi.org/10.1115/1.4038229.

[24] White B, Lewis R. Simulation and understanding the wet-rail phenomenon using twin disc testing. Tribol Int 2019;136:475–86. https://doi.org/10.1016/j.triboint.2019.03.067.

[25] Chen H, Fukagai S, Sone Y, Ban T, Namura A. Assessment of lubricant applied to wheel/rail interface in curves. Wear 2014;314:228–35. https://doi.org/10.1016/j.wear.2013.12.006.

[26] Lewis SR, Lewis R, Olofsson U, Eadie DT, Cotter J, Lu X. Effect of humidity, temperature and railhead contamination on the performance of friction modifiers: pin-on- disk study. Proc Inst Mech Eng F J Rail Rapid Transit 2013;227:115–27. https://doi.org/10.1177/0954409712452239.

[27] Moreno-Ríos M, Gallardo-Hernández EA, Vite-Torres M, Peña-Bautista A. Field and laboratory assessments of the friction coefficient at a railhead. Proc Inst Mech Eng F J Rail Rapid Transit 2016;230:313–20. https://doi.org/10.1177/0954409714536383.

[28] Zhu Y, Olofsson U, Persson K. Investigation of factors influencing wheel–rail adhesion using a mini-traction machine. Wear 2012;292–293:218–31. https://doi.org/10.1016/j.wear.2012.05.006.

[29] Kalin M, Velkavrh I, Vižintin J. The Stribeck curve and lubrication design for non-fully wetted surfaces. Wear 2009;267:1232–40. https://doi.org/10.1016/j.wear.2008.12.072.

[30] Chen H, Ishida M, Namura A, Baek KS, Nakahara T, Leban B, et al. Estimation of wheel/rail adhesion coefficient under wet condition with measured boundary friction coefficient and real contact area. Wear 2011;271:32–9. https://doi.org/10.1016/j.wear.2010.10.022.

[31] Wang WJ, Zhang HF, Wang HY, Liu QY, Zhu MH. Study on the adhesion behavior of wheel/rail under oil, water and sanding conditions. Wear 2011;271:2693–8. https://doi.org/10.1016/j.wear.2010.12.019.

[32] Wang WJ, Shen P, Song JH, Guo J, Liu QY, Jin XS. Experimental study on adhesion behavior of wheel/rail under dry and water conditions. Wear 2011;271:2699–705. https://doi.org/10.1016/j.wear.2011.01.070.

[33] Kimura Y, Okada K. Lubricating properties of oil-in-water emulsions. Tribology Trans 1989;32:524–32. https://doi.org/10.1080/10402008908981921.

[34] Fujita N, Kimura Y, Kobayashi K, Amanuma Y, Sodani Y. Estimation model of plate-out oil film in high-speed tandem cold rolling. J Mater Process Technol 2015;219:295–302. https://doi.org/10.1016/j.jmatprotec.2015.01.002.

[35] Nakahara T, Makino T, Kyogoku K. Observations of liquid droplet behavior and oil film formation in O/W type emulsion lubrication. J Tribol 1988;110:348–53. https://doi.org/10.1115/1.3261630.

[36] Benner JJ, Sadeghi F, Hoeprich MR, Frank MC. Lubricating properties of water in oil emulsions. J Tribol 2006;128:296–311. https://doi.org/10.1115/1.2164464.

[37] Wilson WRD, Sakaguchi Y, Schmid SR. A dynamic concentration model for lubrication with oil-in-water emulsions. Wear 1993;161:207–12. https://doi.org/10.1016/0043-1648(93)90471-W.

[38] Chiu YP. An analysis and prediction of lubricant film starvation in rolling contact systems. A S L E Trans 1974;17:22–35. https://doi.org/10.1080/05698197408981435.

[39] Zhu D, Biresaw G, Clark SJ, Kasun TJ. Elastohydrodynamic lubrication with O/W emulsions. J Tribol 1994;116:310–9. https://doi.org/10.1115/1.2927216.

[40] Yang H, Schmid SR, Kasun TJ, Reich RA. Elastohydrodynamic film thickness and tractions for oil-in-water emulsions. Tribol Trans 2004;47:123–9. https://doi.org/10.1080/05698190490278976.

[41] Liang H, Guo D, Ma L, Luo J. Investigation of film formation mechanism of oil-in-water (O/W) emulsions at high speeds. Tribol Int 2017;109:428–34. https://doi.org/10.1016/j.triboint.2017.01.006.

[42] Zhang F, Fillot N, Bouscharain N, Devaux N, Philippon D, Matta C, et al. Water droplets in oil at the inlet of an EHD contact: A dual experimental and numerical investigation. Tribol Int 2023;177:108015. https://doi.org/10.1016/j.triboint.2022.108015.

[43] Liu X, Wang J, Huang L, Zhang J, Xu C, Tong L, et al. Direct observation of the impact of water droplets on oil replenishment in EHD lubricated contacts. Friction 2022;10:388–97. https://doi.org/10.1007/s40544-020-0466-0.

[44] Cyriac F, Lugt PM, Bosman R. Impact of water on the rheology of lubricating greases. Tribol Trans 2016;59:679–89. https://doi.org/10.1080/10402004.2015.1107929.

[45] Gurt A, Khonsari M. An overview of grease water resistance. Lubricants 2020;8:86. https://doi.org/10.3390/lubricants8090086.

[46] Cann PME, Damiens B, Lubrecht AA. The transition between fully flooded and starved regimes in EHL. Tribol Int 2004;37:859–64. https://doi.org/10.1016/j.triboint.2004.05.005.

[47] Jacod B., Pubilier F, E. Cann P.M., Lubrecht A.A. An Analysis of Track Replenishment Mechanisms in the Starved Regime, 1999, p. 483–492. ⟨https://doi.org/10.1016/S0167–8922(99)80069–8⟩.

[48] Cyriac F, Lugt PM, Bosman R, Venner CH. Impact of water on EHL film thickness of lubricating greases in rolling point contacts. Tribol Lett 2016;61:23. https://doi.org/10.1007/s11249-016-0642-6.

[49] Hudedagaddi CB, Raghav AG, Tortora AM, Veeregowda DH. Water molecules influence the lubricity of greases and fuel. Wear 2017;376–377:831–5. https://doi.org/10.1016/j.wear.2017.02.002.

[50] Li Q, Zhang S, Wu B, Lin Q, Ding H, Galas R, et al. Analysis on the effect of starved elastohydrodynamic lubrication on the adhesion behavior and fatigue index of wheel-rail contact. Wear 2022;510–511:204506. https://doi.org/10.1016/j.wear.2022.204506.

[51] Chen Z, He X, Xiao C, Kim S. Effect of humidity on friction and wear—a critical review. Lubricants 2018;6:74. https://doi.org/10.3390/lubricants6030074.

[52] White B, Kempka R, Laity P, Holland C, Six K, Trummer G, et al. Iron oxide and water paste rheology and its effect on low adhesion in the wheel/rail interface. Tribol Lett 2022;70:8. https://doi.org/10.1007/s11249-021-01549-0.

[53] Galas R, Omasta M, Shi L bing, Ding H, Wang W jian, Krupka I, et al. The low adhesion problem: The effect of environmental conditions on adhesion in rolling-sliding contact. Tribol Int 2020;151:106521. https://doi.org/10.1016/j.triboint.2020.106521.

[54] Arias-Cuevas O, Li Z, Lewis R, Gallardo-Hernández EA. Rolling-sliding laboratory tests of friction modifiers in dry and wet wheel-rail contacts. Wear 2010;268:543–51. https://doi.org/10.1016/j.wear.2009.09.015.

[55] Pieringer A, Kropp W. Model-based estimation of rail roughness from axle box acceleration. Appl Acoust 2022;193:108760. https://doi.org/10.1016/j.apacoust.2022.108760.

[56] Chen H, Namura A, Ishida M, Nakahara T. Influence of axle load on wheel/rail adhesion under wet conditions in consideration of running speed and surface roughness. Wear 2016;366–367:303–9. https://doi.org/10.1016/j.wear.2016.05.012.

[57] Zhu Y, Chen X, Wang W, Yang H. A study on iron oxides and surface roughness in dry and wet wheel-rail contacts. Wear 2015;328–329:241–8. https://doi.org/10.1016/j.wear.2015.02.025.
[58] Tyfour W.R., Beynon J.H., Kapoor A. The steady state wear behaviour of pearlitic rail steel under dry rolling-sliding contact conditions. vol. 180. 1995.
[59] Harmon M, Santa JF, Jaramillo JA, Toro A, Beagles A, Lewis R. Evaluation of the coefficient of friction of rail in the field and laboratory using several devices. Tribol Mater Surf Interfaces 2020;14:119–29. https://doi.org/10.1080/17515831.2020.1712111.

Tribology International 189 (2023) 108910

Contents lists available at ScienceDirect

Tribology International

journal homepage: www.elsevier.com/locate/triboint

A benchmarking methodology for top-of-rail products

Radovan Galas [a,*], Simon Skurka [a], Martin Valena [a], Daniel Kvarda [a], Milan Omasta [a], Haohao Ding [b], Qiang Lin [b], Wen-jian Wang [b], Ivan Krupka [a], Martin Hartl [a]

[a] Faculty of Mechanical Engineering, Brno University of Technology, Technicka 2896/2, 616 69 Brno, Czech Republic
[b] Tribology Research Institute, State Key Laboratory of Traction Power, Southwest Jiaotong University, Chengdu 610031, China

ARTICLE INFO

Keywords:
Rail-wheel tribology
Rolling-sliding
Friction modifier
Top-of-rail lubricants

ABSTRACT

Top-of-rail (TOR) products are designed to optimize adhesion, reduce wear and mitigate noise from the wheel-rail interface. Prior to testing these products in field conditions, a laboratory approach is suitable because it is not time-consuming and expensive. This study aims to design a benchmarking methodology to investigate the performance of TOR products using a standard tribometer in a ball-on-disc configuration. The resulting methodology is based on a multi-parameter approach enabling the assessment of TOR products from multiple perspectives. The core of the methodology is formed by traction tests and a robust evaluation phase resulting in a performance map dividing TOR products into four performance classes, Q1-Q4, based on which a suitable TOR product can be chosen for further testing.

1. Introduction

TOR products represent a progressive approach to modification of friction between the wheel tread and the rail head. In contrast with other conventional methods, such as sanding and flange lubrication, TOR products are designed to control friction at a desired level, referred to as an intermediate level of friction [1]. Besides that, the presence of TOR product in the contact should avoid a negative slope of the creep curve occurring in untreated contact [2]. According to the state of matter, TOR products are classified into solid and liquid. Solid TOR products are usually called “solid sticks” or “HPF solid sticks”, while there are different, sometimes confusing, terms for liquid products. Water-based products (drying products) are called friction modifiers (FMs), while oil- or grease-based products (non-drying products) are called TOR lubricants (TORLs). There is also a third category of TOR products containing both water and oil/grease. These products are called TOR hybrids [1,2].

The possible benefits of TOR products have been intensively studied since 1992, when Kalousek et al. [3] published a pilot study on railway friction management. This study was conducted on the Vancouver mass transit system line, where severe short pitch wheel and rail corrugation developed only a few months after its opening. This investigation showed that applying a solid stick to the wheel tread prevented corrugation formation as roll-slip oscillations were eliminated due to a positive creep curve. The ability to reduce or completely avoid the corrugation growth for different mass transit systems was later confirmed for FMs [4–7]. Other field studies [7–11] showed that suppression of roll-slip oscillations via solid or liquid TOR products reduced curve squeal noise. Moreover, these studies clarified the benefits of TOR products for several transit systems that differ in curve radii, track structures and track conditions. Besides this, it was shown that reducing the coefficient of traction (CoT) to the intermediate level brings other benefits, such as saving fuel consumption [12], reducing the risk of derailment [13,14], and no risk of isolation of track circuits [15] as can occur for sanding [16].

Although field studies have proved many benefits of TOR products, some negative effects related to their application have been revealed as well. One of the most severe drawbacks is the risk of a very low CoT compromising traction and braking. This undesirable phenomenon was observed for both FM [17] and TOR lubricants [18–20]. FMs may cause a very low CoT immediately after their application when a high amount of FM enters the contact [21]. In addition, a significant drop in the CoT was observed during the drying of FM when a viscous film was formed between the contacting surfaces [22]. In the case of TOR lubricants as oil or grease-based products, the applied amount strongly affects product performance [23,24]. A high amount of these non-drying products (TORLs and TORHs) in the contact can lead to the extension of braking distance and can promote the growth of pre-existing cracks and spalling formation [19,25]. Besides these security risks, recently published studies [26–28] showed that the expected benefits of TOR products, such as squeal noise reduction and long carry distance, cannot be

* Corresponding author.
E-mail address: Radovan.Galas@vut.cz (R. Galas).

https://doi.org/10.1016/j.triboint.2023.108910
Received 3 May 2023; Received in revised form 25 July 2023; Accepted 28 August 2023
Available online 29 August 2023

Nomenclature

CTZ	critical traction zone
FM	friction modifier
HPF	high positive friction
ITZ	intermediate traction zone
LTZ	low traction zone
MTM	mini-traction machine
PT, PT_1-PT_5	performance test
Q1-Q4	performance classes
RCF	rolling contact fatigue
RTZ	retentivity traction zone
S1-S6	steps of the experimental phase
S7-S9	steps of the evaluation phase
TOR	top-of-rail
TORP	model TOR product
TORL	TOR lubricant
c, c_1-c_5	critical traction parameter for individual PT (m)
C	average critical traction parameter (m)
CoT	coefficient of traction (1)
F_N	normal force (N)
F_T	traction force (N)
i, i_1-i_5	intermediate traction parameter for individual PT (m)
I	average intermediate traction parameter (m)
j	index representing different values of SRR (1)
k	index representing the number of PT (1)
n, n_1-n_5	number of creep curves within individual PT (1)
N	average number of creep curves for five PTs (1)
$N_{c,j}$, N_{c1}- N_{c5}	number of points of the creep curve(s) for a specific SRR in the CTZ (1)
$N_{i,j}$, N_{i1}- N_{i5}	number of points of the creep curve(s) for a specific SRR in the ITZ (1)
$N_{r,j}$, N_{r1}- N_{r5}	number of points of the creep curve(s) for a specific SRR in the RTZ (1)
OLF	over-lubrication factor (1)
r, r_1-r_5	retentivity for individual PT (m)
r_b	ball radius (m)
r_d	disc radius (m)
R	average retentivity (m)
Sa	average Roughness (m)
S_i	area defining the ideal product (m^2)
S_p	area defining the tested TOR product (m^2)
Sq	root mean square roughness (m)
SRR	slide/roll ratio (1)
t	duration of friction test (s)
t_r	duration of the run-in process (s)
t_w	duration of the wear-in process (s)
v	mean speed (m/s)
w	disc path width (m)
ω_b	ball angular speed (1/s)
ω_d	disc angular speed (1/s)

achieved.

These negative findings indicate that several aspects should be considered before implementing the friction modification method into real operation. One of the most important aspects is the purpose for which the TOR product is used. This factor should be considered together with the type of transit system because the performance of the same product may substantially vary for different systems. Another aspect relates to the application strategy that covers application amount, application interval, and application method. Two methods are currently used to apply TOR products: wayside units along the tracks and on-board vehicle units. Moreover, both methods enable applying TOR products on one or both wheels/rails.

It is evident that the successful implementation of friction management methods into operation involves many aspects that should be considered beforehand. Then, however, the question arises: How to choose a suitable product and its application strategy? One of the options represents field tests that provide reliable results but are costly and time-consuming. Therefore, this approach seems reasonable as a final step of testing. In contrast, laboratory tests seem suitable for comparing different TOR products in different aspects. These tests are inexpensive, time-saving, and usually can be performed under well-controlled conditions, which are difficult to achieve for field tests.

Several experimental approaches have been used to study TOR products in laboratory conditions. Full-scale devices were used to investigate the effect of TOR products on wear, rolling contact fatigue (RCF) [29,30] and bogie-curving performance [31]. In the case of small-scale devices, several types of devices were utilised to study TOR products: pin-on-disc tribometer [32,33], ball-on-disc tribometer [22,24,34], twin-disc machine [19,35–40], plate-on-plate tribometer [41], high-pressure torsion (HPT) tribometer [23,42], pendulum tester [43,44] and hand-push tribometer [44,45]. Note that the latter two approaches are mainly used in field measurements; thus, they can represent an intermediate step between operational and laboratory tests. This literature review showed that the adhesion/friction/traction level, retentivity, and creep curve are the most frequently evaluated parameters to assess the performance of TOR products in laboratory conditions. However, comparing the results across these studies is difficult, sometimes even impossible, because most studies on TOR products utilise non-commercial devices. It means that the contact bodies differ in many aspects, such as size, material, hardness, roughness, etc. Furthermore, the test procedure and parameters can also vary significantly, which further complicates the comparison of results. Based on these findings, it is clear that a unified testing methodology is required to standardize the design and assessment of TOR products under laboratory conditions. Recently published standard no. CEN/TS 15427–2–2:2021 [46] partially deals with this topic for a twin-disc machine and a Mini-Traction machine (MTM). This standard defines two types of tests for twin-disc machines whose result is product retentivity, CoT, and the creep curve. In addition, the test for creep curve investigation is described for MTM. This approach to determining product suitability relies on a single, basic criterion that provides limited insight into the product's behaviour, indicating a need for a more comprehensive testing methodology that can assess TOR products from multiple perspectives.

This study proposes a benchmarking methodology for assessing the performance of various TOR products under rolling-sliding conditions. A standard MTM tribometer in a ball-on-disc configuration was employed to ensure the future transferability and comparability of the results across different laboratories. A robust evaluation phase is an integral part of the comparative test methodology to ensure clarity of the assessment. This approach enables the complex assessment of TOR products from multiple perspectives and improves the reliability and accuracy of TOR product testing. In order to validate the proposed benchmarking methodology, the performance of three TOR products and one bleed oil (the oil separated from the TOR product) is tested and compared within the case study.

2. Material and methods

2.1. Introduction to the methodology development process

The methodology presented in this paper is based on the following assumptions:

I. **Single device:** A single widely used device is utilized to assess TOR products from various perspectives.
II. **Multi-parametric approach:** The product assessment is based on a combination of several important parameters of TOR products:
   - o Retentivity: time, number of cycles or sliding distance for which the product influences the CoT.
   - o Performance parameters: Parameters that express the duration for which a TOR product causes insufficient CoT level and the duration for which it provides a desired intermediate CoT level. These parameters are expressed as a function of sliding distance.
   - o These parameters are considered together to provide a single parameter expressing the product's relative performance.
III. **Traction zones:** Several zones of CoT, defined as a fixed ratio to the baseline (dry) CoT, are used to cover the changing CoT from product application until the moment when its effect is negligible.
IV. **Variable creep:** Benchmarking performance tests are done under different creep to assess product behaviour in different regions on the creep curve (CoT-SRR dependency).
V. **Amount dependence:** Some TOR products, especially oil- and grease-based, are strongly amount-dependent. It is not possible to compare the products regardless of the applied amount. This means that one product may perform better at a specific amount while another product may perform better at a different amount. A final assessment should clearly show which of the tested amount is appropriate for the tested TOR products and identify the TOR product that has the best potential for further testing using full-scale devices or in the field.
VI. **Run-in/wear-in process:** These processes were established specifically to provide the same initial state for all tests and to avoid excessive wear that negatively affects test repeatability.
VII. **Consecutive tests using the same specimens:** A number of consecutive tests are required to cover the variability of the results and gradual changes in the surface topography of the specimens.

2.2. Instruments and specimens

The MTM tribometer in a ball-on-disc configuration was used to develop and validate a benchmarking methodology for assessing TOR products. This tribometer was chosen because it simulates rolling-sliding conditions, similar to the real wheel-rail contact, and is widely used for tribological testing, including the above-mentioned CEN/TS standard [46]. The MTM tribometer and its scheme are depicted in Fig. 1. This configuration consists of a steel ball and a steel disc leading to non-conformal point contact. Both these standard specimens are independently driven; thus, desired slide/roll ratio (SRR) can be set. The SRR value is calculated according to Eq. (1), where ω_b and ω_d are the angular speeds of the ball and the disc, and r_b and r_d represent their radii. To investigate the CoT (Eq. (2)) the tribometer is equipped with load and traction sensors providing information about the normal force F_N and the traction force F_T. Detailed information about the specimens and sensors is listed in Table 1 and Appendix A, respectively.

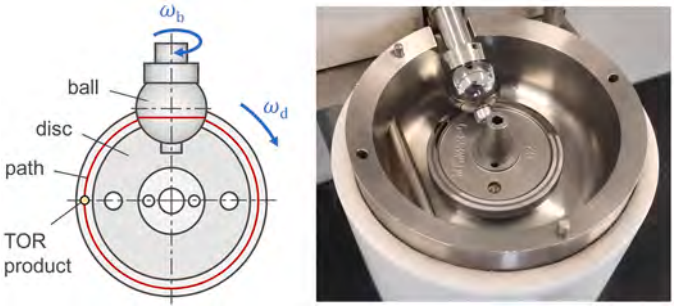

Fig. 1. MTM in ball-on-disc configuration.

$$SRR = \frac{\omega_b \cdot r_b - \omega_d \cdot r_d}{\omega_b \cdot r_b + \omega_d \cdot r_d} \cdot 200\% \quad (1)$$

$$CoT = \frac{F_T}{F_N} \quad (2)$$

2.3. Initial tests: methodology input parameters investigation

Several parameters had to be investigated as input parameters to the proposed methodology. These input parameters included: (1) the duration of the wear-in process, (2) the duration of the run-in process, (3) the creep curve for dry conditions (baseline), and (4) the traction zones and threshold curve. These input parameters are an integral part of the methodology, and the initial tests to investigate them are described in this Subchapter, while the proposed methodology is presented in Subchapter 2.4.

Two sets of tests were conducted under dry conditions to investigate the required input parameters. The experimental conditions of these initial tests are described in Table 2. This table shows that all tests were performed with a load of 18 N, corresponding to a maximum Hertzian pressure of 800 MPa. A mean speed was chosen to be 1 m/s because this value is frequently used for tribological testing on small-scale devices [38,39,47]. This relatively low speed was used because of the device limitation and the stability of tests. According to [48], a speed of 1 m/s on MTM corresponds to a higher train speed (tens of km/h) based on comparing the lambda parameter between MTM and the train.

Set no. 1 in Table 2 aimed to find a suitable duration of the wear-in and run-in process. The wear-in process is always performed when new contact pair is used to overcome excessive wear occurring when new bodies come into contact. In contrast, the run-in process is designed to stabilize the CoT and the surface roughness of worn contact pairs that were already used for TOR product testing. Suitable durations of wear-in process t_w and run-in process t_r were investigated based on the 20 consecutive 30-minute friction tests (CoT-time dependency) under dry conditions (600 min in total), see Table 2. All these friction tests were carried out at 2% SRR, which is a representative value for real wheel-rail contact. After each friction test, both specimens were cleaned in a solvent, and then the surface roughness (Sq and Sa) and the width of the contact path w were analysed for both contact specimens using an optical profilometer. The required time for the wear-in process t_w was chosen based on the evolution of the path width over time. The aim was to select a time at which excessive wear had already occurred. It means that the contact path became more stable for subsequent testing with TOR products. In the case of the run-in process, the required time t_r was chosen as the time needed to stabilise the CoT during the 20 friction tests mentioned above.

Set no. 2 in Table 2 was performed to investigate a creep curve (baseline) for dry conditions. This baseline was subsequently used as a reference curve to design the traction zones and the threshold curve, which are important for the evaluation phase of the proposed methodology (described below). While the maximum Hertzian pressure and mean speed of this set are consistent with set no. 1, SRR varied from 0% to 20%. However, there are two ranges of SRR listed in Table 2. Initially, a range of SRR from 0% to 50% was tested, but it was revealed that SRR values higher than 20% might not be appropriate for testing TOR products. The reason for this SRR limitation is described in the

Table 1
Detailed information about MTM specimens.

	diameter (mm)	material	hardness (HV)	roughness (μm)
ball	19.05	AISI 52100	800 – 920	0.01
disc	46		720 – 780	0.01

Table 2
Experimental conditions of initial tests: friction and traction tests.

set no.	conditions	Hertzian pressure	mean speed	SRR (%)	test duration	measured parameters	evaluated parameters	Fig. No.
1	dry (no TOR product)	800 MPa	1 m/s	2%	20 × 30 min	CoT, *Sq*, *w*	t_w, t_r	6
2				0–20% (0–50%)	6x (8 ×25 s)[a]	CoT	traction zones and threshold	7

[a] 60-minute wear-in process was carried out before this test.

discussion. Therefore, the SRR range was limited to 0–20% (specifically: 0%, 2%, 5%, 10%, 15%, and 20%) for all other tests in this study. As noted in Table 2, the creep curve for dry conditions was measured six times consecutively. These creep curves were obtained based on the series of friction tests (CoT-time dependency). Finally, the average baseline was determined.

The next step was to design the threshold curve and the traction zones. While the threshold curve is important for the measurement phase, the traction zones play a crucial role in the evaluation phase, see Fig. 3. As shown in Fig. 2, the following four traction zones have been defined for the proposed methodology: critical traction zone (CTZ), low traction zone (LTZ), intermediate traction tone (ITZ), and retentivity traction zone (RTZ).

The CTZ is marked in red because it represents a zone with very low CoT that may not provide enough traction and braking capability for vehicles. In contrast, the ITZ (the green zone) represents the range of CoT optimal for traction and braking while reducing significant wear occurring under dry conditions (baseline). As evident from Fig. 2, there is another zone labelled as the LTZ. The CoT values in the LTZ are no longer critical for traction and braking but are not optimal. The presence of this zone between CTZ and ITZ is meaningful because it prevents a sudden transition between critical CoT values and optimal ones. Moreover, this "transition" zone between CTZ and ITZ is commonly considered in the literature [30,49].

The last zone is the RTZ, which is important for evaluating the so-called retentivity parameter. This parameter is usually defined as the interval from product application until the product becomes ineffective regarding expected benefits [46]. Note that this parameter is typically expressed in the number of cycles. Based on its value, different TOR products can be compared in terms of expected carry distance representing one of the key parameters assessed in TOR products [46]. The carry distance defines how far the product is spread in real operation.

Considering the above, the RTZ is defined by zero at the lower boundary and by the upper limit of the ITZ at the upper boundary, as shown in Fig. 2. This upper limit of ITZ and RTZ is simultaneously considered as a threshold value for stopping the performance test (PT, described below) because, beyond this limit, the behaviour of the contact becomes similar to that of dry contact. In other words, the effect of TOR products becomes negligible beyond this limit.

The traction zones mentioned above have been defined as percentage values of the baseline, see Fig. 2. The percentage values were chosen according to [50,51], where the dry level of friction was considered 0.6,

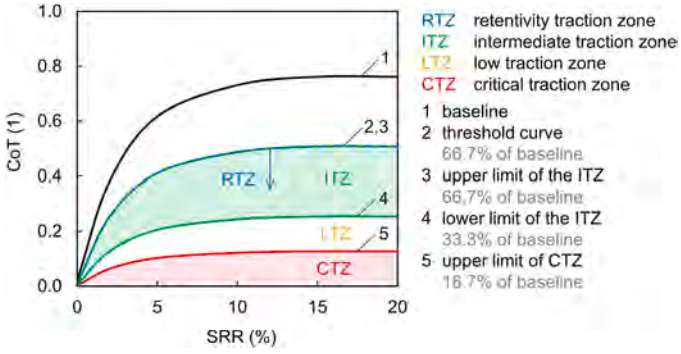

Fig. 2. Baseline, traction zones and threshold curve.

and the intermediate and low friction levels were 0.2–0.4 and 0.1, respectively. With respect to these values, the lower and upper intermediate limits were calculated to be 33.3% and 66.7% of the dry CoT. The limit value of a critical traction zone (CTZ) was 16.7% of the dry CoT.

Note that the specific values on the y-axis in Fig. 2 were obtained from the initial tests conducted under dry conditions (set no. 2 according to Table 2). Detailed descriptions of these test results can be found in Subchapter 3.1. This subchapter includes not only information about traction zones and the threshold curve but also describes other important input parameters for the proposed methodology, specifically the duration of the wear-in and run-in process. Once these parameters were determined in Subchapter 3.1, they were used as fixed values for all subsequent tests with TOR products described in Subchapter 3.2.

2.4. The proposed methodology and its steps

Fig. 3 provides a schematic representation of the proposed benchmarking methodology. The methodology consists of the experimental and evaluation phases, as shown in Fig. 3(a) and (b). The experimental phase includes five consecutive PTs (PT1-PT5), which are required to investigate the performance of one TOR product for one specific applied amount. It is important to note that all five PTs are carried out using the same contact pair. It means that the initial conditions (such as the path width, roughness, pressure, etc.) are not the same for individual PTs due to wear from the previous PT(s). This approach is beneficial because it enables the investigation of the performance of TOR products under a wide range of conditions, and the resulting product assessment is thus more representative.

Each of the five PTs is composed of a preparation phase (indicated by blue colour) and the measurement phase (indicated by red colour), as shown in Fig. 3(a). These two phases comprise six consecutive steps (S1-S6), but only step S4 (traction test) is considered as the measurement step. In this step (S4), The CoT is measured for six SRR values ranging from 0% to 20% (the detailed test procedure is described below). The result of this traction test is plotted to form the creep curve, as depicted in Fig. 4. This figure provides a detailed view of steps S4 and S5. Once the traction test S4 is completed and the creep curve is obtained, checkpoint S5 must be performed. Depending on the result of checkpoint S5, the PT continues by S6 or is finished, and another PT can start by S1. If PT continues, more creep curves are obtained within one PT. It indicates that several creep curves can be obtained during one PT, as in the example in Fig. 4 – step S5, where three creep curves are obtained before checkpoint S5 is met. This procedure is repeated until the fifth PT is completed.

As was mentioned in the previous paragraph, the experimental phase is completed after the fifth PT. Subsequently, the evaluation phase begins with step S7, as illustrated in Fig. 3(b). It should be emphasized that the traction zones depicted in Fig. 2 are crucial for the first evaluation step (S7). This step focuses on the calculation of the performance parameters noted in Table 3.

At first, three performance parameters denoted with lowercase letters (*c*, *i*, and *r*) are evaluated for each PT. As evident from Table 3, each of these parameters is named according to the related traction zone (CTZ, ITZ, and RTZ). These parameters are calculated as the cumulative sliding distance over which the contact was operating in the related traction zone. It means that a total of fifteen parameters (c_1-c_5, i_1-i_5, and

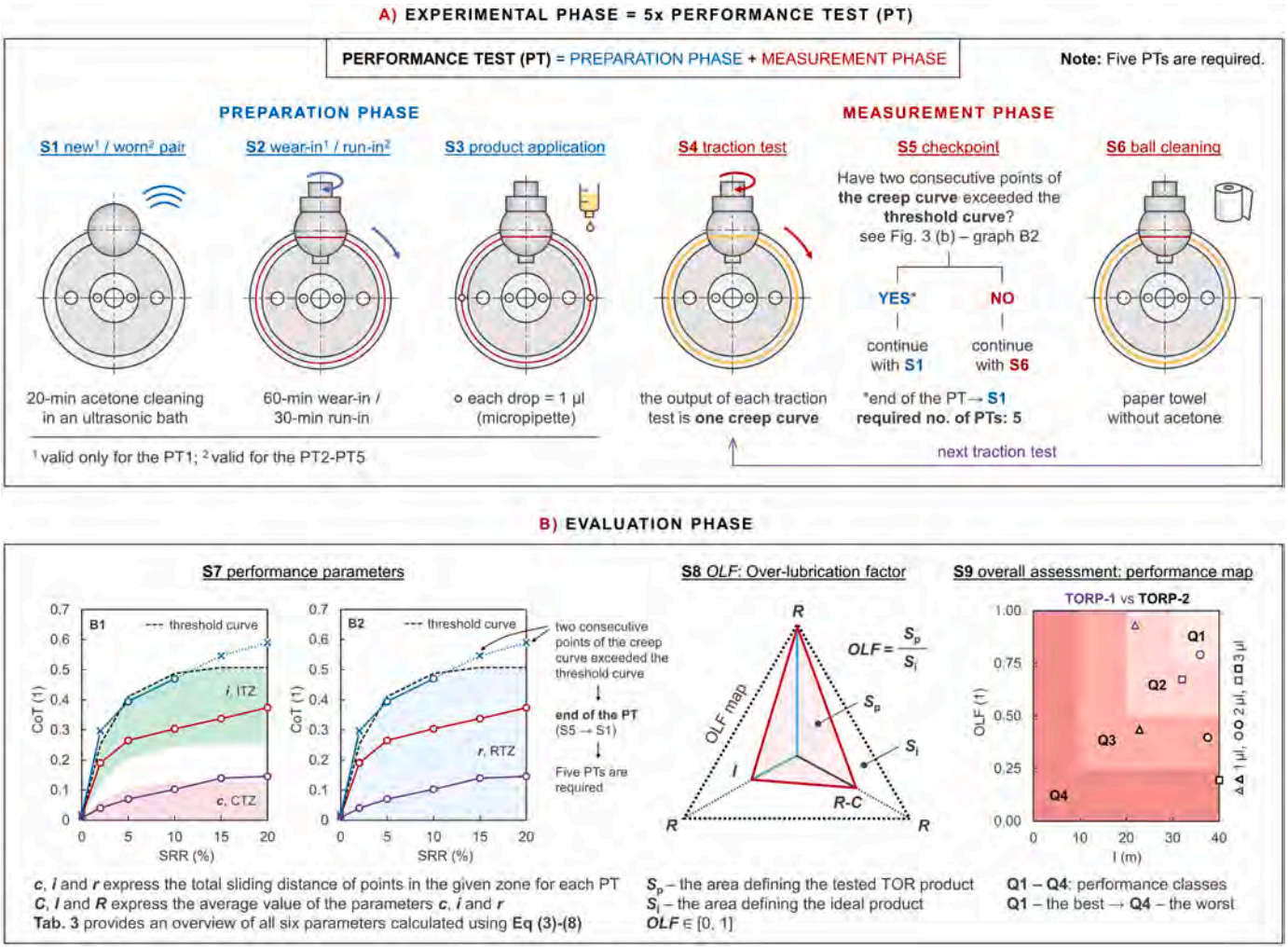

Fig. 3. A benchmarking methodology for assessing the performance of TOR products: (a) experimental phase and (b) evaluation phase.

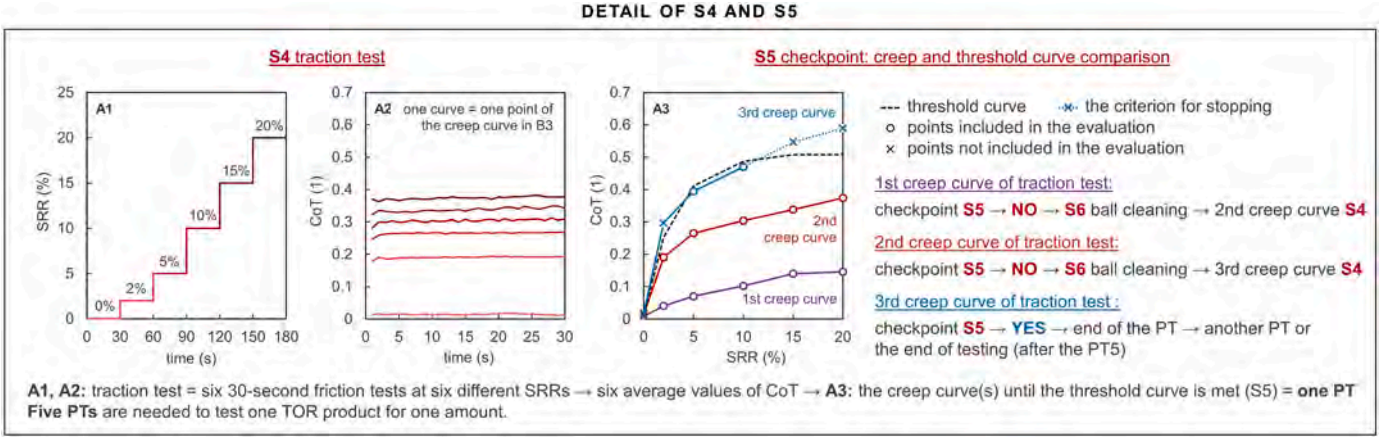

Fig. 4. Detailed information about methodology steps S4 and S5.

r_1-r_5) are obtained for the five required PTs. Subsequently, these sets of parameters are used to determine the average performance parameters denoted by capital letters (C, I, and R). A more detailed description of the parameter calculations is provided below.

Individual PT test parameters (c, i, and r) are calculated according to Eqs. (3)–(5), where index k represents the number of PTs (k = 1–5). Note that it is necessary to know the values of the traction zones to calculate these parameters. As noted earlier, each performance parameter expresses the cumulative sliding distance over which the contact was operating in the related traction zone. It is important to emphasize that the sliding distance is calculated as cumulative, using the sum, because the individual points of the creep curve are measured for different SRRs. Each of these individual points of the creep curve is determined based on a 30-second friction test (CoT-time dependency, see Fig. 4); thus, the

Table 3
Overview of the performance parameters evaluated in step S7.

	symbol	related traction zone	related Eq. no.
Critical traction parameter	c, (c_1-c_5)	CTZ	3
Intermediate traction parameter	i, (i_1-i_5)	ITZ	4
Retentivity	r, (r_1-r_5)	RTZ	5
Average critical traction parameter	C	CTZ	6
Average intermediate traction parameter	I	ITZ	7
Average retentivity	R	RTZ	8

time t in Eqs. (3)–(5) is equal to 30 s and remains constant. In addition, the velocity $v = 1$ m/s also remains constant for calculating all parameters.

On the contrary, each point of the creep curve is measured for different SRR values; therefore, a summation with an index j is included in the equations. This index describes the variation in SRR during the measurement of individual points (friction tests) of the creep curves. The index j ranges from 1 to 5, corresponding to the SRR values in the table in Fig. 5. Note that an SRR of 0% is not included in the calculation because the sliding distance equals zero for this SRR value (pure rolling conditions).

The last parameters in Eq. (3)-(5), $N_{c,j}$, $N_{i,j}$, $N_{r,j}$, represent the number of points of the creep curve(s) (obtained for one PT) within a given traction zone and at a given SRR. In other words, the first character of the index determines from which traction zone the points of the creep curve(s) are selected, while the second character further narrows down the selection of points based on the desired SRR value. This desired SRR value ranges from 2% to 20%, as defined by the summation index j and table in Fig. 5.

Fig. 5 provides an example of how $N_{c,1}$-$N_{c,5}$ can be determined. For simplicity, Fig. 5 depicts only one traction zone (CTZ) and two creep curves. The red points represent the points belonging to the related traction zone (CTZ, based on the first character of the index). If the second character of the index equals "3", for example, then only the points corresponding to a 10% SRR are counted, resulting in $N_{c,3} = 2$. The same procedure also applies to ITZ and RTZ.

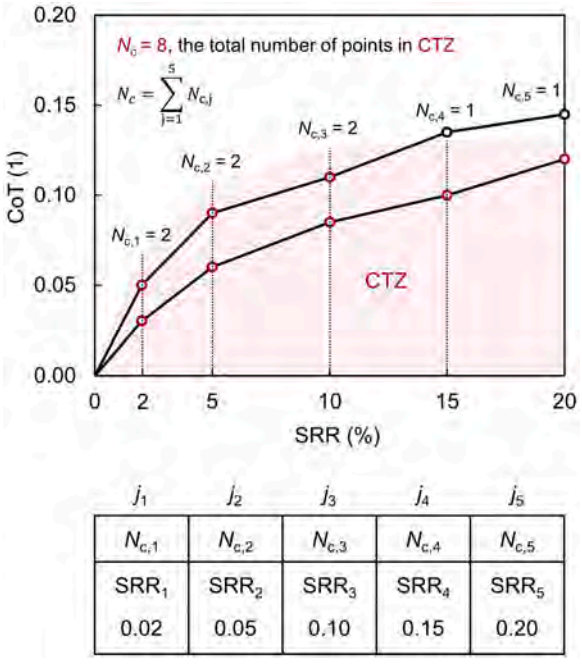

Fig. 5. Example illustrating the determination of $N_{c,j}$ points.

$$c_k = \sum_{j=1}^{5} t \cdot v \cdot \mathrm{SRR}_j \cdot N_{c,j} \tag{3}$$

$$i_k = \sum_{j=1}^{5} t \cdot v \cdot \mathrm{SRR}_j \cdot N_{i,j} \tag{4}$$

$$r_k = \sum_{j=1}^{5} t \cdot v \cdot \mathrm{SRR}_j \cdot N_{r,j} \tag{5}$$

When the performance parameters are evaluated for each PT, three sets of parameters are obtained: c_1-c_5, i_1-i_5, and r_1-r_5. These sets are subsequently used to calculate the average performance parameters C, I, and R using Eqs. (6)-(8).

$$C = \frac{1}{5} \sum_{k=1}^{5} c_k \tag{6}$$

$$I = \frac{1}{5} \sum_{k=1}^{5} i_k \tag{7}$$

$$R = \frac{1}{5} \sum_{k=1}^{5} r_k \tag{8}$$

When S7 is completed, performance parameters C, I, and R are used to assess the overall performance of TOR products. The overall performance is based on two parameters. The first one is the average intermediate traction parameter I described above. This parameter is crucial because it expresses the average sliding distance over which the TOR product provides the desired intermediate level of CoT. As the second parameter, the aim was to use a parameter that would not only indicate whether a tested TOR product may be risky in terms of low (LTZ) and critical CoT (CTZ) but also quantify the degree of this risk. For this purpose, an Over-Lubrication Factor (OLF) was defined. As can be seen in see Fig. 3(b) – step S9 and Eq. (9), the OLF is defined as the ratio of the triangle area of the tested TOR product S_p (the red triangle) to the area of the ideal product S_i (the black dotted triangle).

$$\mathrm{OLF} = \frac{S_p}{S_i} = \frac{R \cdot I + R \cdot (R - C) + I \cdot (R - C)}{3 \cdot R^2} \tag{9}$$

The pair of triangles in Fig. 3(b) is further referred to as the OLF map. Note that the OLF ranges between 0 and 1 depending on the values of the average performance parameters C, I, and R. It means that the calculation of the OLF includes data from all proposed traction zones, including the LTZ. Although the LTZ does not have a corresponding average performance parameter, its data are included in the RTZ, contributing to the parameter R. It should be pointed out that the angles between the directions in which the parameters of triangles are plotted are 120°.

Fig. 3 shows that the triangle representing the tested product is defined by the following vertices: R, R-C, and I. The vertex R was chosen because it directly represents the retentivity of the tested product. The second vertex is defined as the difference between R and C. This vertex ensures that with an increase in the "undesirable" parameter C, the triangle size decreases, resulting in a lower OLF value. The last vertex is defined by the average performance parameter I expressing the sliding distance over which the product provides the desired intermediate level of CoT. As evident from Fig. 3(b) – S8, this red triangle is compared with the black triangle defining the ideal product. This black triangle is drawn solely based on the parameter R (all vertices). The term "ideal" is used because $C = 0$ and $R = I$, which means that the product provides only the desired intermediate level of CoT (all points of creep curves lie within the ITZ, $R = I$) without any risk of low and critical CoT ($C = 0$).

Because OLF is defined as the ratio of the above-described triangles, the OLF value represents the deviation of the test TOR product's performance from the ideal product's performance. The closer the OLF

value is to 1, the better the behaviour of the TOR product can be expected in real operation. In contrast, lower OLF values indicate a risk of over-lubrication, which may lead to traction and braking issues. Once the OLF is calculated, the overall performance of the tested TOR product can be evaluated by considering both the OLF and parameter *I*.

The overall assessment is built on the I-OLF map defined in this study. This map represents the final step of the proposed methodology, Fig. 3(b) – step S9. This I-OLF map, further referred to as a "performance map", is plotted to compare the performance of different TOR products under varying applied amounts. An example of this performance map is in Fig. 3(b) – step S9, where the performances of two model TOR products (TORP-1 and TORP-2) are plotted for three different amounts. These different amounts are represented using different shapes of data points/markers.

When the performance map is plotted, the graph is divided into four equidistantly ranked performance classes/quartiles Q1-Q4, ranked from the best to the worst. If the tested TOR product reaches group Q1, it shows its ability to provide a long effective carry distance without a high risk of over-lubrication. Note that the effective carry distance is defined as the carry distance where the CoT lies within the intermediate traction zone. Compared to the Q1 class, reaching the Q4 class for the TOR product is likely to result in a significantly shorter effective carry distance and/or a higher risk of over-lubrication. Using these four performance classes makes it possible to compare and select the optimal TOR product and its amount for further testing. It should be noted that the y-axis range (OLF) is fixed from 0 to 1, representing absolute categorization. In contrast, the x-axis is relative, as the best tested TOR product (in terms of the parameter *I*) determines its range. However, it should be noted that future studies should set the x-axis range based on the best-performing TOR product obtained so far. If not, the classification of products into classes Q1-Q4 may be significantly affected.

The individual steps of the proposed methodology are summarized in the following points:

- S1 new/worn pair: Cleaning the specimens in a solvent ultrasonic bath for 20 min to remove any preservative oil (for the new pair) or TOR product residue (for the already used pair).
- S2 wear-in/run-in process: The wear-in process is performed only before the first PT when the new pair is used. The run-in process is performed instead of the wear-in process for the second and subsequent PTs. The wear-in and run-in process duration is 60 and 30 min, respectively.

Note: These durations represent the input parameters investigated during the initial tests (set no. 1 in Table 2). These tests and their results are described in the following chapter.

- S3 product application: All tested products are applied to the disc path using an electronic micropipette with a tip volume of 0.1 ml. This configuration allowed for the maintenance of systematic and random errors below ± 1.6% and ± 2.5%, respectively, while also ensuring a minimum dosage of 1 μl. Note that an application jig can be employed with the micropipette to increase the accuracy of the product application. All applications are made at zero speed of samples immediately after finishing the wear-in/run-in process. As depicted in Fig. 3(a) – step S3, the lubricant dose is split into a series of 1 μl drops, which are distributed evenly around the circumference of the contact path to achieve uniform application.
- S4 traction test: Each traction test includes six 30-second friction tests (CoT-time dependency at a specific SRR). Fig. 4 shows that each of these 30-second friction tests is conducted at a different specific SRR value, ranging from 0% to 20%. These tests result in six friction curves for six different SRR values describing the evolutions of the CoT over time, see Fig. 4 – graph A2. Based on these friction curves, six average values of CoT are calculated for each tested SRR. These average values of CoT are used to plot a single creep curve, see Fig. 4 – graph A3. When the creep curve is completed, checkpoint S5 must follow.
- S5 checkpoint: An obtained creep curve from S4 is compared with the threshold curve (depicted in Fig. 2 and described in detail below), and the following criterion is checked: "Have two consecutive points of the creep curve exceeded the threshold curve?" Please note that it requires two consecutive points on a single creep curve, as depicted in Fig. 3(b) – graph B2. As a result of checkpoint S5, there are two following possibilities:

  - NO (the criterion has not been met): No two consecutive CoT points on a single creep curve exceeded the threshold curve (e.g. purple and red creep curves in Fig. 4 – graph A3). In this case, the PT continues at step S6.
  - YES (the criterion has been met): Two or more consecutive CoT points on a single creep exceeded the threshold curve (e.g. blue curve in Fig. 4 – graph A3). After that, another PT should begin with step S1 if the fifth traction test has not been completed yet.

- S6 ball cleaning: When the traction test S4 has been completed, and criterion S5 has not been met, the ball path is cleaned with a paper towel without solvents. The subsequent traction test S4 begins after this cleaning, as indicated by the purple arrow in Fig. 3(a). This cycle of steps S4 and S6 is repeated until criterion S5 is met. Note that there are two reasons for ball cleaning. Firstly, the cleaning decreases the amount of TOR product in the contact path, which leads to the shortening of the traction test. This shortening helps avoid the undesired smoothing effect described in the Discussion. This aspect is important because it enables testing larger applied amounts of TOR products without the risk of smoothing. The second reason is to simulate a situation in the field where a product covers only one surface, and the second is "fresh" without any TOR product. White et al. [49] used a similar cleaning approach where the retentivity of traction gels was studied.
- S7 performance parameters: Based on the results of PTs and designed traction zones, the *c*, *i*, and *r* parameters are calculated according to Eqs. (3)–(5) for each PT. Subsequently, the average performance parameters *C*, *I*, and *R* are evaluated using Eqs. (6)-(8).
- S8 OLF: The average performance parameters are plugged into Eq. (9) to calculate the OLF.
- S9 performance map: This map is drawn based on the OLF and the parameter *I*, where each point on the map corresponds to the performance of the TOR product at a specific tested amount. This approach enables a comprehensive comparison of the performance of TOR products for various amounts.

2.5. Case study

The proposed methodology was verified using a case study where two TOR lubricants (TORL-A and TORL-B) and one FM were tested for different amounts. It should be pointed out that FM was tested for both wet and dry conditions (the terms wet-FM and dry-FM are used below) to describe the possible change in its performance due to the evaporation of the base medium. In addition, the performance of TORL-A bleed oil was investigated for two amounts to show the difference between the behaviour of TORL and bleed oil. The experimental conditions of this case study are listed in Table 4. Note that the maximum Hertzian pressure, mean speed, and SRR range were the same as in the initial tests described in Subchapter 2.4.

3. Results

3.1. Results of the initial tests

Fig. 6 shows the results of set no. 1 according to Table 2, which aimed to find necessary methodology input parameters. These input

Table 4
Experimental conditions of the case study: traction tests.

set no.	TOR product	applied amount	Hertzian pressure	mean speed	SRR	test duration	measured param.	evaluated param.	Fig. No.
3	wet-FM	1, 2, 3, 12 μl	800 MPa	1 m/s	0–20%	to threshold value[1]	*CoT*	*5x (c, i, r),*	8, 10
4	dry-FM	12 μl						*C, I, R*	8, 10
5	TORL-A	1, 2, 3, 5 μl						*OLF*	9, 10
6	TORL-B	1, 2, 3 μl							9, 10
7	TORL-A	1, 3 μl							10
	bleed oil								
	overview of all results using the performance map of TOR products								11

[1] 60-minute wear-in process was carried out before the application of the TOR product.

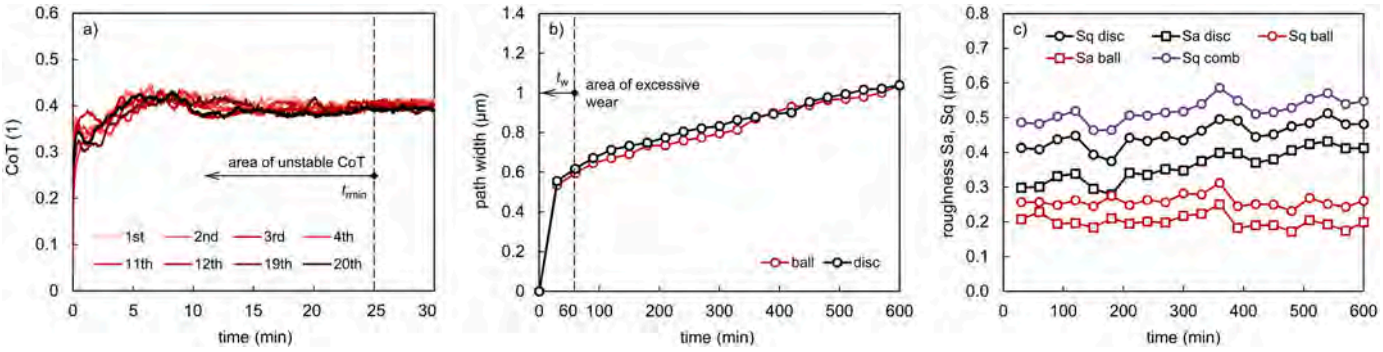

Fig. 6. The results of initial tests under dry conditions (set no. 1 according to Table 2): (a) the examples of friction tests, (b) the development of the ball and disc path during twenty consecutive friction tests, (c) the evaluation of disc and ball roughness during twenty consecutive friction tests.

parameters included the time needed for the run-in and wear-in process, which were determined based on twenty consecutive friction tests (CoT-time dependency) that were measured for various SRRs. Examples of these friction tests are depicted in Fig. 6(a), where only eight curves are drawn for clarity. These curves indicate that the CoT is unstable in the first hundreds of seconds and becomes stable after approximately 1 500 s. Therefore, a time of 1 800 s (t_r =30 min) was finally chosen as the required time for the run-in process. After each friction test, the path width of both contact bodies was evaluated to identify the time needed for the initial wear-in process of the new contact pair, see Fig. 6(b). The results show that excessive wear occurred during the first 40–60 min; after that, the path width grew steadily. Therefore, the time required for the wear-in process t_w was chosen to be 60 min. This wear-in time ensured that the path width was around 0.6 mm before the traction test with the TOR product (step S4). Fig. 6(c) shows the development of surface roughness of both specimens. It is evident that the ball roughness remained almost the same, whereas a gradual increase in the disc roughness was observed. As a result, the calculated combined roughness of the ball and the disc fluctuated between 0.46 and 0.59 μm.

Fig. 7 shows the results of set no. 2 according to Table 2. The purpose of this set was to investigate a creep curve (baseline) under dry conditions and to design the traction zones, which are crucial for the evaluation phase of the methodology. Six creep curves under dry conditions were evaluated for eight different SRR values, see Fig. 7(a). It can be seen that there is no substantial difference among these creep curves. CoT saturates at SRR values between 10% and 20% in all cases. However, a further SRR increase led to a gradual CoT reduction accompanied by an interfacial layer formation, see Fig. 7(c). This layer covered most of the contact path, and its thickness reached up to 2.5 μm. Therefore, the range of SRR was limited to 20% for other tests to mitigate interfacial layer formation. A threshold curve and adhesion zones were then designed for the SRR range from 0% to 20% according to the proposed percentage values of the creep curve under dry conditions. The resulting threshold curve and traction zones are plotted in Fig. 7(b), and CoT values of individual points and related performance parameters are given in Table 5.

3.2. Results of the case study

After initial tests under dry conditions, the measurement phase (steps

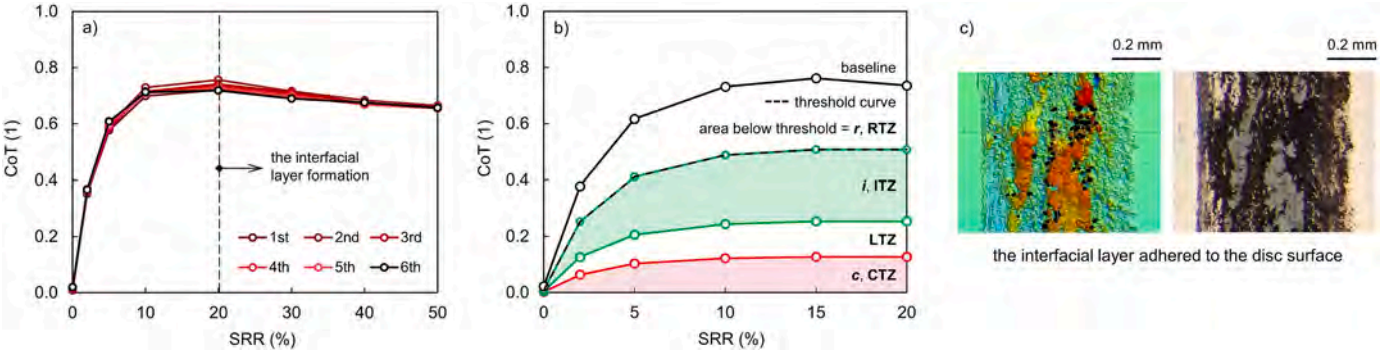

Fig. 7. The results of initial tests under dry conditions (set no. 2 according to Table 2): (a) reference creep curves (baselines) under dry conditions, (b) designed traction zones and threshold curve, (c) the disc surface covered by an interfacial layer after the test at high SRR.

Table 5
Baseline, traction zones, threshold curve and performance parameters.

Traction zones	SRR	0%	2%	5%	10%	15%	20%	perform. param.
	% of dry CoT							
baseline	100%	0.022	0.379	0.617	0.731	0.762	0.736	-
threshold curve; retentivity	66.7%	0.015	0.253	0.411	0.487	0.508	0.508[1])	*r, R*
intermediate zone upper limit	66.7%	0.015	0.253	0.411	0.487	0.508	0.508[1])	*i, I*
intermediate zone lower limit	33.3%	0.007	0.126	0.206	0.244	0.254	0.254[1])	
very low zone (upper limit)	16.7%	0.004	0.063	0.103	0.122	0.127	0.127[1])	*c, C*

[1]) The same value as for 15% SRR was used to avoid the negative trend of the creep curve behind the saturation point occurring under dry conditions.

S4-S6) and the evaluation phase (step S7) were performed to calculate the individual and average performance parameters. These tests correspond with set no. 3–7 in Table 4, where one FM, two TOR lubricants and one bleed oil of one TORL were tested for different applied amounts. Investigating the effect of applied amounts for several products resulted in many large data sets; therefore, only some of them are presented in the following paragraphs. It is important to note that only the points that are included in the evaluation of performance parameters (prior to checkpoint S6 being met) are displayed in the graphs below. Complete results for all products and tested amounts are summarised in Fig. 11. Appendix B lists the performance parameters for all tested conditions.

Fig. 8 presents the results of wet-FM (a-c) and dry-FM (d-f) for the amount of 12 µl (set no. 3 and 4 according to Table 4). The left and middle graphs show examples of PTs, specifically the third and fifth, which were performed according to steps S4 and S5 in Figs. 3 and 4. A summary of the result of all five PTs, which were required to assess the performance of one product, is shown in the graphs to the right (c,f). These bar charts show the values of the performance parameters *c*, *i* and *r* obtained for individual PTs. Moreover, this figure also includes their average values *C*, *I*, and *R*, which define the performance of the tested product throughout the whole testing. Besides this, parameters n_1-n_5 represent the number of traction tests performed in each PT, and the *N* parameter was calculated as an average value. The results in Fig. 8 give evidence that wet-FM provides a longer period of intermediate CoT (the *I* parameter) and a longer retentivity (the *R* parameter) compared to dry-FM. In these cases, the *I* parameter is equal to the *R* parameter because there are no points of creep curves in the very low (the *C* parameter) and low traction zones.

Fig. 9 shows the results of TORL-A (a-c) and TORL-B (d-f) for the lowest tested amount of 1 µl (set no. 5 and 6 according to Table 4). As in the case of FM results, the left and middle graphs show the results of the 3rd and 5th PTs, based on which the individual and average performance parameters were evaluated and displayed in the bar charts on the right. The results revealed that both TOR lubricants provided longer retentivity than FM, even though the applied amount was twelve times smaller. However, for TORL-A and TORL-B, only 40% and 55% of the parameter *R* is made up of the points in the intermediate zone (the *I* parameter). The rest of the *R* parameter is given mainly by points in the low traction zone because parameter *C* was negligible for both tested TOR lubricants.

After the completion of steps S1-S7, the OLF was calculated to reveal the tendency of tested TOR products for different amounts to over-lubricate the contact. The example of OLF maps for tests depicted in Figs. 8 and 9 are shown in Fig. 10. Moreover, Fig. 10 also includes the OLF maps for two tested amounts of the TORL-A bleed oil in order to show the difference between the behaviour of TORL and its bleed oil. It

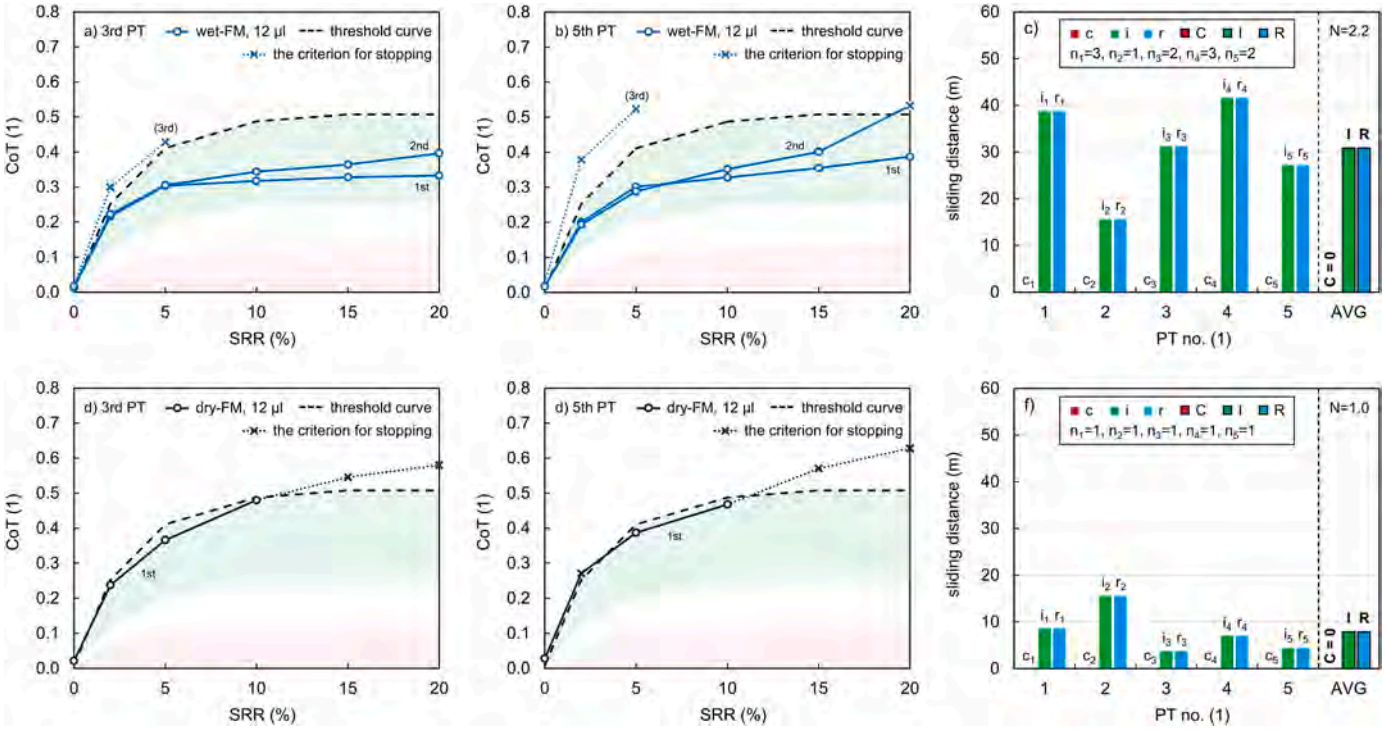

Fig. 8. The results of FM (set no. 3 and 4 according to Table 4, 12 µl): (a) the 3rd PT of wet-FM, (b) the 5th PT of wet-FM, (c) the performance parameters of wet-FM, (d) the 3rd PT of dry-FM, (b) the 5th PT of dry-FM, (c) the performance parameters of dry-FM.

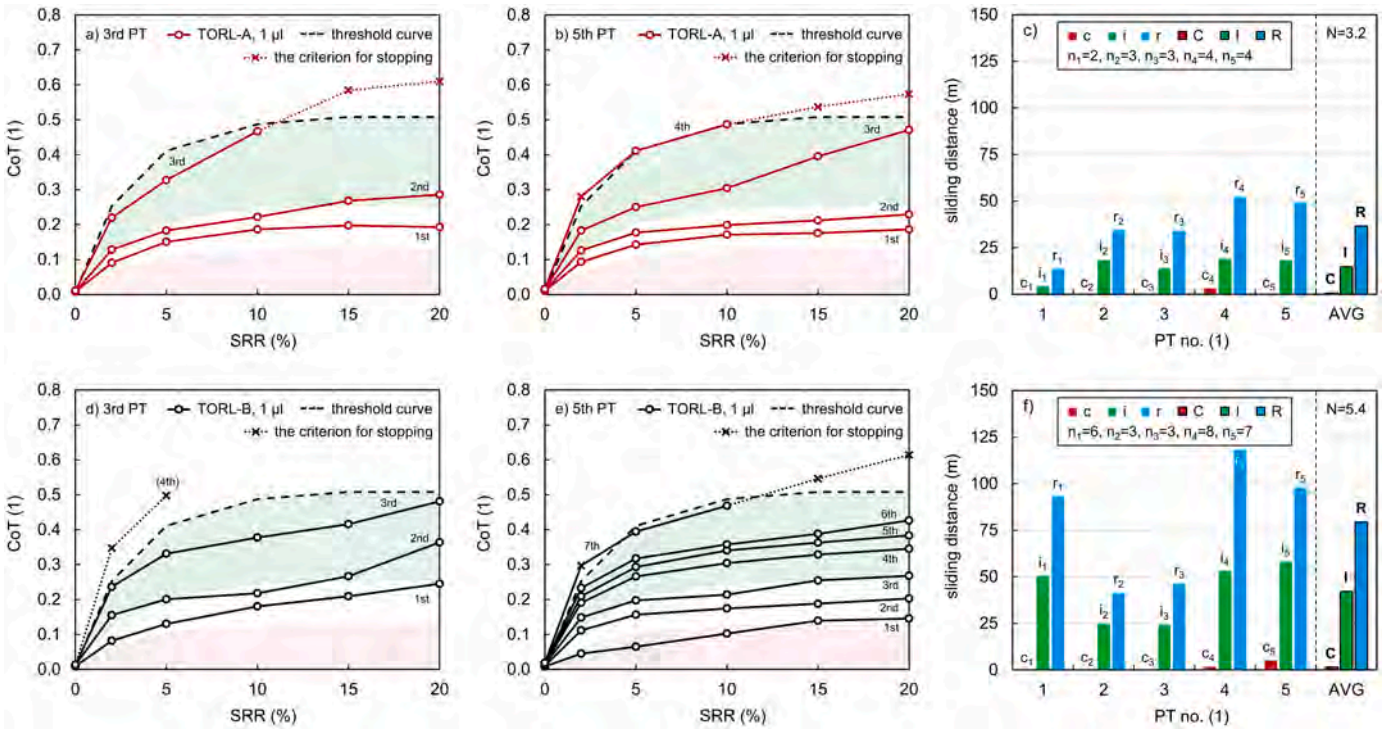

Fig. 9. The results of TORL-A and TORL-B (set no. 5 and 6 according to Table 4, 1 µl): (a) the 3rd PT of TORL-A, (b) the 5th PT of TORL-A, (c) the performance parameters of TORL-A, (d) the 3rd PT of TORL-B, (b) the 5th PT of TORL-B, (c) the performance parameters of TORL-B.

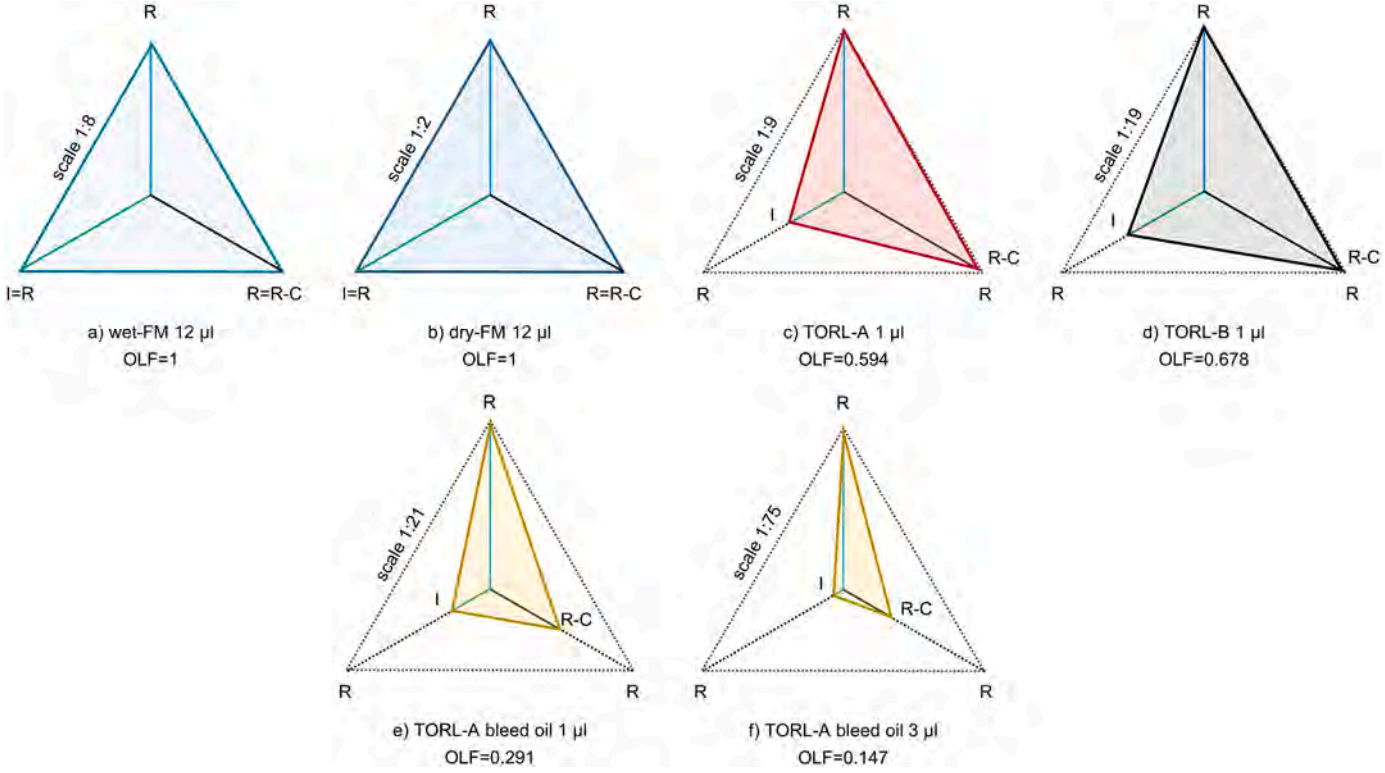

Fig. 10. OLF maps: (a) wet-FM, (b) dry-FM, (c) TORL-A, (d) TORL-B, (e) and (f) TORL-A bleed oil.

should be pointed out that the triangles are drawn at different scales because the tested products achieved significantly different retentivity (the *R* parameter). The first two maps (a) and (b) demonstrate the performance of wet-FM and dry-FM for 12 µl. In both cases, the triangle defining the product performance is identical to the triangle representing the best possible score; therefore, the OLF equals 1. Maps (c) and (d) show the results of TORL-A and TORL-B for the applied amount of 1 µl. As was mentioned above, TORL lubricants caused low and even very low CoT, which indicates that the *R* and *I* parameters are not equal. Therefore, the OLF parameters are lower than 1, specifically

0.594 for TORL-A and 0.678 for TORL-B. The last pair of OLF maps (e) and (f) show the results of TORL-A bleed oil. Comparing the scales with the other maps, it is evident that the bleed oil provided much longer retentivity, as expected. However, the *C* parameter significantly reduced the OLF, resulting in values of 0.291 and 0.147 for 1 μl and 3 μl, respectively. When comparing the performance triangles of tested products with those representing the best possible scores, it is evident that TOR products achieve a significantly better result in preventing over-lubrication than bleed oil.

Fig. 11 (a) shows the performance map and amount-OLF relationship representing the final assessment of tested products. None of the tested products was classified as Q1, the highest-performing class. Wet-FM (12 μl) and TORL-B (1 μl) were the top performers in this study, achieving a Q2 performance class. The rest of the products/amounts fell into the performance classes in Q3 and Q4. As is evident from Fig. 11 (a), FM is limited by very short retentivity, whereas a worse rating of oil-based products results from the low values of OLF. Fig. 11 (b) shows that the higher the amount of oil-based products, the lower the OLF. In contrast, no effect of the applied amount on OLF was observed for FM. Fig. 11 also illustrates the contrasting frictional behaviour between TOR lubricant and its bleed oil. It was revealed that bleed oil led to significantly lower OLF values for both tested amounts compared to TORL.

4. Discussion

This section is divided into four parts. In the first part (4.1), the individual steps of the experimental phase of the proposed methodology are discussed. Moreover, the discussion of initial tests dealing with the input parameters is included in this part. Note that the evaluation steps are omitted because they have been described and explained in Subchapter 2.4. The second part (4.2) focuses on analysing and interpreting the performance of tested products investigated according to the proposed methodology. In addition, the reliability of the methodology is discussed. In the third part (4.3), the proposed methodology is discussed in relation to the CEN/TS standard [46]. Finally, the last part of the discussion (4.3) describes possible future extensions of the methodology.

4.1. Discussion of the methodology: experimental phase

S1 new/worn pair and cleaning: both the new and worn pairs were cleaned in an ultrasonic bath with solvent for 20 min. It should be pointed out that Areiza et al. [45] revealed that solvent cleaning could not completely remove strongly-adhered oxide layers forming during the tests. Therefore, an effective cleaning method was introduced by Navrátil et al. [39], where solvent cleaning was combined with water and mechanical cleaning/grinding with sandpaper. This cleaning method resulted in a clean surface without any visible residue, and the required time for a subsequent run-in process was reduced. Although this method has proven very effective, applying it to MTM samples is difficult because of their narrow contact paths. Therefore, in this study, solvent cleaning in an ultrasonic bath was always followed by a relatively long run-in process to remove the residue of tested products and the interfacial layer.

The material of the contact bodies was bearing steel AISI 52100 100Cr6, which differs in chemical composition and hardness compared to rail and wheel steel. However, the use of these original specimens, offered directly by the tribometer manufacturer, allows future comparison and transferability of the results across laboratories, which is one of the main requirements for any methodology and standard. Furthermore, higher hardness and higher wear resistance of AISI 52100 lead to milder wear and less surface damage than in the case of softer wheel and rail steels. It means that the tests with bearing steel are less affected by changes in surface topography and contact pressure, and the impact of wear debris on the test is not so substantial. This behaviour is crucial for the stability and repeatability of tests, especially for small point contact, as in the case of the MTM tribometer. Therefore, the high carbon-chromium steel seems suitable for friction tests, where the effect of TOR products or another material on friction is investigated. Due to these material properties, this type of steel has been commonly utilized in many previous studies [22,23,47,48,52]. As demonstrated by Harmon et al. [44] for rail materials with varying hardness, higher hardness in specimens may result in slightly lower CoT values compared to softer materials.

S2 wear-in/run-in process: the primary purpose of the run-in process is to stabilize the CoT and roughness. In addition, this process is important to remove residual layers that were formed on the surfaces during tests with TOR products or as a consequence of solvent cleaning. The required time of the run-in process was determined based on the shape of the curves in Fig. 6(a). These data showed that at least 25 min (finally chosen 30 min) was necessary to stabilize the CoT. After 30 min, the CoT was stable and reached almost the same value for all tests. The shape of the curves in Fig. 6(a) is typical for non-lubricated steel-on-steel contact because this type of contact needs some time to stabilise roughness and surface conformity [53]. Optical analysis showed that the combined roughness Sq of specimens was almost the same at the end of each test. The average value of combined Sq was 0.52 ± 0.03 μm, which is in the expected range of wheel/rail roughness [54].

The wear-in process aims to overcome the initial excessive wear occurring when new specimens are rubbed against each other. This process ensures that subsequent tests with TOR products are not significantly affected by the effect of wear debris and related changes in contact geometry. The results revealed that a suitable wear-in process length is 60 min. This length also ensured that the width of the contact path increased to 0.6 mm. This path width allows the solid particles contained in TOR products to come into contact because the typical

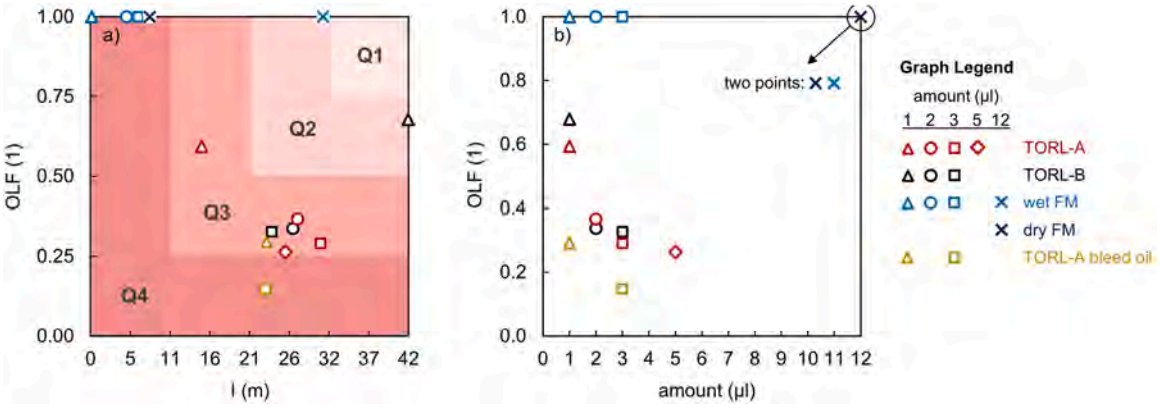

Fig. 11. The final assessment: (a) performance map, (b) amount-OLF relationship.

particle size is in the units to tens of micrometres. Moreover, the wider path allows for a more accurate application of TOR products to the centre of the contact path, compared to a narrow path (without a wear-in process).

S3 product application: there are several methods for the application of TOR products: brush, nozzle, syringe or micropipette. While brush and nozzle were used mainly for field testing [13,45], syringe and micropipette were typically utilized for laboratory testing [34,55]. This is because the required doses are very small in the laboratory, and also high application accuracy is needed. It means that a relatively narrow contact path between the ball and the disc does not allow the application of TOR products using a brush or nozzle.

The micropipette used in this study enables the application of a minimum dosage of 1 μl with a low error guaranteed by the manufacturer. However, since the tested TOR products were viscous liquids containing many solid particles, the application accuracy might have been compromised. Therefore, additional tests focused on application accuracy were conducted where the applied amounts were weighed using a precise analytical balance. These measurements showed that the application error was not higher than 6% except for 12 μl of FM, where the error reached 12%. This larger error resulted from the accumulation of smaller errors due to the application of twelve doses of 1 μl (same as in the PTs). Although this error is not negligible, the application accuracy is still sufficient to study the effect of the applied amount.

As mentioned above, all tested amounts were applied using several 1 μl doses. This application strategy was chosen because it ensures that almost the whole product dose ends up in contact. Note that the application was always performed when both contact bodies were stopped. These conditions are beneficial because it is possible to check whether the application was accurate (based on the position of each drop relative to the centre of the contact path). If not, the whole test has to be repeated. The authors recommend using the application jig to achieve a higher application accuracy. This jig precisely sets the position of the micropipette tip relative to the centre of the contact path.

S4 traction test: this step is a crucial part of the measurement phase in the proposed methodology. This step includes several 180-second tests with different SRR values based on which tested product performance is evaluated. A similar approach to studying TOR products was used in previous studies [19,35]. However, there is also a second and more often used approach to investigate the performance of TOR products in laboratory conditions. Traditionally, the performance of TOR products has been evaluated by measuring the CoT over time at a specific SRR. This friction test begins with the application of TOR product and ends with contact starvation. Note that this test typically has a duration of a few minutes to tens of minutes. Although this experimental approach was previously used in many studies dealing with TOR products [55–60], this approach was found to be unsuitable for tests using the MTM tribometer.

The authors of this study performed these friction tests during the initial testing phase; however, the results were not fully satisfactory. Fig. 12 (a) schematically shows some selected results of these friction tests. The results were acceptable for some kinds of TOR products and very small amounts; see curves no. 1a-1c in Fig. 12 (a). However, the repeatability of these tests was not always good enough to evaluate the performance parameters of TOR products, such as retentivity [24,58] or CoT rate (ratio between CoT difference and time difference) [61]. An unexpected change in the trend of the friction curve was observed for small and medium applied amounts of TOR product (mainly TOR lubricants); see curve no. 2 in Fig. 12 (a). The surface analyses revealed that these unexpected changes occurred due to surface smoothing. A comparison between Fig. 12 (b) and (c) highlights this effect. This smoothing effect was previously described as one of the consequences of applying TOR products [4,30]. This effect was even more significant for tests on the MTM tribometer because of the small contact area and a relatively high amount of TOR product in the contact path compared to real contact. As a consequence of roughness smoothing, the lambda parameter defining the lubrication regime was considerably changed; thus, the test conditions were also changed. Therefore, this result could not be considered relevant because the retentivity was much longer for the lower roughness [62]. Similar behaviour was observed for large amounts of TOR products (curve no. 3 in Fig. 12), where the CoT was very low throughout the whole test, similar to Sánchez et al. [59].

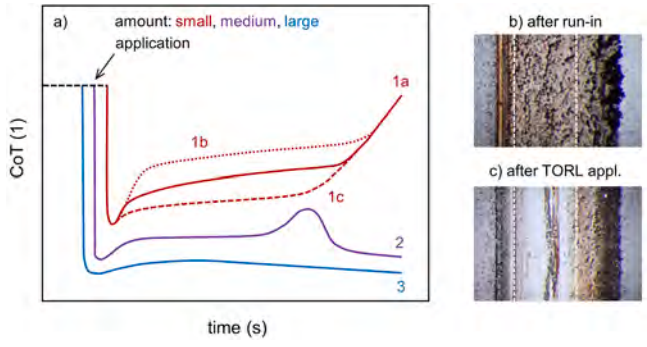

Fig. 12. (a) Schematic results of friction tests, (b) rough path after run-in process, and (c) smooth path after test with higher amount of TOR lubricant and at a low SRR value.

With respect to the findings, a traction test with the range of SRR from 0% to 20% was finally chosen as a suitable approach to investigate the performance of TOR products. Increasing the SRR to higher values raises the shear stress in the TOR product layer; thus, the smoothing effect is suppressed by the gradual starvation of the contact. This approach enables investigating the performance of TOR products for a wider range of applied amounts compared to fixed friction tests at a specific SRR value. The ability to test the performance of TOR products depending on the applied amount is one of the objectives of the proposed methodology.

S5 checkpoint: the creep curve obtained in step S4 was always compared with the threshold curve. This threshold curve was designed as a percentage value of the CoT for a given SRR under dry conditions, see Table 5. The PT was stopped when two neighbouring points of the tested TOR product were above the threshold curve. The reason for choosing two neighbouring points, as a criterion for stopping the PT, instead of one point was that there were many tests where the threshold value was exceeded at lower SRR values. However, the following points of the creep curve were below the threshold curve. Therefore, the criterion was extended to two neighbouring points to ensure that the PT was not stopped too early (before the contact starvation).

If the criterion for stopping the PT has been met, another PT follows. As was mentioned above, five consecutive PTs on the same specimens are needed to investigate the performance of one TOR product for one tested amount. This approach ensures that the performance of each tested product is investigated for a wide range of conditions; thus, the obtained results are more valuable. The most significant change occurs for the geometry of the contact path, while the combined roughness remains almost the same due to the wear-in process between the PTs. The width of the contact path was between 0.6 (after the run-in process) and 0.9 mm (after the fifth PT). This increase in the path width caused a drop in pressure leading to an increase in the value of the Lambda ratio. This ratio defines the lubrication regime and extends the consumption time of TOR products as the load decreases [63]. Moreover, a wider contact path can slightly increase the amount of TOR product which comes into contact while the rest of the dose is pushed out of the contact [64]. These facts explain why the parameter n usually grew with the number of PTs, see Figs. 9(c) and 8 (f).

S6 ball cleaning: the ball is cleaned with a paper tissue without any solvent before the next traction test if the criterion for stopping the test has not been met, see Fig. 3(a). However, it is important to note that this cleaning introduces certain uncertainties in the experiment, as it cannot be easily checked and quantified. Therefore, the cleaning must be

carried out with great precision, using a wipe that does not leave any residues on the surface. It is recommended to check the surface using a microscope. It is important to note that a solvent is not suitable for ball cleaning as it affects the CoT.

As mentioned in Subchapter 2.4, the primary aim of cleaning is to enable testing of higher product amounts without the risk of the smoothing effect depicted in Fig. 12. However, if these higher amounts (e.g. higher than 4 μl) are not being tested, it is possible to omit the ball cleaning and simplify the measurement phase in Fig. 3(a). In that case, the PT will be continued to S4 instead of S6 if the criterion in S5 has not been met. However, it is necessary to decide at the beginning of the testing whether cleaning will be performed or not, as it is essential to maintain the same testing methodology for all tests. The omission of cleaning simplifies the test procedure but can also limit the comparability with this or future studies that employ the proposed methodology (including ball cleaning).

4.2. Case study discussion

In the beginning, the traction tests under dry conditions were performed to evaluate the creep curve under dry conditions. The traction zones and the threshold curve were designed based on this creep curve under dry conditions. The creep curve under dry conditions was found to have a negative trend beyond the saturation point. Although this negative trend is expected under dry conditions, the saturation point should occur at significantly lower slip values [65,66]. This contrast can be explained by different slip conditions in contacts. Whereas MTM contact operates at a fixed SRR, real wheel-rail contact operates at a variable SRR dependent on CoT. At higher SRR/slip, the contact shifts into the unstable region of the creep curve, where sliding may occur. Under these conditions, significant thermal effects arise, and the creep curve declines [23,67].

The results of the presented study are in good agreement with the previous authors' study [24], where no saturation point was observed for SRR values up to 10%. The negative trend of the creep curve in Fig. 7 (a) was not caused primarily by the thermal effects. According to Ertz et al. [68], the calculation revealed that the mean and maximum temperature in the contacts did not exceed 55 °C and 95 °C, respectively. The decline of the creep curve mainly occurred due to the formation of a higher amount of wear debris that adhered to the disc surface; see the interfacial layer in Fig. 7(c). Therefore, the range of SRR was limited to values from 0% to 20% to avoid the formation of this interfacial layer that would affect the results of the test with the TOR product.

The traction test results for several TOR products and one bleed oil are summarized in Fig. 11. These results clearly display a difference in frictional behaviour between water-based (FM) and oil-based TOR products (TORL-A and TORL-B). While increasing the applied amount of FM does not affect the OLF, a significant drop in OLF is found for both TORLs as the amount increases. This result indicates that the application of FM is not risky in terms of a very low CoT, even if the applied amount is large. In contrast, the performance of TORLs is very sensitive to the applied amount, and even a slight increase can lead to a very low CoT. These findings are consistent with Ref. [1], where the dependence of the coefficient of friction on application rate was plotted for both water-based and oil-based products. Besides that, a very low CoT occurrence after the application of TORL was previously reported in both laboratory [20,24] and field studies [18,69].

The second difference between water-based and oil-based products lies in the *I* parameter defining the "effective" retentivity. The results show that the *I* parameter is much more sensitive to the applied amount for TORLs than FM. It means that oil-based products can provide a longer retentivity than water-based products. Moreover, the behaviour of water-based products is extremely influenced by product drying, as observed in the laboratory [22] and field tests [27].

Although the results of the presented study generally agree with previously published studies, it should be noted that the proposed methodology was designed as a comparative test whose aim is to choose a suitable product for further testing. Therefore, the results are divided into four performance groups Q1-Q4 that define the performance class of TOR product for a given amount. Based on the performance map in Fig. 11, TORL-B and FM could be used for further testing because these TOR products were able to reach the performance class Q2 while the class Q3 and Q4 were found for the other two tested products. It is essential to note that class Q3 and Q4 do not necessarily mean that unsatisfactory results will be achieved on the track, but it mainly says that there is a better TOR product or a more suitable amount for its application. On the other hand, recently published studies [44,70] have shown a reasonable correlation between small and full-scale tests.

Finally, the performance of the bleed oil of TORL-A was investigated to verify the sensitivity of the proposed methodology. When comparing the results, it can be seen that TORL-A achieved a higher performance group for both tested amounts (Q2, Q3) than was found for bleed oil (Q3, Q4). Therefore, the proposed methodology can be considered reliable based on these results. Note that some of the tests were repeated to evaluate the repeatability. It was difficult to achieve the same performance parameters because many factors affect the results of traction tests, such as the width of the contact path, surface topography, roughness, etc. However, the same performance group was always achieved for the original and the repeated test. Therefore, it can be concluded that the proposed methodology is robust enough because the final product assessment (Q1-Q4) is not affected by parameters that cannot be precisely controlled during testing.

4.3. Comparison of the proposed methodology and CEN/TS standard

The main parameters of the proposed methodology, further referred to as the I-OLF methodology, and CEN/TS standards [46] are listed in Appendix C. Both methods utilize the MTM tribometer in a ball-on-disc configuration, where specimens are manufactured from AISI 52100. Both approaches involve an initial wear-in process before TOR product testing using traction tests. The CEN/TS standard prescribes only one set of traction tests for one contact pair, while in the I-OLF methodology, five consecutive tests (PTs) are conducted using the same pair. This allows the I-OLF methodology to provide more reliable and representative results, as the individual PTs are performed for a wider range of contact conditions. It should be noted that the higher number of tests in the case of the I-OLF methodology results in a significantly longer total test time, as shown in Appendix C. Therefore, the CEN/TS standard may be suitable when there is a need for rapid testing of a higher number of TOR products.

Another significant difference between the I-OLF methodology and the CEN/TS standard lies in the evaluation phase. While CEN/TS uses only one simple criterion to decide whether the product's performance is good or not in terms of a low CoT, the I-OLF methodology employs four traction zones to evaluate several performance parameters based on which the performance map is plotted. This performance map provides a more comprehensive assessment of TOR products and categorizes them, based on the applied amounts, into four performance classes Q1-Q4.

In terms of individual test parameters, the approaches differ mainly in the contact pressure and the SRR range, see Appendix C. Both contact pressures, used in the I-OLF methodology and CEN/TS standard, represent typical pressure in the wheel tread-rail head contact. The lower pressure in the I-OLF methodology was chosen to reduce wear since the contact pair is used for several consecutive PTs. The higher range of SRRs was selected in the I-OLF methodology to enable testing larger amounts of TOR products and mitigate the smoothing effect depicted in Fig. 12.

4.4. Possible future extension of the methodology

There are several possibilities to extend the proposed methodology in the future. Possible extensions of the methodology may be the

following:

- Test the performance of TOR products together with a representative natural interfacial layer which must be prepared on the surface in advance.
- Test the performance of TOR products for different temperatures, air humidity and various contaminants because all these factors can limit the usage of TOR products.
- Connect the ultrafine particle counter to investigate the number of airborne particles generated from the contact. These particles, mainly ultrafine particles, are dangerous for human health.
- Design a circuit for measuring contact impedance that is crucial to shunting.
- Implementing an optical method to evaluate the film thickness of TOR products could provide valuable insights for modelling and clarifying friction mechanisms.
- Modify the methodology to investigate wear rate, surface and subsurface damage, and RCF propagation. This task could be the most challenging because representative materials of specimens are needed. Therefore, manufacturing samples from wheel and rail steel seems to be necessary. Note that the pin-on-disc configuration (possible for MTM) may be considered in case of manufacturing difficulties of the ball from wheel steel.
- The performance parameters can be redefined to apply the methodology for evaluating oil and grease performance (e.g., products used for wheel flange lubrication).

5. Conclusions

This paper introduced a novel benchmarking methodology for assessing the performance of TOR products, which are applied in rail transportation to manage friction, noise and wear. The methodology was proposed for the MTM tribometer in ball-on-disc configuration to allow future comparison of results across different laboratories. The proposed methodology consists of nine consecutive steps describing the testing from the initial wear-in process to the final assessment of TOR products. A core of the methodology is formed by traction tests and a robust evaluation phase resulting in a performance map that compares different TOR products and their amounts. It should be highlighted that this performance map is plotted based on several performance parameters that are crucial for ensuring traffic safety and reaching the expected benefits associated with TOR products. This multi-parametric approach makes the assessment of TOR products highly representative. The resulting performance map shows the performances of tested TOR products depending on the applied amount and categorizes them into four performance classes Q1-Q4. Based on this, a suitable TOR product can be chosen for further testing because the proposed comparative test is considered the first step towards applying the product to real operation. Therefore, full-scale and operational tests should follow this initial testing with a small-scale tribometer.

The suitability of the proposed methodology was confirmed by testing three TOR products (1x FM and 2x TOR lubricants) and one bleed oil using varying amounts. The results led to the following conclusions:

- Increasing the applied amount of FM did not lead to any risks related to a very low CoT. In contrast, both tested TOR lubricants caused a very low CoT when increasing the amount applied.
- The retentivity of TOR lubricants was affected by the applied amount more notably than was found for FM.
- The previous two points show that the performance of oil-based TOR products is much more sensitive to applied amounts than water-based products.
- The retentivity of FM is significantly shortened if the base medium is evaporated before the test. However, the evaporation of the base medium did not influence the product behaviour regarding the occurrence of a very low CoT.
- Based on the case study results, the most suitable TOR products for further testing have been identified.
- TOR lubricant reached a higher performance class for both tested amounts than its bleed oil. This conclusion gives evidence that the methodology is appropriately designed.

Declaration of Competing Interest

The authors declare that they have no known competing financial interests or personal relationships that could have appeared to influence the work reported in this paper.

Data availability

Data will be made available on request.

Acknowledgements

The work was supported by the project LTACH19001 with financial support from the Ministry of Education, Youth and Sports of the Czech Republic.

Appendix A. Sensors parameters

sensor	range	accuracy	nonlinearity
load cell for normal force	2–75 N	±0.3 N	±1% of full scale
load cell for friction force	–20 to + 20 N	±0.3 N	±2% of full scale
servo-drives	–4 to + 4 m/s	±1 mm/s or 0.1% of speed, whichever is larger	not applicable

Appendix B. – Overview of performance parameters for all tested conditions

set	TOR product	amount (μl)	*C* (m)	*I* (m)	*R* (m)	*N* (1)*	*OLF* (1)	Class (1)
3	wet-FM	1	0	0.1	0.1	0.4	1	Q4
		2	0	4.8	4.8	1.0	1	Q4
		3	0	6.3	6.3	1.0	1	Q4
		12	0	30.9	30.9	2.2	1	Q2
4	dry-FM	12	0	7.9	7.9	1	1	Q4
5	TORL-A	1	0.6	14.7	36.6	3.2	0.594	Q3
		2	35.3	27.5	98.7	6.8	0.367	Q3

(*continued on next page*)

(*continued*)

set	TOR product	amount (μl)	*C* (m)	*I* (m)	*R* (m)	*N* (1)*	*OLF* (1)	Class (1)
		3	62.6	30.5	128.8	9.0	0.291	Q3
		5	82.6	25.8	200.1	13.2	0.264	Q3
6	TORL-B	1	1.5	42.1	79.2	5.4	0.678	Q2
		2	41.6	26.9	104.7	7.2	0.338	Q3
		3	40.5	24.1	103.6	7.0	0.328	Q3
7	TORL-A	1	45.6	23.2	88.3	6.4	0.291	Q3
	bleed oil	3	201.2	21.6	308.7	20.2	0.147	Q4

* N – average value of n_1-n_5

Appendix C. Comparison of the proposed methodology (I-OLF methodology) and CEN/TS standard

I-OLF methodology	pressure (GPa)	speed (m/s)	SRR (%)	duration (min)
wear-in	0.8	1	2	60
run-in			2	30
TOR product testing			0–20	~25[1)]
type of test for TOR product testing	traction test (creep curves)			
more tests using the same pair	yes (5 in total)			
total test time	~5–7 h[1)]			
comparative methodology	YES			
assessment based on	traction zones and several performance parameters			
overall assessment	performance map (classes Q1-Q4)			
CEN/TS standard	pressure (GPa)	speed (m/s)	SRR (%)	duration (min)
wear-in (run-in)[2)]	1	0.1	50	30
TOR product testing		1, 3.8	0.25–10	22
type of test for TOR product testing	traction test (creep curves)			
more tests using the same pair	no			
total test time	~1 h[1)]			
comparative methodology	YES			
assessment based on	CoT value at 10% SRR			
overall assessment	good/bad			

[1)] It is only an estimate of the duration as it depends on the number of creep curves.
[2)] Only the term "run-in" is used in the CEN/TS standard.
[3)] Time needed for specimens cleaning is not included as this information is not provided.

References

[1] Stock R, Stanlake L, Hardwick C, Yu M, Eadie D, Lewis R. Material concepts for top of rail friction management – Classification, characterisation and application. Wear 2016;366–367:225–32. https://doi.org/10.1016/j.wear.2016.05.028.

[2] Harmon M, Lewis R. Review of top of rail friction modifier tribology. Tribology - Mater, Surf Interfaces 2016;10:150–62. https://doi.org/10.1080/17515831.2016.1216265.

[3] Kalousek J, Johnson KL. An Investigation of Short Pitch Wheel and Rail Corrugations on the Vancouver Mass Transit System. Proc Inst Mech Eng, Part F: J Rail Rapid Transit 1992;206:127–35. https://doi.org/10.1243/PIME_PROC_1992_206_226_02.

[4] Eadie DT, Kalousek J, Chiddick KC. The role of high positive friction (HPF) modifier in the control of short pitch corrugations and related phenomena. Wear 2002;253:185–92. https://doi.org/10.1016/S0043-1648(02)00098-4.

[5] Egana JI, Vinolas J, Gil-Negrete N. Effect of liquid high positive friction (HPF) modifier on wheel-rail contact and rail corrugation. Tribol Int 2005;38:769–74. https://doi.org/10.1016/j.triboint.2004.11.006.

[6] Eadie DT, Santoro M, Oldknow K, Oka Y. Field studies of the effect of friction modifiers on short pitch corrugation generation in curves. Wear 2008;265:1212–21. https://doi.org/10.1016/j.wear.2008.02.028.

[7] Eadie DT, Santoro M. Top-of-rail friction control for curve noise mitigation and corrugation rate reduction. J Sound Vib 2006;293:747–57. https://doi.org/10.1016/j.jsv.2005.12.007.

[8] Eadie DT, Santoro M, Kalousek J. Railway noise and the effect of top of rail liquid friction modifiers: changes in sound and vibration spectral distributions in curves. Wear 2005;258:1148–55. https://doi.org/10.1016/j.wear.2004.03.061.

[9] Kwong M, Frossinakis R, Makowsky T, Yu M, Lu X, O'Grady J. Wayside top of rail friction control: an embedded track solution in a high density tram. Netw, Ausrail 2019;2019:1–14.

[10] FUKAGAI S, BAN T, OGATA M, ISHIDA M, NAMURA A. Development of wheel/rail friction moderating system (FRIMOS). Q Rep Rtri 2008;49:26–32. https://doi.org/10.2219/rtriqr.49.26.

[11] Anderson D, Wheatley N. Mitigation of wheel squeal and flanging noise on the australian rail network. Noise Vib Mitig Rail Transp Syst 2008:399–405. https://doi.org/10.1007/978-3-540-74893-9_56.

[12] Davis K, Stickland W. Eval a Top–rail Lubr Syst 1999:1–120.

[13] Suda Y, Iwasa T, Komine H, Tomeoka M, Nakazawa H, Matsumoto K, Nakai T, Tanimoto M, Kishimoto Y. Development of onboard friction control. Wear 2005;258:1109–14. https://doi.org/10.1016/j.wear.2004.03.059.

[14] Matsumoto K, Suda Y, Fujii T, Komine H, Tomeoka M, Satoh Y, Nakai T, Tanimoto M, Kishimoto Y. The optimum design of an onboard friction control system between wheel and rail in a railway system for improved curving negotiation. Veh Syst Dyn 2006;44:531–40. https://doi.org/10.1080/00423110600875294.

[15] Ishida M, Ban T, Iida K, Ishida H, Aoki F. Effect of moderating friction of wheel/rail interface on vehicle/track dynamic behaviour. Wear 2008;265:1497–503. https://doi.org/10.1016/j.wear.2008.02.041.

[16] Lewis R, Dwyer-Joyce RS, Lewis J. Disc machine study of contact isolation during railway track sanding. Proc Inst Mech Eng, Part F: J Rail Rapid Transit 2003;217:11–24. https://doi.org/10.1243/095440903762727311.

[17] Lundberg J, Rantatalo M, Wanhainen C, Casselgren J. Measurements of friction coefficients between rails lubricated with a friction modifier and the wheels of an IORE locomotive during real working conditions. Wear 2015;324–325:109–17. https://doi.org/10.1016/j.wear.2014.12.002.

[18] Galas R, Omasta M, Klapka M, Kaewunruen S, Krupka I, Hartl M. Case Study: the Influence of Oil-based Friction Modifier Quantity on Tram Braking Distance and Noise. Tribology Ind 2017;39:198–206. https://doi.org/10.24874/ti.2017.39.02.06.

[19] D.V. Gutsulyak, L.J.E. Stanlake, H. Qi, Twin disc evaluation of third body materials in the wheel/rail interface, 15 (2021) 115–126. ⟨https://doi.org/10.1080/17515831.2020.1829878⟩.

[20] Liu X, Meehan PA. Investigation of squeal noise under positive friction characteristics condition provided by friction modifiers. J Sound Vib 2016;371:393–405. https://doi.org/10.1016/j.jsv.2016.02.028.

[21] Li Q, Wu B-nan, Ding H-hao, Galas R, Kvarda D, Liu Q-yue, Zhou Z-rong, Omasta M, Wang W. Numerical prediction on the effect of friction modifiers on adhesion behaviours in the wheel-rail starved EHL contact. Tribol Int 2022;170. https://doi.org/10.1016/j.triboint.2022.107519.

[22] Galas R, Kvarda D, Omasta M, Krupka I, Hartl M. M. The role of constituents contained in water–based friction modifiers for top–of–rail application. Tribology Int 2018;117:87–97. https://doi.org/10.1016/j.triboint.2017.08.019.

[23] D. Kvarda, R. Galas, M. Omasta, M. Hartl, I. Krupka, M. Dzimko, Shear properties of top-of-rail products in numerical modelling, Proceedings Of The Institution Of Mechanical Engineers, Part F: Journal Of Rail And Rapid Transit. ⟨https://doi.org/10.1177/09544097221138374⟩.

[24] Galas R, Omasta M, Krupka I, Hartl M. Laboratory investigation of ability of oil-based friction modifiers to control adhesion at wheel-rail interface. Wear 2016;368–369:230–8. https://doi.org/10.1016/j.wear.2016.09.015.

[25] Hardwick, Lewis R, Stock R. The effects of friction management materials on rail with pre existing rcf surface damage. Wear 2017;384–385:50–60. https://doi.org/10.1016/j.wear.2017.04.016.
[26] Curley D, Anderson DC, Jiang J, Hanson D. Field trials of gauge face lubrication and top-of-rail friction modification for curve noise mitigation. Noise Vib Mitig Rail Transp Syst 2015:449–56. https://doi.org/10.1007/978-3-662-44832-8_54.
[27] Khan SA, Lundberg J, Stenström C. Carry distance of top-of-rail friction modifiers. Proc Inst Mech Eng, Part F: J Rail Rapid Transit 2018;232:2418–30. https://doi.org/10.1177/0954409718772981.
[28] Chen H, Fukagai S, Sone Y, Ban T, Namura A. Assessment of lubricant applied to wheel/rail interface in curves. Wear 2014;314:228–35. https://doi.org/10.1016/j.wear.2013.12.006.
[29] Eadie DT, Elvidge D, Oldknow K, Stock R, Pointner P, Kalousek J, Klauser P. The effects of top of rail friction modifier on wear and rolling contact fatigue: Full-scale rail–wheel test rig evaluation, analysis and modelling. Wear 2008;265:1222–30. https://doi.org/10.1016/j.wear.2008.02.029.
[30] Stock R, Eadie DT, Elvidge D, Oldknow K. Influencing rolling contact fatigue through top of rail friction modifier application – A full scale wheel–rail test rig study. Wear 2011;271:134–42. https://doi.org/10.1016/j.wear.2010.10.006.
[31] Matsumoto A, Sato Y, Ohno H, Mizuma T, Suda Y, Tanimoto M, Oka Y. Study on curving performance of railway bogies by using full-scale stand test. Veh Syst Dyn 2006;44:862–73. https://doi.org/10.1080/00423110600907402.
[32] Abbasi S, Olofsson U, Zhu Y, Sellgren U. Pin-on-disc study of the effects of railway friction modifiers on airborne wear particles from wheel–rail contacts. Tribology Int 2013;60:136–9. https://doi.org/10.1016/j.triboint.2020.106566.
[33] Lewis SR, Lewis R, Olofsson U, Eadie DT, Cotter J, Lu X. Effect of humidity, temperature and railhead contamination on the performance of friction modifiers: Pin-on-disk study. Proc Inst Mech Eng, Part F: J Rail Rapid Transit 2013;227:115–27. https://doi.org/10.1177/0954409712452239.
[34] Kvarda D, Skurka S, Galas R, Omasta M, Shi L-bing, Ding H, Wang W-jian, Krupka I, Hartl M. The effect of top of rail lubricant composition on adhesion and rheological behaviour. Eng Sci Technol, Int J 2022;35. https://doi.org/10.1016/j.jestch.2022.101100.
[35] Tomeoka M, Kabe N, Tanimoto M, Miyauchi E, Nakata M. Friction control between wheel and rail by means of on-board lubrication. Wear 2002;253:124–9. https://doi.org/10.1016/S0043-1648(02)00091-1.
[36] Liu X, Meehan PA. Investigation of squeal noise under positive friction characteristics condition provided by friction modifiers. J Sound Vib 2016;371:393–405. https://doi.org/10.1016/j.jsv.2016.02.028.
[37] Vélez JC, Cornelio JAC, Sierra RB, Santa JF, Hoyos-Palacio LM, Nevshupa R, Toro A. Development of a composite friction modifier with carbon nanotubes for applications at the wheel–rail interface. Adv Compos Lett 2020;29. https://doi.org/10.1177/2633366X20930019.
[38] Buckley-Johnstone L, Harmon M, Lewis R, Hardwick C, Stock R. A comparison of friction modifier performance using two laboratory test scales. Proc Inst Mech Eng, Part F: J Rail Rapid Transit 2019;233:201–10. https://doi.org/10.1177/0954409718787045.
[39] Navrátil V, Galas R, Klapka M, Kvarda D, Omasta M, Shi L, Ding H, Wang W-J, Krupka I, Hartl M. Wheel Squeal Noise in Rail Transport: The Effect of Friction Modifier Composition. Tribology Ind 2022;44:361–73. https://doi.org/10.24874/ti.1211.11.21.02.
[40] Song J, Shi L, Ding H, Galas R, Omasta M, Wang W, Guo J, Liu Q, Hartl M. Effects of solid friction modifier on friction and rolling contact fatigue damage of wheel-rail surfaces. Friction 2022;10:597–607. https://doi.org/10.1007/s40544-021-0521-5.
[41] Harmon M, Lewis R. New laboratory methodologies to analyse the top of rail friction modifier performance across different test scales. Proc Inst Mech Eng, Part F: J Rail Rapid Transit 2021;235:191–200. https://doi.org/10.1177/0954409720913759.
[42] Evans M, Skipper WA, Buckley-Johnstone L, Meierhofer A, Six K, Lewis R. The development of a high pressure torsion test methodology for simulating wheel/rail contacts. Tribology Int 2021;156. https://doi.org/10.1016/j.triboint.2020.106842.
[43] Lewis SR, Lewis R, Olofsson U. An alternative method for the assessment of railhead traction. Wear 2011;271:62–70. https://doi.org/10.1016/j.wear.2010.10.035.
[44] M. Harmon, J.F. Santa, J.A. Jaramillo, A. Toro, A. Beagles, R. Lewis, Evaluation of the coefficient of friction of rail in the field and laboratory using several devices, 14 (2020) 119–129. ⟨https://doi.org/10.1080/17515831.2020.1712111⟩.
[45] Areiza YA, Garcés SI, Santa JF, Vargas G, Toro A. Field measurement of coefficient of friction in rails using a hand-pushed tribometer. Tribology Int 2015;82:274–9. https://doi.org/10.1016/j.triboint.2014.08.009.
[46] CEN/TS 15427–2-2:2021. Railway applications - Wheel/Rail friction management - Part 2–2: Properties and Characteristics - Top of Rail materials, 2021.
[47] Cann PM. The “leaves on the line” problem—a study of leaf residue film formation and lubricity under laboratory test conditions. Tribology Lett 2006;24:151–8. https://doi.org/10.1007/s11249-006-9152-2.
[48] Zhu Y, Olofsson U, Persson K. Investigation of factors influencing wheel–rail adhesion using a mini-traction machine. Wear 292- 2012;293:218–31. https://doi.org/10.1016/j.wear.2012.05.006.
[49] White B, Hyland-Knight J, Lewis R. Assessing the effectiveness of traction gels using full-scale and field testing. Proc Inst Mech Eng, Part F: J Rail Rapid Transit 2021;235:690–9. https://doi.org/10.1177/0954409720953943.
[50] Kalousek J, Magel E. Modifying and managing friction. Railw Track Struct 1997;93:31–6.
[51] Arias-Cuevas O. Low Adhesion in the Wheel-Rail Contact, PhD Thesis. Netherlands: Delft University of Technology,; 2010.
[52] Oomen MA, Bosman R, Lugt PM. Characterization of friction and wear behavior of friction modifiers used in wheel-rail contacts. Int J Progn Health Manag 2017;8. https://doi.org/10.36001/ijphm.2017.v8i3.2663.
[53] Blau PJ. On the nature of running-in. Tribol Int 2005;38:1007–12. https://doi.org/10.1016/j.triboint.2005.07.020.
[54] Chen H, Namura A, Ishida M, Nakahara T. Influence of axle load on wheel/rail adhesion under wet conditions in consideration of running speed and surface roughness. Wear 2016;366–367:303–9. https://doi.org/10.1016/j.wear.2016.05.012.
[55] Li Z, Arias-Cuevas O, Lewis R, Gallardo-Hernández EA. Rolling–Sliding Laboratory Tests of Friction Modifiers in Leaf Contaminated Wheel–Rail Contacts. Tribology Lett 2009;33:97–109. https://doi.org/10.1007/s11249-008-9393-3.
[56] Wang W, Li S, Ding H, Lin Q, Galas R, Omasta M, Meli E, Guo J, Liu Q. Wheel/rail adhesion and damage under different contact conditions and application parameters of friction modifier. Wear 2023. https://doi.org/10.1016/j.wear.2023.204870.
[57] Li JX, Wu BN, Ding HH, Galas R, Omasta M, Wen ZF, Guo J, Wang WJ. Wear and damage behaviours of wheel and rail materials: Effects of friction modifier and environmental temperature. Wear 2023. https://doi.org/10.1016/j.wear.2023.204796.
[58] Arias-Cuevas O, Li Z, Lewis R, Gallardo-Hernández EA. Rolling–sliding laboratory tests of friction modifiers in dry and wet wheel–rail contacts. Wear 2010;268:543–51. https://doi.org/10.1016/j.wear.2009.09.015.
[59] Sánchez JC, Jaramillo JA, Santa JF, Toro A. Twin-disc assessment of the effect of top-of-rail friction modifiers on the tribological response of er8-r370ht pairs for use in wheel-rail systems. Rev Latinoam De Metal Y Mater 2019;39:2–15.
[60] Trummer G, Lee ZS, Lewis R, Six K. Modelling of Frictional Conditions in the Wheel–Rail Interface Due to Application of Top-of-Rail Products. Lubricants 2021;9. https://doi.org/10.3390/lubricants9100100.
[61] Omasta M, Galas R, Knapek J, Hartl M, Krupka I. Development of an adaptive top-of-rail friction modification system. In: Stephenson Conference: Research For Railways 2017. London: Institution of Mechanical Engineers; 2017. p. 325–32.
[62] Lewis SR, Lewis R, Evans G, Buckley-Johnstone LE. Assessment of railway curve lubricant performance using a twin-disc tester. Wear 2014;314:205–12. https://doi.org/10.1016/j.wear.2013.11.033.
[63] Aldajah S, Ajayi OO, Fenske GR, Kumar S. Investigation of Top of Rail Lubrication and Laser Glazing for Improved Railroad Energy Efficiency1. J Tribology 2003;125:643–8. https://doi.org/10.1115/1.1537745.
[64] White B, Lee ZS, Lewis R. Towards a Standard Approach for the Twin Disc Testing of Top-Of Rail Friction Management Products. Lubricants 2022;10. https://doi.org/10.3390/lubricants10060124.
[65] Polach O. Creep forces in simulations of traction vehicles running on adhesion limit. Wear 2005;258:992–1000. https://doi.org/10.1016/j.wear.2004.03.046.
[66] Six K, Meierhofer A, Müller G, Dietmaier P. Physical processes in wheel–rail contact and its implications on vehicle–track interaction. Veh Syst Dyn 2015;53:635–50. https://doi.org/10.1080/00423114.2014.983675.
[67] Vollebregt E, Six K, Polach O. Challenges and progress in the understanding and modelling of the wheel–rail creep forces. Veh Syst Dyn 2021;59:1026–68. https://doi.org/10.1080/00423114.2021.1912367.
[68] Ertz M, Knothe K. A comparison of analytical and numerical methods for the calculation of temperatures in wheel/rail contact. Wear 2002;253:498–508. https://doi.org/10.1016/S0043-1648(02)00120-5.
[69] Khan SA, Lundberg J, Stenström C. The effect of third bodies on wear and friction at the wheel-rail interface. Proc Inst Mech Eng, Part F: J Rail Rapid Transit 2022;236:662–71. https://doi.org/10.1177/09544097211034688.
[70] Buckley-Johnstone L, Harmon M, Lewis R, Hardwick C, Stock R. A comparison of friction modifier performance using two laboratory test scales. Proc Inst Mech Eng, Part F: J Rail Rapid Transit 2019;233:201–10. https://doi.org/10.1177/0954409718787045.

Tribology Letters (2024) 72:90
https://doi.org/10.1007/s11249-024-01889-7

ORIGINAL PAPER

Assessing the Performance of TOR Lubricants in Humid Environments and Under Dew Conditions

Simon Skurka[1] · Radovan Galas[1] · Milan Omasta[1] · Haohao Ding[2] · Wen-Jian Wang[2] · Ivan Krupka[1] · Martin Hartl[1]

Received: 6 May 2024 / Accepted: 3 July 2024 / Published online: 16 July 2024

Abstract

Top-of-rail (TOR) lubricants are commonly used for friction control in railway operations. They aim to lower friction and reduce noise and wear while ensuring sufficient transmission of traction/braking forces. However, the wheel–rail interface is an open system, so the conditions may suddenly change due to the weather, and different contaminants may enter the contact and influence the performance of these lubricants. Thus, this study examined the effect of humidity and dew on two commercial products, as these conditions often occur on the track. A methodology based on a creep curves measurement approach was used to assess product performance under various scenarios. All measurements were conducted on a universal tribometer in the ball-on-disc configuration covered with a climate chamber. The results show a strong influence of dew on the tested products, as dew lowered their performance parameters and caused low adhesion problems. Possible mechanisms of water–oil interaction and formation of oxidic third body layers were discussed. The main findings indicate that TOR lubricants may cause traction/braking problems if used in dew conditions. The present study may be helpful in optimising friction management methods in the future.

Graphical Abstract

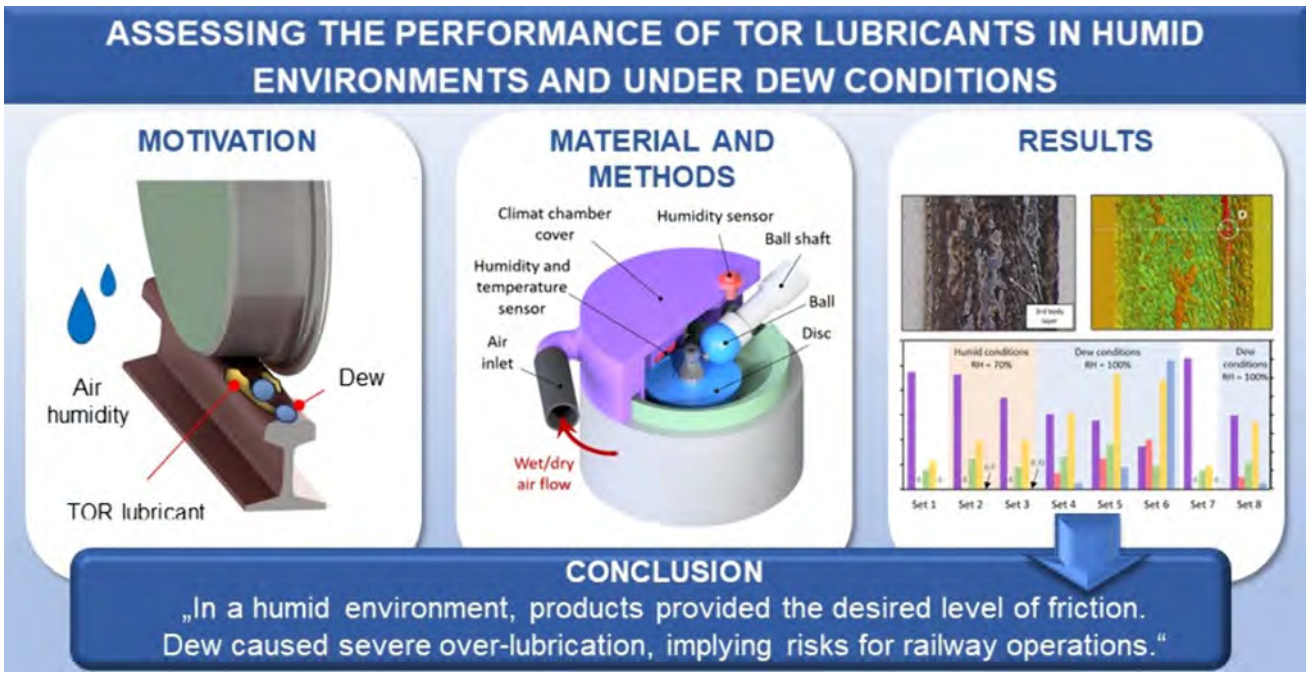

Keywords Wheel–rail tribology · Friction modification · Humidity · TOR lubricants · Dew · Contamination

Extended author information available on the last page of the article

1 Introduction

Railway transportation is an ecologically friendly way of transporting passengers and goods, and its energy efficiency can be further improved by reducing the adverse effects of friction in the wheel–rail (W/R) contact. Too high friction is the cause of excessive fuel consumption [1]. Furthermore, it causes wear of contact surfaces, leading to more frequent wheel changes and rail grinding [2, 3], increasing maintenance costs [4]. Lastly, friction is a source of noise pollution [5, 6]. At the same time, keeping a certain minimum level of friction is necessary. Otherwise, the effectivity of tangential forces transmission from the wheel to the rail will drop, which can result in the vehicle being unable to accelerate and break effectively [7]. A normal and tangential force ratio can quantify frictional conditions in the rolling–sliding contacts. In the literature, this parameter is called the traction (or sometimes adhesion) coefficient (CoT) and depends on several parameters, e.g. load and creepage. Values higher than 0.09 and 0.2 are sufficient for braking and traction, respectively [8].

Top-of-rail (TOR) products were developed to maintain friction at the desired levels, where noise and wear are reduced, but sufficient CoT for traction and braking is maintained. Initially, these products were solid sticks containing lubricants like graphite or molybdenum disulphide. They were used with great success back in the 90 s in the Vancouver mass transit system to overcome problems with corrugation [9]. Since then, TOR products have undergone intensive development, and new liquid-form types have been established. Following [10], liquid TOR products can be divided into two groups depending on their base medium type: Friction modifiers (FMs), which are water-based and TOR lubricants (grease/oil-based products). The difference between these two groups lies in the friction modification mechanism [11]: Water in FMs acts as a transport medium and helps to distribute solid lubricants on the rail head. After that, water evaporates, and the friction is reduced by the shear–displacement mechanism of solid lubricants. In the case of TOR lubricants, grease/oil forms a thin lubricating film on the rail head, contact operates in a boundary/mixed lubricating regime, and solid particles in the product composition help maintain the desired CoT levels. Please note that in general tribology, the term "friction modifier" is used for various additives added to the lubricant to modify its frictional properties. However, in W/R tribology, the term is commonly used for one specific group of TOR products to distinguish between different base-medium types [10]. So, in this paper, "friction modifier" (or "FM") always refers to the group of water-based TOR products. Intensive research over the past decade has already proven the benefits of TOR products. Field studies showed that lower friction was measured on rails where TOR products are applied [12–15], resulting in wear [16–18] and noise reduction [5, 6] and even the number of air-born particles generated from the contact decreased [18].

However, the W/R contact is an open system, which means that besides the intentionally applied TOR products, it is also influenced by various contaminants naturally present on the rail [19]. One of the most common is water. Several studies have shown that water is a good lubricant that can reduce CoT significantly and cause low adhesion problems [20–23]. Furthermore, low adhesion problems are typically linked to the so-called "wet–rail phenomenon" [24, 25]. In that case, a small amount of water mixes with iron oxides, which are inevitably present on the rail surface. Together, they form a thick layer with high viscosity, capable of reducing CoT to as low as 0.05 [25]. It was shown that low adhesion problems are most probable in the morning when dew is present on the track [8], concluding that a small amount of water rather than large amounts causes low adhesion problems. Furthermore, several tests in a climate chamber were conducted to examine the effect of humidity on friction [22, 26]. The results show that with the rise in relative humidity (RH) %, the CoT decreases.

Moreover, the study [27] found that it is even worse when the dew point is reached and water condenses on the specimen surfaces. CoT drop is significantly more substantial in that case than in the humid conditions without dew. In addition, it was shown that temperature influences this behaviour, as it determines how much water can be contained in the air before dew conditions happen. It was found that the effect of humidity is most substantial for temperatures below 24 °C. On the contrary, it is almost negligible for temperatures over 30 °C [27].

Even though contamination significantly influences CoT, little is known about the interaction between TOR products and contaminants. Although TOR products are designed to maintain the CoT required for traction/braking, their effect has been tested primarily in laboratory-clean conditions, or the effect of contaminants has not been evaluated. There are only a few studies addressing this problem. In [28], two FMs were tested under water contamination. Water influenced both products and caused a drop of CoT below 0.1 when applied. However, these products contained friction enhancers like stainless steel particles or sand with high particle diameters, which are not typically found in modern TOR products [29, 30]. It can be assumed that the influence of water on products that do not contain such particles can be even more significant. This conclusion is supported by [31], where different amounts of water were applied to three commercial TOR products (one FM and two TOR lubricants). It was shown that water mixes with the oil in TOR

lubricants and causes a long-lasting period of very low CoT. This observation is also supported by a study [32] that showed that a mixture of rail oil and water leads to even lower CoT than the oil itself. Finally, in [26], an FM mixed with iron oxide particles was tested in a climate chamber under high-humidity conditions. It was shown that with an increase in % of RH, the performance of FM was influenced, and CoT decreased. It was also noted that for a higher % of RH, FM stayed wet for a more extended period, suggesting that the base medium evaporates slowly in a humid environment. Although the increase in % of RH caused a decrease in CoT, it stayed in the interval of desired friction levels as it did not drop below 0.2.

Although testing of FMs in a humid environment did not result in low adhesion in the study [26], it must be noted that as the RH ranged between 40 and 90%, severe water condensation probably did not occur. Previously, in [27], it was shown that there is a significant drop in CoT when dew is present due to the water acting as a lubricant. Furthermore, it was shown in [31] that water influences the performance of TOR products significantly, and oil-based products even cause low adhesion problems in these conditions.

So, based on [27, 31], the question arises about what would happen if condensation occurs and dew is mixed with the product. Although this scenario may happen in the field, the interaction between dew and TOR lubricants has not yet been thoroughly examined. So, this study aims to explore the effect of humidity and dew on two commercial TOR lubricants. Experiments follow an approach based on the creep curve measurement described in [33]. A laboratory tribometer in a ball-on disc configuration equipped with a climate chamber was used for all experiments.

2 Material and Methods

2.1 Test Setup and Specimens

A laboratory tribometer MTM (Mini-Traction Machine, PCS Instruments) in a ball-on-disc configuration was used for all tests and wear-ins/run-ins, see Fig. 1. The specimens were disc with 46 mm in diameter and a ball with 19.05 mm in diameter. According to the Hertz theory, the contact area was circular at the beginning with a diameter of 0.2 mm (the Poisson's ratio of 0.33 and Elastic modulus of 205 GPa was considered for this material). Both specimens were loaded against each other and driven by independent servo motors so the required slide–roll ratio (SRR) could be achieved according to the given equation:

$$\mathrm{SRR} = \frac{w_{\mathrm{ball}} \cdot r_{\mathrm{ball}} - w_{\mathrm{disc}} \cdot r_{\mathrm{disc}}}{w_{\mathrm{ball}} \cdot r_{\mathrm{ball}} + w_{\mathrm{disc}} \cdot r_{\mathrm{disc}}} \cdot 200\% \tag{1}$$

where w_{ball} and w_{disc} are angular speeds of specimens and r_{ball} and r_{disc} stands for its radii. The embedded sensor measures the normal force (N) with ± 0.3 N accuracy with a 1 Hz sampling frequency. However, this signal results from averaging a non-specified higher frequency input signal. Traction force (T) is calculated from the torque measured by the transducer attached to the disc shaft, so the traction coefficient (CoT) could be determined as follows:

$$\mathrm{CoT} = \frac{T}{N} \tag{2}$$

The specimens were made of AISI 52100 bearing steel with a Vickers macro-hardness of 800–920 and 720–780 HV for ball and disc, respectively. Although bearing steel is not a typical rail material, its higher hardness ensures stable conditions during experiments and better repeatability

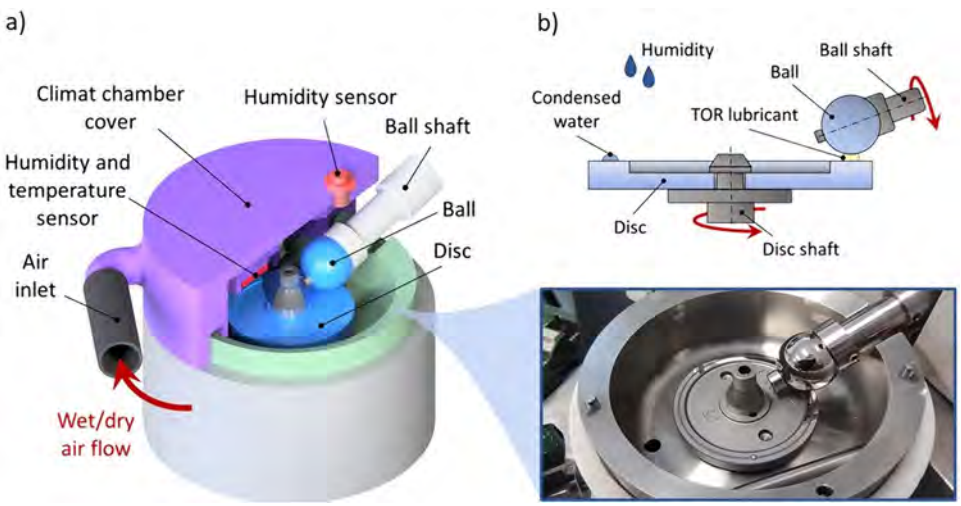

Fig. 1 Test setup: **a** climate chamber and **b** detail of the specimens inside. Part of **b** redrawn from [31] with the Publisher's permission (Elsevier)

due to reduced wear compared to standard wheel/rail steel. The choice of specimen material and geometry follows the benchmarking methodology [33] and enables results to be compared between different laboratories. The impact of the selection of bearing steal over authentic rail steal on measured results and all other study limitations derived from the simplified ball-on-disc configuration will be thoroughly discussed in Sect. "Study limitations". Before tests (after running-in), the surface roughness of specimens was checked using an optical profiler Contour GT (Bruker), and it varied around Ra 0.15 µm for the ball and Ra 0.3 µm for the disc. The same profiler was used to study topography changes and observe oxide layer formation.

The stability of the environment was ensured by a climate chamber mounted on the top of the pot of the tribometer, see Fig. 1a. The chamber had two sensors for monitoring RH and air temperature. The first sensor was mounted in the upper part of the chamber and provided feedback to the humidification unit. Based on the data from this sensor, the humidification unit runs the mixture of wet and dry air into the chamber in a specific ratio, achieving the desired value of RH. The second sensor (HTU21D) was placed near the contact area to enable online monitoring of RH and air temperature near the contact inlet. This sensor measures RH in the 5–95% range with an accuracy of ± 2%. It is also possible to measure outside these borders but with slightly lower accuracy. However, this should not affect the tests conducted since the 100% RH was achieved by running only wet air in the climate chamber. The climate chamber did not enable air temperature control, so all tests were conducted at room temperature of 22 ± 1 °C. However, due to the rise of air temperature due to heat generated in the contact during tests, the HTU21D sensor was also used for air temperature monitoring with ± 0.3 °C accuracy (declared in the range from − 40 to 125 °C).

2.2 Tested TOR Lubricants

The TOR lubricant used in most tests is referred to as "TORL-A". It is a commercially available product used for friction modification in railway operations. Additionally, several tests were conducted using a second TOR lubricant labelled "TORL-B". These tests investigated whether similar phenomena can occur for products with different compositions, indicating that they are not specific to TORL-A alone. Essential information about the composition of both products obtained from datasheets can be seen in Table 1.

2.3 Methodology

Studies on friction modification usually use time tests (CoT on time dependency) [17, 30, 31] or creep curve measurements (CoT on SRR dependency) [14, 28, 34] for testing FMs and TOR lubricants. A study [33] shows that results obtained during time tests can be influenced by the ever-changing topography of the contact surfaces. On the contrary, results based on creep curve measurements are less influenced by topography changes and enable the study of TOR lubricants in a wide range of conditions typical for railway operations. Also, a higher % of slip prevents the contact path surface smoothening effect (the major drawback of time tests), enabling the testing of TOR lubricants in higher quantities. So, in this study, the authors chose to follow a creep curve measurement approach proposed in [33] to examine the effect of humidity and dew on TOR lubricants, which is the main objective of this paper. As seen in Fig. 2, this Sect. "Methodology" is divided into four consecutive parts describing the fundamental principles of the methodology. Readers are encouraged to see the study [33], where the detailed reasoning behind each step was explained.

2.3.1 Cleaning and Running-ing

Before each test, specimens were cleaned manually with a paper towel and ultrasonically in an acetone bath for 10 min. After that, specimens were runned-in for 30 min to stabilise surface roughness and remove residual contaminants. The run-in parameters were 2% SRR, a speed of 1000 mm/s and a normal force of 18 N (corresponding to 0.8 GPa Hertz pressure for unworn specimens). For a given set of humidity/dew conditions, every test was repeated five times on the same pair of specimens to obtain results from a wide range of conditions, as the contact path width and depth changes during tests due to wear. Before each of these five tests, the run-in was conducted the same way except for the first one, which was extended to 60 min to overcome the initial rapid topography changes of unworn surfaces and form a stable contact path.

Table 1 Composition and characteristics of tested TOR lubricants

TOR lubricant	Structure	NLGI grade	Base oil	Thickener	Particles	Base oil viscosity at 40 °C (mm^2/s)
TORL-A	Paste	0	Biodegradable ester	Organic	Soft metal	41–53
TORL-B	Gel paste	00	Synthetic ester	Inorganic (silicate)	Soft metal	46

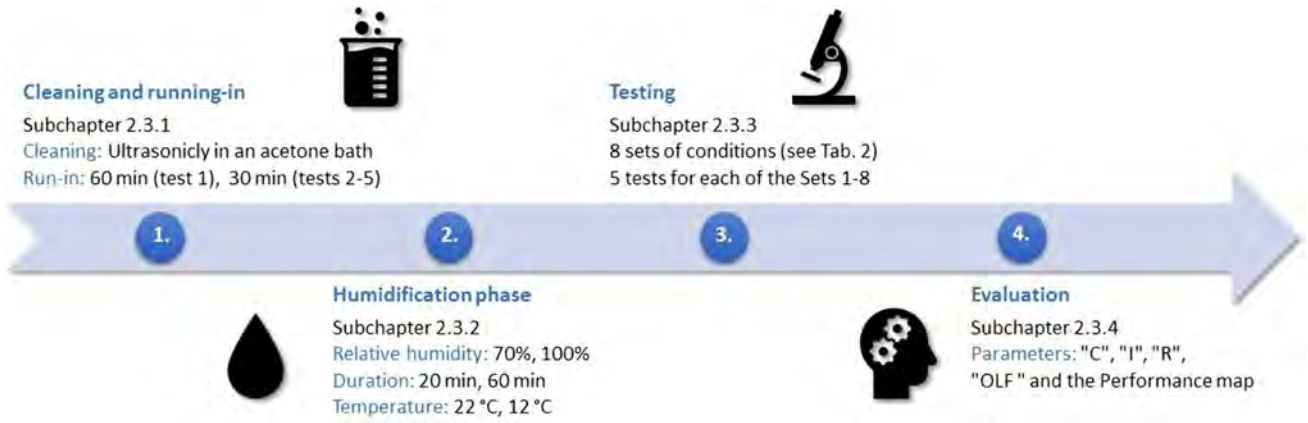

Fig. 2 The individual steps of the methodology

2.3.2 Humidification Phase

Next, TOR lubricant was applied to the contact path of the disc. Then, the tribometer pot was covered with a climate chamber, and the mixture of wet and dry air in the specific ratio was run inside to achieve the desired % of RH (this step is further referred to as the "Humidification phase"). It can be assumed that water condensation only occurred during this step since after the start of the test, the surface temperature quickly rose due to the heat generated by friction, and water could no longer condense on the specimens. The humidification phase was skipped in Sets 1 and 7 (see Table 2), where TOR lubricants were tested under laboratory ambient conditions.

2.3.3 Testing

The test starts when the Humidification phase is ended (see Table 2). One test consists of repetitive creep curve measurements with the same specimen pair, see Fig. 3a. TOR lubricant is applied only once before the first creep curve measurement. So, as the starvation progresses, every consecutive curve reaches higher values of CoT until the threshold criterion is met. This approach enables testing the product under a wide range of topography conditions and evaluating its lasting effect. Every creep curve consists of six points, each evaluated from a 30-s time test as an average CoT at a given SRR value, namely 0, 2, 5, 10, 15, and 20%. Please note that time tests with 0% SRR were only to redistribute

Table 2 The testing parameters and conditions

Set	Product	Amount (µl)	SRR (%)	Normal force[d] (N)	Speed (mm/s)	RH (%)	Humidification phase (min)	Specimen temp. (°C)
1	TORL-A	1	0–20	18	1000	Ambient[a]	–	Ambient[a]
2	TORL-A	1	0–20	18	1000	70[b]	20	Ambient[a]
3	TORL-A	1	0–20	18	1000	70[b]	20	12 ± 2
4	TORL-A	1	0–20	18	1000	100[c]	20	Ambient[a]
5	TORL-A	1	0–20	18	1000	100[c]	60	Ambient[a]
6	TORL-A	1	0–20	18	1000	100[c]	20	12 ± 2
7	TORL-B	1	0–20	18	1000	Ambient[a]	–	Ambient[a]
8	TORL-B	1	0–20	18	1000	100[c]	20	Ambient[a]

[a]Laboratory ambient conditions: RH = 34 ± 2%, temperature = 22 ± 1 °C

[b]Tests with RH = 70 ± 5% are labelled as "humid conditions" in the text

[c]Tests with RH = 100% are labelled as "dew conditions" in the text

[d]According to the Hertz theory, 18 N normal force results in 0.8 GPa contact pressure in the given configuration and unworn specimens

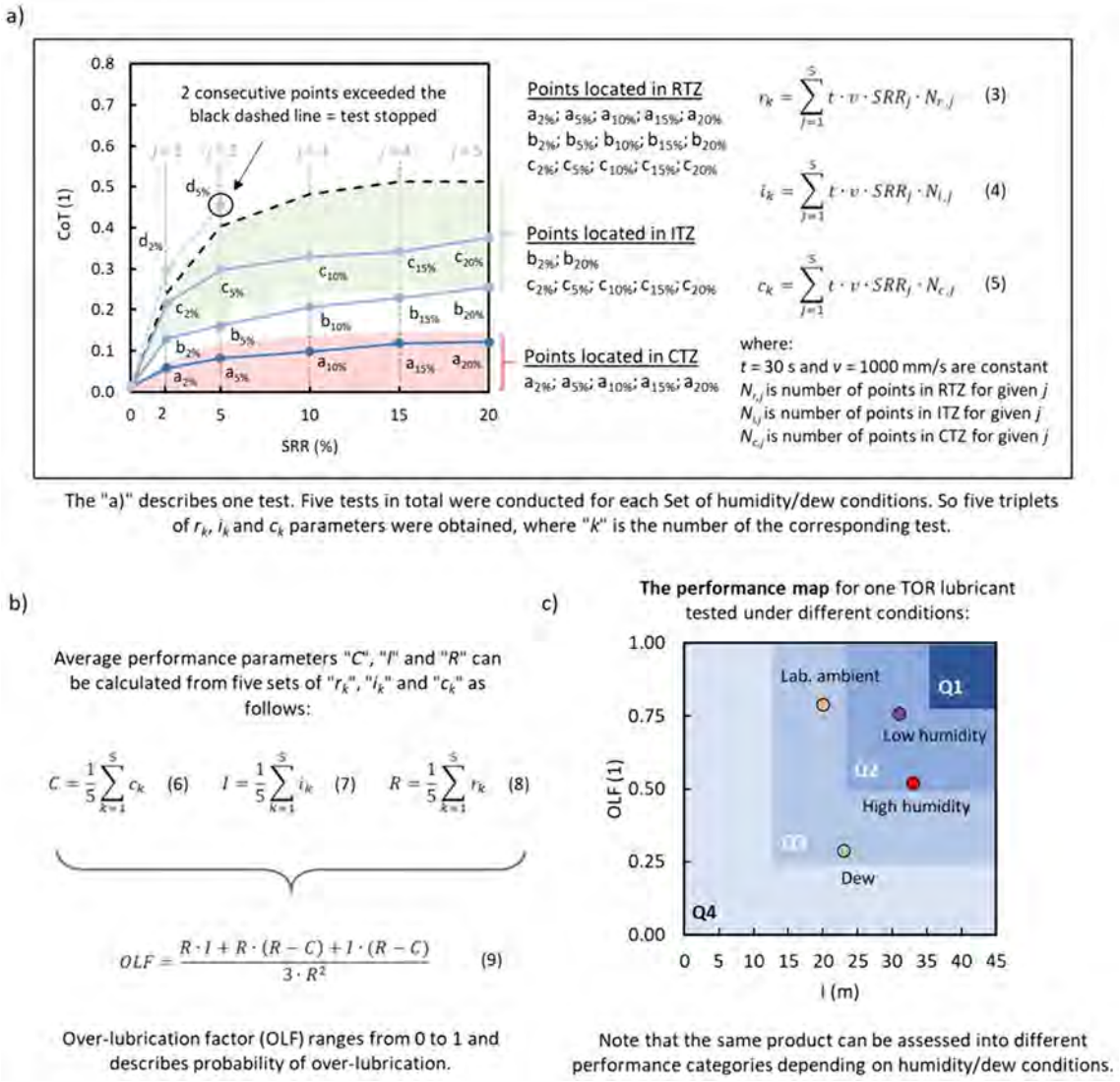

The "a)" describes one test. Five tests in total were conducted for each Set of humidity/dew conditions. So five triplets of r_k, i_k and c_k parameters were obtained, where "k" is the number of the corresponding test.

Fig. 3 **a** Model example of one test. Each test is repeated five times, so five triplets of "r", "i", and "c" parameters are obtained. **b** Average parameters "R", "I", and "C" are calculated and used for the "OLF" evaluation. **c** Product performance is assessed into four categories Q1–Q4 based on "OLF" and "I" for each set of humidity/dew conditions

TOR lubricant on the surfaces evenly, and these tests were not used in the evaluation. The threshold criterion was as follows: If two consecutive points exceeded the threshold curve (black dashed line in Fig. 3a), the test was ended. If not, another creep curve was measured. "Consecutive points" are two neighbouring SRRs from the sequence 2, 5, 10, 15 and 20% and corresponding values of CoT.

Three traction zones located under the threshold curve were defined: Critical traction zone (CTZ), Intermediate traction zone (ITZ) and Retentivity traction zone (RTZ). These zones represent different frictional levels: "CTZ" for levels insufficient for reliable traction/braking, "ITZ" represents levels desired for operating the rail vehicles, and "RTZ" which shows the distance for which the TOR lubricant has a noticeable effect on friction. If a point is placed in "CTZ" (red area in Fig. 3a), the CoT decreases to very low values for a given SRR, indicating that over-lubrication occurs. On the other hand, in "ITZ" (green area in Fig. 3a), the CoT reaches intermediate values, meaning the product performed well (that is where, on actual track, adverse effects of friction are reduced but sufficient transmission of traction/braking forces is ensured). Finally, "RTZ" is the entire area under the threshold curve and contains all points measured during the test (except those that exceeded the threshold criterion). Lastly, there is a blank area between "CTZ" and "ITZ", in which CoT acquires values that are not considered critical nor optimal. If a point is placed in this area, this does not directly benefit or penalise the product in the evaluation but influences the retentivity and prolongs test time. Exact values for the threshold

curve and "CTZ", "ITZ", and "RTZ" boundary points were calculated as a defined fraction [33] of dry and clean contact CoT for a given % of SRR and are listed in Appendix A.

2.3.4 Evaluation

From each test, three performance parameters were calculated, namely: "*c*" (critical traction parameter), "*i*" (intermediate traction parameter), and "*r*" (retentivity parameter). These parameters represent the cumulative sliding distances for which CoT stayed in "CTZ", "ITZ", and "RTZ" during the test (see Fig. 3a) Eqs. 3–5) and their unit is one meter. In other words, each parameter is calculated as a sum of weighted distances for which the contact operated in the corresponding zone, where the weight is the value of the corresponding SRR %. The ideal TOR lubricant would aim to maintain the intermediate friction level for as long as possible (represented by the high value of the "*i*" parameter) and simultaneously reduce the probability of low adhesion problems (zero or low value of the "c" parameter). The values of these parameters are limited by the product retentivity (expressed by the "*r*" parameter), which shows how long the effect of the product is noticeable (in this methodology, this parameter represents the whole test duration). Five tests were performed for each set of humidity/dew conditions, resulting in the five triplets of these parameters. From those, average parameters "C", "I", and "R" were calculated, and the over-lubrication factor ("OLF") was evaluated, see Fig. 3b) Eqs. 6–9. The "OLF" describes the probability of over-lubrication (ranges from 0 to 1; the lower the number, the higher the probability of over-lubrication). The ideal product would score "OLF" equal to 1, meaning only desirable CoT values were measured during the test duration.

Finally, a 2D Performance map was constructed in which the *x*-axis contains the value of "*I*", and the *y*-axis has the value of "OLF" for each set of humidity/dew conditions (see Fig. 3c). In this map, four performance categories Q1–Q4 were defined (these categories divide the performance map into quartiles). To be placed into Q1, both "I" and "OLF" values have to lay in the upper 25% on each axis, for Q2 in the upper 50%, for Q3 in the upper 75% and for Q4 at least one value is in the bottom 25%. If the TOR lubricant scores in Q1, that means that the risk of low adhesion problems due to over-lubrication (or condensed water, in this study) is not significant, and the product maintains the desired frictional conditions for a very long time. A change in the performance category caused by humidity/dew indicates how the product performs under different scenarios that can occur on the rail.

2.4 Test Conditions

TOR lubricants were tested in various conditions to evaluate which factors (% RH value, duration of the Humidification phase, etc.) affect their performance the most. TORL-A was chosen for the majority of experiments. However, some experiments were performed with the second lubricant, TORL-B, to ensure that observed phenomenons are not limited to the composition of TORL-A alone but can be generalised to other TOR lubricants with different compositions. All the information about humidity/dew conditions and performed tests is listed in Table 2. In this table, each set of conditions is labelled as "Set 1–8". The purpose of testing these sets is as follows:

(1) Set 1 was conducted under laboratory ambient conditions, specifically RH = 34 ± 2% and temperature of 22 ± 1 °C. This set shows how the TOR lubricant performs in "normal conditions" and was used as the base reference.
(2) In Set 2, TORL-A was exposed to "humid conditions" (specifically RH = 70 ± 5%) for 20 min.
(3) Set 3 was also conducted under "humid conditions" (RH = 70 ± 5%) for 20 min. However, specimens were first put into the refrigerator and cooled to 12 ± 2 °C (measured on the surface). A comparison between Sets 2 and 3 can highlight the importance of the temperature and the dew point.
(4) In Set 4, the TOR lubricant was exposed to RH = 100% ("dew conditions") for 20 min during the Humidification phase. A comparison between Sets 1, 2 and 4 shows how the change in RH % value influences the performance parameters.
(5) In Set 5, TORL-A was exposed to RH = 100% ("dew conditions") for a prolonged duration of 60 min. A comparison between Sets 4 and 5 reveals how the duration of exposure to the humidity will affect the performance parameters.
(6) In Set 6, TORL-A was exposed to RH = 100% ("dew conditions") for 20 min, but first, specimens were put into a refrigerator and cooled down to 12 ± 2 °C (same procedure as in Set 3). The difference in temperature between the surface and surrounding air lowers the dew point and speeds up the water condensation. Thus, more water could condense during the Humidification phase in Set 6 compared to Set 4, where the temperature of the specimens was the same as that of the surrounding air.
(7) Set 7 was conducted with TORL-B under laboratory ambient conditions, specifically RH = 34 ± 2% and temperature of 22 ± 1 °C to obtain the reference for this TOR lubricant under "normal conditions".
(8) In Set 8, the TORL-B was exposed to RH 100% ("dew conditions") for 20 min during the Humidification phase. Sets 7 and 8 were designed to validate results for TOR lubricants with different compositions.

2.5 Additional Experiments

Before the tests mentioned above, several experiments were performed to quantify how much water condenses on the disc surface during the Humidification phase for conditions defined in Table 2, Sets 2–6 (and 8). Only the Humidification phase was performed in these experiments (without any running-in or testing; the goal was to quantify the amount of water). Then, the discs were weighed, and the amount of water was calculated based on the disc weight difference before and after the Humidification phase. So, the change in TOR lubricant performance could be linked to the explicit water quantity.

3 Results and Discussion

First, experiments defined in Sect. "Additional Experiments" were performed to quantify water amounts that condense on the disc surface during the Humidification phase. The results of these experiments can be seen in Table 3 (an average value of 5 measurements). Please note that these are the quantities condensated on the entire disc surface. It is expected that most of the water did not enter the contact because it did not lay in the contact path, as can be seen in pictures from the optical microscope, see Fig. 4. So, there are two more columns in Table 3: corresponding amounts of water in the contact path and amounts of water in W/R contact. These values were calculated based on the ratio between the entire disc surface area, contact path area, and actual W/R contact area. Note that the "contact path area" was measured using an optical profiler, and an approximated value of 1 cm^2 was used as the "actual W/R contact area" based on the literature [11].

3.1 The Effect on TOR Lubricant Creep Curves

The results for Sets 1–8 are summarised in Fig. 5. From each Set, only one out of five tests was randomly selected to be displayed for the sake of clarity. However, average

Table 3 Weighed amounts of water during the Humidification phase and corresponding amounts for the contact path and actual W/R contact

Amount of water	Set 1 (7)	Set 2	Set 3	Set 4 (8)	Set 5	Set 6
On disc (µl)	–	0.2	0.72	7	30	180
In contact path (µl)[a]	–	0.007	0.03	0.26	1.2	7.2
In W/R contact (ml)[b]	–	0.01	0.04	0.37	1.7	10.3

[a]Calculated based on the disc surface and contact path area ratio

[b]Calculated based on the ratio between the MTM and the actual W/R contact areas

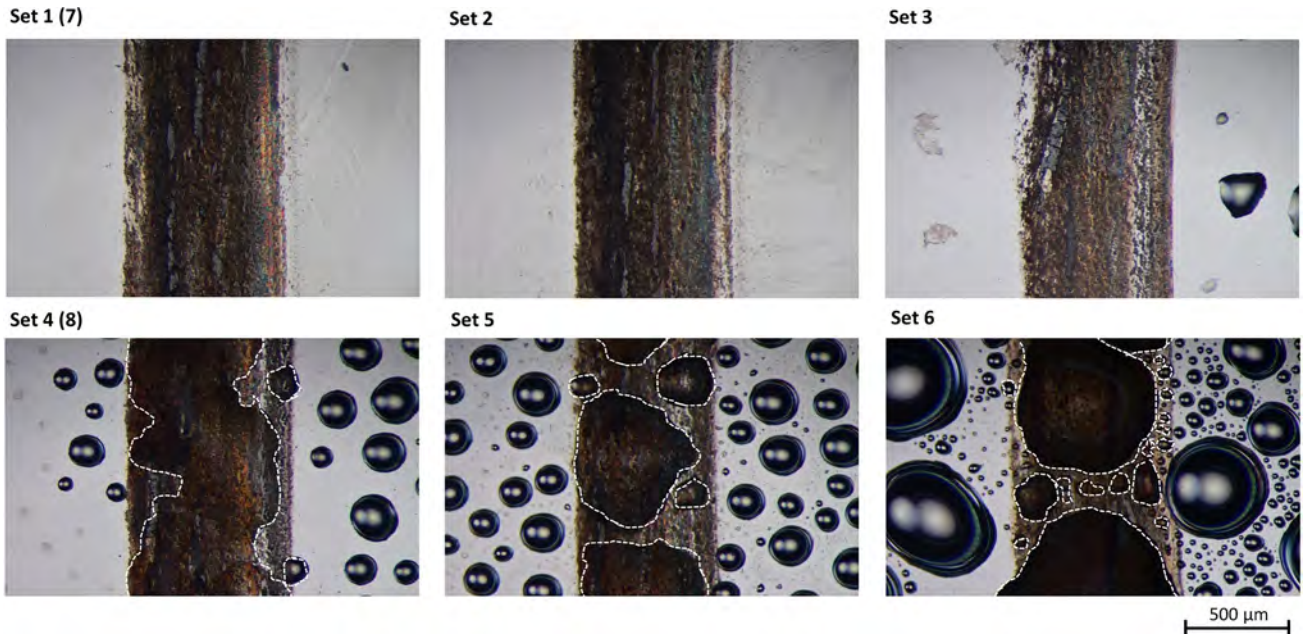

Fig. 4 Photo of the contact path after the Humidification phase in Sets 1–8. A white dashed line highlights water droplets lying in the contact path

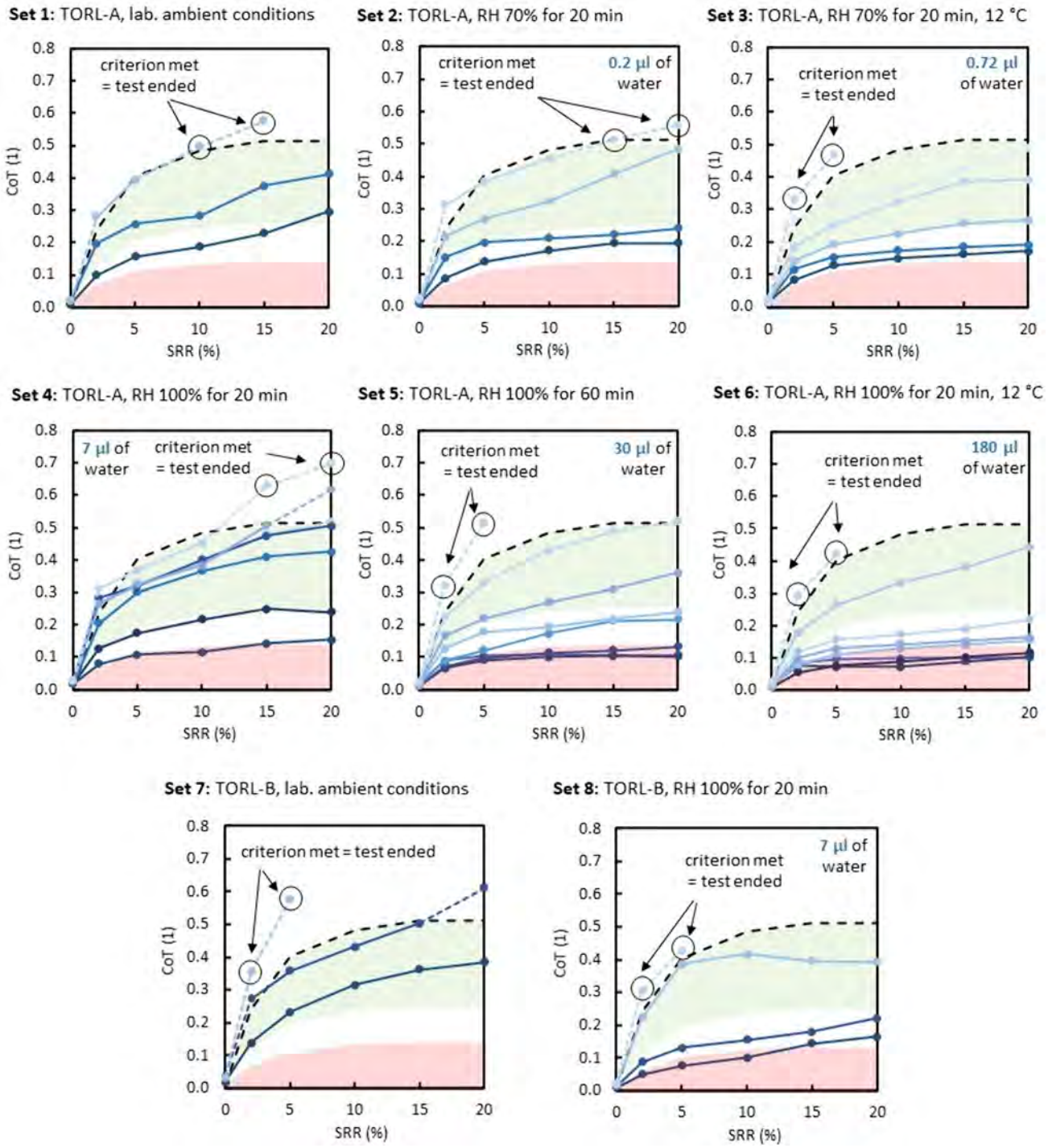

Fig. 5 One selected test for each of Sets 1–8. A black dashed line shows the threshold criterion. Creep curves are depicted in shades of blue. "CTZ" and "ITZ" are highlighted by the red and green areas, respectively

performance parameters were calculated based on all five tests and will be discussed later in the text. These charts show creep curves constructed from SRR value on the *x*-axis and CoT on the *y*-axis. Each creep curve has six points (the last creep curve in each chart may be an exception). The threshold limit is displayed in these charts by a dashed black line. Creep curves are shown by solid lines in shades of blue. If some point of the creep curve is placed outside the black threshold curve, this point is excluded from the evaluation and connected with other points by a dashed line of the

same colour. If two consecutive points are placed outside the threshold line, the criterion for ending the test was met, and the test was stopped (which is why the last creep curve in each test may consist of less than six points). Furthermore, the red area highlights the "CTZ", and the green area highlights "ITZ" in these charts.

First, the effect of humidity/dew on TORL-A creep curves will be discussed. After linking the results for Sets 1–6 from Fig. 5 to corresponding amounts of water from Table 3, it is clear that with increased water amount, more creep curves are measured during the single test, and CoT decreases to lower values. During the displayed test for Set 1, in which measurements were conducted under laboratory ambient conditions to obtain the reference, only two creep curves lay entirely under the threshold, and the test was stopped during the third one. In the beginning, when the TOR lubricant is applied, the contact is flooded. A uniform layer of oil may be formed for sufficient speeds, preventing direct contact between surface asperities, resulting in low CoT for a given % of SRR. However, at some point, starvation occurs, and the load is transmitted partly by the oil film and partly by the direct contact between the surface asperities, which is typical for mixed/boundary lubrication regimes. At this point, higher values of CoT are measured until the threshold criterion is finally met.

During the displayed test for Set 2, where specimens were exposed to RH 70% for 20 min, one extra creep curve was measured compared to the previous test. However, as shown in Fig. 4, no water was present in the contact path after the Humidification phase. This slight difference is not out of the range in which this product performs under normal conditions (topography changes and precision of application play a role), concluding that RH 70% had no significant effect on the TORL-A. On the contrary, a noticeable effect was seen during Set 3, where precooling of the specimen led to higher water condensation compared to Set 2, see Table 3. In this test, not only were more creep curves measured, but some of these curves also approached boundaries of the "CTZ".

The most significant effect was observed during Sets 4–6 with RH 100% when dew conditions occurred. During Set 4, some points fell into the "CTZ" for the first time, meaning very low CoT was measured for these SRRs. Furthermore, the situation worsens in Set 5 when the Condensation period is extended to 60 min. Finally, the highest number of creep curves placed in "CTZ" were measured during Set 6, where precooling of the specimens led to the condensation of excessive amounts of water of 180 µl on the disc surface.

Lastly, Sets 7 and 8 were performed with TORL-B to see if this behaviour is exclusive to TORL-A or may occur for products with different compositions and rheological properties. Although the number of creep curves did not rise dramatically under the dew conditions, significantly lower values of CoT were measured, and points for some of the SRRs were moved from "ITZ" to the "CTZ", showing an apparent effect of water on TORL-B, as in the case of TORL-A.

It is clear that water interacts with the product and mixes with its base medium, which is grease/oil in this case. The interaction between oil and water can be described based on Oil-in-water (O/W) emulsion theories, especially the plate-out theory (valid for lower running speeds). This theory says that in the case of O/W emulsion, contact is predominantly lubricated by the oil as it has stronger wetting abilities [35, 36]. This means that even if the mixture consists mainly of water, the oil forms a pool before the contact inlet and prevents water from entering the contact. Thus, the lubricating film is entirely composed of oil, and water does not negatively influence film thickness in the contact [37]. Furthermore, the study [32] experimentally confirmed that water may even improve the lubricating abilities of oil in some cases, as an oil and water mixture provided lower CoT than pure oil in experiments conducted in the study. This scenario may describe the situation in the contact during a couple of first points of the creep curve(s).

At some point, starvation occurs, meaning water can no longer be excluded from the contact [38]. Without water, CoT would rise at this point (as was seen in Sets 1, 2 and 7). However, in this case, water can refill starved contact and maintain low CoT. It is important to note that the base medium of tested TOR lubricants also contains thickeners and other additives, and the lubricating mechanism may differ from O/W emulsions. So, in this case, water will influence not only the oil pool formed before the contact inlet but also the rheology and structure of the grease itself. It was shown that grease bulk can absorb water due to the polar nature of the thickener [39]. Usually, grease tends to be pushed to the sides of the contact path, and then, the contact replenishment is inversely proportional to viscosity [40, 41]. Water may influence stiffness and oil-bleeding ability, which could lead to higher contact replenishment and prolong the duration of low CoT. So, a higher number of creep curves is measured in Sets 4–6 compared to those with lower amounts or no water at all.

3.2 The Effect on TOR Lubricant Performance Parameters

The values of average performance parameters "C", "I", and "R" were computed using Eqs. 3–8 (Fig. 3) from five triplets of "c", "i", and "r" for each of the Set 1–8. Together with "OLFs" and corresponding amounts of water, they are summarised in Table 4 and depicted in Fig. 6. In this figure, the x-axis is divided into eight parts, one for each Set 1–8. The

purple *y*-axis is for "OLF", and the black *y*-axis is for sliding distances of "*C*", "*I*", and "*R*". Finally, the blue *y*-axis on the right stands for water amounts that condensated. Furthermore, tests under humid and dew conditions are differentiated by brown and blue, respectively.

A clear relation between the change in "OLF" and the amount of water can be seen: with an increase in water amount, "OLF" gradually decreases between Sets 1–6 and 7–8, which means that the risk of low adhesion problems is dependent on the water amount, which follows findings in [8]. This trend is also valid for "*C*" and "*R*" parameters (with a slight exception for "*R*" between Sets 5 and 6)—the higher the water amount, the longer the duration of critical traction and the longer the retentivity. On the other hand, parameter "*I*" did not show any clear trend, which can be interpreted as follows: water does not strongly influence the

Table 4 The exact values of "C", "I", and "R" parameters and "OLF" for Sets 1–8

	Set 1	Set 2	Set 3	Set 4	Set 5	Set 6	Set 7	Set 8
C (m)	0	0	0	16	31	50	0	12
I (m)	20	31	22	33	45	23	19	27
R (m)	29	49	50	77	116	111	24	68
OLF (1)	0.79	0.76	0.63	0.52	0.47	0.29	0.88	0.51

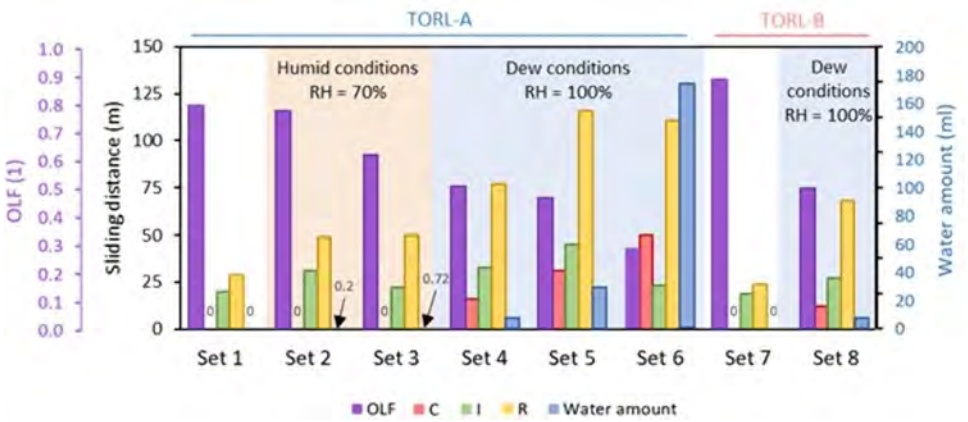

Fig. 6 The final results: Summary of "OLF", "*C*", "*I*", and "*R*" parameters and corresponding amounts of water

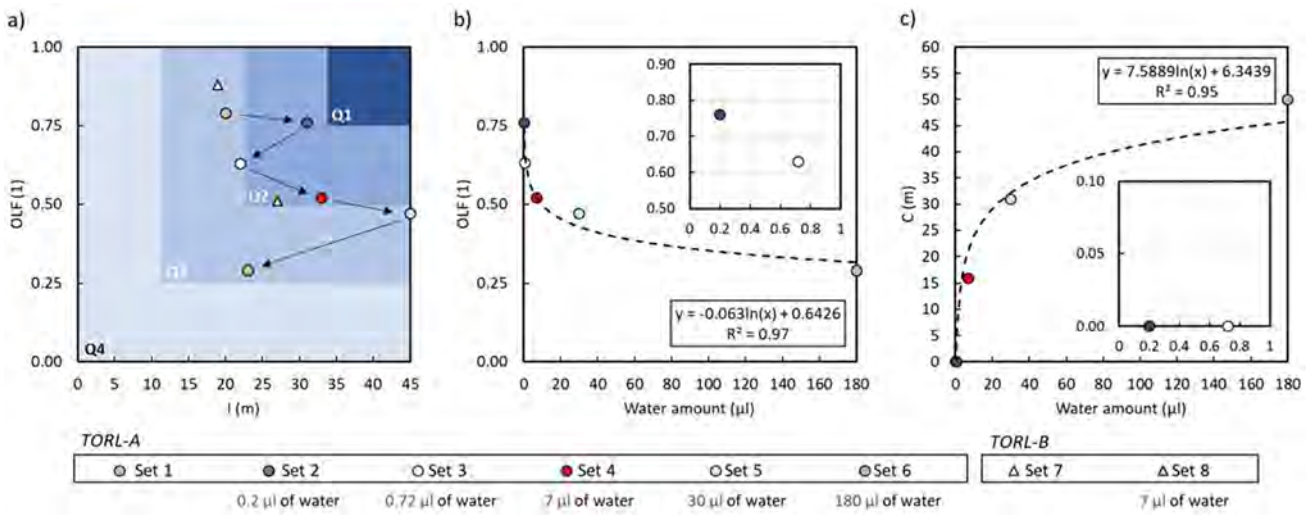

Fig. 7 The final results: **a** performance map, **b** the dependency of "OLF" on water amount for TORL-A and **c** the dependency of average critical traction parameter "C" on water amount for TORL-A

duration of positive effects of TOR lubricants. However, it enhances the time of undesirable critical traction, which also prolongs retentivity and, in the end, lowers "OLF". To sum it up, water does not influence the desired effects of TOR lubricants but enhances their adverse effects.

Next, the performance map was constructed. In Fig. 7a, four performance classes Q1–Q4 are highlighted in shades of blue. Placing in the best-performing class (Q1) requires scoring high values for both parameters. This requirement was met under no set of conditions. Although in Sets 1, 2 and 7, the "OLF" of TORL-A and TORL-B was sufficient for the Q1 class, their "I" parameter was good enough only for the Q2 or Q3 class, resulting in a lower product overall assessment, meaning that in these tests, products provided desired frictional levels, but only for a limited sliding distance. In Sets 2, 4 and 8, tested products provided a good compromise between the provided CoT and the duration of its performance and were assessed in the Q2 class. In Sets 1, 3, 5 and 6, products lacked sufficient duration, or low adhesion problems occurred, and Q3 class was assessed.

TORL-A performed the worst in Set 6, where a large amount of water nearly caused a drop from Q3 to the worst Q4 category. In the performance map, arrows between points show the direction in which the performance class changed with increased water amount.

Furthermore, "OLF" on water amount dependency was plotted in Fig. 7b. Please note that the results are shown only for TORL-A, and only Sets 2–6 in which the water amount was non-zero are displayed. There is a clear trend that with increased water amount, "OLF" decreases to lower values. However, this behaviour is not linear—a slight increase in small amounts of water leads to a significant "OLF" change. On the other hand, with larger amounts of water, a further increase leads only to a negligible change in "OLF". This behaviour can be explained by the fact that there is a limit to the amount of water that can enter the contact, depending on the contact size. The reference logarithmic curve is plotted as a black dashed curve over measured results. However, there is not enough evidence to state that the "OLF"—water amount dependency is logarithmic. More tests should be conducted to support this conclusion, and the logarithmic curve is displayed only to highlight that the severity of the impact of the change in water amount differs for small and large amounts.

In addition, parameter "C" on water amount dependency was plotted in Fig. 7c). A similar trend can be seen in this case as for lower amounts of water, a slight increase in water amount causes a significant increase in the sliding distance in the "CTZ". However, when larger amounts of water are present, further increase leads only to a slight rise in parameter "C", which is probably also linked to the contact size area and the fact that only a limited amount of water can enter the contact with TOR lubricant.

3.3 The General Discussion and Implications for Railway Operation

To better understand the results, it is necessary to put them in the context of the rest of the scientific work. The Fig. 8 shows a selection of published papers on this topic.

The *y*-axis has the value of CoT/CoF measured in dry conditions (grey bars), under humid/water/dew conditions (blue bars) and a combination of humidity/water/dew and TOR products (brown bars). Moreover, essential parameters (e.g. measuring configuration, range of RH or temperature, etc.) are noted, and the "CTZ" for 20% SRR used in this study is highlighted in red.

The left part of Fig. 8 shows that in dry contact, CoT (or CoF in case of pure sliding contact) usually vary from 0.4 to 0.8 depending on the presence of third body layers and also measurement method, as studies with different measurement configurations (rail tribometer, ball-on-disc and twin-disc) were chosen on purpose to gain a broader overview. Studies in the middle show that under humid conditions, CoT decreases slightly compared to dry contact. However, the decrease is not significant. A more substantial effect was shown in [42], where RH 60% and water caused the reduction of CoT to 0.3. This value was measured also in [27] under RH 70%. However, in the same study, the author raised RH further to 100%, which caused severe condensation, lowering CoT to 0.13. A comparison between grey and blue bars shows that although humidity somewhat reduces CoT, a more substantial CoT drop occurs only when water is introduced to the contact through direct application [42] or condensation [27]. The right part of Fig. 8 shows that the situation worsens when TOR products come into play. First, a study [26] tested the effect of humidity and iron oxides on FM. Although very low CoT was not measured, another study [31] showed that FMs are generally more resistant to contamination (in terms of low adhesion), and the problem arises when oil contained in TOR lubricants mixes with water. In that case, CoT as low as 0.015 was measured in [31], even lower than in the present study. However, as different tests were performed in both studies, the comparison of the results is slightly limited. Also, different amounts of water were tested, from which the most comparable are results for 8 µl of water, which caused a long-lasting period of very low CoT in [31], similar to the effect of 7.2 µl of water in Set 6 in the present study.

Another critical factor is the presence of a third body layer. A study [8] suggests that low adhesion problems are more probable in the morning when dew is present, as a

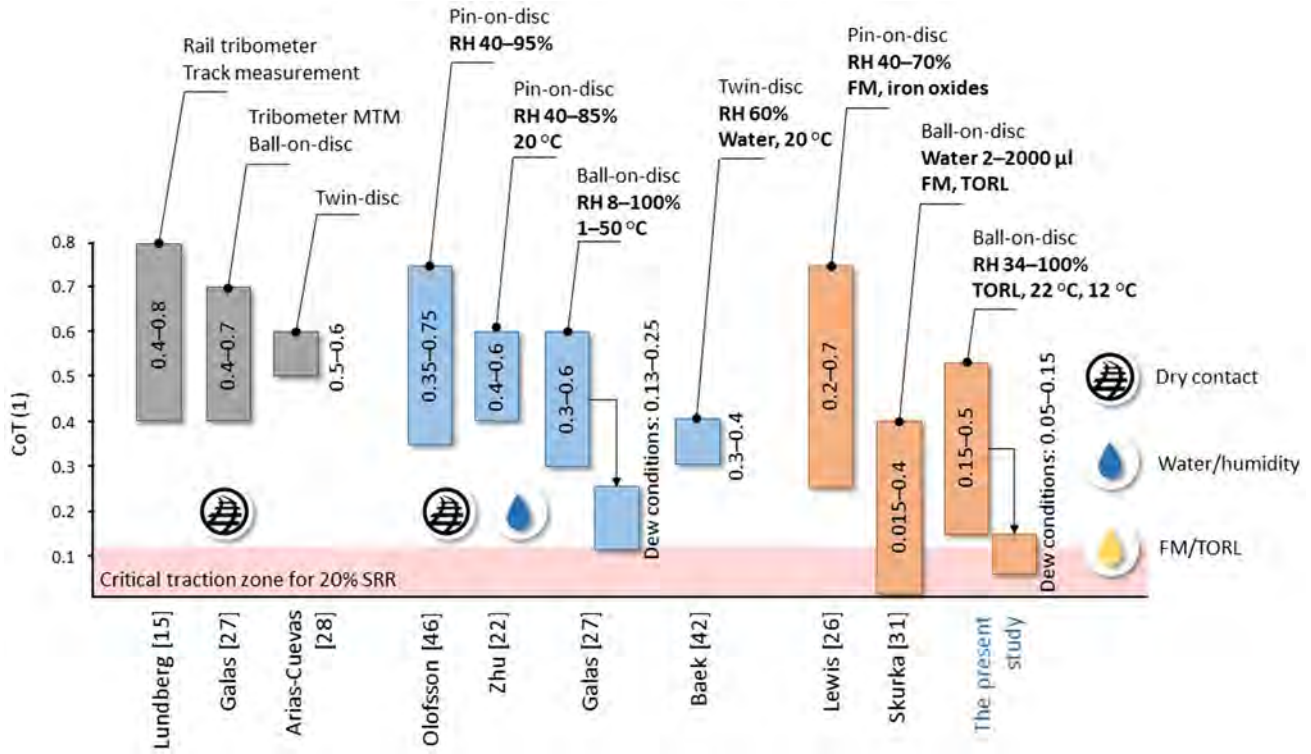

Fig. 8 The comparison of measured CoT/CoF under humid/water/dew conditions across different studies

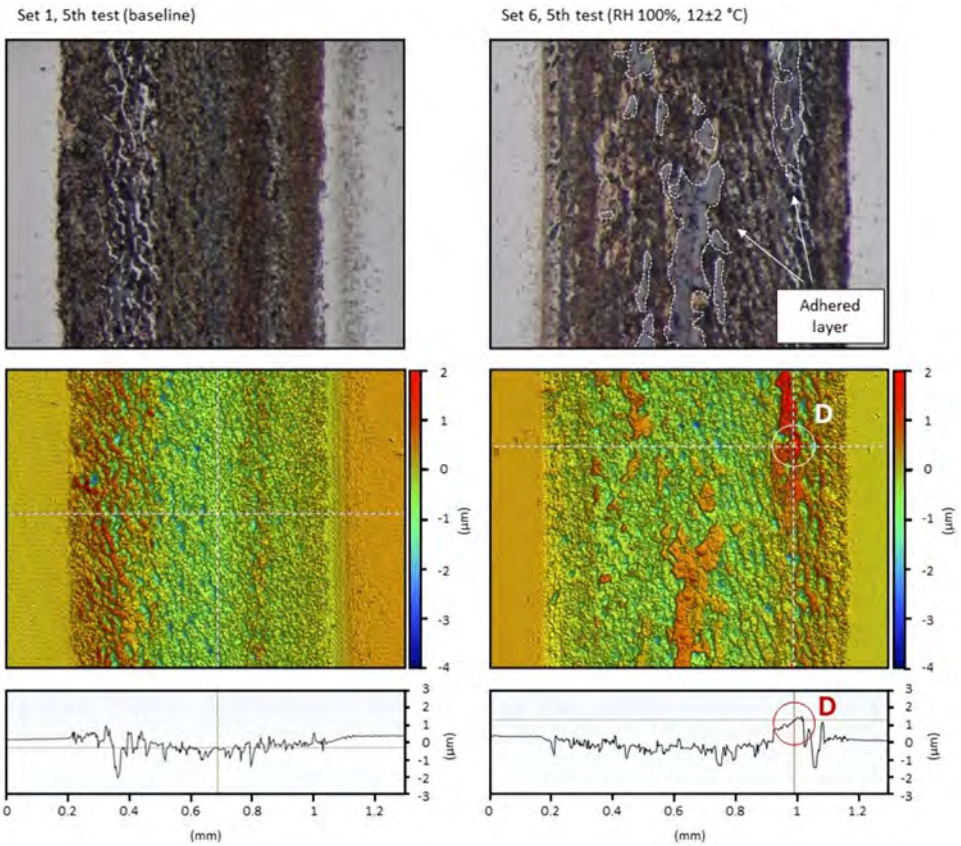

Fig. 9 The images of the contact path surface after the 5th test of Sets 1 and 6. The white dashed line highlights the thick adhered layer

small amount of water is mixed with particles and wear debris [25]. This follows the results of the presented study, where low adhesion problems occurred only under dew conditions, where water droplets on the specimen surfaces were eye-visible. As water–particle interaction plays a crucial role in low adhesion problems [25], the contact path surface was checked on an optical profiler after tests, during which low adhesion problems occurred. The images of the contact path after the last tests in Sets 1 and 6 can be seen in Fig. 9. These images show that at the end of Set 6, an eye-visible layer up to 2 µm thick has formed and covered part of the contact path. The highest amount of water was weighed during these tests, and its influence on "OLF" was the most significant.

On the contrary, at the end of Set 1, the contact path was covered by wear particles, but there was no sign of the "thick adhered layer" as in Set 6. The difference in the third body layer formed in those two Sets was that the wear particles (found in both Sets 1 and 6) could be easily removed by simply cleaning the surface with a paper towel and acetone. However, the thick layer found in Set 6 (and also other Sets where the dew conditions occurred) firmly adhered to the surface, and removing it requires increased effort (e.g. sandpaper, but it was tested that this layer was completely removed during the run-in process). This layer probably consists of iron oxides, which could explain low "OLF" scores in these tests, as the mixture of water and iron oxides is known for reducing CoT. This behaviour was previously observed in [43], where an adhered layer of Fe_2O_3 was mixed with condensed water and caused a stable period of low CoT. Several factors may influence the formation of the oxidic layer, and temperature is one of them. Based on numerical calculations computed in [33], the highest temperature in the contact should not exceed 95 °C (and the average temperature will be significantly lower), which does not seem very high at first glance. Still, the oxides can form under sliding conditions even at room temperature when metal surfaces are exposed to the air and in the absence of water, as these factors may alter/enhance the oxidation but are not the necessary conditions for oxides to be formed. As iron oxides are naturally present on the railhead, mixing them with TOR lubricants is inevitable. On the other hand, water seems more likely to pose a risk to TOR lubricants in terms of low adhesion, as these problems were observed only in tests where severe condensation occurred.

Unlike in the case of iron oxides, water contamination can be potentially avoided by carefully planned friction management, depending on weather conditions, and by avoiding applying TOR lubricant when dew is on the railhead in the morning. A possible benefit of contamination is that water prolonged retentivity, as in the tests where the highest quantities were present, the "*R*" parameter scored the highest values, which can help to extend the carry distance on the actual track.

When transferring results to the actual track, the drop of CoT is expected to be less significant for *W/R* contact (larger area compared to the one between specimens in the ball-on-disc configuration) and farther distances from the application unit (as every pass of the wheel remove TOR lubricant and redistribute it further). Even if a low CoT occurs, this should not pose a considerable risk to passengers' safety on a straight, long track where braking is not expected. However, this may be an issue on tram loops, where, after completing the ride, vehicles are parked one after another. There are reported cases from Brno, Czechia, in which vehicles experience braking problems on tram loops due to low adhesion, and collisions between vehicles often occur. As TOR product application units are commonly placed in front of these loops to reduce friction when the tram is driving into the curve, there is a real risk of TOR lubricants being contaminated by morning dew or rainwater, which may further worsen this issue. In the future continuation of this work, the focus should be on the actual track measurements in these loops.

3.4 Study Limitations

Regarding laboratory testing, measurements in humid conditions were previously performed in several studies. Shen [44] used a twin-disc device to measure CoT in the 5–99% RH range. Baek [42] tested 60% RH under different air temperatures. Zhu [22] also tested under different air temperatures but used a 40–95% RH, and Lyu [45] performed experiments under 40–85% RH. Next, Olofsson [46] tested two different levels of RH: 40% and 95%. Finally, Galas [27] conducted tests in the 8–100% RH range. In all these studies, higher humidity always led to a decrease in measured friction/CoT, supporting the validity of the presented results. Regarding testing conditions, 34 and 70% of RH used in this study fit into these ranges and represent normal and higher humidity conditions (e.g. in tunnels), and 100% RH was chosen to achieve dew conditions.

The most significant study limitation lies in simplified apparatus, as the ball-on-disc configuration leads to point contact rather than the elliptical, which is standard on the actual track. The measured CoT values are firmly dependent on the device and method of measurement [15]. Thus, adapting a universal benchmarking methodology and a commercial tribometer MTM with certified specimens is the most suitable option for laboratory CoT measurement to compare

results between different workplaces [33]. The MTM tribometer allowed precise control over test parameters in a wide range and was used in several studies focusing on W/R tribology before [29–31]. Although the transferability of laboratory results into actual W/R contact may be slightly challenging due to measuring configuration limitations, these measurements are useful in preliminary testing to identify the most reasonable conditions and parameters, as laboratory tests are fast and cost-effective. However, these results should be verified using a testing rig with more realistic geometry and conditions.

Together with measuring configuration, the most significant difference from the actual track conditions lies in the material of specimens. Specimens used in this study were made of AISI 52100 bearing steel with macrohardness of 820–920 and 720–780 HV for ball and disc, respectively. These values are significantly higher than those of typical rail materials. For example, one of the most common rail steel used in Europe is R260, with a bulk hardness around 275 HV, although there are also special heat-treated steels with bulk hardness as high as 350 HV [47]. It is also estimated that due to the work-hardening effect, the hardness close to the surfaces can be up to 2.5 times higher [48]. The AISI 52100 steel was chosen for two reasons. First, these specimens are provided directly by the tribometer manufacturer, enabling comparability of contact conditions across different workplaces. The second reason is that due to the higher hardness, the surfaces of the specimens were more resistant to wear, so topography changes of contact path groove were reduced, and relatively stable conditions could be maintained for all tests. However, it is necessary to remember that wear debris oxidises and forms a third body layer on the rail. Thus, less wear debris means the third body layer formed in these tests was less developed compared to field conditions. Furthermore, when interpreting results, it is essential to note that lower CoT values can usually be measured for specimens with higher hardness than those with lower hardness [12].

It is important to note that although the bearing steel experiences lower wear than the rail materials, it still occurs to some extent and influences contact conditions. The wear-in was always conducted on a new pair of specimens to create a stable contact path with an initial width of around 0.6 mm, which is sufficient for particles in TOR products to enter the contact, as their diameter typically ranges in tens of micrometres [29]. However, as the wear progresses, the contact path becomes wider. The width was measured at the end of the fifth test from each of the Sets 1–8, and the results (average from three values measured on different cross-sections of the disc) in order from the first to the eighth are as follows: 0.85 ± 0.01, 0.92 ± 0.02, 0.93 ± 0.02, 1.09 ± 0.08, 1.00 ± 0.02, 1.03 ± 0.06, 0.92 ± 0.01, and 1 ± 0.05 mm. The contact path's width increases with the experiment's length, although the increase is not proportional. This is probably caused by the fact that in the experiments with longer duration, the extra creep curves are measured in the areas of low CoT, in which a lower wear rate is also expected. However, the last couple of creep curves in each test have the most significant effect on wear as they reach higher values of CoT.

On the other hand, a larger contact area and more conformal contact results in a decrease in contact pressure. Evaluating the change in contact pressure is not an easy task, as during the assembly of specimens at the start of each test, specimens may be positioned slightly differently due to small clearances in the mounting mechanism. The contact is then realised on different radii in each test, which means that the size of the contact is not equal to the width of the contact path but is smaller. This is a limitation of the measuring device and means that the initial conditions for each of the five tests in the set will inevitably differ. However, from one perspective, this may be seen as beneficial because the final parameters are computed as an average and thus can be related to a broader range of conditions like on the actual track, where the ever-changing topography of surfaces also leads to a variety of contact conditions after each pass of the wheel.

In addition, the transfer mechanism of TOR lubricant under this configuration differs from the situation on the actual track. The contact is in a ball-on-disc configuration realised repeatedly on the same pair of points on both surfaces, and lubricant cannot easily leave the contact path, resulting in delayed starvation. On the railhead, TOR lubricant is spread at a longer distance [34]. Thus, after several dozen meters from the application unit, a significantly smaller amount of TOR lubricant is present, meaning that the effect on CoT will probably be less severe than in the MTM case. The recently published second part of the methodology [49] utilises a more realistic testing device, which incorporates a piece of actual rail, a scaled wheel and a hand-pushed tribometer. In this configuration, TOR products are tested in conditions close to the actual track, as the lubricant transfer mechanism is more realistic and the contact area is larger. The same TOR products were tested in both studies [33, 49]. Although the exact numerical values of CoT differed due to the different measuring methods and apparatus, strong correlations were found in the behaviour of the tested TOR products. Testing under contamination was not part of the study. However, the results imply that

a similar correlation may exist for testing under humidity/dew conditions, and these tests will be the next step in our future research.

4 Conclusion

This study investigated the influence of air humidity and dew on the performance of TOR lubricants. The universal methodology based on creep curve measurement was adapted to enable comparability of results across different workplaces. This methodology uses the coefficient of traction (CoT) and several performance parameters to evaluate the risk of low adhesion problems and the retentivity of TOR lubricants. Based on these parameters, TOR lubricants are assessed into four performance classes: Q1–Q4. The tribometer MTM in a ball-on-disc configuration was used for all measurements. The pot of the tribometer was covered with a climate chamber to control RH %. Tested TOR lubricants were exposed to three RH levels: laboratory ambient (34%), 70%, and 100%, simulating different situations on the track, e.g., morning dew, tunnels, etc. In some tests, specimens were precooled to create a temperature gradient and lower the dew point. The findings can be summarised as follows.

In tests with RH 70%, the effect of humidity on TOR lubricant was insignificant, as there was almost no water condensation. Although humidity influences friction in nonlubricated contacts, the effect is negligible compared to the effect of TOR lubricant. The cooling of specimens enhanced water condensation, resulting in worse product performance in terms of CoT. However, the product still performed sufficiently well, showing that TOR lubricants can be safely used in humid environments without significant risk of low adhesion problems.

A substantial effect was observed in tests under dew conditions. There is a clear relationship between the amount of water and its impact on performance. With the increase in water amount, the severity of low adhesion problems also increases, and lower values of CoT are measured. However, this behaviour is not linear, as a slight change in water amount causes a significant change for small amounts of water, but a substantial change in water amount causes only a slight difference for larger water amounts. This may be related to the fact that only a limited amount of water/lubricant can enter the contact area. The second TOR lubricant with a different composition was tested to confirm that this behaviour is not exclusive to the first product. The effect of dew was even more significant in this case, meaning that the resistance to contamination, besides others, depended on the product composition.

Results presented in this study imply that without significant water condensation, humidity has a less substantial effect on TOR lubricants. If the dew point is not reached, the low adhesion problems are more likely to occur due to the other impacts, e.g. contact over-dosing. However, when the dew point is reached and water condenses, it can significantly affect the performance of the TOR lubricant. This study showed that dew severely worsens the performance of tested TOR lubricants and, in some cases, can even cause low adhesion problems. These findings can be used to optimise friction management methods.

Appendix A

See Table 5.

Table 5 The limits of traction zones and the threshold curve

SRR (%)	0[a]	2	5	10	15	20
Dry contact CoT	0.008	0.361	0.605	0.724	0.769	0.773
CTZ upper limit CoT	0.001	0.060	0.101	0.121	0.128	0.128
ITZ lower limit CoT	0.002	0.120	0.202	0.241	0.256	0.256
ITZ upper limit[b] CoT	0.003	0.240	0.403	0.483	0.513	0.513

[a]Values for SRR 0% were not used in the evaluation

[b]ITZ Upper limit was also used as a threshold curve

Author contributions Simon Skurka: Conceptualization, Methodology, Investigation, Data curation, Writing—original draft. Radovan Galas: Conceptualization, Investigation, Methodology, Writing—review & editing. Milan Omasta: Conceptualization, Investigation, Methodology, Writing—review & editing, Project administration. Haohao Ding: Writing—review & editing. Wen-Jian Wang: Project administration. Ivan Krupka: Data curation, Writing—review & editing. Martin Hartl: Supervision, Funding acquisition.

Funding Open access publishing supported by the National Technical Library in Prague. This work was carried out in the framework of the project "Bozek Vehicle Engineering National Center of Competence" (TN02000054), which was co-financed from the state budget by the Technology Agency of the Czech Republic within the programme "National Centres of Competence". The work was also supported by the National Natural Science Foundation of China (No. 52320105007) and the 2024 Excellent Youth Team Training Program of Southwest Jiaotong University.

Declarations

Conflict of interests The authors declare that they have no known competing financial interests or personal relationships that could have appeared to influence the work reported in this paper.

References

1. Szablewski, D., LoPresti, J., Sultana, T.: Testing of latest top-of-rail friction modification materials at FAST. Railway Track and Struct. **111**, 13–16 (2015)
2. Wang, R.X., Zhou, K., Yang, J.Y., Ding, H.H., Wang, W.J., Guo, J., et al.: Effects of abrasive material and hardness of grinding wheel on rail grinding behaviors. Wear. pp 454–455 (2020). https://doi.org/10.1016/j.wear.2020.203332.
3. Niu, L., Yang, F., Deng, X., Zhang, P., Jing, G., Qiang, W., et al.: An assessment method of rail corrugation based on wheel–rail vertical force and its application for rail grinding. J. Civ. Struct. Health Monit. **13**, 1131–1150 (2023). https://doi.org/10.1007/s13349-023-00700-w
4. Krishna, V. V., Hossein-Nia, S., Casanueva, C., Stichel, S.: Long term rail surface damage considering maintenance interventions. Wear, pp 460–461 (2020). https://doi.org/10.1016/j.wear.2020.203462.
5. Han, J., He, Y., Xiao, X., Sheng, X., Zhao, G., Jin, X.: Effect of control measures on wheel/rail noise when the vehicle curves. Appl. Sci. **7**, 1144 (2017). https://doi.org/10.3390/app7111144
6. Meehan, P.A., Liu, X.: Wheel squeal noise control under water-based friction modifiers based on instantaneous rolling contact mechanics. Wear **440–441**, 203052 (2019). https://doi.org/10.1016/j.wear.2019.203052
7. Galas, R., Omasta, M., Klapka, M., Kaewunruen, S., Krupka, I., Hartl, M.: Case Study: the Influence of Oil-based Friction Modifier Quantity on Tram Braking Distance and Noise. Tribol. Ind. **39**, 198–206 (2017). https://doi.org/10.24874/ti.2017.39.02.06.
8. Ishizaka, K., Lewis, S.R., Lewis, R.: The low adhesion problem due to leaf contamination in the wheel/rail contact: bonding and low adhesion mechanisms. Wear **378–379**, 183–197 (2017). https://doi.org/10.1016/j.wear.2017.02.044
9. Kalousek, J., Johnson, K.L.: An Investigation of short pitch wheel and rail corrugations on the Vancouver mass transit system. Proc. Inst. Mech. Eng. F. J. Rail Rapid Transit. **206**, 127–135 (1992). https://doi.org/10.1243/PIME_PROC_1992_206_226_02
10. Stock, R., Stanlake, L., Hardwick, C., Yu, M., Eadie, D., Lewis, R.: Material concepts for top of rail friction management—classification, characterisation and application. Wear **366–367**, 225–232 (2016). https://doi.org/10.1016/j.wear.2016.05.028
11. Harmon, M., Lewis, R.: Review of top of rail friction modifier tribology. Tribol. Mater. Surf. Interfaces **10**, 150–162 (2016). https://doi.org/10.1080/17515831.2016.1216265
12. Harmon, M., Santa, J.F., Jaramillo, J.A., Toro, A., Beagles, A., Lewis, R.: Evaluation of the coefficient of friction of rail in the field and laboratory using several devices. Tribol. Mater. Surf. Interfaces **14**, 119–129 (2020). https://doi.org/10.1080/17515831.2020.1712111
13. Moreno-Ríos, M., Gallardo-Hernández, E.A., Vite-Torres, M., Peña-Bautista, A.: Field and laboratory assessments of the friction coefficient at a railhead. Proc. Inst. Mech. Eng. F J. Rail Rapid Transit. **230**, 313–320 (2016). https://doi.org/10.1177/0954409714536383
14. Areiza, Y.A., Garcés, S.I., Santa, J.F., Vargas, G., Toro, A.: Field measurement of coefficient of friction in rails using a hand-pushed tribometer. Tribol. Int. **82**, 274–279 (2015). https://doi.org/10.1016/j.triboint.2014.08.009
15. Lundberg, J., Rantatalo, M., Wanhainen, C., Casselgren, J.: Measurements of friction coefficients between rails lubricated with a friction modifier and the wheels of an IORE locomotive during real working conditions. Wear **324–325**, 109–117 (2015). https://doi.org/10.1016/j.wear.2014.12.002
16. Eadie, D.T., Elvidge, D., Oldknow, K., Stock, R., Pointner, P., Kalousek, J., et al.: The effects of top of rail friction modifier on wear and rolling contact fatigue: full-scale rail–wheel test rig evaluation, analysis and modelling. Wear **265**, 1222–1230 (2008). https://doi.org/10.1016/j.wear.2008.02.029
17. Galas, R., Omasta, M., Krupka, I., Hartl, M.: Laboratory investigation of ability of oil-based friction modifiers to control adhesion at wheel-rail interface. Wear **368–369**, 230–238 (2016). https://doi.org/10.1016/j.wear.2016.09.015
18. Abbasi, S., Olofsson, U., Zhu, Y., Sellgren, U.: Pin-on-disc study of the effects of railway friction modifiers on airborne wear particles from wheel–rail contacts. Tribol. Int. **60**, 136–139 (2013). https://doi.org/10.1016/j.triboint.2012.11.013
19. Olofsson, U., Lyu, Y.: Open system tribology in the wheel–rail contact—a literature review. Appl. Mech. Rev., 69 (2017). https://doi.org/10.1115/1.4038229.
20. Wang, W.J., Shen, P., Song, J.H., Guo, J., Liu, Q.Y., Jin, X.S.: Experimental study on adhesion behavior of wheel/rail under dry and water conditions. Wear **271**, 2699–2705 (2011). https://doi.org/10.1016/j.wear.2011.01.070
21. Gallardo-Hernandez, E.A., Lewis, R.: Twin disc assessment of wheel/rail adhesion. Wear **265**, 1309–1316 (2008). https://doi.org/10.1016/j.wear.2008.03.020
22. Zhu, Y., Lyu, Y., Olofsson, U.: Mapping the friction between railway wheels and rails focusing on environmental conditions. Wear

324–325, 122–128 (2015). https://doi.org/10.1016/j.wear.2014.12.028
23. Chen, H., Ban, T., Ishida, M., Nakahara, T.: Experimental investigation of influential factors on adhesion between wheel and rail under wet conditions. Wear **265**, 1504–1511 (2008). https://doi.org/10.1016/j.wear.2008.02.034
24. Kempka, R., Falconer, R., Gutsulyak, D., Lewis, R.: Effects of oxide and water on friction of rail steel–new test method and friction mapping. Tribol. Mater. Surf. Interfaces **15**, 80–91 (2021). https://doi.org/10.1080/17515831.2020.1765611
25. White, B., Lewis, R.: Simulation and understanding the wet-rail phenomenon using twin disc testing. Tribol. Int. **136**, 475–486 (2019). https://doi.org/10.1016/j.triboint.2019.03.067
26. Lewis, S.R., Lewis, R., Olofsson, U., Eadie, D.T., Cotter, J., Lu, X.: Effect of humidity, temperature and railhead contamination on the performance of friction modifiers: Pin-on-disk study. Proc. Inst. Mech. Eng. F J. Rail Rapid Transit. **227**, 115–127 (2013). https://doi.org/10.1177/0954409712452239
27. Galas, R., Omasta, M., Shi, L., Ding, H., Wang, W., Krupka, I, et al.: The low adhesion problem: the effect of environmental conditions on adhesion in rolling-sliding contact. Tribol. Int. **151**, 106521 (2020). https://doi.org/10.1016/j.triboint.2020.106521.
28. Arias-Cuevas, O., Li, Z., Lewis, R., Gallardo-Hernández, E.A.: Rolling–sliding laboratory tests of friction modifiers in dry and wet wheel–rail contacts. Wear **268**, 543–551 (2010). https://doi.org/10.1016/j.wear.2009.09.015
29. Kvarda, D., Skurka, S., Galas, R., Omasta, M., Shi, L., Ding, H., et al.: The effect of top of rail lubricant composition on adhesion and rheological behaviour. Eng. Sci. Technol. Int. J. **35**, 101100 (2022). https://doi.org/10.1016/j.jestch.2022.101100
30. Galas, R., Kvarda, D., Omasta, M., Krupka, I., Hartl, M.: The role of constituents contained in water–based friction modifiers for top–of–rail application. Tribol. Int. **117**, 87–97 (2018). https://doi.org/10.1016/j.triboint.2017.08.019
31. Skurka, S., Galas, R., Omasta, M., Wu, B., Ding, H., Wang, W.J., et al.: The performance of top-of-rail products under water contamination. Tribol. Int. 188 (2023). https://doi.org/10.1016/j.triboint.2023.108872.
32. Wang, W.J., Zhang, H.F., Wang, H.Y., Liu, Q.Y., Zhu, M.H.: Study on the adhesion behavior of wheel/rail under oil, water and sanding conditions. Wear **271**, 2693–2698 (2011). https://doi.org/10.1016/j.wear.2010.12.019
33. Galas, R., Skurka, S., Valena, M., Kvarda, D., Omasta, M., Ding, H., et al.: A benchmarking methodology for top-of-rail products. Tribol. Int. **189**, 108910 (2023). https://doi.org/10.1016/j.triboint.2023.108910
34. Valena, M., Omasta, M., Kvarda, D., Galas, R., Krupka, I., Hartl, M.: An approach for the creep-curve assessment using a new rail tribometer. Tribol. Int. 191 (2024). https://doi.org/10.1016/j.triboint.2023.109153.
35. Kimura, Y., Okada, K.: Lubricating properties of oil-in-water emulsions. Tribol. Trans. **32**, 524–532 (1989). https://doi.org/10.1080/10402008908981921
36. Fujita, N., Kimura, Y., Kobayashi, K., Amanuma, Y., Sodani, Y.: Estimation model of plate-out oil film in high-speed tandem cold rolling. J. Mater. Process. Technol. **219**, 295–302 (2015). https://doi.org/10.1016/j.jmatprotec.2015.01.002
37. Nakahara, T., Makino, T., Kyogoku, K.: Observations of Liquid Droplet Behavior and Oil Film Formation in O/W Type Emulsion Lubrication. J. Tribol. **110**, 348–353 (1988). https://doi.org/10.1115/1.3261630
38. Wilson, W.R.D., Sakaguchi, Y., Schmid, S.R.: A dynamic concentration model for lubrication with oil-in-water emulsions. Wear **161**, 207–212 (1993). https://doi.org/10.1016/0043-1648(93)90471-W
39. Cyriac, F., Lugt, P.M., Bosman, R.: Impact of water on the rheology of lubricating greases. Tribol. Trans. **59**, 679–689 (2016). https://doi.org/10.1080/10402004.2015.1107929
40. Cann, P.M.E., Damiens, B., Lubrecht, A.A.: The transition between fully flooded and starved regimes in EHL. Tribol. Int. **37**, 859–864 (2004). https://doi.org/10.1016/j.triboint.2004.05.005
41. Jacod, B., Pubilier, F., Cann, P.M., Lubrecht, A.A.: An analysis of track replenishment mechanisms in the starved regime. In: Dowson, D. et al (eds) Lubrication at the frontier, tribology series, 36,. Elsevier, Amsterdam, pp 483–492 (1999). https://doi.org/10.1016/S0167-8922(99)80069-8.
42. Baek, K.S., Kyogoku, K., Nakahara, T.: An experimental investigation of transient traction characteristics in rolling-sliding wheel/rail contacts under dry-wet conditions. Wear **263**, 169–179 (2007). https://doi.org/10.1016/j.wear.2007.01.067
43. Shi, L.B., Ma, L., Guo, J., Liu, Q.Y., Zhou, Z.R., Wang, W.J.: Influence of low temperature environment on the adhesion characteristics of wheel-rail contact. Tribol. Int. **127**, 59–68 (2018). https://doi.org/10.1016/j.triboint.2018.05.037
44. Shen, M., Li, J., Li, L., Li, S., Ma, C.: Adhesion and damage behaviour of wheel-rail rolling–sliding contact suffering intermittent airflow with different humidities and ambient temperatures. Tribol. Lett. **72**, 18 (2024). https://doi.org/10.1007/s11249-023-01817-1
45. Lyu, Y., Zhu, Y., Olofsson, U.: Wear between wheel and rail: a pin-on-disc study of environmental conditions and iron oxides. Wear **328–329**, 277–285 (2015). https://doi.org/10.1016/j.wear.2015.02.057
46. Olofsson, U., Sundvall, K.: Influence of leaf, humidity and applied lubrication on friction in the wheel-rail contact: pin-on-disc experiments. Proc. Inst. Mech. Eng. F J. Rail Rapid Transit. **218**, 235–242 (2004). https://doi.org/10.1243/0954409042389364
47. Lewis, R., Christoforou, P., Wang, W.J., Beagles, A., Burstow, M., Lewis, S.R.: Investigation of the influence of rail hardness on the wear of rail and wheel materials under dry conditions (ICRI wear mapping project). Wear **430–431**, 383–392 (2019). https://doi.org/10.1016/j.wear.2019.05.030
48. Tyfour, W.R., Beynon, J.H., Kapoor, A.: The steady state wear behaviour of pearlitic rail steel under dry rolling-sliding contact conditions. Wear. **180**, 79–89 (1995).
49. Galas, R., Valena, M., Jordan, T., Kvarda, D., Omasta, M., Skurka, S., et al.: A benchmarking methodology for top-of-rail products: Carry distance and retentivity. Tribol. Int. **197**, 109810 (2024). https://doi.org/10.1016/j.triboint.2024.109810

Authors and Affiliations

Simon Skurka[1] · Radovan Galas[1] · Milan Omasta[1] · Haohao Ding[2] · Wen-Jian Wang[2] · Ivan Krupka[1] · Martin Hartl[1]

✉ Simon Skurka
Simon.Skurka@vut.cz

[1] Faculty of Mechanical Engineering, Brno University of Technology, Technicka 2896/2, 616 69 Brno, Czech Republic

[2] State Key Laboratory of Rail Transit Vehicle System, Tribology Research Institute, Southwest Jiaotong University, Chengdu 610031, China

Wear 588 (2026) 206520

Contents lists available at ScienceDirect

Wear

journal homepage: www.elsevier.com/locate/wear

Performance of top-of-rail products under contaminated conditions with pre-existing cracks: Impacts on traction and surface damage

Simon Skurka [a,*], Radovan Galas [a], Jiaxin Li [b], Honghao Wang [b], Milan Omasta [a], Haohao Ding [b], Wenjian Wang [b], Ivan Krupka [a], Martin Hartl [a]

[a] Faculty of Mechanical Engineering, Brno University of Technology, Technicka 2896/2, 616 69, Brno, Czech Republic
[b] Tribology Research Institute, State Key Laboratory of Rail Transit Vehicle System, Southwest Jiaotong University, Chengdu, 610031, China

ARTICLE INFO

Keywords:
Friction modification
Rolling-contact fatigue
Wear
Low friction
Wheel-rail contact
Iron oxides
Water

ABSTRACT

Top-of-rail (TOR) products are used to optimise friction and reduce wear in the wheel–rail contact. However, their performance is affected by the presence of oxide layers naturally formed on the rail surface and by other environmental contaminants such as water. In this study, two types of TOR products (one friction modifier and one TOR lubricant) were tested under dry and wet conditions on both clean and oxidised specimens. In addition, some specimens were preconditioned to form pre-existing cracks, allowing a comparison between undamaged and damaged surfaces. The investigation focused on traction (CoT), wear rate, and rolling contact fatigue (RCF). The results showed that, with respect to CoT, water influenced the TOR lubricant much more than the friction modifier, as it extended its retentivity and led to extremely low friction levels (CoT down to 0.05). Both products effectively reduced wear and prevented crack initiation. However, when pre-existing cracks were present, the combination of water and the liquid base of TOR products accelerated crack propagation and caused severe spalling. Interestingly, oxidation also contributed to crack growth, as oxide formation inside the crack induced internal pressure that promoted secondary crack propagation.

1. Introduction

In railway operation, top-of-rail (TOR) products are applied to the wheel-rail (W/R) interface to mitigate the adverse effects of friction, such as increased fuel consumption [1], wear, and noise [2–7]. Generally, two types of TOR products are used: solid sticks pressed against the wheel [8] or liquid-based suspensions sprayed onto the railhead. Liquid TOR products can be divided into two main groups based on their base medium. The first group includes friction modifiers, which use water as the base, while the second group includes TOR lubricants, which use an oil or grease base [9]. The difference between these two types lies in their friction modification mechanisms, which result from their drying/non-drying nature. In friction modifiers (FMs), water acts as the transport medium, carrying solid lubricants along the rail. When it evaporates, it leaves behind a dry layer with low shear strength, typically composed of solid lubricants like graphite or molybdenum disulfide, which reduces friction [10]. On the contrary, due to their oil/grease base, TOR lubricants do not dry out. Instead, they form a thin lubricating film on the rail surface, providing boundary or mixed lubrication regimes [11].

Frictional conditions in the W/R contact are often described by the coefficient of traction (CoT), defined as the ratio of the traction force to the normal force. Several studies have assessed the effectiveness of TOR products in reducing wear and noise while maintaining sufficient CoT [12–17]. Recently, the possibility of using TOR products to mitigate rolling contact fatigue (RCF) was investigated. RCF is caused by the traction force, which induces minor plastic deformation that accumulates over time. Once the ductility of the material is exhausted, small cracks form in the deformed subsurface layer. These cracks then grow larger until a chunk of the material is removed from the surface, a process known as spalling [18]. Typically, there is competition between wear and RCF, as cracks are naturally removed due to wear [19,20]. In some cases, when wear rates are very high, RCF may not develop at all.

Some papers have reported the ability of TOR products to prevent crack formation, as they reduce CoT and thus the traction force, which results in a transition from plastic shakedown limit to the elastic region in the shakedown map [21–23]. However, a recent study by Hardwick et al. [24] reported results of tests where cracks already existed in the specimen surface before the TOR product was applied. The results showed that although FMs were effective, water and TOR lubricant

* Corresponding author.
E-mail address: Simon.Skurka@vut.cz (S. Skurka).

https://doi.org/10.1016/j.wear.2026.206520
Received 28 July 2025; Received in revised form 3 December 2025; Accepted 3 January 2026
Available online 5 January 2026

accelerated the growth of pre-existing cracks, causing massive surface delamination and material loss of up to 1740 % compared to dry conditions. Similar findings were also reported by Maya-Johnson et al. [25]. Hardwick et al. [24] identified that the varying effects of different TOR products on RCF and crack growth depend on whether the product is drying or non-drying. In the case of drying products (FMs), water evaporates quickly, leaving only dry particles on the surface. However, for non-drying products (TOR lubricants), the base medium may enter cracks and accelerate their growth due to fluid pressurisation and flank lubrication, as shown by Xavier et al. in their study [26]. The viscosity of the base medium significantly influences this effect, as TOR lubricants with low-viscosity oil have a much more substantial impact on crack growth than those based on high-viscosity grease. In addition, Seo et al. [27] investigated the effect of the liquid quantity. In their experiments, FM was not effective in preventing RCF, and interestingly, the most significant crack growth was observed in so-called "mixed conditions", referring to the situation when FM is almost dried out, so only a negligible amount of fluid is present. Then, the crack growth is enhanced due to the combination of the adverse effects of both dry friction (high CoT) and fluid-driven mechanisms of accelerated RCF.

Based on studies [21–24], applying FMs or high-viscosity TOR lubricants may seem an effective way to deal with wear and RCF, as FMs dry out and grease may struggle to penetrate cracks. However, the study by Seo et al. [27] challenges this, as it showed that RCF may develop under FMs, and the reason for this is the water contained in their composition. It is essential to note that the experiments in most of the studies are typically conducted under clean conditions, free from contaminants. On the actual track, water is often present (e.g. from rain or morning dew), as it is the most common contaminant [28]. Many studies experimentally confirmed the role of water as a lubricant in the W/R contact [29–33]. In addition, various numerical models were developed to describe the influence of specific parameters in water-contaminated contact. These studies have shown that surface roughness has a significant effect on CoT [34,35], together with water temperature [36–38], as it influences viscosity and thus film thickness [36]. Moreover, rolling speed plays a critical role, as at higher speeds, a thicker film forms, causing a transition to fluid film lubrication regime [39,40].

So, in water-contaminated contacts, it seems that TOR products will influence RCF differently than in dry conditions, as water has a significant effect on their performance [41,42]. However, it is not clear to what extent. Moreover, the state of the wheel and rail surfaces will also play a significant role, as they are naturally subject to oxidation. As the surfaces oxidise, the upper layer turns to a layer of iron oxides with lower shear strength than steel [43]. The crack growth, geometry and capillary forces between the crack face and entrapped liquid will differ in the oxidised layer compared to the conditions tested before, as previous studies usually used clean and non-oxidised specimens. The need for research on how iron oxides and water, combined with TOR products, affect wear has been highlighted in a study by Zhu et al. [43].

So, in the present study, the effectiveness of two commercial TOR products on reducing wear, RCF and their ability to maintain intermediate CoT was tested. A drying FM and a high-viscosity TOR lubricant (NLGI 0) were selected to address the problems discussed in this chapter. The novelty lies in the special attention paid to how water contamination and oxide layer will impact the performance of TOR products. Tests were conducted on both oxidised and non-oxidised specimens under dry and wet conditions. Additionally, specimens with and without pre-existing cracks were used to evaluate the ability of these products to prevent crack formation. This study addresses whether TOR products can maintain sufficient CoT and effectively mitigate wear and RCF in contact with oxidised surfaces and water contamination, simulating near-field conditions in a laboratory environment.

2. Material and methods

2.1. Experimental setup

All tests were conducted on a twin-disc machine (MJP-30A, Southwest Jiaotong University) capable of simulating rolling-sliding contact under various conditions. In this setup, the rail disc (mounted on an upper shaft) and wheel disc (mounted on a lower shaft) are driven by separate servo motors, allowing different percentages of slip to be set by varying the speed of both motors, see Fig. 1. The final slip (λ) value in % is a result of the wheel disc running faster than the rail disc and can be

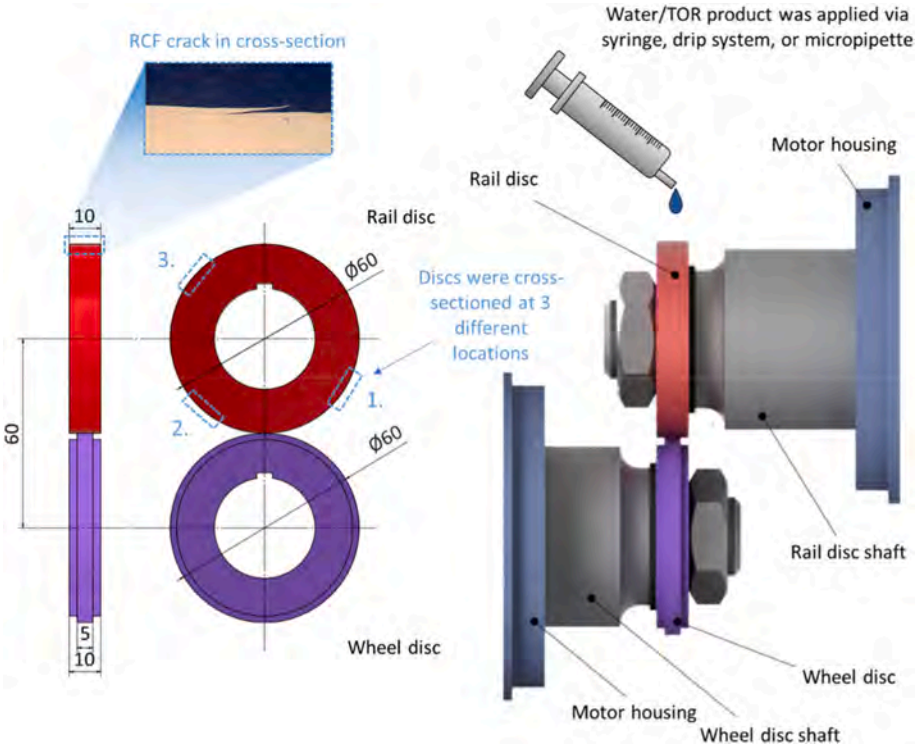

Fig. 1. Specimens dimensions and the MJP-30A twin-disc machine setup.

calculated as follows:

$$\lambda = \frac{w_{wheel} \cdot r_{wheel} - w_{rail} \cdot r_{rail}}{w_{wheel} \cdot r_{wheel}} \cdot 100\% \quad (1)$$

where w_{wheel} and w_{rail} are angular speeds (r/min) of discs and r_{wheel} and r_{rail} are their radii (mm). Both discs were loaded against each other by a hydraulic loading system. The frictional conditions were quantified in terms of CoT, which can be calculated as follows:

$$CoT = \frac{M_{wheel}}{r_{wheel} \cdot F_N} \quad (2)$$

where M_{wheel} is the torque (N · m) measured on the wheel shaft, r_{wheel} is the wheel disc radius (mm) and F_N stands for the normal force measured by the attached load sensor. The control of all test parameters and data acquisition was performed by the desktop computer connected to the machine.

The MJP-30A enables testing in various conditions typical for W/R contact. In this study, a Hertz contact pressure of 1.1 GPa (exerted by a normal force of 2500 N) was chosen for all experiments, as it falls within the typical range of contact pressures between the wheel tread and the top of the rail. The mean speed of 1.5 m/s (corresponding to a rotational speed of 500 RPM) was set. To achieve 2 % slip (a value from the effective part of the creep curve near the saturation point), the wheel disc rotates slightly faster and the rail disc slightly slower, resulting in the desired slip value. This study carried out two types of tests: "friction tests" and "wear and RCF tests". The friction tests focus on evaluating the influence on the CoT, whereas in the wear and RCF tests, metallographic samples will be prepared to investigate the effects on surface damage and crack propagation. Further details will be provided later in the paper.

2.2. Tested TOR products, contaminants and specimens

One FM and one TOR lubricant were selected for testing to examine both drying and non-drying types of TOR products. The manufacturers do not provide information about the composition of these products. However, the datasheets for the TOR lubricant indicate that the base is a biodegradable ester oil with a viscosity between 41 and 53 mm^2/s at 40 °C. It also contains an organic thickener and particles of soft metals and their compounds. The NLGI grade for this product is "0". The suitable application quantity for a downscaled twin-disc machine differs from field recommendations. Therefore, preliminary friction tests were conducted to examine the effects of varying application quantities in down-scaled contact. As detailed in the Results chapter, suitable quantities were chosen for each product based on their performance: 20 μl for FM and 10 μl for the TOR lubricant (see Fig. 3).

Water was applied to the contact in two different ways. In the "friction test" (where CoT was recorded as a function of the number of cycles), water was applied using a pipette (error ± 0.04 μl) in the following quantities: 30 μl, 120 μl and 480 μl. In the case of "wear and RCF tests", water was applied continuously from a drip system hung above the testing machine via a needle at the rate of one drop per second. The number of cycles during which water was fed to the contact is specified in Table 3.

In "wear and RCF tests", the influence of an oxide layer was investigated. In these tests, specimens were first run-in for 5000 dry cycles to form pre-existing cracks. After that, the oxidation process was carried out as follows: after the initial run-in, the discs were placed in a chamber preheated at 60 °C for 24 h, during which vapours from a solution of water, ethanol, and magnesium dichloride induced oxidation. Then, the discs were weighed to quantify the amount of oxide, and the tests were carried out. Please note that the mass of the resulting iron oxide includes both the mass of the original metal and the mass of the oxygen that has been added. X-ray diffraction (XRD) analysis showed that the oxide layer was composed primarily of magnetite, hematite, goethite, and akaganeite.

Regarding the specimens, both wheel and rail discs were cut from the actual wheel and rail, respectively. In the case of wheel discs, the material was C-class steel with a hardness of 388 ± 9 $HV_{0.5}$. Rail discs were made of U71Mn steel with a hardness of 290 $HV_{0.5}$. The detailed chemical composition of both materials is given in Table 1. Furthermore, both discs had the same diameter of 60 mm, and the width of the contact path was 5 mm (linear contact), see Fig. 1.

2.3. Test methodology

2.3.1. Friction tests

First, preliminary friction tests were performed without contaminants to select a suitable quantity of FM and TOR lubricant, as the manufacturer's recommendation for field application may not be ideal for the downscaled linear contact in the used apparatus. Both TOR products were applied using an electronic micropipette (error ± 0.04 μl) in the following amounts: 5 μl, 10 μl, 20 μl, and 30 μl for FM, and 5 μl, 10 μl, and 15 μl for TOR lubricant. All details are summarised in Table 2. Furthermore, the chosen quantity was tested three times to check repeatability. A model friction test is depicted in Fig. 2 a). The criterion for selecting the optimal amount was that the products provide intermediate CoT levels (green zone) for a reasonable time and do not cause low CoT (red zone).

The CoT levels were defined as follows: according to the benchmarking methodology for TOR products [44], the intermediate CoT level, where wear is reduced, but CoT is still sufficient for traction/-braking, is defined between 1/3 and 2/3 of dry contact CoT. Typical CoT values for dry contact measured on the MJP-30A are between 0.4 and 0.5 [45]. Thus, the intermediate CoT level was defined between 0.15 and 0.3 (1/3 and 2/3 from 0.45 – the middle interval value where CoT stabilises for the dry contact). The value of 0.4, the minimum boundary of the dry contact CoT interval, was considered the threshold at which the product no longer had any significant effect. The test was stopped when this value was reached.

Furthermore, CoT lower than 1/6 of dry contact CoT is considered low [44], leading to a value of approx. 0.075 under these conditions. Moreover, Ishizaka et al. [46] state that a CoT higher than 0.09 is usually required for effective braking. However, they don't specify for which slip % this CoT value is relevant. Thus, this study defined a low CoT level for values lower than 0.1, similar to the previous study [42], to stay conservative on the low CoT definition. Regarding the above-stated intervals for CoT levels, the well-performing TOR product maintains CoT in the 0.15–0.3 interval for as long as possible (marked as "effective retentivity" in Fig. 2 a) and never causes a drop below 0.1. Friction tests are categorised into two groups based on the presence of oxides, see Table 2.

In tests conducted under wet conditions, water was always applied before the TOR products. Preliminary experiments showed that reversing the order led to inconsistent wetting. When the TOR product, particularly the TOR lubricant, was applied first, it spread across the surface and formed a continuous film due to its strong wetting ability. As

Table 1
Chemical composition of specimen materials (wt.%).

Disc	Steel	C	Si	Mn	P	S
Wheel	C-class	0.67–0.77	0.15–1.00	0.60–0.90	0.030	0.005–0.040
Rail	U71Mn	0.65–0.75	0.10–0.50	0.80–1.30	≤0.025	≤0.025

Table 2
The parameters and conditions of friction tests.

	TOR product; quantity (μl)	Water quantity (μl)	Run-in	Test duration	Slip; speed; pressure	Fig. #
No oxides	–	–	–	500 cycles	2 %; 1.5 m/s; 1.1 GPa	3 a)
	–	30, 120, 480	To stable CoT 0.4–0.5	CoT reached 0.4		3 b–d)
	FM; 20[1)]	–				3 i)
	TOR lubricant; 10[2)]	–				3 l)
	FM; 20	30, 120, 480				3 j)
	TOR lubricant; 10	30, 120, 480				3 m)
With oxides	–	–	–	500 cycles	2 %; 1.5 m/s; 1.1 GPa	3 e)
	–	30, 120, 480	To stable CoT 0.4–0.5[3)]	CoT reached 0.4		3 f–h)
	FM; 20	30, 120, 480				3 k)
	TOR lubricant; 10	30, 120, 480				3 n)

[1] The FM was tested in the following quantities: 5 μl, 10 μl, 15 μl and 20 μl, from which 20 μl was chosen for further testing as it provided the optimal results.
[2] The TOR lubricant was tested in the following quantities: 5 μl, 10 μl and 15 μl, from which 10 μl was chosen for further testing as it provided the optimal results.
[3] The run-in was conducted before the creation of the oxide layer.

Table 3
The testing parameters and conditions of wear and RCF tests.

	Labeled as	TOR product; quantity (μl)	The TOR product is applied when	Water	Pre-existing cracks	Test duration (cycles)	Slip; speed; pressure	Fig. #
No oxides With pre-existing cracks	Test 1	–	–	–	No cracks were present at the time of application	5000	2 %; 1.5 m/s; 1.1 GPa	4 a)
	Test 2	–	–	–		25 000		4 b)
	Test 3	FM; 20	CoT = 0.3	–		25 000		4 c)
	Test 4	TOR lubricant; 10	CoT = 0.3	–		25 000		4 d)
	Test 5	–	–	1 drop/s		25 000		4 e)
	Test 6	FM; 20	CoT = 0.3	–	Run-ins were conducted to form pre-existing cracks	20 000 (+5000 cycles dry run-in)		4 f)
	Test 7	TOR lubricant; 10	CoT = 0.3	–				4 g)
	Test 8	–	–	1 drop/s				4 h)
	Test 9	FM; 20	Every 600 cycles[1)]	1 drop/s				4 i)
	Test 10	TOR lubricant; 10	Every 2200 cycles[2)]	1 drop/s				4 j)
With oxides	Test 11	FM; 20	Every 600 cycles[1)]	1 drop/s	Run-ins were conducted to form pre-existing cracks	20 000 (+5000 cycles dry run-in)		9 a)
	Test 12	TOR lubricant; 10	Every 2200 cycles[2)]					9 b)
	Test 13	–	–					9 c)

[1] FM was applied once every 600 cycles to match the total amount used in the test without water contamination, see 4 c).
[2] TOR lubricant was applied once every 2200 cycles to match the total amount used in the test without water contamination, see 4 d).

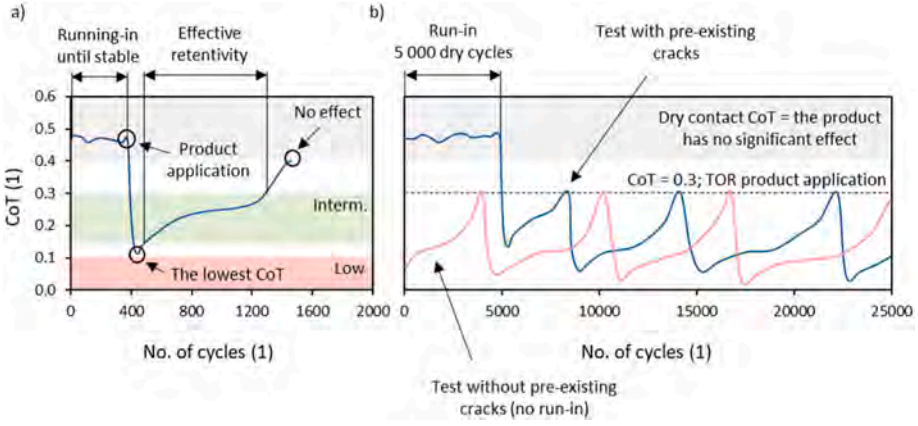

Fig. 2. a) The "optimal" TOR product performance and b) the wear and RCF tests procedure.

a result, the subsequently applied water could not reach the contact because it slid over the lubricant film and ran off the disc surfaces.

2.3.2. Wear and RCF tests

Parameters of wear and RCF tests are summarised in Table 3, with each test labeled as Test 1–13. The fundamental categorisation of the tests is based on the presence/absence of a pre-prepared oxide layer (as was described in Subchapter 2.2). Furthermore, 5000 cycles of dry run-in were conducted in tests 6–13 to create pre-existing cracks, so the ability of TOR products to prevent their formation could be evaluated by comparing tests with and without run-ins. Then, the test started, and depending on the type of the test, the water/TOR product was added

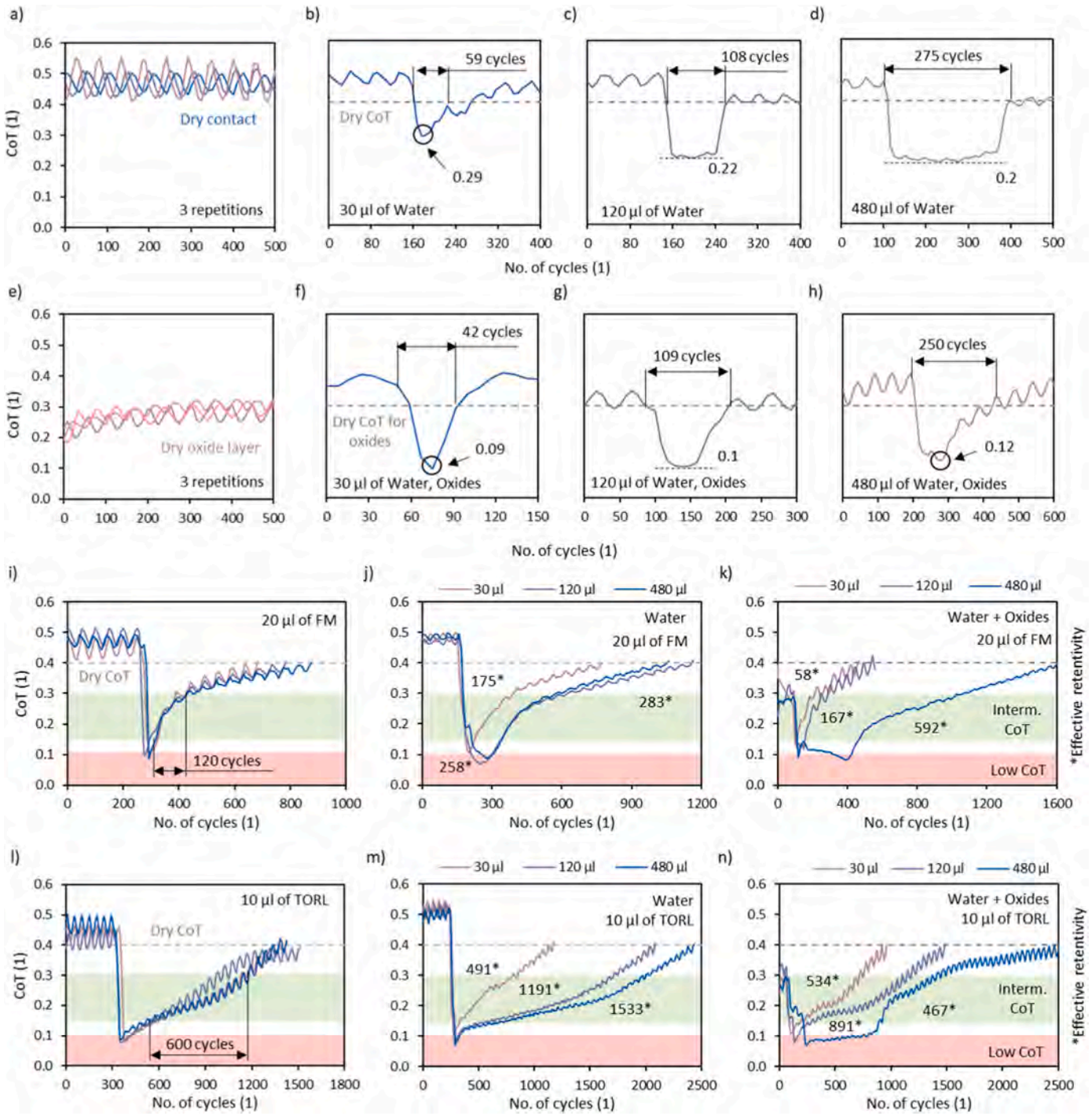

Fig. 3. a) Dry contact CoT, b–d) Different quantities of water on clean discs, e) Dry oxide layer CoT, f–h) Different amounts of water on oxidised discs, i–k) Tests with FM under various conditions, l–n) Tests with TOR lubricant under different conditions.

either from the beginning or after the initial run-in. TOR products were applied each time CoT reached the value of 0.3, an upper boundary of the intermediate traction level, see Fig. 2 b). Contrary to friction tests, water was continuously added from a drip system at a rate of 1 drop/s. All test parameters, applied quantity, etc., are summarised in Tab. 3.

In wear and RCF tests, the discs were weighed before and after testing to determine the total mass loss. The wear rate was calculated as the average mass loss normalised per 1 m sliding distance. After the test, discs were sectioned at three different locations (see Fig. 1), and polished samples were observed via optical (OM) and electron (SEM) microscopes for cracks and other surface damage. Furthermore, energy-dispersive spectroscopy (EDS) was used to analyse whether FM and TOR lubricant can enter the cracks.

In the preliminary phase of the study, several friction tests and selected wear and RCF tests were repeated to check the consistency of the procedure. However, full repetition of all wear and RCF tests was not conducted, as each experiment required destructive sectioning of the discs for metallographic analysis. Given the large number of test conditions investigated, repeating every case would have required preparing a proportionally large number of additional wheel and rail specimens, since each disc could be used for only a single test. The authors acknowledge that for future research, a more narrowly focused

study design with a higher number of repetitions would be preferable.

3. Results

3.1. Results of friction tests

The results of tests with water without the TOR product are depicted in Fig. 3b–d). It can be seen that with an increase in water amount, the CoT decreases to lower values and the recovery time to dry values of CoT is prolonged. Next, the same tests with water were repeated on specimens with an oxide layer, see Fig. 3f–h). Compared to tests with clean specimens, CoT has now decreased to lower values. However, it can be attributed to the fact that while the CoT for clean specimens stabilises above 0.4, the corresponding value for specimens with an oxide layer is 0.3, see Fig. 3 a) and e). Therefore, the higher decrease in CoT is probably caused by lower initial values, which is also supported by the fact that the drop duration was similar for both types of tests.

In the next step, TOR products in different quantities were tested to choose the optimal dosage. The following quantities were tested: 5 μl, 10 μl, 20 μl, and 30 μl for FM, and 10 μl, 15 μl, and 20 μl for the TOR lubricant. For the FM, 20 μl was selected, as lower quantities did not provide a sufficient duration of effective retentivity. However, increasing the quantity beyond 20 μl did not bring any benefits. After application, the CoT briefly dropped to 0.08 as the liquid phase flooded the contact, temporarily separating the surfaces with a thin fluid film. Still, after a few cycles, the CoT rose to the desired levels. The duration of effective retentivity was approximately 120 cycles. Please note that the "duration of effective retentivity" refers to the number of cycles for which the value of CoT belonged to the intermediate interval, see Fig. 2 a). This test was repeated three times to check the repeatability, see Fig. 3 i).

Subsequently, the same amount was tested on clean and oxidised specimens under wet conditions, see Fig. 3 j) and k). Water was applied first to wet the surfaces, simulating wet rail conditions. The application of FM followed immediately. On clean specimens, the duration of the initial drop and the effective retentivity of the FM increased with the increase in applied water amounts. The situation was less clear with oxides, as their presence sometimes led to prolonged retentivity and sometimes had the opposite effect. The most significant impact was seen on oxidised specimens when 480 μl of water was applied, resulting in a drop lasting several hundred cycles. However, after the evaporation of water, the product behaved similarly to the case where the FM was applied under dry conditions. In this context, "performed similarly" refers to the stage that typically occurs near the upper boundary of the Intermediate CoT zone. Once most of the water has evaporated, the contact gradually transitions toward dry conditions but still contains residual solid lubricants originating from the FM. Beyond this point, the behaviour corresponds to dry contact with a thin layer of solid lubricants, influencing the friction level. This trend was consistent across most tests, except for those with oxide contamination and the test with 480 μl of water, where the surface may have remained partially wetted and the presence of oxides may have affected the contact mechanics, resulting in longer retentivity of the FM.

The same tests were conducted for the TOR lubricant. Following the same criteria, the quantity of 10 μl was assessed as optimal. TOR lubricants are known to cause over-lubrication when applied in excessive amounts. In the context of this paper, the term over-lubrication refers to a condition in which the CoT falls below the intended range. As TOR products are designed to provide an intermediate level of friction (low enough to reduce wear and noise, yet high enough to maintain effective traction and braking), this condition is undesirable. Although over-lubrication did not occur with any tested quantity, it is expected that in wear and RCF tests, where TOR lubricant is applied repeatedly, TOR lubricant would accumulate over time, preventing CoT recovery if a higher quantity were selected.

Under wet conditions, the lasting effect was significantly prolonged, see Fig. 3 m). The water has a substantially more pronounced impact on the TOR lubricant than on FM. For clean discs, the TOR lubricant follows the same trend as FM, and with an increase in water amount, effective retentivity also increases. This is not the case when oxides are present – while the CoT recovery took longer under 480 μl of water, the effective retentivity was the longest under 120 μl. It seems that the influence of oxide layers on TOR products cannot be generalised as purely increasing or decreasing CoT, as it depends on several factors such as oxide type, hardness and layer thickness. A possible explanation for the irregular behaviour observed in the case where 120 μl of water resulted in the longer effective retentivity than 480 μl is that oxide layers have low shear strength, and they break down in a non-uniform way during rolling–sliding. As a result, local cracking and flaking may disturb or partially remove the TOR lubricant film and change the contact conditions. This may explain why the expected trend of increasing effective retentivity with increasing water amount was not observed and why some CoT curves show unexpected shapes or sudden changes.

3.2. Results of wear and RCF tests: No oxides

First, tests 1 and 2 under dry conditions were conducted: the first for 5000 cycles to check the formation of pre-existing cracks after the run-ins and the second for 25 000 cycles for comparison with tests with water/TOR products. In these tests, the CoT stabilised in the 0.4–0.5 interval after the initial 2500 cycles, see Fig. 4 a) and b).

Tests 3–5 were conducted without any run-ins, so the water/TOR product was applied right from the beginning. Thus, no major cracks were present on the surface at the moment of application. While FM and TOR lubricant were applied each time the CoT reached 0.3 (resulting in 36 and 10 applications for FM and TOR lubricant, respectively), water was applied continuously with a rate of 1 drop/s, see Fig. 4c–e). Each application of the TOR product led to a similar CoT curve. Both TOR products were able to provide values from the intermediate CoT level throughout the test, which was achieved with a total amount over 7 times lower for TOR lubricant than for FM. Water maintained stable CoT values between 0.1 and 0.2, see Fig. 4 e). Although those values are not considered optimal, they are still above the low CoT level.

From the friction perspective, there was no significant difference in the performance of TOR products in tests without (3 and 4) and with pre-existing cracks (6 and 7), see Fig. 4 f) and g). However, when comparing tests with water (5 and 8), there is a clear difference in frictional behaviour, see Fig. 4 e) and h). In the first 5000 cycles of water application, CoT in test 8 had a similar development to that in test 5. But then, CoT gradually rose and became less stable, almost reaching dry contact values at the end of the test. A similar phenomenon, although to a limited extent, was also observed in test 9, where FM was applied together with water, see Fig. 4 i). As it was limited to tests where water and pre-existing cracks were present, it is most likely a result of RCF, which will be discussed later. This behaviour was not observed in test 10 with TOR lubricant and water, see Fig. 4 j). Under wet conditions, neither of the TOR products could maintain intermediate CoT. The combination of water and TOR product caused over-lubrication, and CoT values dropped below 0.1.

For the wear analysis, specimens were weighed before and after each test to evaluate the mass loss of the wheel disc and rail disc separately. The "total system" represents the combined mass loss of both discs. Fig. 5 a) shows mass loss of discs after tests 1–10 (no oxides). The chart is divided into two parts: tests without pre-existing cracks (1–5) and tests where an initial 5000 dry cycles were conducted before the water/TOR application to form pre-existing cracks. Fig. 5 b) is divided into two parts in the same way as Fig. 5 a) and displays information about wear rate, which was calculated as total system mass loss per 1 m of sliding distance. Please note that, in tests with pre-existing cracks, the initial 5000 dry cycles were excluded from the evaluation, so the number represents only the part of the test under lubricated conditions.

Fig. 5 a) shows that under dry conditions, the mass loss of the wheel

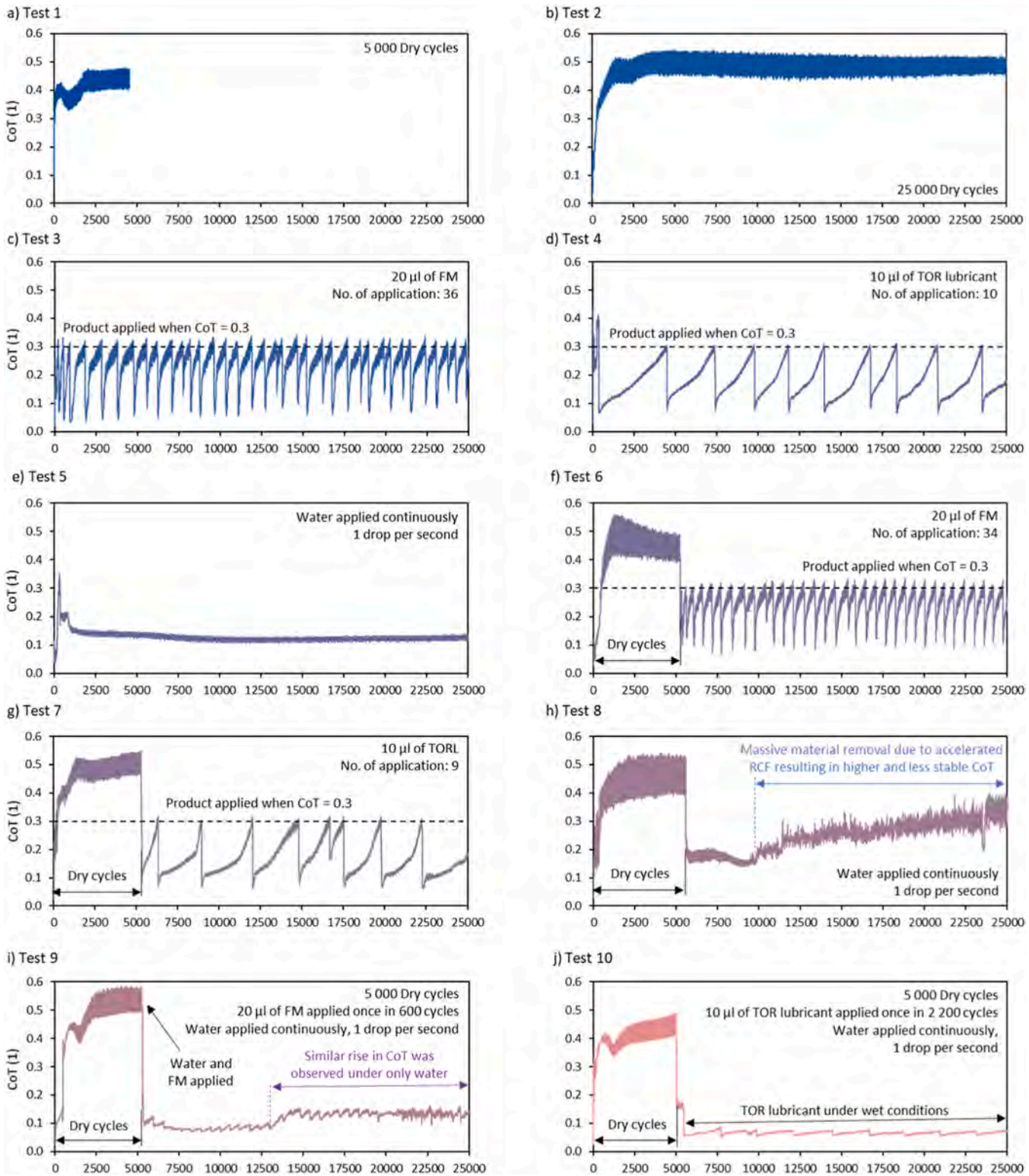

Fig. 4. Friction data for wear and RCF tests: No oxides. Tests 1–5 (a–e) were conducted without run-ins. Tests 6–10 (f–j) are with pre-existing cracks. No oxides.

disc is higher than that of the rail discs (tests 1 and 2), but the opposite was true in the rest of the tests. Both TOR products effectively reduce wear, as the total system mass loss decreased 10 times when using FM and 35 times when using the TOR lubricant. In a direct comparison of both products, the TOR lubricant proved to be more than three times as effective as FM in reducing wear. Water achieved similar wear reduction as TOR lubricant, resulting from maintaining low and stable CoT throughout the test and, thus, lower adhesive wear.

The situation changed significantly in tests with pre-existing cracks. The increase in mass loss was observed in all cases, although it is essential to point out that TOR products, when applied to dry surfaces, still provided wear reduction to some extent. Wear rate, calculated as total system mass loss normalised per 1 m of sliding distance, is a better indicator of changes in wear intensity in tests 6–10, as it excludes wear

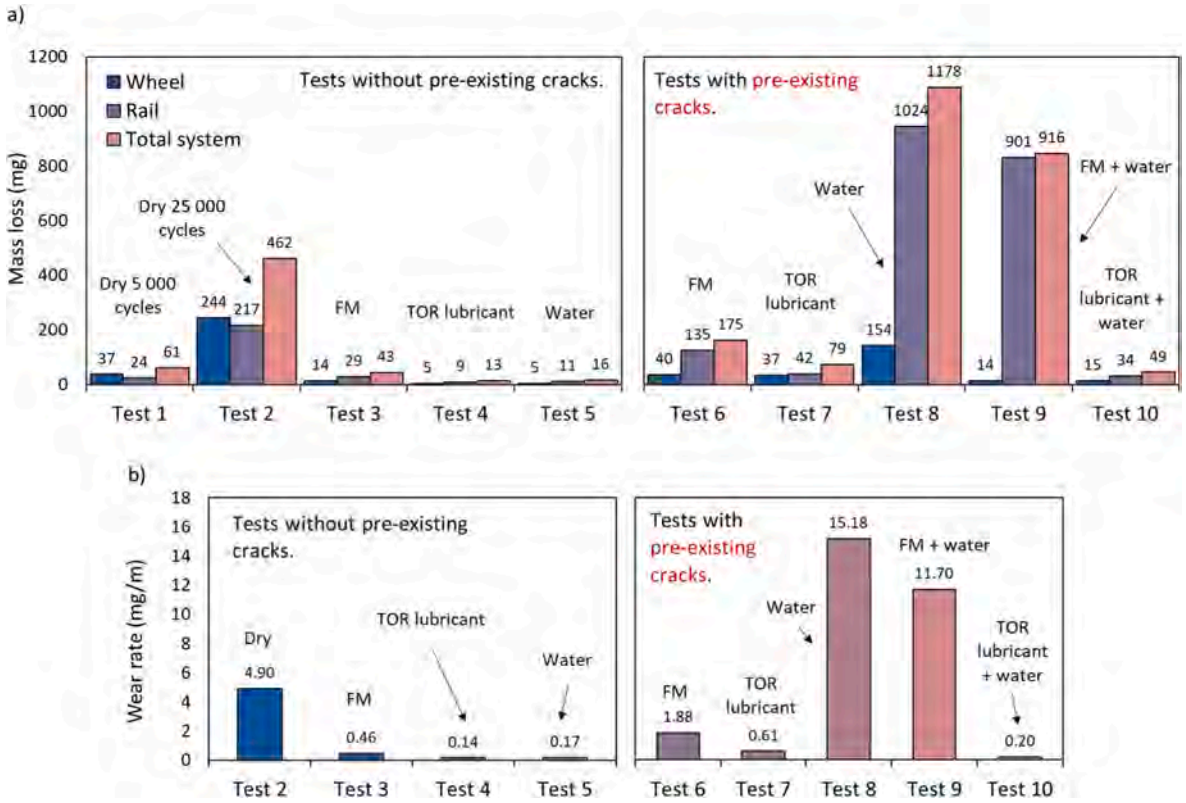

Fig. 5. a) Mass loss of wheel disc, rail disc and total system. Part b) shows the total system wear rate in mg per 1 m of sliding distance (run-ins were excluded from the evaluation). No oxides.

during the first 5000 dry cycles, see Fig. 5 b). The presence of pre-existing cracks and water resulted in an 89 times increase between tests 5 and 8.

Furthermore, the wear rate in test 8 was three times higher than in dry tests without lubrication (test 2). An increased wear rate was also observed in test 9, where FM was applied together with water. Although it was lower than in test 8, it remained more than six times higher than when FM was used alone (test 6) and more than twice the wear rate under dry conditions. On the contrary, the effect of water was less pronounced in test 10, where TOR lubricant was used, suggesting that wet conditions influence TOR products differently depending on their base medium type.

After mass loss/wear rate evaluation, surfaces were observed under an optical microscope, see Fig. 6. OM analysis showed signs of minor spalling in tests 3 and 4 but no visible cracks, meaning that both TOR products were more or less effective in preventing crack initiation. However, surfaces in tests with pre-existing cracks exhibited severe spalling and extensive cracking, with the most pronounced damage observed in tests 8, 9, and 10, where water was present.

As the wear and RCF were more severe for the rail discs (see Fig. 5), and the wheel discs often showed no noticeable cracks, the following crack analysis will focus only on the rail discs, which are of greater interest. After 5000 and 25 000 dry cycles, the surfaces showed signs of adhesive wear and minor spalling (see Fig. 6, tests 1 and 2). The black areas represent material peeled off the original surface and then adhered to a different location. As shown in Fig. 7), the median length and depth of cracks were similar in these tests, suggesting that 5000 cycles of running-in are sufficient to create pre-existing cracks. Fig. 8 a) shows that cracks run parallel to the surface, entering at an average angle of around 10°.

The cracks observed in tests 4 and 5, where water and TOR lubricant were used, were very short and shallow and ran under an average angle of around 12°. Only a few turned towards the bulk under a steep 25–50° angle. In contrast, the cracks in test 3 with FM ran under a much smaller angle of 6° and were similar in size to those observed under dry conditions.

Regarding tests with TOR products and pre-existing cracks (Fig. 8b and c), the final length and depth of cracks were somewhat similar to tests without pre-existing cracks. However, there was a substantial difference when TOR products were applied in wet conditions (Fig. 8e–h), as the length of the cracks in test 10 was, on average, almost 58 times longer than in test 4, and their depth increased 94 times. There was an even more significant change in the case of water alone, where cracks in test 8 were, on average, more than 200 times longer and more than 150 times deeper than in test 5. Numerous cracks were found running above one another, causing extensive material peeling. These cracks entered the surface at a shallow angle at first, similar to earlier tests, but then turned towards the bulk and propagated at a much steeper angle, reaching depths of nearly 600 μm, see Fig. 8 d).

Fig. 8 presents SEM images of typical cracks observed in cross-sections from tests 6–10. In tests where water was present (8–10), the cracks propagated deep into the bulk material, exhibiting branching and coalescence. In contrast, in tests 6 and 7, the cracks remained shallow. So, water was able to enter cracks and played a crucial role in crack propagation. In addition, an EDS analysis was conducted to confirm whether TOR products can also enter cracks. As a result, EDS detected carbon particles inside the cracks (see Fig. 8 b) and f). The only possible carbon source was the FM, which usually contains graphite or carboxymethyl cellulose (although authors do not know the exact composition of used TOR products, EDS analysis confirmed carbon as one of the constituents of FM). It is important to note that although the steel used for the discs also contains a trace amount of carbon, it was likely too low to form the thick black coating observed on the crack faces.

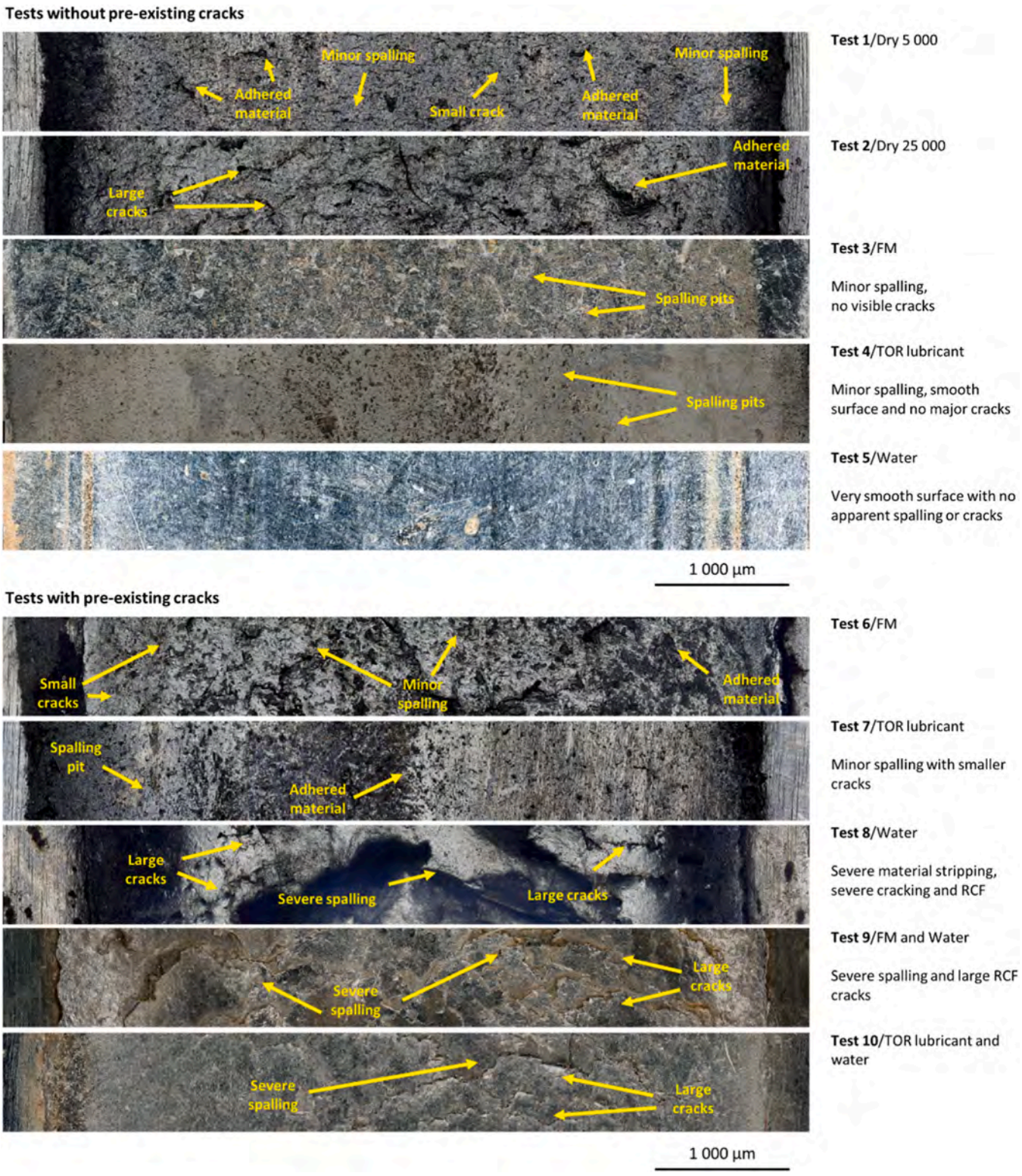

Fig. 6. OM pictures of the surface after testing (rail disc). No oxides.

3.3. *Results of wear and RCF tests: with oxides*

In tests 11–13, specimens were first run-in for 5000 cycles to create pre-existing cracks. After that, both discs were put in a climate chamber for 24 h to form an oxide layer. Then, the test was conducted the same way as in tests 8–10. Regarding friction, CoT measured in tests where TOR products were applied on oxidised specimens stayed in the same range as in tests where clean specimens were used (9 and 10). For FM, this range was between 0.1 and 0.15, see Fig. 9 a). For TOR lubricant, CoT values were slightly lower, as they stayed below 0.1 for most of the test, see Fig. 9 b). However, a difference was observed in tests with water, as the CoT now remained stable around 0.2, unlike in test 8, where CoT gradually increased to values approaching dry contact friction (see Fig. 4 h). This behaviour resembled test 5 (Fig. 4 e), where

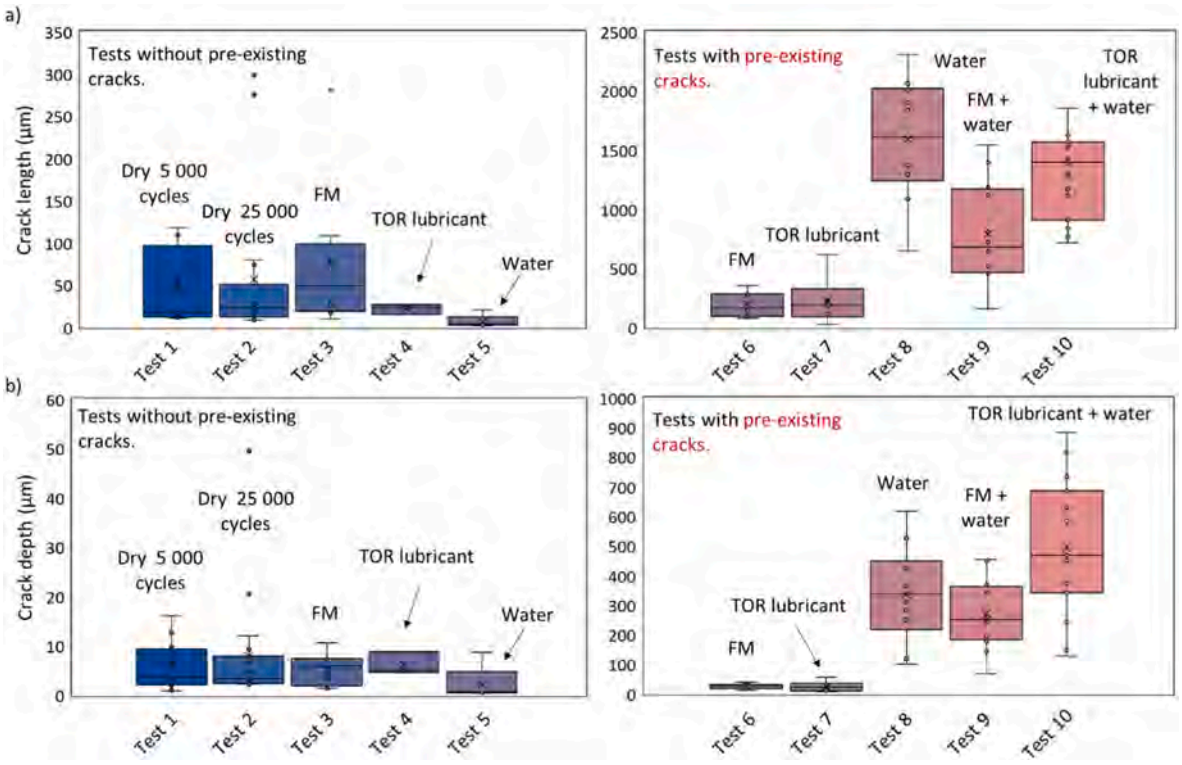

Fig. 7. RCF crack parameters: a) length and b) depth. Tests without and with pre-existing cracks are displayed in separate figures. No oxides.

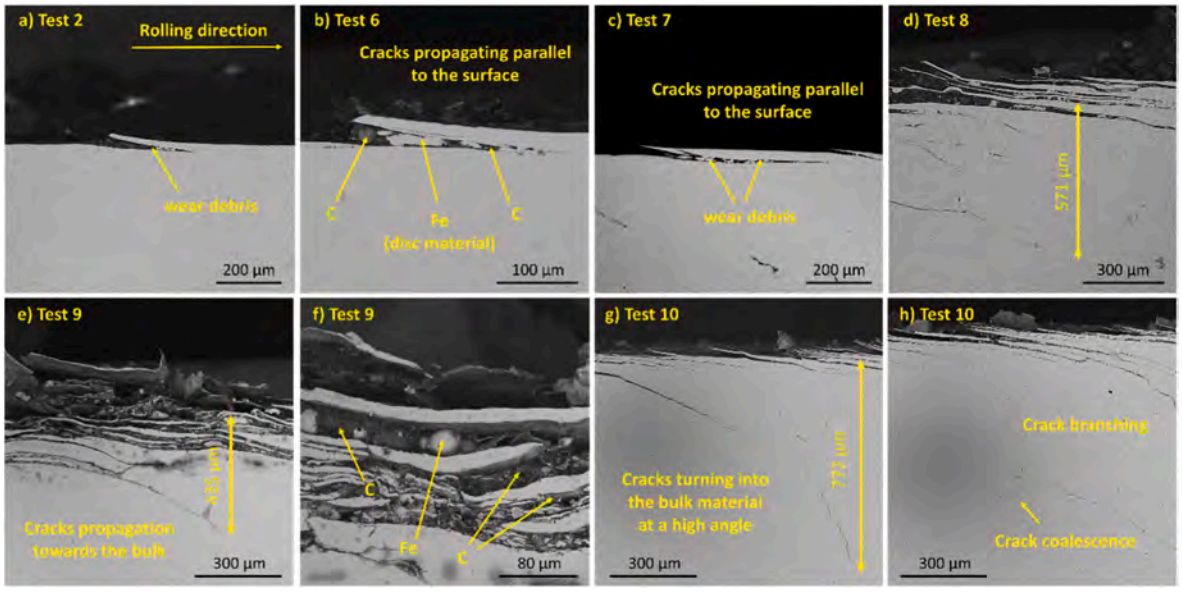

Fig. 8. SEM pictures of cracks: a) Dry 25 000 cycles, b) FM (with pre-existing cracks), c) TOR lubricant (with pre-existing cracks), d) Water (with pre-existing cracks), e) and f) FM in wet conditions (with pre-existing cracks), g) and h) TOR lubricant in wet conditions (with pre-existing cracks). No oxides.

water was used, but no pre-existing cracks were present. This suggests that, from a frictional perspective, an oxide layer suppresses the influence of pre-existing cracks, allowing water to affect CoT like in conditions without cracks.

Specimens were weighed before and after the test to evaluate the mass loss and wear rate. However, it is essential to note that it was impossible to distinguish between the mass loss of the oxides and the bulk steel. As the oxide layer has lower shear strength than steel and is easily worn, the mass loss and wear rate calculated for specimens with oxides could not be meaningfully compared to the wear rate of the specimens in the previous tests without oxides. Nevertheless, the results showed that in the case of the TOR lubricant under wet conditions, the mass loss and wear rate were higher for oxidised specimens than for those without oxide layers (see Fig. 10, test 12), which can be explained by the fact that oxide layers are easily worn due to their low shear strength. However, in tests with water alone and those with water together with FM, the opposite was true (see Fig. 10, tests 11 and 13), as the mass loss and wear rate of specimens with an oxide layer were lower than in tests without oxides. The reason for this was that the exceptionally high mass loss observed for the unoxidised discs was mainly a

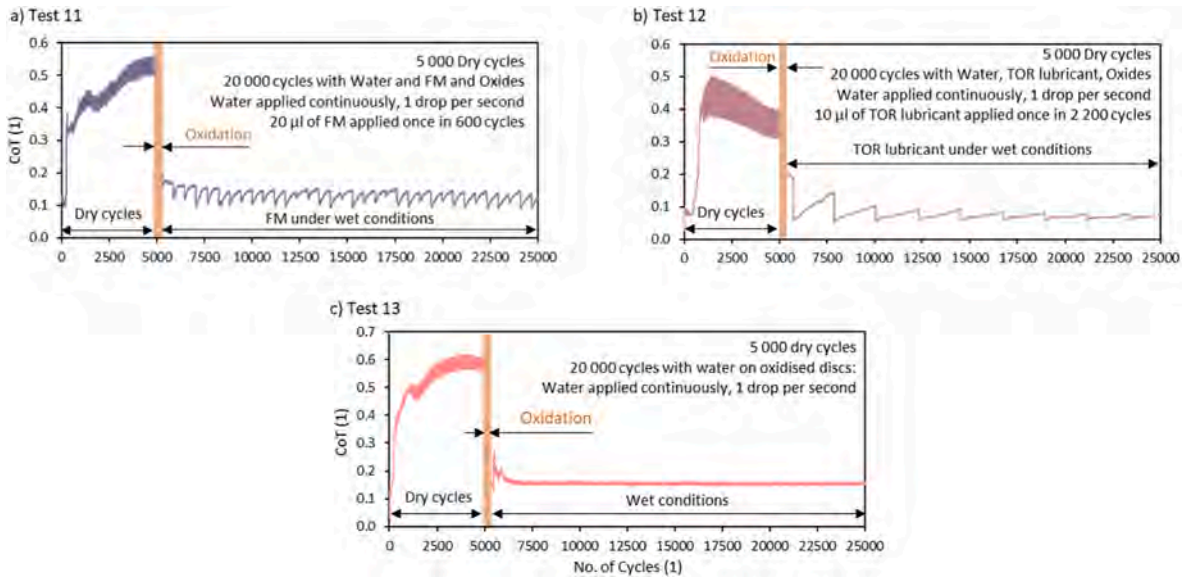

Fig. 9. Friction data for wear and RCF tests: With oxides. All tests were conducted on specimens with pre-existing cracks. a) FM and water, b) TOR lubricant and water, c) water.

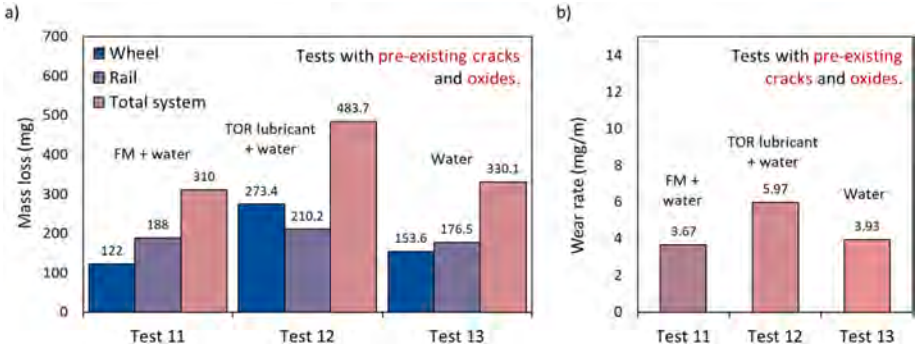

Fig. 10. a) Mass loss of wheel disc, rail disc and total system. Part b) shows the total system wear rate in milligrams per 1 m of sliding distance (run-ins were excluded from the evaluation). Specimens with an oxide layer.

result of severe RCF damage. In contrast, in the tests with oxidised surfaces, water could not enter the cracks, and the mass loss was therefore primarily due to wear. Unlike FM, the TOR lubricant was more effective in preventing mass loss due to the RCF. This is discussed in

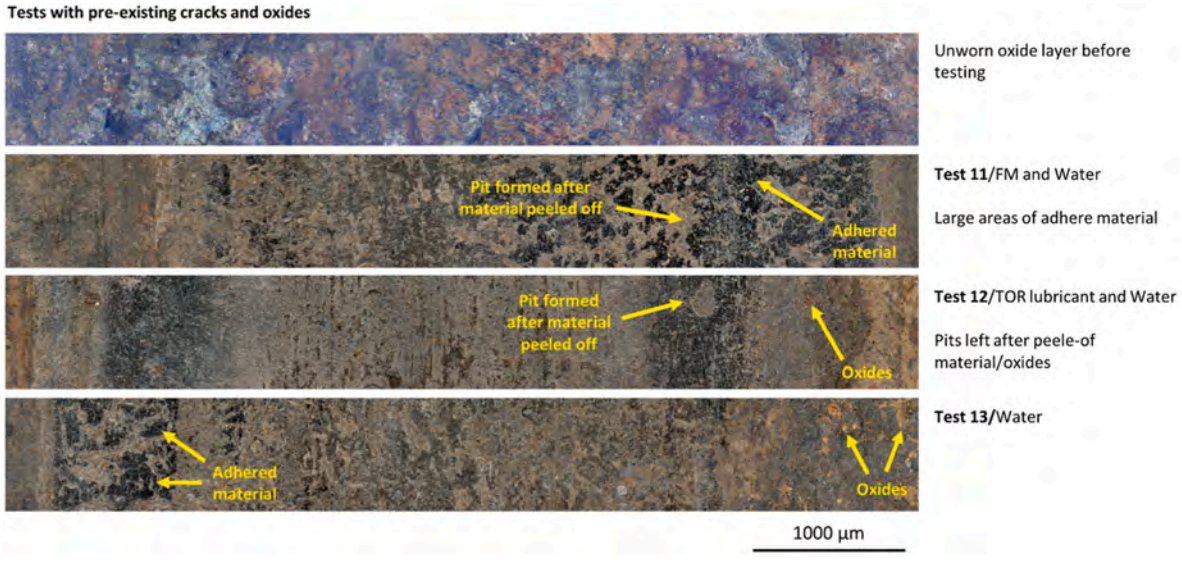

Fig. 11. OM pictures of the surface after testing (rail disc). No oxides.

more detail later in the text in the Discussion section.

The unworn oxide layer can be seen in Fig. 11, with its thickness and cross-section visible in SEM images in Fig. 12a–d). SEM images show that the oxides uniformly covered the surface in a layer with thicknesses varying in the order of micrometres. After the tests, OM observation of the surface did not reveal any major signs of RCF. The oxide layer was visibly worn, and several pits were found, most likely due to peeled-off oxides or bulk material (see Fig. 11). The pre-existing cracks are visible in cross-section images in Fig. 12a–d). After testing, crack measurements revealed that their parameters were comparable to those in tests under dry conditions, despite expectations that water or the combination of water and TOR product would enhance crack growth like in previous cases, see Fig. 13 a) and b). A possible explanation for why discs with oxides did not experience severe RCF, as in the case with clean specimens, will be discussed next in the Discussion section.

4. Discussion

4.1. Tests without oxides

In this study, the authors used the interval application of TOR products. Although smart application units that control lubricant applications based on real-time friction data have recently been implemented, interval application remains the dominant method. In this approach, TOR products are applied after a certain number of vehicle passes or a fixed time interval, regardless of weather conditions. Thus, over-lubrication due to lubricant accumulation or contamination is more likely, as was the case in this study. As suggested in the study by Seo et al. [27], potentially interesting phenomena may be observed if the water/TOR product application is less frequent and starvation occurs, requiring application not in fixed intervals but instead depending more on actual CoT data. The author used interval application to examine the worst-case scenario from the point of view of traction/adhesion problems that may occur on the track. From the perspective of future research, the authors will focus on what happens when contact starves, and CoT reaches higher values, approaching dry contact, as it may reveal interesting phenomena. While this aspect is undoubtedly relevant, addressing it in the present study would go beyond its intended scope, making it a natural subject for future investigation.

Problems with over-lubrication did not occur after a single water application in any of the friction tests. However, the situation changed when water was continuously applied in wear and RCF tests. Although water also affected FM somewhat, the results with TOR lubricant were more interesting, see Fig. 4 j). CoT reached the lowest values in this test, staying between 0.05 and 0.07, as the water stopped its recovery. This indicates that TOR lubricants may cause over-lubrication even in recommended dosages when used under wet conditions. A possible explanation may be based on studies describing water–oil/grease interactions, which explain that combining water and grease may lead to a better lubrication effect [47–49]. At first, due to the higher wetting ability of oil, the lubricating film is predominantly formed by the oil phase, even when water is present in larger quantities [49,50]. This allows the film to maintain low shear stress within the contact and consequently a low CoT. When starvation occurs, water now takes a larger part in the lubrication process, and CoT rises [51]. Subsequently, a larger portion of the load is carried by direct asperity and particle contacts, leading to an increase in CoT [42]. Several studies suggest that some thickeners can absorb water, which may lower grease viscosity and enhance contact replenishment and thus delay starvation [52–54]. Furthermore, the manufacturer lists an organic thickener, and the formulation appears consistent with a polyurea-based system commonly used in the industry. Polyurea greases, particularly those based on biodegradable esters, can emulsify water up to several per cent and, under intense mixing, absorb as much as 70–80 % of water without losing structural integrity. This remarkable water uptake likely accounts for the prolonged period of low traction coefficient ("over-lubricated" state) observed during continuous wetting in the TOR lubricant tests.

However, a more detailed understanding of the water absorption behaviour would require additional testing, which was beyond the scope of this study. Such testing could include the construction of a water uptake curve using standardised methods such as ASTM D4049 (spray test) or ASTM D7342 (Karl-Fischer titration) to track moisture content over time. Polyurea/ester-based greases absorb up to approximately 5–10 wt % of water under mild exposure and considerably more under blending conditions. A previous study [42] examined water interactions with TOR lubricant in more detail using a ball-on-disc tribometer. It confirmed that the two phases do mix, leading to a temporary drop in CoT. Since the same product was tested here, these conclusions are also applicable to this work. Since the present study focuses mainly on wear and RCF, readers are referred to that paper for a more detailed discussion of the friction behaviour.

Now, the effect of pre-existing cracks will be discussed. FM reduced

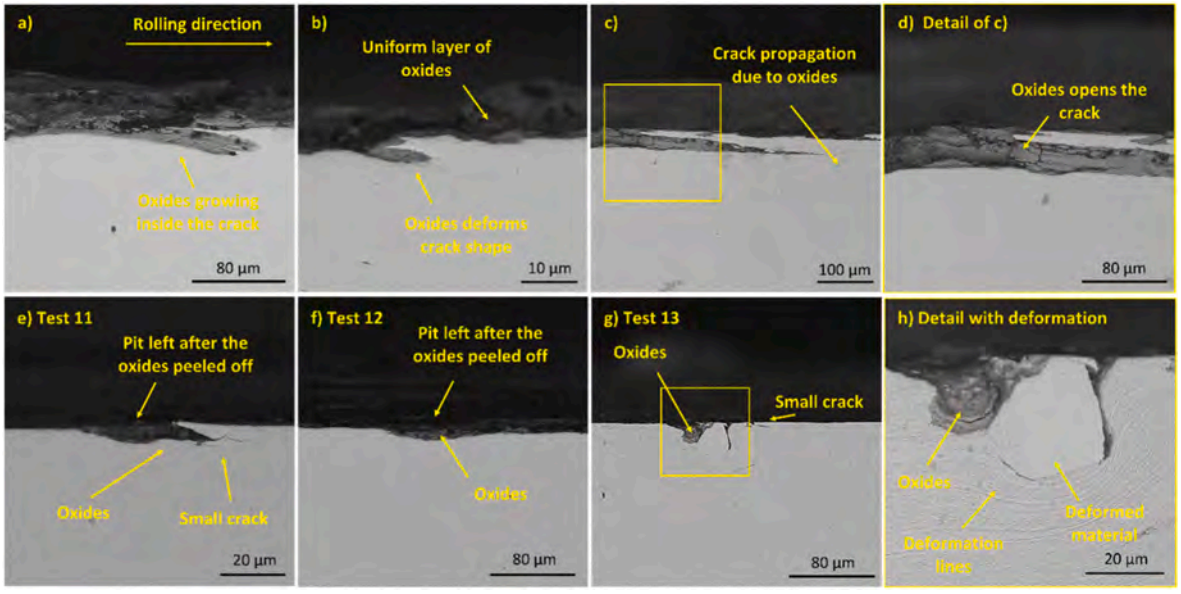

Fig. 12. SEM pictures: a–d) intact oxide layer before testing, e) after test with FM and water, f) TOR lubricant and water, g) water, h) detail on deformed material. Tests with oxides and pre-existing cracks.

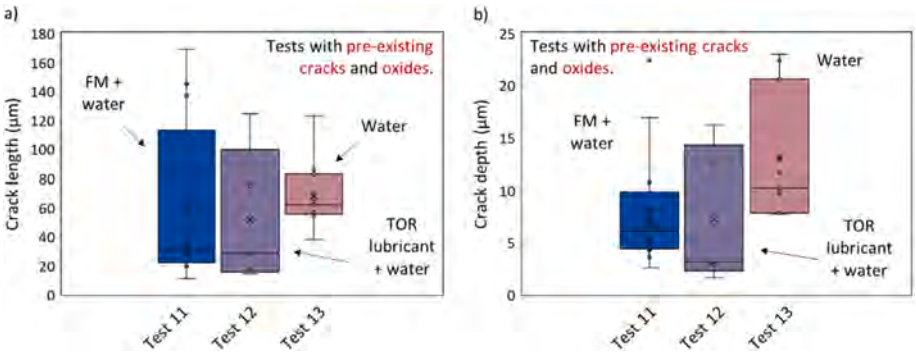

Fig. 13. Crack a) length and b) depth. Tests with oxides and pre-existing cracks.

the wear rate in tests without pre-existing cracks by a factor of 10 (test 3), while the TOR lubricant achieved a 35-fold reduction (test 4). Meanwhile, water in test 5 led to a 29 times reduction compared to dry conditions, see Fig. 5 b). FM achieved worse wear reduction than the TOR lubricant as it repeatedly dried out, causing an increase in CoT and, consequently, higher adhesive wear. In contrast, water maintained a stable and low CoT. Although the TOR lubricant also periodically reached a CoT of 0.3 like FM, it exhibited a longer-lasting effect than FM, providing a lower CoT for an extended period. Overall, it can be said that both TOR products were effective in reducing wear, and no significant signs of RCF were found, but TOR lubricant was more effective.

In tests with pre-existing cracks, all aspects of RCF increased substantially. A crack length and depth comparison with previous tests showed that a liquid base of both TOR products accelerated crack growth (see Fig. 7 a). However, water on its own had an even more significant effect on RCF, as under these conditions, the crack depth and length were an order of magnitude higher than under TOR products. In reality, cracks are always present in the rail surface. Thus, applying TOR products may severely impact rail service life, which may not be apparent from testing in laboratory conditions if new specimens without cracks are used for testing. Thus, more interest should be placed on testing specimens with pre-existing cracks and surface damage. These findings follow the study by Hardwick et al. [24], where a similar change in RCF behaviour was observed when pre-existing cracks were present, but for different material pairs and TOR products than used in this study.

The behaviour of TOR products under wet conditions from the perspective of RCF has not been studied yet. Tests 9 and 10 showed that crack lengths were up to five times longer under FM in wet conditions than in tests where FM was applied in dry conditions, and in some cases, cracks propagated up to ten times deeper beneath the surface. The combination of water and TOR lubricant accelerated crack growth even further, reaching depths of up to 900 µm (see Fig. 7 b), the deepest from all tests. Those cracks and signs of spalling were visible to the naked eye (Fig. 6), showing that TOR products affect RCF differently in wet than dry conditions. In the tests with FM, it is more likely that the exceptionally high mass loss resulted from the presence of water rather than from the FM itself. Unlike TOR lubricant, FM could not prevent it, as it is soluble in water, and thus, the mass loss was similar to water-only conditions. Instead of drying out, the base medium of FM remains liquid and, together with water, enters cracks, accelerating their growth due to crack face lubrication and hydropressurization mechanisms [55].

EDS detected carbon particles inside the cracks for FM but not for the TOR lubricant. However, the influence of oil-based products has been previously investigated in several studies, which have concluded that these products are capable of penetrating cracks and influencing RCF, despite their relatively high viscosity [5,24]. Since water influences grease and enhances replenishment, as stated in Refs. [52–54], it may make it even easier for bleed oil from a TOR lubricant to get into cracks under wet conditions, which EDS would not have detected. In that case, crack faces would be well-lubricated (as CoT decreases as low as 0.05). Thus, internal friction would be very low, allowing cracks to propagate easily. Usually, if the friction between the crack faces is lower than 0.2, cyclic shear crack growth may occur [56]. The CoT was considerably below this value. In addition, any trapped liquid (TOR lubricant, its bleed oil or water) becomes pressurised by load and causes a phenomenon similar to the oil wedge effect [57]. As evident from test 10, the combination of TOR lubricant and water accelerated crack growth the most, as cracks penetrated the deepest into the bulk. This was likely because the TOR lubricant was more effective in reducing wear than the FM. As mentioned earlier, a competitive mechanism exists between wear and RCF, where an increase in wear can shorten or even eliminate cracks [19,20]. In this case, the lower wear rate achieved with the TOR lubricant allowed the cracks to grow deeper compared to the tests where the wear rate was higher.

4.2. *The effect of oxides*

In this study, the authors used a modified approach proposed by Sone [58], which was also adopted in several other studies [59–62]. The adopted procedure involved exposing the specimens to vapours of water, ethanol and magnesium dichloride at 60 °C. As a result, the entire surface was covered with a thick and uniform oxide layer, consisting of magnetite (Fe_3O_4), hematite (Fe_2O_3), goethite (α-FeOOH) and akaganeite (β-FeOOH), see Fig. 14 a) and b). Godfrey [63] provided an overview of fifteen iron oxides and their rust forms and summarised their key characteristics. In rail-tribology, laboratory studies typically focus on hematite and magnetite [64], which are arguably the most frequently tested oxides. In addition, Kempka et al. [65] conducted XRD analysis on railhead swabs collected on the track and identified that goethite and akaganeite were always present when drivers reported problems with traction. Thus, the oxide layer formed in this study was representative of actual track conditions.

Studies often report that hematite and some other oxides increase friction [63]. However, this was not observed in any of the friction tests, where it caused a reduction in CoT under dry conditions from 0.4 to 0.3, see Fig. 3 e). On the contrary, Kempka et al. [65] linked the presence of goethite and akaganeite to low-adhesion problems, and Beagley [66] showed that when mixed with water, even hematite can cause low friction, likely because its particles are strong enough to carry the load but have low shear strength, allowing them to act as an effective lubricant. This was further confirmed in another study by Lu et al. [67]. Thus, while hematite may increase friction under dry conditions, its interaction with moisture in the ambient air, together with the presence of goethite and akaganeite, may explain why lower CoT values were measured on the oxidised specimens. This behaviour is consistent with the fact that oxide layers generally exhibit relatively low shear strength, which reduces the available traction.

The effect of iron oxides on friction has been well examined in many studies [59–62], but their impact on wear and RCF is still unclear [43]. It

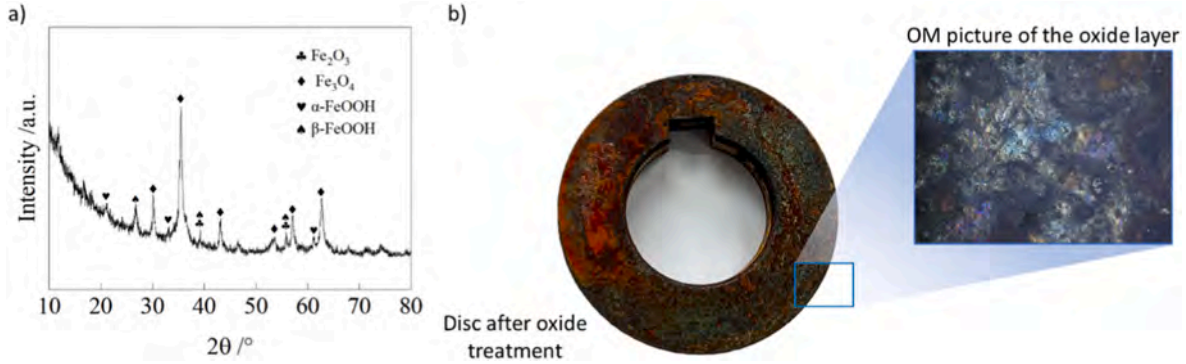

Fig. 14. a) The results of XRD analysis and b) a picture of a disc after oxide treatment.

is true that due to its low shear strength, oxide layers are also easily worn. Yet, the total mass loss in tests involving water was usually higher with unoxidised discs compared to those with oxides. The explanation for that is that while oxides increase wear, they also suppress RCF. The exceptionally high mass loss in tests with water and water together with FM was due to massive delamination and spalling caused by RCF, which was not the case for oxidised specimens.

In Fig. 12, SEM images of cross-sections show that the oxide layer was several microns thick. More importantly, it was observed that the crack faces were also oxidised. As the oxides grow bigger, they fill the insides of cracks and separate their faces. At some point, the oxides start to press against internal surfaces, causing localised stress at the crack tip, potentially initiating further propagation [68]. This process occurs during oxidation, so the crack growth is accelerated even before any testing is conducted. This is supported by the fact that some cracks found after the oxide treatment were significantly larger than those typically created during the run-in, with the oxide being the likely cause. However, at this stage, this hypothesis is based on a simple observation only and will be subject to further research. Once the oxides fill the cracks, they prevent fluids from entering. This means that water or TOR products cannot go inside, and mechanisms such as face lubrication or hydropressurisation cannot occur. As a result, cracks did not grow further during testing, even though liquid was on the surface.

Oxides have low shear strength, so the top layer was quickly worn, meaning cracks could not grow and were also worn. This can be seen in Fig. 12, where images a–d) show the surface and cracks before the test, and e–h) show the surface after the test. After testing, the surface was very smooth, with only small pits in areas where oxides or cracks were previously present before being worn off. An interesting phenomenon is observed in Fig. 12 h), where a crack with an unusual shape was detected. The corrosive solution was sprayed on the crossectioned surface to highlight the deformation lines around this crack (see the detail in Fig. 12 h). Deformation lines are visible on one side of the crack but absent on the other. A possible explanation is that this is not an RCF crack but rather a piece of material initially located on the left side in an upward position. A hole formed next to it due to oxidic wear, and this material was deformed by traction forces and indented into the hole left by the worn oxides. Similar behaviour was also observed in Ref. [69].

The effect of oxides can be summarised as follows. Oxides enhance crack propagation even before the start of the test by exerting pressure on internal faces. However, they also block any liquid from entering, preventing the usual mechanisms responsible for further crack growth. As the top layer is easily worn due to its low shear strength, the result is smooth surfaces without any apparent cracks, see Fig. 12e–h). Thus, RCF is less likely to occur on oxidised surfaces.

5. Conclusion

This study investigated whether TOR products can effectively reduce wear and prevent rolling contact fatigue (RCF) while maintaining an intermediate coefficient of traction (CoT) in the presence of contaminants typically found on the railhead. All tests were conducted on a twin-disc machine, using conditions representative of wheel-rail (W/R) contact. Two types of TOR products were selected: a water-based friction modifier (FM) and a grease-based TOR lubricant, allowing for a comparison between drying and non-drying compositions. Specimens were cut from authentic materials, and some of them were run-in to create pre-existing surface cracks. Given its significant impact on traction and braking, water was chosen as the primary contaminant. Additionally, some discs underwent an oxidation treatment to form an oxide layer on the surface, enabling an examination of the influence of third-body layers on RCF and wear.

From the perspective of CoT, the results can be summarised as follows. Water influenced both TOR products differently. In the case of FM, water delayed the evaporation of the base medium, prolonging friction-modifying effects. For the TOR lubricant, the impact on retentivity was even more substantial. Over-lubrication was observed in tests with repeated applications, primarily due to the product accumulation over time and as a result of the thickener absorbing water. This led to conditions of extremely low friction, with CoT values dropping as low as 0.05 – a value considered insufficient for safe railway vehicle operation. The oxide layer decreased CoT in dry and wet conditions, but the effect was negligible in the presence of the TOR product.

Adhesive wear was the dominant wear mechanism observed under dry conditions. Both TOR products effectively reduced wear rate, with the TOR lubricant proving the most efficient. The FM was less effective, likely due to its tendency to dry quickly. Both products effectively prevent crack formation and reduce mass loss. However, in tests where cracks were formed before the application of products, severe RCF was observed as the liquid component of products accelerated crack propagation due to crack face lubrication and hydropressurisation. RCF damage intensified when TOR products were contaminated by water. The combined effect of FM and water resulted in significant mass loss, whereas TOR lubricant, though not experiencing as high mass loss, exhibited deeper crack penetration. These deeper cracks posed a risk of substantial spalling if allowed to merge, which would possibly happen if the test duration was prolonged.

An interesting phenomenon was found in tests with oxidised specimens. It was observed that the crack faces also oxidise. As the oxides grow, they fill the crack interior, creating pressure and initiating crack propagation. This effect resembled hydropressurisation but occurred under dry conditions without any external load. Furthermore, water or liquid components of TOR products could not enter cracks due to oxides suppressing the usual mechanisms of liquid-driven crack propagation. And, as the oxidised surface is easily worn due to the low shear strength of oxides, the cracks were quickly removed, leaving a smooth surface after testing with no signs of RCF.

CRediT authorship contribution statement

Simon Skurka: Writing – original draft, Methodology, Investigation, Data curation, Conceptualization. **Radovan Galas:** Writing – review & editing, Methodology, Investigation, Conceptualization. **Jiaxin Li:** Methodology, Investigation. **Honghao Wang:** Writing – review & editing, Investigation. **Milan Omasta:** Writing – review & editing, Project administration, Methodology, Investigation, Conceptualization. **Haohao Ding:** Writing – review & editing. **Wenjian Wang:** Writing – review & editing, Project administration, Data curation, Conceptualization. **Ivan Krupka:** Writing – review & editing, Data curation. **Martin Hartl:** Supervision, Funding acquisition.

Declaration of generative AI and AI-assisted technologies in the manuscript preparation process

During the preparation of this work the author(s) used ChatGPT and Grammarly in order to improve the clarity and correctness of the English language in this manuscript. After using this tool/service, the author(s) reviewed and edited the content as needed and take(s) full responsibility for the content of the published article.

Declaration of competing interest

The authors declare that they have no known competing financial interests or personal relationships that could have appeared to influence the work reported in this paper.

Acknowledgements

This publication was supported by the project "Mechanical Engineering of Biological and Bio-inspired Systems", funded as project No. CZ.02.01.01/00/22_008/0004634 by Programme Johannes Amos Comenius, call Excellent Research, administrated by Ministry of Education, Youth and Sports of the Czech Republic. The work was also supported by the National Natural Science Foundation of China (No. 52320105007).

Data availability

The data supporting the findings of this study have been deposited in the Zenodo repository (https://doi.org/10.5281/zenodo.15744531), and the preprint of this manuscript has been archived at https://doi.org/10.5281/zenodo.15910051.

References

[1] D. Szablewski, J. LoPresti, T. Sultana, Testing of latest top-of-rail friction modification materials at FAST, Railw. Track Struct. 111 (2015) 13–16.
[2] X. Liu, P.A. Meehan, Investigation of squeal noise under positive friction characteristics condition provided by friction modifiers, J. Sound Vib. 371 (2016) 393–405, https://doi.org/10.1016/j.jsv.2016.02.028.
[3] P.A. Meehan, X. Liu, Wheel squeal noise control under water-based friction modifiers based on instantaneous rolling contact mechanics, Wear 440–441 (2019) 203052, https://doi.org/10.1016/j.wear.2019.203052.
[4] J. Han, Y. He, X. Xiao, X. Sheng, G. Zhao, X. Jin, Effect of control measures on wheel/rail noise when the vehicle curves, Appl. Sci. 7 (2017) 1144, https://doi.org/10.3390/app7111144.
[5] M. Harmon, R. Lewis, Review of top of rail friction modifier tribology, Tribol. Mater. Surface Interfac. 10 (2016) 150–162, https://doi.org/10.1080/17515831.2016.1216265.
[6] U. Olofsson, Y. Zhu, S. Abbasi, R. Lewis, S. Lewis, Tribology of the wheel–rail contact – aspects of wear, particle emission and adhesion, Veh. Syst. Dyn. 51 (2013) 1091–1120, https://doi.org/10.1080/00423114.2013.800215.
[7] D.T. Eadie, M. Santoro, Top-of-rail friction control for curve noise mitigation and corrugation rate reduction, J. Sound Vib. 293 (2006) 747–757, https://doi.org/10.1016/j.jsv.2005.12.007.
[8] J. Kalousek, K.L. Johnson, An investigation of short pitch wheel and rail corrugations on the Vancouver mass transit system, Proc. Inst. Mech. Eng. F J. Rail Rapid Transit 206 (1992) 127–135, https://doi.org/10.1243/PIME_PROC_1992_206_226_02.
[9] R. Stock, L. Stanlake, C. Hardwick, M. Yu, D. Eadie, R. Lewis, Material concepts for top of rail friction management – classification, characterisation and application, Wear 366–367 (2016) 225–232, https://doi.org/10.1016/j.wear.2016.05.028.
[10] R. Galas, D. Kvarda, M. Omasta, I. Krupka, M. Hartl, The role of constituents contained in water–based friction modifiers for top–of–rail application, Tribol. Int. 117 (2018) 87–97, https://doi.org/10.1016/j.triboint.2017.08.019.
[11] D. Kvarda, S. Skurka, R. Galas, M. Omasta, L. Shi, H. Ding, et al., The effect of top of rail lubricant composition on adhesion and rheological behaviour, Eng. Sci. Technol. Int. J. 35 (2022) 101100, https://doi.org/10.1016/j.jestch.2022.101100.
[12] M. Harmon, J.F. Santa, J.A. Jaramillo, A. Toro, A. Beagles, R. Lewis, Evaluation of the coefficient of friction of rail in the field and laboratory using several devices, Tribol. Mater. Surface Interfac. 14 (2020) 119–129, https://doi.org/10.1080/17515831.2020.1712111.
[13] M. Moreno-Ríos, E.A. Gallardo-Hernández, M. Vite-Torres, A. Peña-Bautista, Field and laboratory assessments of the friction coefficient at a railhead, Proc. Inst. Mech. Eng. F J. Rail Rapid Transit 230 (2016) 313–320, https://doi.org/10.1177/0954409714536383.
[14] Y.A. Areiza, S.I. Garcés, J.F. Santa, G. Vargas, A. Toro, Field measurement of coefficient of friction in rails using a hand-pushed tribometer, Tribol. Int. 82 (2015) 274–279, https://doi.org/10.1016/j.triboint.2014.08.009.
[15] D.T. Eadie, D. Elvidge, K. Oldknow, R. Stock, P. Pointner, J. Kalousek, et al., The effects of top of rail friction modifier on wear and rolling contact fatigue: full-Scale rail–wheel test rig evaluation, analysis and modelling, Wear 265 (2008) 1222–1230, https://doi.org/10.1016/j.wear.2008.02.029.
[16] J. Lundberg, M. Rantatalo, C. Wanhainen, J. Casselgren, Measurements of friction coefficients between rails lubricated with a friction modifier and the wheels of an IORE locomotive during real working conditions, Wear 324–325 (2015) 109–117, https://doi.org/10.1016/j.wear.2014.12.002.
[17] R. Galas, M. Omasta, I. Krupka, M. Hartl, Laboratory investigation of ability of oil-based friction modifiers to control adhesion at wheel-rail interface, Wear 368–369 (2016) 230–238, https://doi.org/10.1016/j.wear.2016.09.015.
[18] A.F. Bower, K.L. Johnson, Plastic flow and shakedown of the rail surface in repeated wheel-rail contact, Wear 144 (1991) 1–18, https://doi.org/10.1016/0043-1648(91)90003-D.
[19] H.H. Wang, W.J. Wang, Z.Y. Han, Y. Wang, H.H. Ding, R. Lewis, et al., Wear and rolling contact fatigue competition mechanism of different types of rail steels under various slip ratios, Wear 522 (2023) 204721, https://doi.org/10.1016/j.wear.2023.204721.
[20] K. Luo, X. Liu, Y. Yang, T. Cong, F. Zhang, W. Wang, Modeling the competitive relationship between wear and rolling contact fatigue of railway wheel steel, Wear 560–561 (2025) 205615, https://doi.org/10.1016/j.wear.2024.205615.
[21] R. Stock, D.T. Eadie, D. Elvidge, K. Oldknow, Influencing rolling contact fatigue through top of rail friction modifier application – a full scale wheel–rail test rig study, Wear 271 (2011) 134–142, https://doi.org/10.1016/j.wear.2010.10.006.
[22] D.T. Eadie, D. Elvidge, K. Oldknow, R. Stock, P. Pointner, J. Kalousek, et al., The effects of top of rail friction modifier on wear and rolling contact fatigue: full-scale rail–wheel test rig evaluation, analysis and modelling, Wear 265 (2008) 1222–1230, https://doi.org/10.1016/j.wear.2008.02.029.
[23] R. Reiff, Top of rail friction control on rail surface performance and grinding, TTCI Technology Digest TD-07-039 4 (2007).
[24] C. Hardwick, R. Lewis, R. Stock, The effects of friction management materials on rail with pre existing rcf surface damage, Wear 384–385 (2017) 50–60, https://doi.org/10.1016/j.wear.2017.04.016.
[25] S. Maya-Johnson, J. Felipe Santa, A. Toro, Dry and lubricated wear of rail steel under rolling contact fatigue - wear mechanisms and crack growth, Wear 380–381 (2017) 240–250, https://doi.org/10.1016/j.wear.2017.03.025.
[26] Y.L. Xavier, A.B. Rezende, S.T. Fonseca, E. Jun Kina, P.R. Mei, Friction modifier performance in twin-disk tests using disks of the same microstructure and hardness, Tribol. Trans. 68 (2025) 1–11, https://doi.org/10.1080/10402004.2024.2429716.
[27] J.-W. Seo, H.-K. Jun, S.-J. Kwon, D.-H. Lee, Effect of friction modifier on rolling contact fatigue and wear of wheel and rail materials, Tribol. Trans. 61 (2018) 19–30, https://doi.org/10.1080/10402004.2016.1271487.
[28] R. Galas, M. Omasta, L. Shi, H. Ding, W. Wang, I. Krupka, et al., The low adhesion problem: the effect of environmental conditions on adhesion in rolling-sliding contact, Tribol. Int. 151 (2020) 106521, https://doi.org/10.1016/j.triboint.2020.106521.
[29] K. Oldknow, D.T. Eadie, R. Stock, The influence of precipitation and friction control agents on forces at the wheel/rail interface in heavy haul railways, Proc. Inst. Mech. Eng. F J. Rail Rapid Transit 227 (2013) 86–93, https://doi.org/10.1177/0954409712452240.
[30] R. Lewis, E.A. Gallardo-Hernandez, T. Hilton, T. Armitage, Effect of oil and water mixtures on adhesion in the wheel/rail contact, Proc. Inst. Mech. Eng. F J. Rail Rapid Transit 223 (2009) 275–283, https://doi.org/10.1243/09544097JRRT248.
[31] T. Nakahara, K.-S. Baek, H. Chen, M. Ishida, Relationship between surface oxide layer and transient traction characteristics for two steel rollers under unlubricated and water lubricated conditions, Wear 271 (2011) 25–31, https://doi.org/10.1016/j.wear.2010.10.030.
[32] K.S. Baek, K. Kyogoku, T. Nakahara, An experimental investigation of transient traction characteristics in rolling-sliding wheel/rail contacts under dry-wet conditions, Wear 263 (2007) 169–179, https://doi.org/10.1016/j.wear.2007.01.067.
[33] W.J. Wang, H.F. Zhang, H.Y. Wang, Q.Y. Liu, M.H. Zhu, Study on the adhesion behavior of wheel/rail under oil, water and sanding conditions, Wear 271 (2011) 2693–2698, https://doi.org/10.1016/j.wear.2010.12.019.

[34] H. Chen, T. Ban, M. Ishida, T. Nakahara, Adhesion Between rail/wheel Under Water Lubricated Contact, vol. 253, 2002.
[35] Z. Wang, B. Wu, J. Huang, Y. Ji, D. Li, S. Wu, Dynamic wheel–rail adhesion characteristics on wet curved tracks considering surface roughness, Phys. Fluids 37 (2025), https://doi.org/10.1063/5.0252179.
[36] B. Wu, T. Wu, B. An, Numerical investigation on the high-speed wheel/rail adhesion under the starved interfacial contaminations with surface roughness, Lubric. Sci. 32 (2020) 93–107, https://doi.org/10.1002/ls.1489.
[37] H. Chen, T. Ban, M. Ishida, T. Nakahara, Experimental investigation of influential factors on adhesion between wheel and rail under wet conditions, Wear 265 (2008) 1504–1511, https://doi.org/10.1016/j.wear.2008.02.034.
[38] H. Chen, T. Ban, M. Ishida, T. Nakahara, Effect of water temperature on the adhesion between rail and wheel, Proc. IME J. J. Eng. Tribol. 220 (2006) 571–579, https://doi.org/10.1243/13506501JET75.
[39] H. Chen, M. Ishida, A. Namura, K.S. Baek, T. Nakahara, B. Leban, et al., Estimation of wheel/rail adhesion coefficient under wet condition with measured boundary friction coefficient and real contact area, Wear 271 (2011) 32–39, https://doi.org/10.1016/j.wear.2010.10.022.
[40] B. Wu, Z. Wen, H. Wang, X. Jin, Analysis of wheel and rail adhesion under wet condition by using elastic–plastic microcontact model, Lubric. Sci. 27 (2015) 297–312, https://doi.org/10.1002/ls.1283.
[41] S. Skurka, R. Galas, M. Omasta, H. Ding, W.-J. Wang, I. Krupka, et al., Assessing the performance of TOR lubricants in humid environments and under dew conditions, Tribol. Lett. 72 (2024) 90, https://doi.org/10.1007/s11249-024-01889-7.
[42] S. Skurka, R. Galas, M. Omasta, B. Wu, H. Ding, W.J. Wang, et al., The performance of top-of-rail products under water contamination, Tribol. Int. 188 (2023), https://doi.org/10.1016/j.triboint.2023.108872.
[43] Y. Zhu, The influence of iron oxides on wheel–rail contact: a literature review, Proc. Inst. Mech. Eng. F J. Rail Rapid Transit 232 (2018) 734–743, https://doi.org/10.1177/0954409716689187.
[44] R. Galas, S. Skurka, M. Valena, D. Kvarda, M. Omasta, H. Ding, et al., A benchmarking methodology for top-of-rail products, Tribol. Int. 189 (2023) 108910, https://doi.org/10.1016/j.triboint.2023.108910.
[45] J.X. Li, B.N. Wu, H.H. Ding, R. Galas, M. Omasta, Z.F. Wen, et al., Wear and damage behaviours of wheel and rail materials: effects of friction modifier and environmental temperature, Wear 523 (2023), https://doi.org/10.1016/j.wear.2023.204796.
[46] K. Ishizaka, S.R. Lewis, R. Lewis, The low adhesion problem due to leaf contamination in the wheel/rail contact: bonding and low adhesion mechanisms, Wear 378–379 (2017) 183–197, https://doi.org/10.1016/j.wear.2017.02.044.
[47] Y. Kimura, K. Okada, Lubricating properties of oil-in-water emulsions, Tribol. Trans. 32 (1989) 524–532, https://doi.org/10.1080/10402008908981921.
[48] N. Fujita, Y. Kimura, K. Kobayashi, Y. Amanuma, Y. Sodani, Estimation model of plate-out oil film in high-speed tandem cold rolling, J. Mater. Process. Technol. 219 (2015) 295–302, https://doi.org/10.1016/j.jmatprotec.2015.01.002.
[49] T. Nakahara, T. Makino, K. Kyogoku, Observations of liquid droplet behavior and oil film formation in O/W type emulsion lubrication, J. Tribol. 110 (1988) 348–353, https://doi.org/10.1115/1.3261630.
[50] J.J. Benner, F. Sadeghi, M.R. Hoeprich, M.C. Frank, Lubricating properties of water in oil emulsions, J. Tribol. 128 (2006) 296–311, https://doi.org/10.1115/1.2164464.
[51] W.R.D. Wilson, Y. Sakaguchi, S.R. Schmid, A dynamic concentration model for lubrication with oil-in-water emulsions, Wear 161 (1993) 207–212, https://doi.org/10.1016/0043-1648(93)90471-W.
[52] B. Jacod, F. Pubilier, P.M. E.Cann, A.A. Lubrecht, An analysis of track replenishment mechanisms in the starved regime, 483–492, https://doi.org/10.1016/S0167-8922(99)80069-8, 1999.
[53] P.M.E. Cann, B. Damiens, A.A. Lubrecht, The transition between fully flooded and starved regimes in EHL, Tribol. Int. 37 (2004) 859–864, https://doi.org/10.1016/j.triboint.2004.05.005.
[54] F. Cyriac, P.M. Lugt, R. Bosman, Impact of water on the rheology of lubricating greases, Tribol. Trans. 59 (2016) 679–689, https://doi.org/10.1080/10402004.2015.1107929.
[55] I.I. Kudish, K.W. Burris, Modeling of Surface and Subsurface Crack Behavior Under Contact Load in the Presence of Lubricant, vol.125, 2004.
[56] A.F. Bower, The influence of crack face friction and trapped fluid on surface initiated rolling contact fatigue cracks, J. Tribol. 110 (1988) 704–711, https://doi.org/10.1115/1.3261717.
[57] S. Bogdański, P. Lewicki, M. Szymaniak, Experimental and theoretical investigation of the phenomenon of filling the RCF crack with liquid, Wear 258 (2005) 1280–1287, https://doi.org/10.1016/j.wear.2004.03.038.
[58] Y. Sone, J. Suzumura, T. Ban, F. Aoki, M. Ishida, Possibility of in situ spectroscopic analysis for iron rust on the running band of rail, Wear 265 (2008) 1396–1401, https://doi.org/10.1016/j.wear.2008.02.027.
[59] Y. Zhu, U. Olofsson, H. Chen, Friction between wheel and rail: a pin-on-disc study of environmental conditions and iron oxides, Tribol. Lett. 52 (2013) 327–339, https://doi.org/10.1007/s11249-013-0220-0.
[60] Y. Zhu, X. Chen, W. Wang, H. Yang, A study on iron oxides and surface roughness in dry and wet wheel−rail contacts, Wear 328–329 (2015) 241–248, https://doi.org/10.1016/j.wear.2015.02.025.
[61] Y. Lyu, Y. Zhu, U. Olofsson, Wear between wheel and rail: a pin-on-disc study of environmental conditions and iron oxides, Wear 328–329 (2015) 277–285, https://doi.org/10.1016/j.wear.2015.02.057.
[62] Y. Zhu, H. Yang, W. Wang, Twin-disc tests of iron oxides in dry and wet wheel−rail contacts, Proc. Inst. Mech. Eng. F J. Rail Rapid Transit 230 (2016) 1066–1076, https://doi.org/10.1177/0954409715575093.
[63] D. Godfrey, Iron oxides and rust (hydrated iron oxides) in tribology, Tribol. Lubric. Technol. 55 (1999) 33.
[64] S. Lewis, B. Steel, D.T. Eadie, S.R. Lewis, R. Lewis, U. Olofsson, et al., The Effect of Temperature, Humidity and Railhead Contamination on the Performance of Friction Modifiers; A pin-on-disk Study, 2011.
[65] R. Kempka, R. Falconer, D. Gutsulyak, R. Lewis, Effects of oxide and water on friction of rail steel–new test method and friction mapping, Tribol. Mater. Surface Interfac. 15 (2021) 80–91, https://doi.org/10.1080/17515831.2020.1765611.
[66] T.M. Beagley, The rheological properties of solid rail contaminants and their effect on wheel/rail adhesion, Proc. Inst. Mech. Eng. 190 (1976) 419–428, https://doi.org/10.1243/PIME_PROC_1976_190_044_02.
[67] X. Lu, J. Cotter, D.T. Eadie, Laboratory study of the tribological properties of friction modifier thin films for friction control at the wheel/rail interface, Wear 259 (2005) 1262–1269, https://doi.org/10.1016/j.wear.2005.01.018.
[68] H.W. Pickering, F.H. Beck, M.G. Fontana, Wedging action of solid corrosion product during stress corrosion of austenitic stainless steels, Corrosion 18 (1962), https://doi.org/10.5006/0010-9312-18.6.230, 230t–9t.
[69] S.Y. Zhang, M. Spiryagin, H.H. Ding, Q. Wu, J. Guo, Q.Y. Liu, et al., Rail rolling contact fatigue formation and evolution with surface defects, Int. J. Fatig. 158 (2022) 106762, https://doi.org/10.1016/j.ijfatigue.2022.106762.

13th International Conference on Contact Mechanics and Wear of Rail/Wheel Systems (CM2025), Tokyo, Japan, September 22-26, 2025

INSIDE RCF CRACKS: OXIDATION AS A FACTOR IN RAIL DAMAGE

Simon Skurka[1]; Mengxuan Li[2]; Honghao Wang[2*]; Radovan Galas[1]; Milan Omasta[1]; Haohao Ding[2]; Wenjian Wang[2]; Ivan Krupka[1]; Martin Hartl[1]

[1]Faculty of Mechanical Engineering, Brno University of Technology
Technicka 2896/2, 616 69 Brno, Czech Republic
[2]Tribology Research Institute, State Key Laboratory of Rail Transit Vehicle System,
Southwest Jiaotong University, Chengdu 610031, China.

[*]E-mail: whh@my.swjtu.edu.cn

Abstract: This study investigates how oxidation affects RCF cracks in three rail steel grades. Pre-existing cracks were formed using a twin-disc machine under dry and wet conditions and then subjected to controlled oxidation in a heated chamber for up to 168 hours. OM/SEM observation revealed progressive growth of an oxide layer and penetration of the oxide deep into cracks.

While oxidation may initially promote crack opening through volume expansion, it also increases crack-face adhesion, preventing water from entering the cracks. Impact testing confirmed that oxides remained in cracks under cyclic loading. Oxidation modifies crack morphology, limits fluid-driven crack propagation, and potentially suppresses RCF progression as the result of increased wear.

Keywords: Rolling Contact Fatigue, Oxidation, Wear, Crack Morphology

1. Introduction

Due to increasing traffic density, rising axle loads, and higher operating speeds, the wheel-rail (W/R) interface is facing growing mechanical challenges [1]. These factors intensify rolling contact fatigue (RCF) and accelerate material degradation [2]. Rail surfaces naturally oxidise, forming a layer of iron oxides that modify the tribological properties of the W/R contact [3]. While RCF mechanisms have been extensively studied [4–9], the influence of oxidation on this process remains insufficiently understood [3].

The low shear strength of oxide layers correlates with increased wear. If an oxide layer forms within a material volume already containing RCF cracks, wear may remove the affected layer before cracks propagate further, potentially mitigating RCF [10]. On the other hand, oxides also cause embrittlement, making the material more susceptible to cracking [11].

In addition, water, a natural contaminant commonly found on the railhead [12]accelerates crack growth due to mechanisms such as crack face lubrication and hydropressurisation [13], often leading to severe spalling and rail damage [14]. However, if oxidation occurs inside cracks, it remains uncertain whether water can penetrate them and whether these two mechanisms can still happen. Thus, it is likely that RCF will progress differently on oxidised rails compared to the well-studied RCF behaviour on non-oxidised specimens. This study will examine how oxidation affects the morphology of pre-existing RCF cracks.

2. Material and Methods

The experimental procedure was conducted in three main stages. First, a twin-disc machine was used to prepare pre-existing cracks. Then, specimens were placed in a heated chamber and exposed to vapours from chemicals accelerating oxidation. After a specified period, the oxidised specimens were cross-sectioned, and polished metallographic samples were examined using OM/SEM to analyse crack morphology. Finally, impact testing was conducted to evaluate the brittleness of the oxide layer, its adhesion to crack faces, and its behaviour under cyclic loading.

2.1. Specimens

The specimens used in this study were discs with a diameter of 60 mm. The contact patch was linear, with a width of 5 mm, see Fig. 1 a). All discs were made of authentic materials. The first set of specimens was cut directly from a train wheel made of CL60 carbon steel. The remaining specimens were cut from rails. Specifically, three different steel grades were selected. Two of them were perlitic steels U75V and U71MnH. The last material was "hyper-eutectoid" chromium-alloyed steel with a high carbon content. Their specific chemical composition is listed in Table 1. These steel grades were selected to test a wide range of macro-hardness, a key parameter influencing the initiation and propagation of cracks under cyclic loading. Please note

Table 1 *Chem. composition (wt. %) and macro-hardness.*

Steel	C	Mn	P	S	$HV_{0.5}$
CL60	0.56-0.60	≤0.80	≤0.020	≤0.015	298±11
U75V	0.71-0.80	0.70-1.05	≤0.030	≤0.030	310±11
U71MnH	0.65–0.75	0.80–1.30	≤0.025	≤0.025	290±9
Hyper-eutectoid	0.90–0.95	0.94–1.02	~0.01	0.04–0.07	405±10

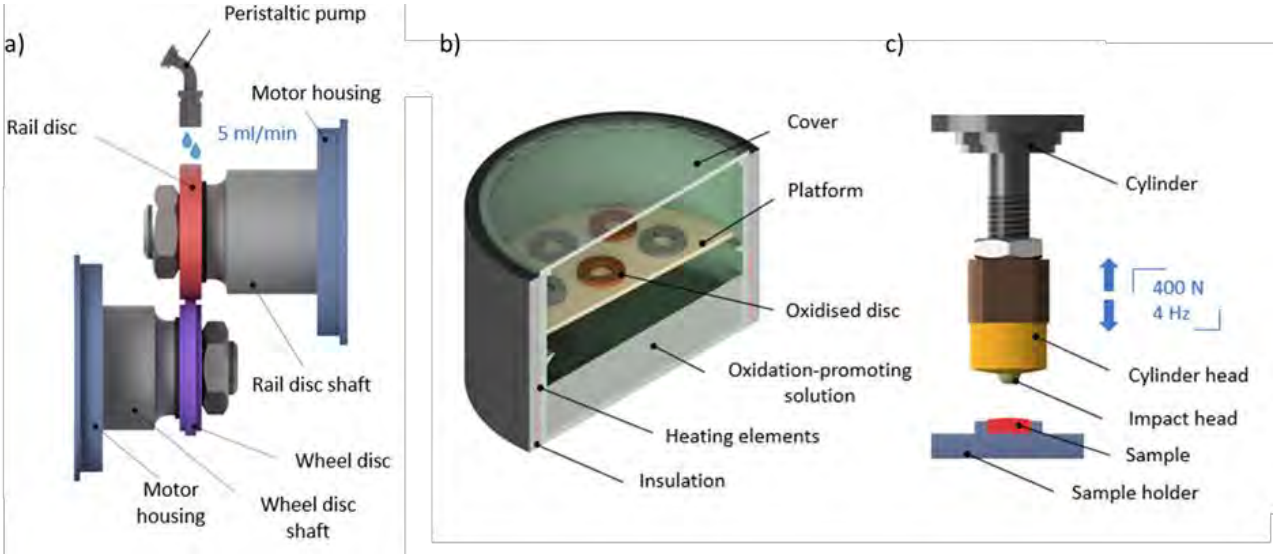

Fig. 1 *Experimental apparatus: a) Twin disc machine, b) heated chamber and c) impact tester.*

that while wheel discs made of CL60 steel were used together with rail discs on the twin-disc machine to prepare pre-existing cracks to maintain the authenticity of this process, the subsequent crack analysis was conducted only on the rail discs, as they exhibit significantly more pronounced RCF.

2.2. Preparation of pre-existing cracks

A twin-disc machine (MJP-30A, Southwest Jiaotong University) with a dry-wet cyclic exposure system was used to form pre-existing cracks. In this setup, the discs are mounted on two horizontally positioned shafts, with the rail disc mounted on the upper shaft and the wheel disc on the lower shaft, as shown in Fig. 1 a). Each shaft is driven by an independent servo motor, enabling precise control of the slip ratio (λ) by adjusting the relative rotational speeds of the two discs, as defined by the following equation:

$$\lambda = \frac{w_{wheel} \cdot r_{wheel} - w_{rail} \cdot r_{rail}}{w_{wheel} \cdot r_{wheel}} \cdot 100\% \qquad (1)$$

where w_{wheel} and w_{rail} are angular speeds (r/min) of discs and r_{wheel} and r_{rail} are their radii (mm). The two discs were loaded against each other via a hydraulic loading system equipped with a force sensor. The normal force was adjusted to achieve a contact pressure representative of the W/R interface. In rolling-sliding contacts, the frictional behaviour is quantified by the CoT, which is calculated using Eq (2):

$$CoT = \frac{M_{wheel}}{r_{wheel} \cdot F_N} \qquad (2)$$

where M_{wheel} is the torque (N·m) measured on the wheel shaft and F_N is the normal force (N). The testing apparatus is depicted in Fig. 1 a). The dry-wet cyclic exposure system was mounted on the twin-disc machine to simulate dry and wet crack initiation mechanisms. In dry conditions with a high coefficient of traction (CoT), tangential forces induce cyclic plastic deformation at the contact interface. As plastic strain accumulates, the material experiences progressive work hardening and loss of ductility. Once the local ductility limit is exceeded, crack initiation occurs [15]. In contrast, the liquid is often trapped within existing cracks in wet conditions, playing a dual role in the propagation of cracks. First, it reduces friction between crack faces, facilitating crack-face displacement. Second, hydrostatic pressure builds up inside the crack due to fluid entrapment under cyclic loading, further driving crack growth through hydropressurisation [14].

The system consisted of a peristaltic pump for controlled water supply during the "wet phase" and an air compressor to facilitate the transition to the "dry phase" by rapidly removing residual water from the contact. During the wet phase, the peristaltic pump applies water onto the disc surface at a 5 ml/min rate. In the dry phase, the water supply was stopped, and high-pressure gas was flown on the surface. The ratio between the wet and dry phases varied, so cracks of different parameters (length, depth) were prepared. All the information about test parameters is provided in Tab. 2.

The tests were conducted as follows. First, an initial run-in phase was performed to establish steady-state contact conditions. After that, dry and wet phases alternated in repeated cycles, with the duration of each phase specified in Tab. 2. Fig. 2 illustrates an example of the test procedure. The effect of various contact parameters (slip, contact pressure) and environmental conditions on crack initiation and propagation was extensively studied. However, these findings are not included here, as they are beyond the scope of this study. Instead, this study focuses on how oxidation influences already existing (thus, "pre-existing") cracks rather than how contact conditions

Table 2 *Test parameters and conditions for pre-existing crack formation..*

Test no.	Steel	Normal force (N)	Contact pressure (MPa)	Slip (%)	Speed (r/min)	Dry phase (s)	Wet phase (s)	Run-in (no. of cycles)	Test duration (no. of cycles)
1	U75V	1300	800	0.6	500	180	0	10 000	60 000
2						150	30		
3						120	60		
4						90	90		
5						60	120		
6						30	150		
7						0	180		
8	U71MnH	2 045	1 000			90	90		40 000
9	Hyper-eutectoid	2 475	1 100			90	90		

influence their initial formation. Therefore, only a brief overview of the crack formation process is provided in this chapter to give context to the reader. From now on, this study will focus on the influence of oxides on pre-existing cracks.

2.3. Oxidation process

The discs underwent an oxidation process in a heated chamber, where they were placed on a platform above a solution containing water, ethanol, and magnesium dichloride. The chamber maintained a constant temperature of 60 °C, enabling slow evaporation of the solution, exposing the discs to vapours and promoting oxidation. Additionally, the discs were dipped into the solution at regular intervals to ensure their surface remained wet, further enhancing oxide formation. This oxidation method was based on a modified approach proposed by Sone [16]. The setup is illustrated in Fig. 1 b).

The discs were removed at each time point listed in Tab. 3, and a small sample was cut using a wire-cut EDM machine. The discs were then placed back into the heated chamber to continue the oxidation process. The samples were prepared as metallographic specimens and analysed for oxides and cracks using optical microscopy (OM), scanning electron microscopy (SEM), and, in specific cases, also energy-dispersive X-ray spectroscopy (EDX). For U75V steel, under conditions where the entire test was conducted either in a dry phase, a wet phase, or a 1:1 wet-to-dry phase ratio, samples were collected at all time points (see Tab. 3). These conditions were selected for full-interval monitoring as they represent the extreme and central cases with the expected most significant variations. However, for other wet-to-dry phase ratios and two remaining steel grades, samples were taken only after 24 hours.

2.4. Impact testing

The impact test was conducted using an impact testing machine powered by an air compressor, which delivered pressurised air to actuate the impact cylinder, see Fig. 1 c). The impact load was monitored in real time using a pressure sensor and a data acquisition card. The machine had a maximum impact load of 600 N, with an accuracy of ±2%, and allowed an impact frequency range of 0 to 8 Hz.

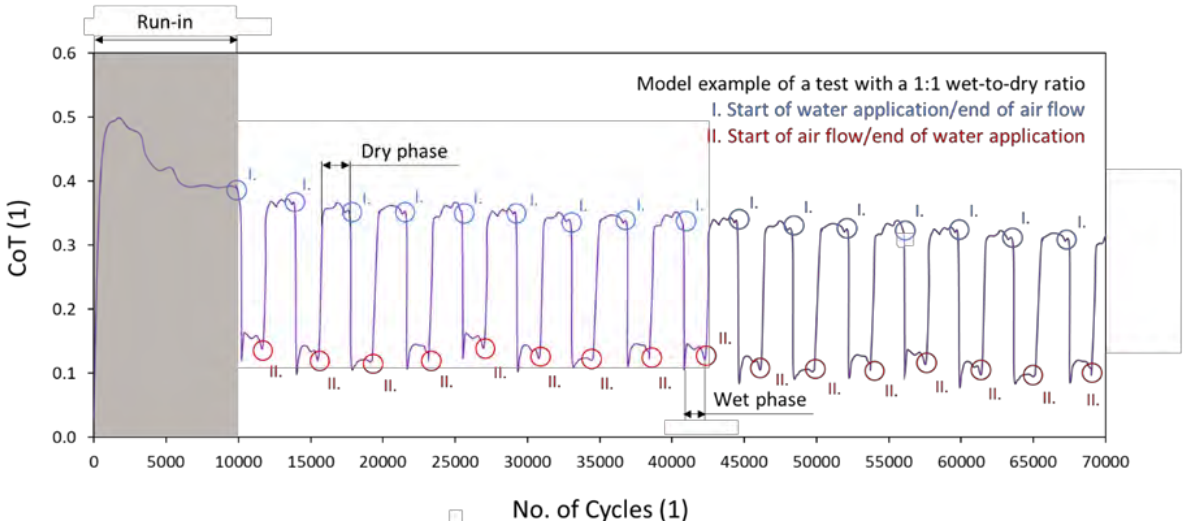

Fig. 2 *Model example of a test with alternating wet and dry phases.*

Table 3 *Intervals of sample analysis during the oxidation process.*

Test no.	1 h	3 h	6 h	12 h	24 h	72 h	168 h
1	✓	✓	✓	✓	✓	✓	✓
2					✓		
3					✓		
4	✓	✓	✓	✓	✓	✓	✓
5					✓		
6					✓		
7	✓	✓	✓	✓	✓	✓	✓
8					✓		
9					✓		

For this study, specimens from Test no. 7 after 168 hours of oxidation were selected, as this condition was expected to produce the most significant cracks and the thickest oxide layer (see Tabs. 2 and 3). The experimental parameters were set to an impact load of 400 N, an impact frequency of 4 Hz, and three different test lengths: 500, 5 000, and 50 000 cycles. These impact tests aimed to evaluate the mechanical integrity of the oxide layer, its adhesion to the crack faces, and whether it remains within the cracks under cyclic loading or disintegrates. A new sample was used for each of the three tests.

3. Results and Discussion

During the process, a large set of OM/SEM images was taken to enable both qualitative and quantitative evaluation of the effect of oxidation on RCF cracks. Although the quantitative analysis was conducted using the entire set, only the most representative and illustrative images are shown here due to space limitations.

Fig. 3 a) shows the progression of oxide layer coverage on the disc surface at selected time intervals (see Tab. 3). Although the images were taken from Test no. 7, they represent all other tests, as the oxidation process was consistent across all experiments. Fig. 3 a) demonstrates a time-dependent increase in the surface area covered by the oxide layer. After 24 hours, some places on the disc surface remain uncovered, indicating that a continuous oxide layer has not yet formed. The images for 72 and 168 hours show that a uniform and continuous thick oxide layer was reliably formed after prolonged oxidation time.

Please note that in the later text, oxide layer thickness values for time points up to 24 hours were calculated only from areas where the oxide layer was present. Regions without any oxide coverage were excluded from the analysis. Consequently, the reported values (e.g., in

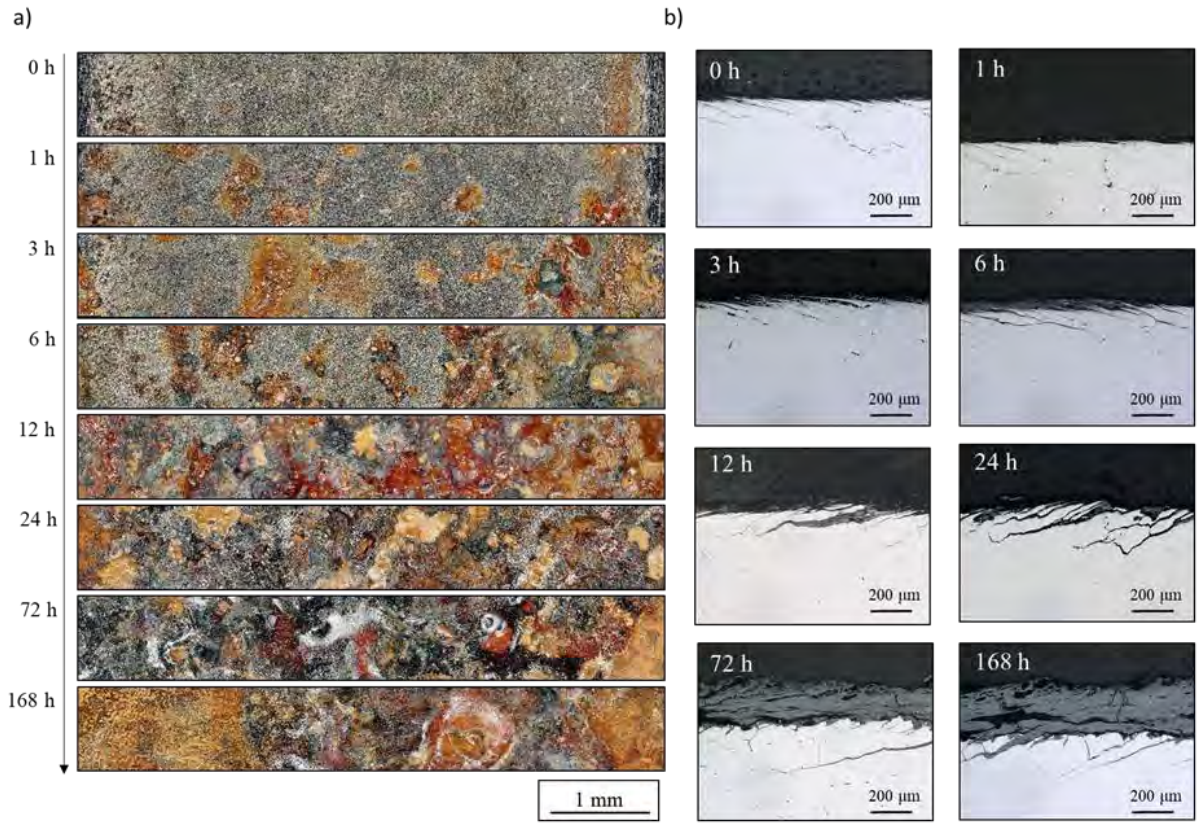

Fig. 3 *Evolution of the oxide layer at selected time intervals: a) on the disc surface and b) within RCF cracks. Test no. 7 (Dry phase: 0 s, Wet phase: 180 s).*

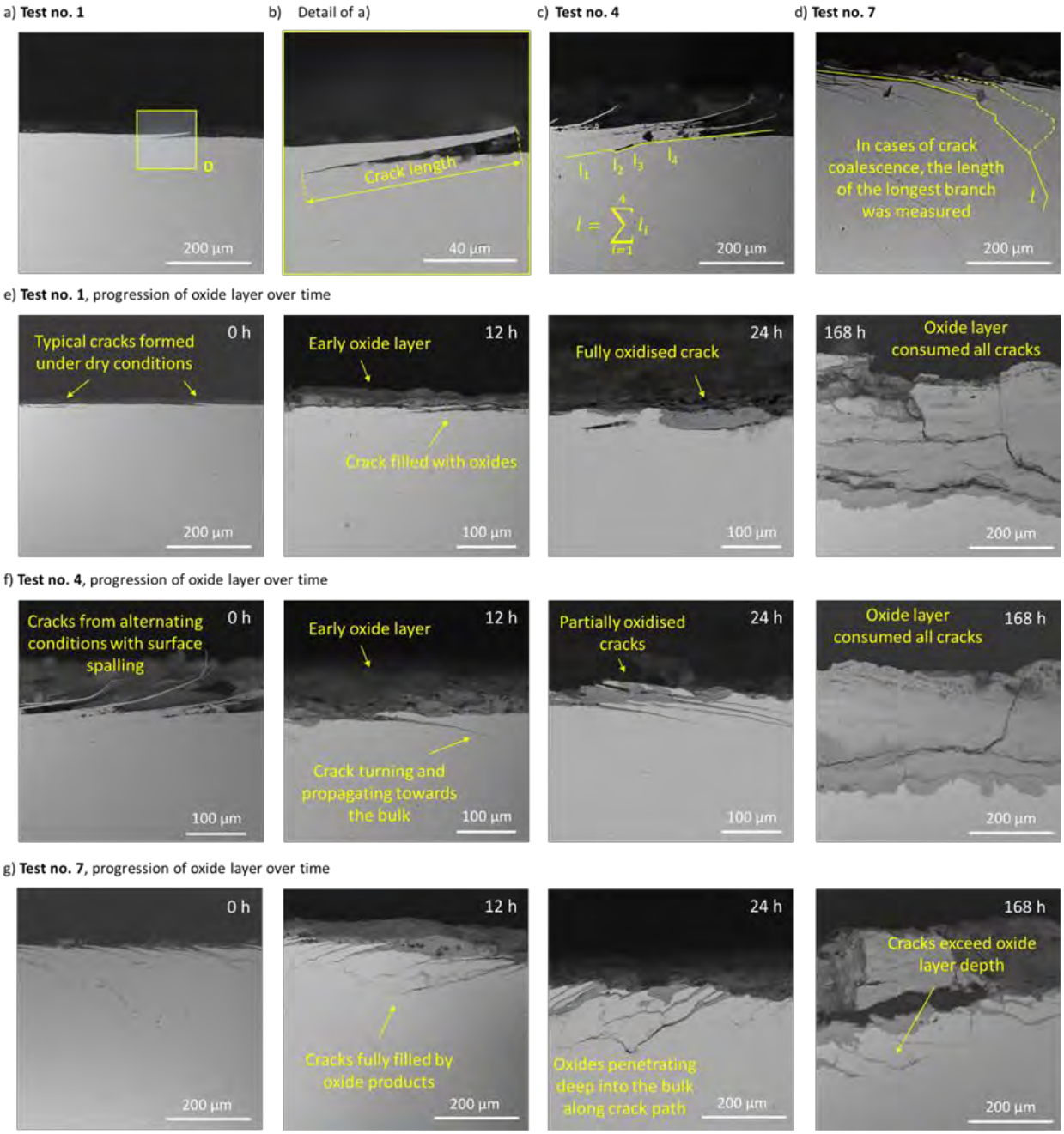

Fig. 4 *Typical crack morphologies observed under different testing conditions: a) and b) dry conditions; c) alternating dry and wet conditions; and d) continuous wet conditions. e–f) progression of the oxide layer over time.*

Fig. 5 does not represent an average over the entire surface but rather the local thickness in oxidised regions. A fully continuous oxide layer can only be assumed after 72 h and 168 h.

Fig. 3 b) demonstrates that oxidation of crack faces occurs even in areas where a continuous oxide layer does not yet cover the surface. Oxide products are visible within the cracks after only a few hours of exposure, as shown in the 6-hour and 12-hour images. This suggests that, even without visible surface coverage, oxidation actively affects RCF cracks by progressing along the crack faces and penetrating the bulk material. The process appears relatively rapid, occurring within just a few hours.

Measuring the maximum crack depth is relatively straightforward; however, determining the crack length is more challenging due to the curved geometry, branching, and coalescence of the crack. Fig. 4 illustrates the typical crack morphologies obtained from varying dry and wet phase ratios, as well as the methodology employed for length measurement. Figs. 4 a) and b) depict cracks formed under dry conditions (Test no. 1). These cracks are short, shallow, and run parallel to the surface. Fig. 4 b) illustrates how the length of such a crack was measured. Fig. 4 c) shows a crack formed under alternating dry and wet conditions with a 1:1 ratio (Test no. 4). The influence of water on crack development is evident when compared to the straight cracks formed in dry conditions. In this case, the crack initially propagates straight but then turns towards the bulk and continues at

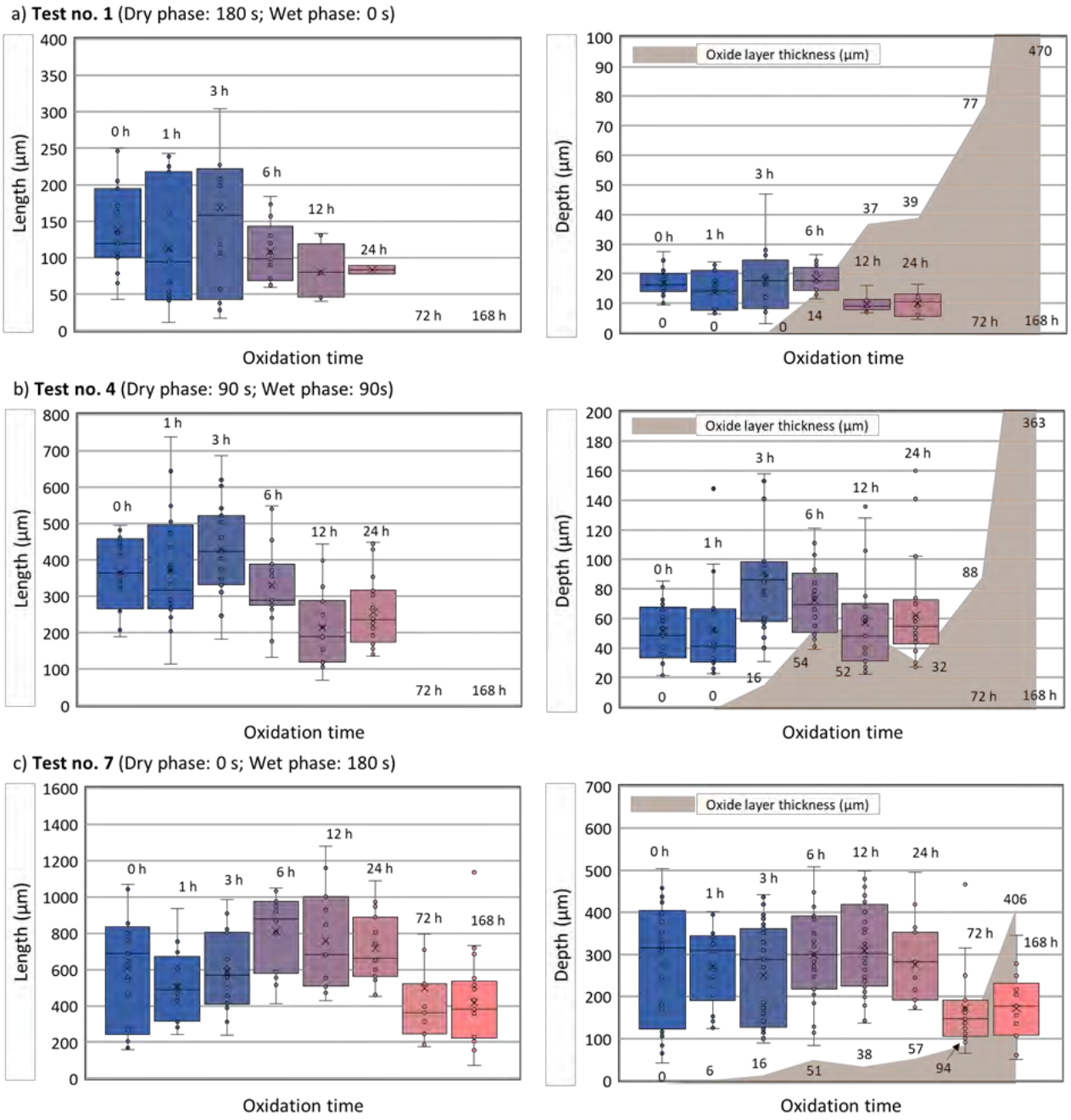

Fig. 5 *Box plots of crack length and depth at different oxidation times for a) dry, b) alternating, and c) wet conditions. Shaded areas in the depth plots indicate average oxide layer thickness.*

a second, steeper angle. In addition, these cracks were also larger in number and, in some cases, layered one on top of another. To determine the length, the crack was divided into several consecutive segments, each of which was measured individually and summed to obtain the final value.

Finally, Fig. 4 d) shows typical cracks formed under wet conditions (Test no. 7). The surface contains a high density of cracks, each of them turning towards the bulk at steep angles, often approaching perpendicularity, and extending significantly deeper into the material compared to cracks formed under dry conditions. These cracks frequently branch and coalesce with neighbouring cracks, creating complex, interconnected structure.

Due to this branching and coalescence, determining crack length is more challenging than in previous cases. Therefore, the measurement approach focused on identifying the longest continuous branch within each crack network, which was considered the main crack. Its length was measured as described in Fig. 4 c).

Fig. 4 e–g) shows typical examples of cracks formed under dry, alternating, and wet conditions, along with the progression of oxide penetration over time. These images are included to provide the reader with a visual understanding of the crack morphology and oxidation patterns and to illustrate the data type used for the quantitative analysis. However, the influence of oxidation on crack behaviour will be primarily discussed

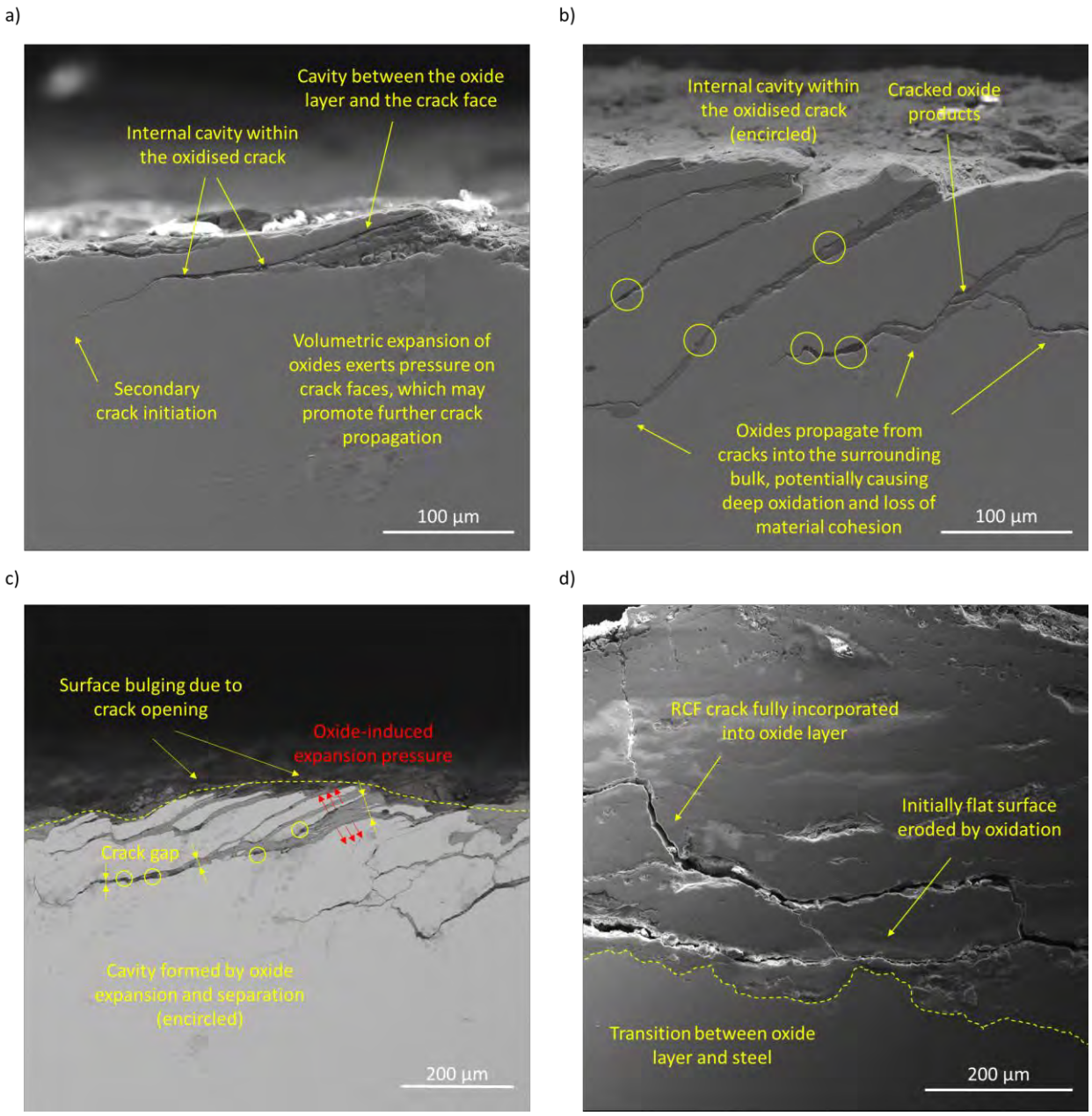

Fig. 6 *SEM pictures of: a) crack mouth opening due to oxide growth, b) deeper cracks filled with oxides, c) surface bulging, cavity formation, and a tapered crack gap, likely caused by oxide-induced wedging and volumetric expansion, d) crack consumed by the oxide layer as a result of progressive surface oxidation.*

based on the measured data presented in Fig. 5.

The quantitative analysis of crack parameters is presented in Fig. 5: a) for dry conditions only (Test no. 1), b) for alternating dry and wet conditions (Test no. 4), and c) for wet conditions only (Test no. 7). For each condition, the first plot shows the measured crack lengths, and the second shows the measured crack depths. Each box corresponds to a different oxidation time interval. The median, mean (marked by ×), minimum and maximum values, and the 25th and 75th percentiles are displayed. Individual data points are also shown. In the depth plots, the shaded area represents the average oxide layer thickness for each time point, providing a visual reference for the extent of surface oxidation relative to the crack penetration depth. The quantitative crack parameters will be discussed in detail with reference to the high-resolution SEM images presented in Fig. 6, which offer further insight into crack morphology and the effects of oxidation.

Previous research suggested that when a surface containing RCF cracks undergoes oxidation, some of the oxidised cracks look wider and extended than those that are not oxidised. This led to the idea that the volumetric expansion of growing oxide products may create internal pressure on the crack faces, helping the crack to grow and become wider and deeper. A clear example supporting this idea is shown in Fig. 6 a), where the crack mouth is wider, and signs of secondary crack propagation can be observed.

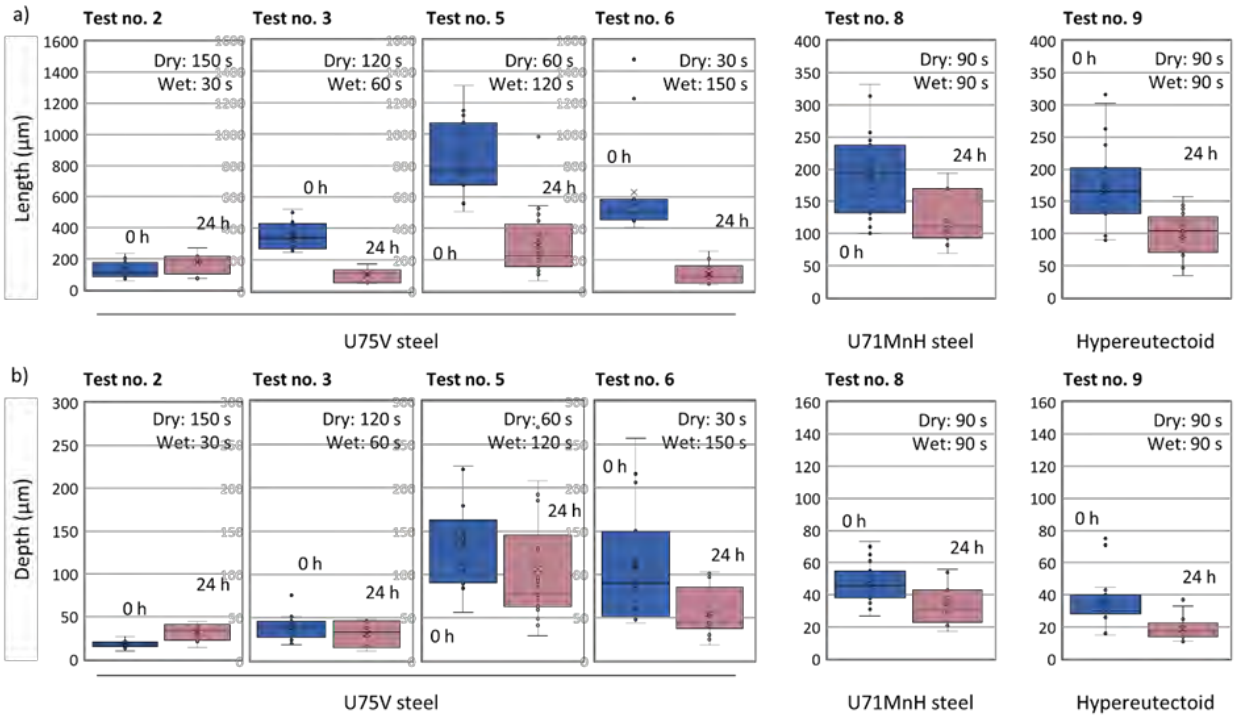

Fig. 7 *Comparison of crack length (a) and depth (b) before and after 24 h of oxidation for various dry/wet phase ratios and three steel grades.*

Additional findings from this study support this idea. In particular, oxidised cracks often exhibit a specific shape: they are wider near the surface and become narrower with depth, which differs from typical RCF cracks. This could be caused by the physical effect of volumetric expansion. The oxide products, which can increase in volume by 2 to 4 times compared to the original metal, likely push against the crack faces. This pressure could gradually separate the crack faces, especially near the surface opening of the crack, where the surrounding material provides less constraint.

Indeed, in several SEM images, such as Fig. 6 a) and b), cavities were seen between the oxide and the steel, suggesting that the oxides did not fully conform to the changing crack geometry. These cavities may have formed because the crack was first completely filled with oxide, which then expanded beyond the available space. This additional growth likely pushed the crack faces apart, creating cavities deep within the crack where the oxides could not adapt to the new shape.

Additionally, fractures within the oxidised material, including internal cracks and delamination of oxide layers, support that the volumetric expansion generates local mechanical stress. In some SEM images, the material above the crack appears slightly raised or deformed, which may reflect local uplift due to oxide-induced expansion. This deformation, often referred to as bulging, provides additional support for the notion that oxide growth can exert outward pressure on the surrounding steel. These stresses may not cause measurable crack growth, but they do suggest that mechanical forces from oxide expansion can change the crack geometry. Additionally, the crack openings are often observed to narrow progressively with depth, forming a wedge-like profile. This geometry suggests that surface oxidation generates stronger expansive

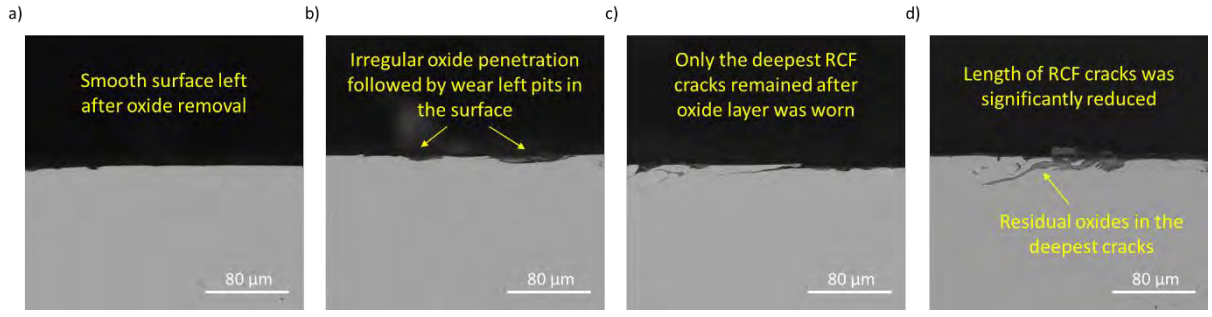

Fig. 8 *a) Surface after oxide removal, b) pit left by removed oxide, c) remainings of a significant crack, and d) residual oxides in the crack remainings.*

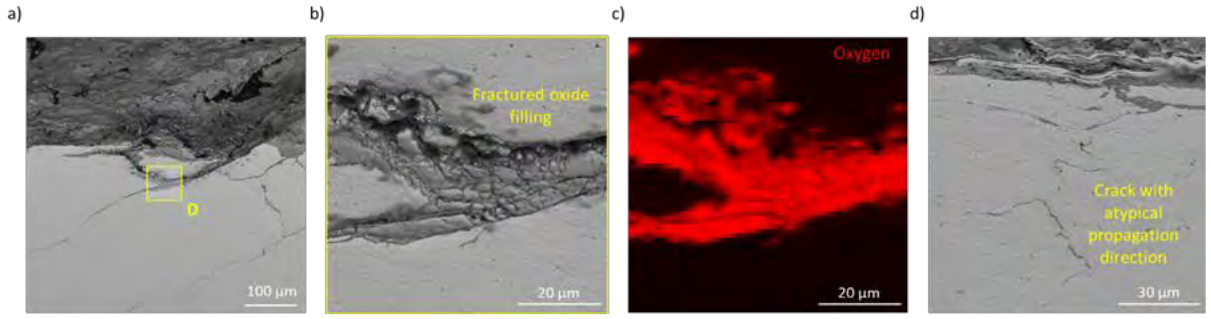

Fig. 9 *a) Impact site from the tester head, b) detail of fractured oxides within a crack, c) EDX mapping confirming the presence of oxides in cracks, and d) atypical crack propagation due to cyclic loading.*

forces near the crack mouth, which then gradually dissipate with increasing depth. Such a wedge-shaped widening is consistent with the idea that oxidation-induced separation acts more intensively near the oxidised surface.

Although the quantitative data in Fig. 5 does not show clear increases in crack length during oxidation (Tests no. 1, 4, and 7), this does not mean there were no local mechanical effects inside the cracks. One issue with the analysis is that it does not follow the same crack before and after oxidation. Instead, measurements were taken from different spots on the sample surface at each time point. Because of this, differences in the original size and shape of the selected cracks might hide real changes. For example, a crack might have grown during oxidation, but if the first measurement came from a spot with large cracks and the second from a spot with smaller ones, the data might falsely suggest the crack got smaller. This type of sampling issue makes it difficult to determine whether oxidation caused the cracks to grow, especially when the changes are small or limited to specific areas. The primary visible effect of oxidation remains crack widening rather than deepening.

The apparent widening of cracks can also be explained by chemical processes. As oxidation progresses, the steel near the crack is converted into brittle iron oxides, which makes the crack appear wider. However, the cracks and cavities seen inside the oxidised areas also suggest local mechanical stress, likely caused by volumetric expansion. These stresses may not be strong enough to cause significant crack growth, but they can influence the shape of the crack.

In the end, even if some crack growth does happen due to pressure from oxide expansion, it is likely much slower than the rate at which oxidation progresses from the surface downwards. As the oxidation front moves deeper into the material, it gradually consumes the crack, regardless of whether secondary crack propagation occurs. Over time, this leads to the crack being entirely embedded within the oxidised layer, as observed in the later stages of oxidation, as shown in Fig. 6 d).

Therefore, the widened appearance of the crack is likely the result of both chemical transformation of the steel into oxide and local mechanical effects from oxide expansion. This conclusion is based on visual evidence and qualitative observations, and while it provides a plausible explanation, a more detailed experimental study would be needed to measure and distinguish the contribution of each mechanism directly. However, such an investigation would require a more complex methodology and is beyond the scope of this study.

Although no clear time-dependent crack length trend was observed between 0 and 24 hours in Fig. 5, a consistent change occurred at longer oxidation times (72 and 168 hours). A noticeable reduction in both crack length and depth was observed in all tests shown in Fig. 5. For the dry and alternating conditions (Tests 1 and 4), cracks completely disappeared from the measured areas. Some cracks remained under wet conditions (Test no. 7), but their length and depth were significantly reduced. This effect correlates with the growth of the oxide layer, as indicated by the shaded area in the crack depth plots, which represents the oxide thickness. In the first few hours, the oxide layer remains very thin and does not significantly affect the cracks. However, some decrease in the typical crack depth can already be seen at 12 and 24 hours. This is especially evident when focusing on the middle of the data range (for example, the median) rather than just examining the extreme values. At 72 and 168 hours, the oxide layer becomes thicker than the deepest cracks, and the cracks are no longer present in the steel; they have been entirely transformed into part of the oxide layer as the surrounding steel oxidises. This process is also visible in the SEM image in Fig. 6 d), which shows a significant RCF crack. As the surface oxidised over time, the entire crack became part of the growing oxide layer.

To confirm the observed effect across a broader range of conditions and crack types, additional tests were conducted using various dry-to-wet phase ratios (see Tab. 2). Additionally, tests were conducted on discs made from two different steel grades to investigate the impact of material properties. The results of these tests are presented in Fig. 7. Please note that this figure compares the non-oxidised condition and the condition after 24 hours of oxidation. In nearly all cases, oxidation led to a consistent reduction in both crack length and depth across all three steel grades. This confirms that oxide layer growth effectively reduces crack dimensions, even in different materials.

A question arises as to how oxidation may influence wear and RCF. To investigate this, a test was carried out in which surface cracks were prepared under dry conditions using the same method as in previous experiments. This approach was chosen because cracks generated in dry conditions were shown to be the most affected by oxidation. Then, the specimens underwent the 24-hour oxidation procedure. Please note that these were not the same discs used in Test no. 1, as the original pair had already been sectioned for earlier analyses.

After the oxidation phase, a wear test was conducted using the twin-disc machine (Fig. 1 a) under conditions representative of the wheel-rail contact: 2% slip, a rolling speed of 1.5 m/s, and a maximum contact pressure of 1.1 GPa. Although the cracks were formed under dry conditions, the wear test was carried out under wet conditions, with water supplied to the contact area. Water was used because it accelerates RCF through several mechanisms, including crack face lubrication and hydropressurisation. After testing, the rail disc specimen was sectioned, and SEM images of the surface and subsurface regions were obtained (see Fig. 8).

Analysis of SEM images revealed that after the wear test, the oxide layer was completely removed, leaving a smooth disc surface (see Fig. 8 a). Small pits were observed in some locations where oxides had detached from the surface. These pits likely originated from regions where oxidation penetrated the steel matrix unevenly (see Fig. 8 b). In addition, traces of cracks were identified in some regions of the surface (e.g., Fig. 8 c). After 24 hours of oxidation, the layer thickness typically ranged from 30 to 60 μm. Some cracks extended deeper than this thickness, which explains why residual portions of cracks were still visible after the oxide layer was removed. Residual oxide products were also found within the remaining crack segments (Fig. 8 d). Notably, the surfaces did not exhibit any visible signs of RCF damage.

It seems that oxidation suppresses RCF by two complementary mechanisms. First, as the crack faces oxidise, the resulting oxide products expand volumetrically and fill the crack volume, preventing water penetration into the cracks and thereby suppressing known fluid-driven crack propagation mechanisms, such as hydropressurisation and crack face lubrication. Second, as the oxide layer is removed, any cracks within it are also removed. While this may lead to increased wear compared to non-oxidised surfaces, it effectively prevents the development of RCF damage.

However, a crucial question remains whether the oxide products can stay in the cracks under real operating conditions, such as during the passage of a railway wheel. The key uncertainty lies in the adhesion of the oxides to the crack faces. It is possible that the oxide material could come loose or fall out under dynamic loading. If the oxides are removed from the cracks, water may again penetrate, potentially reactivating fluid-driven crack propagation mechanisms. A series of tests were conducted using an impact tester to assess the mechanical stability of the oxide layer under such loading. The results of these tests are shown in Fig. 9.

Impact tests demonstrated that even after 50 000 cycles, oxides remained within cracks despite exhibiting fracturing both on the surface and inside the cracks, see Fig 9 a-c). EDX analysis further confirmed the presence of oxygen within the cracks, indicating that oxides were not removed. This suggests that, under actual operating conditions, oxidised cracks would still likely prevent water from penetrating, thereby suppressing liquid-driven RCF propagation. However, as oxidation progresses deeper into cracks, it weakens the material beyond the typical range of surface oxidation. This deeper degradation may, under cyclic loading, facilitate further crack growth (as seen in Fig. 9 d), potentially affecting long-term RCF behaviour as it weakens material integrity to greater depths.

4. Conclusion

The findings indicate that oxidation has a significant impact on the morphology and evolution of RCF cracks. Oxide products were observed not only on the surface but also deep within cracks. The volumetric expansion of these oxides creates pressure on the crack faces, widening them and forming wedge-shaped openings, especially near the surface. While this mechanical effect does not result in clear crack growth across the sample, it may trigger limited secondary propagation in some cases.

As oxidation progresses, the cracks are gradually consumed by the growing oxide layer. This results in a measurable reduction in both crack length and depth. Moreover, because oxides have significantly lower shear strength than the original steel, an increase in wear was observed under loading, however, their presence in the cracks effectively blocks fluid-driven RCF mechanisms. Thus, oxidation plays a dual role: it increases wear susceptibility but simultaneously suppresses RCF.

These findings underscore the importance of considering oxidation processes when assessing the long-term evolution of damage in wheel-rail contacts under realistic operating conditions. Even slow oxidation-induced changes can accumulate over extended service periods, affecting both wear and crack behaviour.

Acknowledgments

This publication was supported by the project "Mechanical Engineering of Biological and Bio-inspired Systems", funded as project No. CZ.02.01.01/00/22_008/0004634 by Programme Johannes Amos Comenius, call Excellent Research. The work was also supported by National Natural Science Foundation of China (No. 52320105007 and No. 52202510).

References

[1] R.A. SMITH, The wheel–rail interface—some recent accidents, Fatigue Fract Eng Mater Struct 26 (2003) 901–907. https://doi.org/10.1046/j.1460-2695.2003.00701.x.

[2] S. Zhang, M. Spiryagin, Q. Lin, H. Ding, Q. Wu, J. Guo, Q. Liu, W. Wang, Study on wear and rolling contact fatigue behaviours of defective rail under different slip ratio and contact stress conditions, Tribol Int 169 (2022) 107491. https://doi.org/10.1016/j.triboint.2022.107491.

[3] Y. Zhu, The influence of iron oxides on wheel–rail contact: A literature review, Proc Inst Mech Eng F J Rail Rapid Transit 232 (2018) 734–743. https://doi.org/10.1177/0954409716689187.

[4] S.T. Hengeveld, D. Leonetti, B. Snijder, J. Maljaars, Prediction of fatigue crack paths including crack-face friction for an inclined edge crack subjected to mixed mode loading, Procedia Structural Integrity 54 (2024) 34–43. https://doi.org/10.1016/j.prostr.2024.01.053.

[5] S.Y. Zhang, M. Spiryagin, H.H. Ding, Q. Wu, J. Guo, Q.Y. Liu, W.J. Wang, Rail rolling contact fatigue formation and evolution with surface defects, Int J Fatigue 158 (2022) 106762. https://doi.org/10.1016/j.ijfatigue.2022.106762.

[6] R. Stock, D.T. Eadie, D. Elvidge, K. Oldknow, Influencing rolling contact fatigue through top of rail friction modifier application – A full scale wheel–rail test rig study, Wear 271 (2011) 134–142. https://doi.org/10.1016/j.wear.2010.10.006.

[7] S. Maya-Johnson, J. Felipe Santa, A. Toro, Dry and lubricated wear of rail steel under rolling contact fatigue - Wear mechanisms and crack growth, Wear 380–381 (2017) 240–250. https://doi.org/10.1016/j.wear.2017.03.025.

[8] N. Fantecelle Strey, A. Bavaresco Rezende, R. da Silva Miranda, S. Tamara da Fonseca, P.R. Mei, C. Scandian, Comparison of rolling contact fatigue damage between railway wheels and twin-disc test specimens, Tribol Int 160 (2021) 107037. https://doi.org/10.1016/j.triboint.2021.107037.

[9] D.T. Eadie, D. Elvidge, K. Oldknow, R. Stock, P. Pointner, J. Kalousek, P. Klauser, The effects of top of rail friction modifier on wear and rolling contact fatigue: Full-scale rail–wheel test rig evaluation, analysis and modelling, Wear 265 (2008) 1222–1230. https://doi.org/10.1016/j.wear.2008.02.029.

[10] G. Donzella, M. Faccoli, A. Mazzù, C. Petrogalli, R. Roberti, Progressive damage assessment in the near-surface layer of railway wheel–rail couple under cyclic contact, Wear 271 (2011) 408–416. https://doi.org/10.1016/j.wear.2010.10.042.

[11] S. Kondo, Y.W. Chai, K. Kanai, L. Dosung, M. Watanabe, S. Ishikawa, T. Yamasita, Y. Kimura, Intermetallic phase precipitation and oxidation behavior of Fe–20Cr–0.5Nb–2Mo (at%) high-Cr ferritic alloy at high temperatures, Acta Mater 246 (2023) 118677. https://doi.org/10.1016/j.actamat.2023.118677.

[12] H. Chen, T. Ban, M. Ishida, T. Nakahara, Adhesion between rail/wheel under water lubricated contact, Wear 253 (2002) 75–81. https://doi.org/https://doi.org/10.1016/S0043-1648(02)00085-6.

[13] A.F. Bower, The Influence of Crack Face Friction and Trapped Fluid on Surface Initiated Rolling Contact Fatigue Cracks, J Tribol 110 (1988) 704–711. https://doi.org/10.1115/1.3261717.

[14] I.I. Kudish, K.W. Burris, Modeling of surface and subsurface crack behavior under contact load in the presence of lubricant, 2004.

[15] A.F. Bower, K.L. Johnson, Plastic flow and shakedown of the rail surface in repeated wheel-rail contact, Wear 144 (1991) 1–18. https://doi.org/10.1016/0043-1648(91)90003-D.

[16] Y. Sone, J. Suzumura, T. Ban, F. Aoki, M. Ishida, Possibility of in situ spectroscopic analysis for iron rust on the running band of rail, Wear 265 (2008) 1396–1401. https://doi.org/10.1016/j.wear.2008.02.027.